



MÁSTER UNIVERSITARIO EN INGENIERÍA INDUSTRIAL

TRABAJO FIN DE MÁSTER

ANAEROBIC CO-DIGESTION STUDY AND CHARACTERISATION OF DIFFERENT DIGESTERS TO MAXIMIZE BIOGAS GENERATION

Autor: Javier Victoria Rodríguez

Director: María del Mar Cledera Castro

Director: Carlos Morales Polo

Madrid

Agosto 2022

Declaro, bajo mi responsabilidad, que el Proyecto presentado con el título
Anaerobic Co-Digestion Study and Characterisation of Different
Digesters to Maximise Biogas Generation en la ETS de Ingeniería - ICAI de la
Universidad Pontificia Comillas en el
curso académico 20221/2022 es de mi autoría, original e inédito y
no ha sido presentado con anterioridad a otros efectos. El Proyecto no es
plagio de otro, ni total ni parcialmente y la información que ha sido tomada
de otros documentos está debidamente referenciada.



Fdo.: Javier Victoria Rodríguez

Fecha: 18/08/2022

Autorizada la entrega del proyecto

EL DIRECTOR DEL PROYECTO



Firmado digitalmente por María del Mar Cledera Castro
Nombre de reconocimiento (DN): cn=María del Mar Cledera
Castro, o=Universidad Pontificia Comillas, ou,
email=mcledera@comillas.edu, c=ES
Fecha: 2022.08.25 10:36:03 +02'00'

Fdo.: María del Mar Cledera Castro

Fecha://

Firmado digitalmente por Carlos Morales Polo
Nombre de reconocimiento (DN): cn=Carlos Morales Polo, o, ou,
email=cmorales@comillas.edu, c=ES
Fecha: 2022.08.25 10:38:56 +02'00'

Fdo.: Carlos Morales Polo

Fecha://



MÁSTER UNIVERSITARIO EN INGENIERÍA INDUSTRIAL

TRABAJO FIN DE MÁSTER

ANAEROBIC CO-DIGESTION STUDY AND CHARACTERISATION OF DIFFERENT DIGESTERS TO MAXIMIZE BIOGAS GENERATION

Autor: Javier Victoria Rodríguez

Director: María del Mar Cledera Castro

Director: Carlos Morales Polo

Madrid

Agosto 2022

ANAEROBIC CO-DIGESTION STUDY AND CHARACTERISATION OF DIFFERENT DIGESTERS TO MAXIMIZE BIOGAS GENERATION

Autor: Victoria Rodríguez, Javier

Directores: María del Mar Cledera Castro y Carlos Morales Polo

Institución Colaboradora: ICAI- Universidad Pontificia Comillas

RESUMEN DEL PROYECTO

Introducción

El principal problema al que se enfrenta la sociedad actualmente es la Transición Ecológica a una economía verde mediante la reducción de los impactos que los humanos tenemos en el planeta como resultado del cambio climático antropogénico. Esta es parte de las “Twin Transitions” (European Commission, 2020) considerada por la UE un pilar en el que basar el liderazgo mundial de Europa. Esto culminó en la creación y aprobación del “European Green Deal” (European Commission, 2021) que busca dar respuesta a las anomalías y desastres causados por el cambio climático.

Para dirigir los esfuerzos e inversiones tanto públicas como privadas, el Acto Delegado sobre el Clima fue aprobado con el objetivo de alinear a los actores clave y tecnologías a emplear. Entre estas tecnologías se encuentra la bioenergía; particularmente el biogás y el biometano, gases bajos en carbono destinados a sustituir al gas natural y producidos mediante la digestión anaerobia (DA) de especial importancia en el sector del transporte pesado (European Biogas Association, 2020).

El COP de Glasgow (United Nations, 2021) enfatizó la necesidad de controlar el incremento de la temperatura global a 1,5 °C sobre niveles preindustriales. Por tanto, los líderes mundiales alcanzaron un compromiso común para eliminar el carbón de la generación eléctrica (Rannard, 2021), considerado como el combustible fósil más contaminante. Además, la UE y EEUU, junto con otros 100 países anunciaron su intención de reducir sus emisiones fugitivas de metano, principalmente las procedentes de escapes de gas natural. Estas han sido consideradas como 1 de las 8 cuñas de estabilización necesarias para prevenir el incremento de la temperatura (Pacala & Socolow, 2004).

A escala nacional, el Ministerio para la Transición Ecológica (MITECO) identificó el biogás como una nueva fuente de energía renovable con una capacidad de evitar la emisión de 2,1 millones de toneladas de CO₂-eq. por año según la Hoja de Ruta del Biogás (Ministero para la Transición Ecológica y el Reto Demográfico, 2022). La HR resalta el uso residual de la DA, la cual produjo 2,74 TWh de energía en 2020. Además, solo hay 5 plantas de biometano en España, siendo la de mayor tamaño la planta de Valdemingomez, Madrid (FCC, 2021).

El último aspecto del contexto en el que ocurre esta investigación está relacionado con el objetivo de conseguir una economía circular en la cual se minimice la producción de residuos, mejorando la reutilización de recursos para extraer todo su potencial (Romero Mora & Tatay Nieto, 2020). La DA propone la conversión del fango de residuo a subproducto que puede ser usado no solo en la generación de energía, sino también en fertilizante a través del digestato. Al considerarse todo el ciclo de vida del fango, así como el eco-diseño del proceso de tratamiento de residuos para conseguir un proceso “cradle-to-cradle”. Estos avances permitirían reducir la intensidad energética del tratamiento de aguas residuales u otros procesos industriales que requieren de depuradoras para cumplir normativa.

Metodología

Todos los experimentos presentaban una característica común, su composición, por tanto, los cálculos realizados para obtener los volúmenes requeridos por cada envase se muestran a continuación en la Tabla-R 1 junto con las fórmulas. Basándose en estudios previos, la proporción fango-sustrato se mantuvo 3:1 (Morales Polo, 2019). Además, se necesitaba una humedad del 50% (FCC, 2021), lo que creó una segunda restricción a la composición. Para crear la mezcla, se empleó calabaza como sustrato.

$$V_{agua}[l] = 0.5 * V_{Total}[ml]$$

$$V_{fangos}[l] = 0.375 * V_{Total}[ml]$$

$$V_{sustrato}[l] = 0.125 * V_{Total}[ml]$$

Tabla-R 1: Proporciones en la Mezcla de Co-Digestión. Fuente: Propia.

Variable	BMP	Reactor
V _{Total} (ml)	300.0	2000.0
V _{water} (ml)	150.0	1000.0
V _{sludge} (ml)	112.5	750.0
V _{substrate} (ml)	37.5	125.0

Diseño y Construcción Ensayos BMP

Los primeros ensayos realizados fueron los ensayos BMP, regidos por la norma ISO 11734:1999 (AENOR, 1999), utilizada en proyectos en los que este estudio se basa. Esta Norma requiere del uso de botellas de 1 litro selladas herméticamente en las que se digiere una muestra de 300 ml de mezcla de DA durante 21 días, midiendo la presión generada a diario. Estas botellas se sellaron con septums y pasta de silicona.

Asimismo, para replica el ensayo semicontinuo a escala de botella, se diseñaron 2 botellas BMP empleando un tapón con válvulas: el puerto de muestreo y el puerto de alimentación. Por último, se empleó una incubadora orbital para la agitación y para mantener la consiga de temperatura de nueve botellas cada vez, limitando las tandas a ese número. Para mantener las condiciones mesofílicas, la consigna se estableció en 38.0°C. En la Figura-R 1 se muestra una botella BMP discontinua; en la Figura-R 2 una botella BMP semicontinua y por último el diseño en la Figura-R 3.



Figura-R 1: Botella BMP Discontinua. Fuente: Propia.



Figura-R 2: Botella BMP Semicontinua. Fuente: Propia.

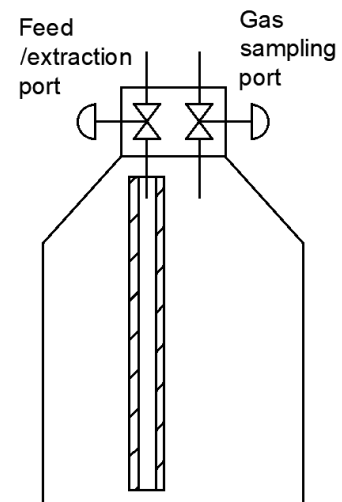


Figura-R 3: Diagrama Botella BMP Semicontinua. Fuente: Propia.

Diseño y Construcción Reactor Discontinuo

El segundo tipo de experimento se realizó en reactores discontinuos de 2 litros, los cuales eran una versión a mayor escala de los ensayos BMP estandarizados. El mayor volumen también requería de ciertos cambios en el diseño. El primero y más relevante fue el cambio de control de temperatura y agitación. En estos, se emplearon termostatos externos para el control de temperatura, lo que requirió de una sonda dentro del reactor.

También se requirió de agitación externa mediante el uso de un eje con una pala de agitación soldada en su punta para mezclar la mezcla del reactor. Esta era accionada por el MiniReactor Scharlau y su motor.

Para conectar los MilliGascounters, se construyó un Sistema basado en una válvula de tres vías para permitir tanto el muestreo de biogás como la medición de la producción de este. En este caso, la válvula se encontraba de manera normal en la posición de producción. La construcción final del reactor se muestra en la Figura-R 4. Asimismo, todos los componentes del reactor se muestran en la Figura-R 5.



Figura-R 4: Construcción Final Reactor Discontinuo. Fuente: Propia.

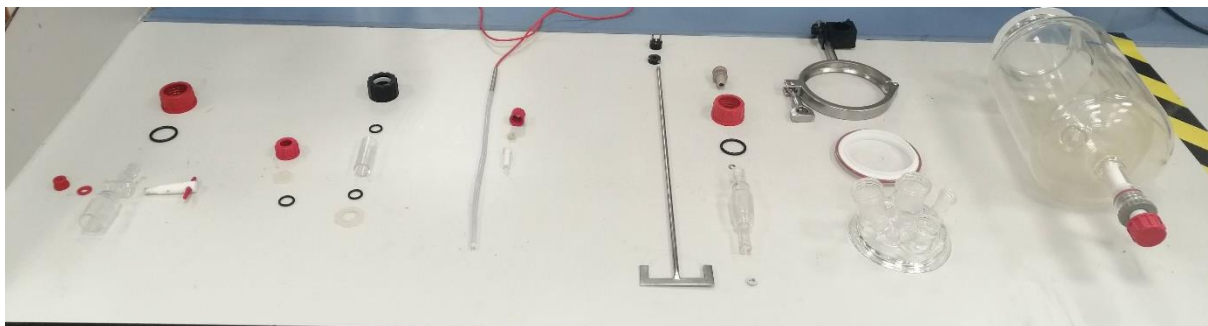


Figura-R 5: Componentes Reactor Discontinuo. Fuente: Propia.

Diseño y Construcción Reactor Discontinuo

El último experimento realizado fue en un reactor semicontinuo. Al igual que el reactor discontinuo, este experimento tenía su equivalente las botellas semicontinuas diseñadas previamente

El reactor escalado presento ciertas dificultades debido a sus características únicas, principalmente de espacio para acomodar el volumen de la mezcla de DA junto con todo el equipo auxiliar, idéntico al del

reactor discontinuo salvo por una excepción. La toma sellada en el discontinuo fue reemplazada por un septum modificado. Este puerto modificado se usó para instalar la manguera de alimentación, la cual conectaba la reserva de sustrato con el reactor a través de la bomba peristáltica Heidolph Hei-FLOW Precision 01 (Heidolph, 2022), la cual proporcionaba el sello hermético. Por último, para conseguir el comportamiento semicontinuo y la salida de digestato, se instaló una válvula de esfera en el puerto inferior para extraer diariamente el volumen necesario. El diseño se muestra en la Figura-R 6.

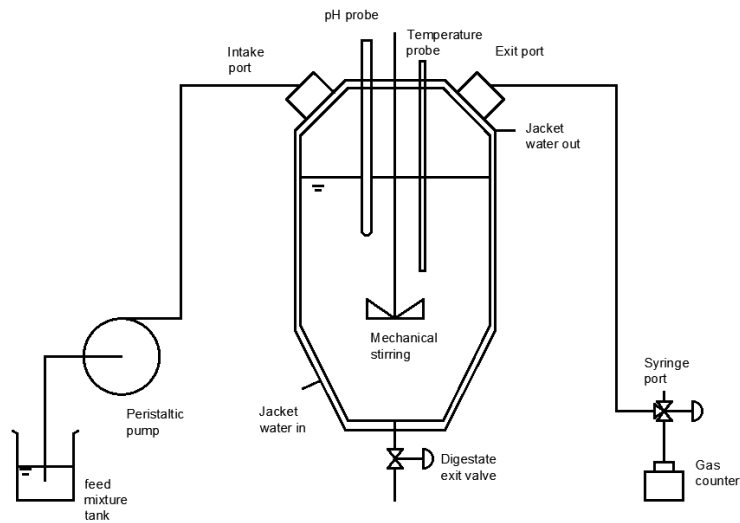


Figura-R 6: Diseño Reactor Semicontinuo. Fuente: Propia.

Medición de Presión y Muestreo de Botellas BMP

Como se ha mencionado, los ensayos BMP se realizaron en botellas selladas de 1 litro, permitiendo la producción de biogás en su interior para su recogida y análisis. Estas botellas se muestreaban diariamente para medir la producción molar de biogás de manera indirecta a través de la ley de los gases ideales. Además, la temperatura se controlaba con el Ivymen orbital shaker incubator, fijándola a 38°C, como se ha explicado previamente. Los moles de biogás se obtienen a través de esta fórmula:

$$[mol] = 0,041 * P[bar]$$

Producción de Biogás y Muestreo de Reactores

De manera similar a las botellas antes descrita, la medición de biogás se realizó de manera diaria. El diseño de los reactores permitió la medición directa de este a través de los MilliGascounters. Se ha de señalar que, debido a la pérdida de carga, estos no funcionaron correctamente durante todo el ensayo.

Test Ácidos Grasos Volátiles

La primera prueba realizada en el sobrenadante extraído de las muestras fue la medición de la alcalinidad dentro del reactor. Este ensayo es una variación de (Tran, 2017). La primera etapa de la valoración empleaba HCl para reducir el pH hasta 5.75, siguiendo la norma. Tanto el volumen como el pH final se anotaban. La segunda etapa del proceso era la valoración final, empleando H₂SO₄ hasta alcanzar 4.3 de pH. Estos era V₁ y V₂, respectivamente. Estas medidas fueron usadas para determinar la Alcalinidad Parcial (AP), Intermedia (AI) y Total (AT); usando la AI para medir los AGVs:

$$AP \left[\frac{mgCaCO_3}{l} \right] = \frac{V_{HCl} * N_{HCl} * 5000}{V_{sample}}$$

$$AI \left[\frac{mgCaCO_3}{l} \right] = \frac{V_{H_2SO_4} * N_{H_2SO_4} * 5000}{V_{sample}}$$

$$AT \left[\frac{mg_{CaCO_3}}{l} \right] = Ap + AI = \frac{(V_{H_2SO_4} * N_{H_2SO_4} + V_{HCl} * N_{HCl}) * 5000}{V_{sample}}$$

Cromatografía de Gases

Las muestras de gas eran extraídas diariamente y analizadas para determinar la composición del biogás producido. El método empleado en el cromatograma se desarrolló en (Morales Polo, 2019) con este fin. El diagrama caudal-temperatura se muestra en la Figura-R 7

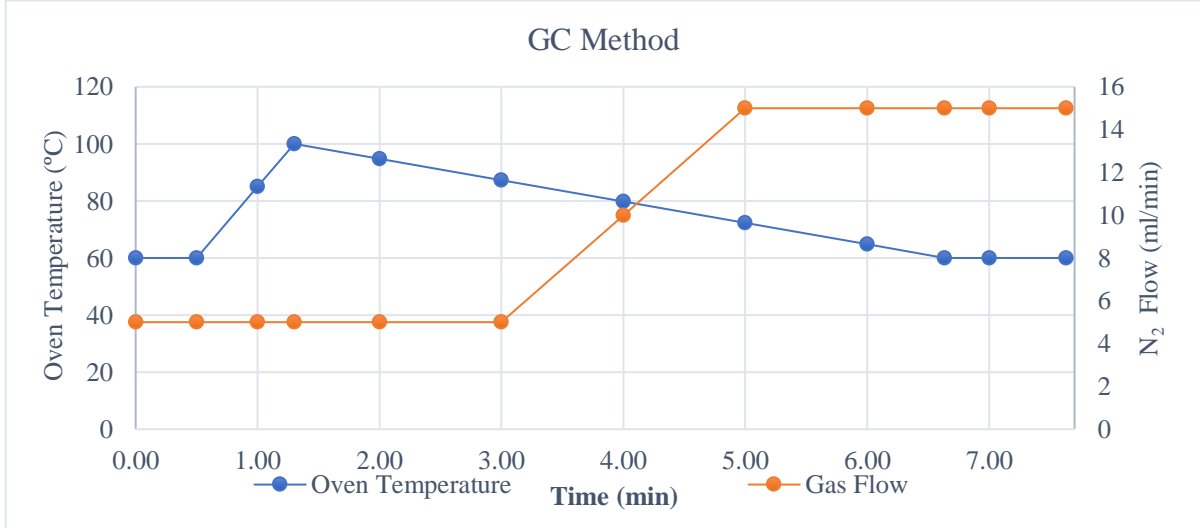


Figura-R 7: Método de Cromatografía de Gases. Fuente: Propia.

Resultados

Resultados Botellas BMP

Tras la recolección de los datos, se calculó la producción media normalizada de cada tipo de botella. Se ha de señalar que no se incluyeron las botellas semicontinuas en el análisis al no producir estos resultados útiles debido a la inhibición del proceso de DA en el día 4. La producción acumulada se muestra en la Figura-R 8.

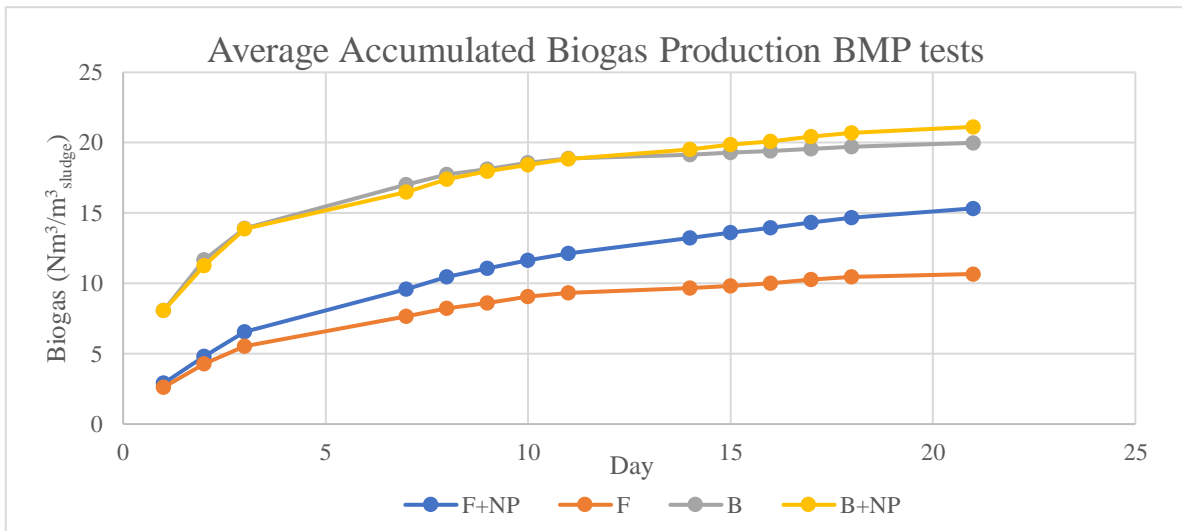


Figura-R 8: Producción Acumulada Normalizada por Tipo de Botella. Fuente: Propia.

Como se puede observar en la Figura anterior, la producción normalizada de biogás en los casos de codigestión fue muy superior al compararse con el fango (F) así como fango y nanopartículas (F+NP).

También se ha de mencionar que la adición de nanopartículas no mejoró la producción de biogás de manera significativa, lo que sugiere que sus efectos en reactores de codigestión estarán más relacionados con la estabilidad del proceso. Par realizar un mejor análisis, los datos de las botellas B y B+NP se compararon en la Figura-R 9

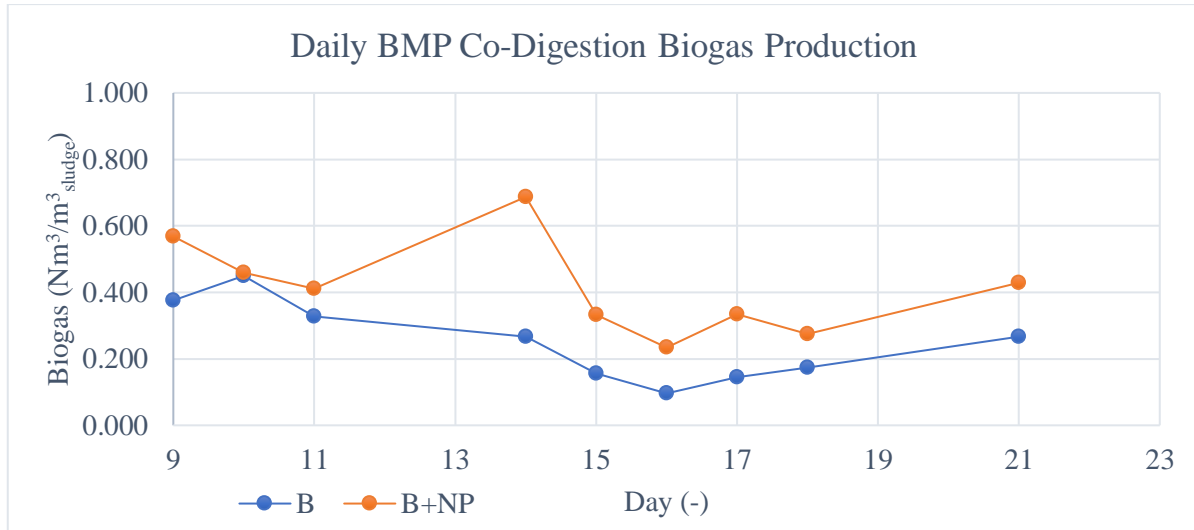


Figura-R 9: Detalle de la Producción diaria de Codigestión de Biogás. Fuente: Propia.

Al contrario que en la Figure-R 8, se aprecia que las nanopartículas sí mejoran ligeramente la producción de biogás después del día nueve. Además, ambas curvas siguen una tendencia similar, aunque la serie B+NP presenta un incremento en su producción en el día 14, lo que sugiere que las nanopartículas aceleran el proceso de DA.

Para determinar el efecto de las nanopartículas, tanto en producción media como en variabilidad de los datos, se realizó un test t de Student para determinar si ambos grupos de datos de producción diaria pudieran tener la misma media (asumiendo un intervalo de confianza del 95% y que ambas poblaciones procedían de distribuciones normales). La hipótesis nula usada era que ambas poblaciones de las que se obtuvieron las muestras presentaban la misma media

De manera similar, se realizó un test f de Snedecor para determinar si las varianzas poblaciones eran iguales (estas se estimaron a partir de las varianzas muestrales, corrigiendo el sesgo). En este test, la hipótesis nula fue la igualdad de varianza de ambas poblaciones, con una significación del 5%.

Todos los test estadísticos realizados se recogieron en la Tabla-R 2 y la Tabla-R 3, conteniendo los resultados de medias y varianzas, respectivamente. Si se aceptó la hipótesis nula, el resultado era de 0. En cambio, si esta era rechazada, el resultado mostrado es un 1. Se ha de señalar que los resultados del test de Snedecor son de la desviación típica

Modelado de Distribución Bi-normal de muestras B

Empleando los resultados antes mostrados, se modelo una distribución bi-normal para la producción media de biogás sin nanopartículas (muestras B). Este se construyó empleando la siguiente ecuación. Las estadísticas de la regresión se muestran a continuación en la Figura-R 10

$$\mu_B(t) \left[\frac{Nm^3}{m_{fangoo}^3} \right] = 4.1587 * e^{-0.192t} *; \quad t[\text{día}]$$

Number of observations: 14, Error degrees of freedom: 12
 Root Mean Squared Error: 0.579
 R-squared: 0.824, Adjusted R-Squared: 0.809
 F-statistic vs. constant model: 56.1, p-value = 7.33e-06

Figura-R 10: Estadísticas Media Modelo B. Fuente: Propia.

Asimismo, la desviación estándar se modeló con una distribución polinómica, cuya fórmula se muestra a continuación. Las estadísticas del modelo se muestran en la Figura-R 11

$$\sigma_B(t) \left[\frac{Nm^3}{m_{fango}^3} \right] = 1.2177 - 0.012 * t^2 + 4.7875 * 10^{-4} * t^3; \quad t[\text{día}]$$

Number of observations: 14, Error degrees of freedom: 11
 Root Mean Squared Error: 0.461
 R-squared: 0.479, Adjusted R-Squared: 0.384
 F-statistic vs. constant model: 5.06, p-value = 0.0277

Figura-R 11: Estadísticas Desviación Estándar Modelo B. Fuente: Propia.

Por último, tras obtener ambos modelos, se construyó la distribución bi-normal, que se muestra a continuación. Asimismo, la distribución se encuentra en la Figura-R 12.

$$n_{biogas} \left[\frac{Nm^3}{m_{fango}^3} \right] = N(4.1587 * e^{-0.192*t}, 1.2177 - 0.012 * t^2 + 4.7875 * 10^{-4} * t^3)$$

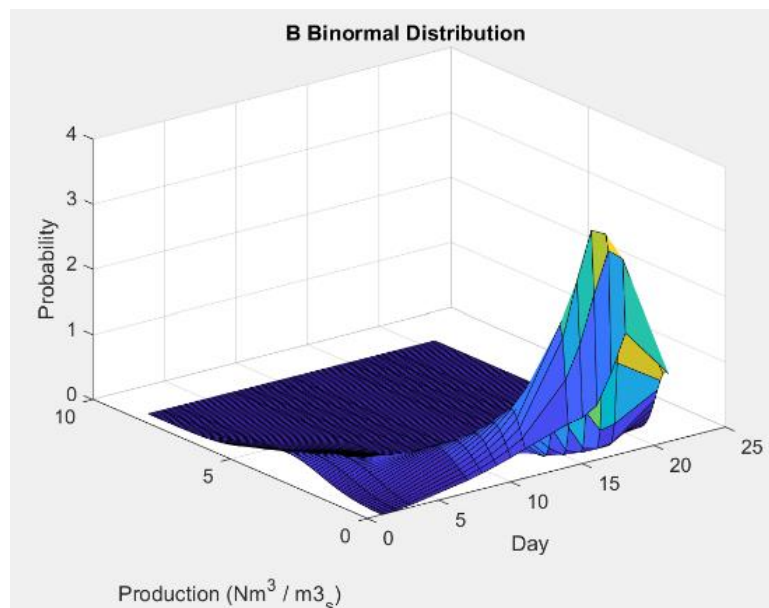


Figura-R 12: Campana Bi-normal Muestras B. Fuente: Propia.

Modelado de Distribución Bi-normal de muestras B-NP

De manera similar al anterior modelado, la distribución bi-normal se separó en media y desviación estándar. En este caso, se construyó el modelo para las muestras B-NP. El modelo de la media se muestra a continuación y sus estadísticas en la Figura-R 13.

$$\mu_{B-NP}(t) \left[\frac{Nm^3}{m_{fangos}^3} \right] = 4.1604 * e^{-0.1531*t}; \quad t[\text{día}]$$

Number of observations: 14, Error degrees of freedom: 12
 Root Mean Squared Error: 0.546
 R-squared: 0.769, Adjusted R-Squared: 0.75
 F-statistic vs. constant model: 40, p-value = 3.78e-05

Figura-R 13: Estadísticas Media Modelo B-NP. Fuente: Propia.

Asimismo, la desviación estándar se modeló con una distribución polinómica, cuya fórmula se muestra a continuación. Las estadísticas del modelo se muestran en la Figura-R 14.

$$\sigma_{B-NP}(t) \left[\frac{Nm^3}{m_{fangos}^3} \right] = 0.8495 - 0.0741 * t^2 + 2.8246 * 10^{-4} * t^3; \quad t[\text{día}]$$

Number of observations: 14, Error degrees of freedom: 11
 Root Mean Squared Error: 0.409
 R-squared: 0.355, Adjusted R-Squared: 0.237
 F-statistic vs. constant model: 3.02, p-value = 0.09

Figura-R 14: Estadísticas Desviación Estándar Modelo B-NP. Fuente: Propia.

Por último, tras obtener ambos modelos, se construyó la distribución bi-normal, que se muestra a continuación. Asimismo, la distribución se encuentra en la Figura-R 15.

$$n_{biogas} \left[\frac{Nm^3}{m_{fangos}^3} \right] = N(4.1604 * e^{-0.1531*t}, 0.8495 - 0.0741 * t^2 + 2.8246 * 10^{-4} * t^3)$$

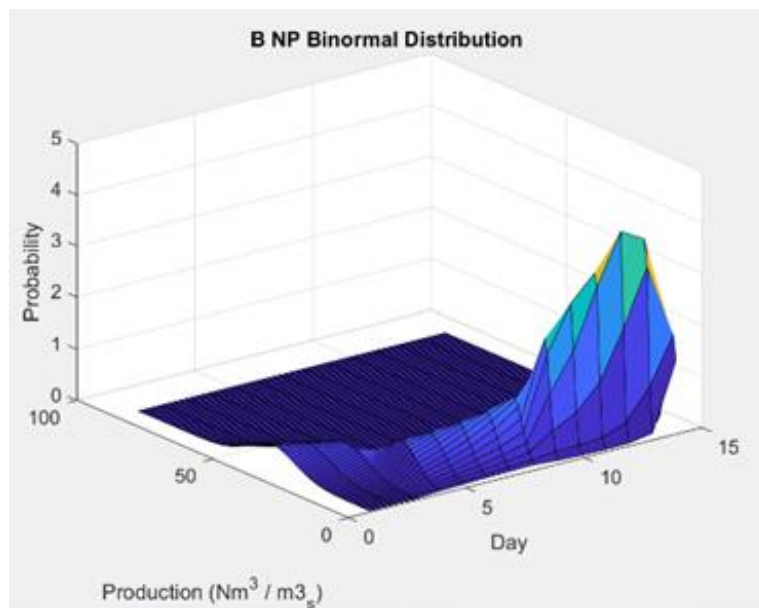


Figura-R 15: Campana Bi-normal Muestras B-NP. Fuente: Propia.

Resultados Reactor Discontinuo

El reactor discontinuo se comportó de una manera similar a las botellas BMP discontinuas, ya que este era una versión de mayor volumen, con sus respectivas modificaciones. Se realizó un análisis en detalle de la composición del biogás y el efecto de las nanopartículas, aunque no se pudieron realizar estudios estadísticos. El resultado más significativo es el referente al comportamiento del metano e hidrógeno, mostrado en la Figura-R 16.

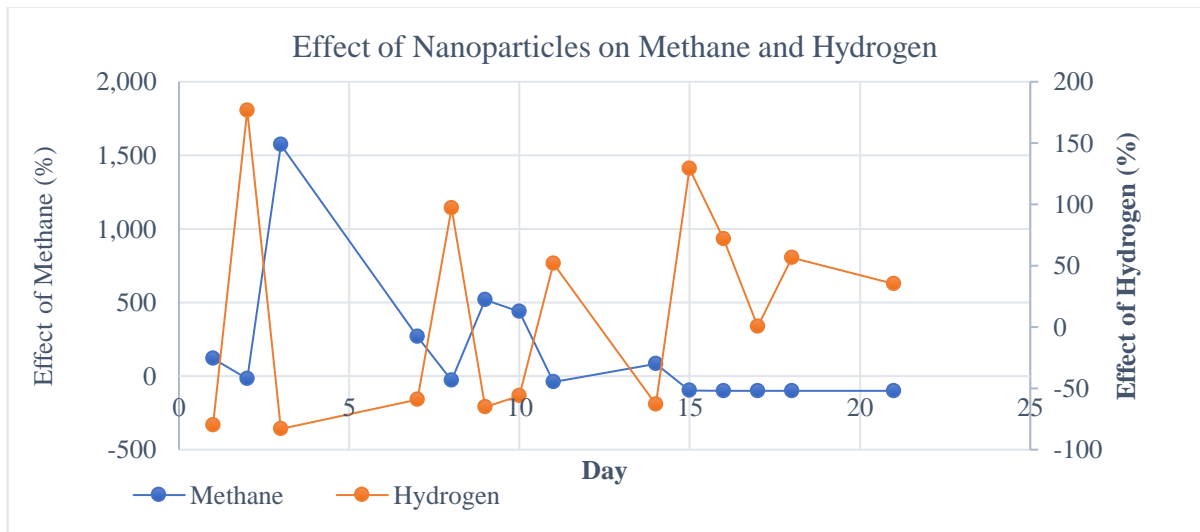


Figura-R 16: Efecto de las Nanopartículas en el CH_4 y el H_2 del Reactor Discontinuo. Fuente: Propia.

Resultados Reactor Semicontinuo

Los resultados más relevantes obtenidos del reactor discontinuo fueron aquellos referidos a la variación de la composición a medida que transcurría el ensayo. Estos resultados se recogieron en la Figura-R 17.

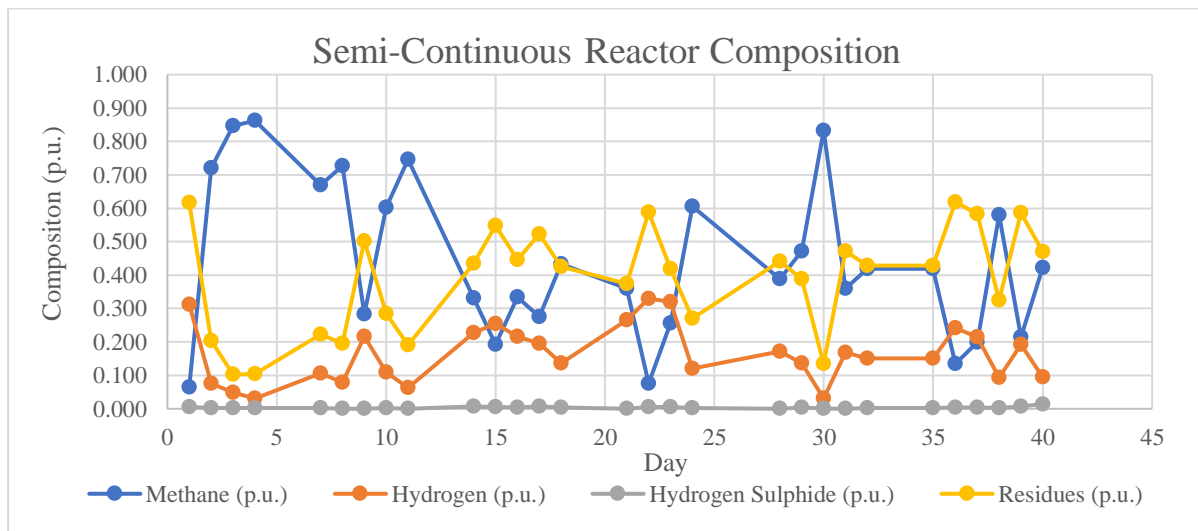


Figura-R 17: Composición del Biogás del Reactor Semicontinuo. Fuente: Propia.

Además, se realizaron ensayos para analizar los AGVs y la DQO. Estos mostraron un incremento en su concentración en los días finales del ensayo, lo que podría causar la inhibición de la metanogénesis si no se controlase.

Por último, se estimó la ratio C/N usando los datos empíricos obtenidos junto con los métodos identificados en el Estado del Arte, sin conseguirse resultados consistentes.

Escenarios de Aplicación

El escenario propuesto se basó en una demanda térmica obtenida de: (Linares Hurtado, 2021). Esta demanda se modeló a partir de una función exponencial. La curva se muestra en la Figura-R 18.

$$\dot{V} (MW_T) = 20 * e^{\frac{-H}{5000}}$$

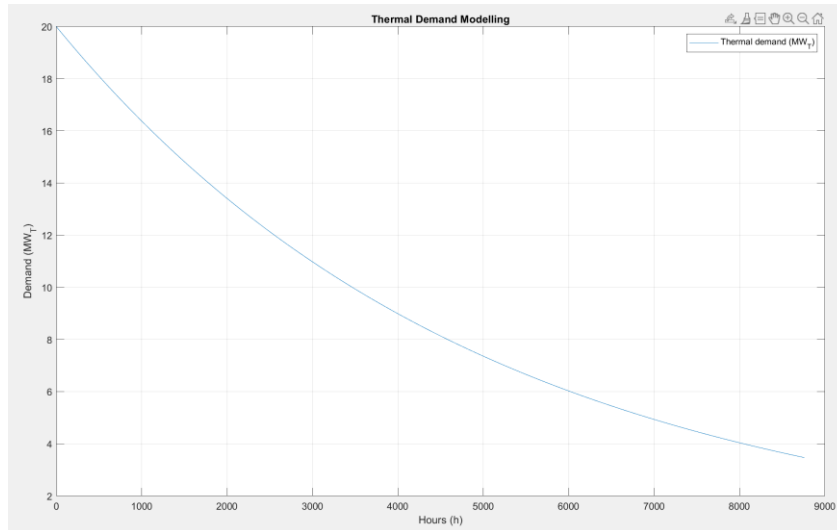


Figura-R 18: Modelado de Demanda Térmica. Fuente: Propia.

El reactor produce el biogás mediante la digestión del sustrato. En ambos escenarios propuestos, la producción se estimó a partir de un reactor sintético construido con los resultados BMP. En consecuencia, la producción diaria de biogás se recogió en la Tabla-R 4.

Tabla-R 4: Producción Diaria de Biogás, Reactor Sintético. Fuente: Propia.

Día (-)	n_{CH_4} (Nm ³ / día-m ³ _s)	n_{H_2} (Nm ³ / día-m ³ _s)	n_{H_2S} (Nm ³ / día-m ³ _s)	n_{RES} (Nm ³ / día-m ³ _s)	N_{tot} (Nm ³ / día-m ³ _s)
Total	1.3601	0.0004	0.0007	0.1214	1.4826

Este biogás fue utilizado en plantas de cogeneración para satisfacer la demanda térmica. Se consideraron dos posibles escenarios. En el primero se empleaba el biogás bruto como combustible, mientras que en el segundo este se limpiaba para obtener biometano. Los resultados de ambos casos se presentan en la Tabla-R 5. Por último, se determinaron las dimensiones del digestor necesarias para producir la cantidad necesaria. Para ello se asumió una base cilíndrica.

Tabla-R 5: Resultados Económicos de Escenarios de Aplicación. Fuente: Propia.

Parámetro	Uso Biogás Bruto	Uso Biometano
H* (h)	5015.31	5016.36
Pe (MW _e)	7.32	7.08
NVA (EUR)	29,880,973.60€	27,953,327.42€
Q _{biogas} (m ³ /h)	3014.3115	1732.5979
V _{sludge} (m ³)	90.4240	60.9337
V _{substrate} (m ³)	30.1413	20.3112
V _{supermatant} (m ³)	120.5653	81.2449
V _{total} (m ³)	241.1306	162.4897
V _{reactor} (m ³)	337.5829	227.4856
D (m)	4.8866	4.0014
h (m)	4.5	4.5

Respecto al tipo de planta modelado, también se calcularon el AEP y el REE. El combustible usado fue el biogás en ambos casos. Además, la planta se asume posterior a 2015 con un rendimiento eléctrico de referencia de 0,42. Se decidió emplear el calor producido para agua caliente, que presenta un rendimiento de referencia de 0,7. Los resultados se encuentran en la Tabla-R 6.

Tabla-R 6: AEP y REE de Escenarios de Aplicación. Fuente: Propia.

Parámetro	Uso Biometano	Uso Biogás Bruto
η_{ER} (-)	0.42	0.42
η_{VR} (-)	0.7	0.7
η_E (-)	0.427	0.426
η_V (-)	0.428	0.441
PES (-)	0.3858	0.3918
EEE (-)	1.0990	1.1514

Diseño Columna de Absorción Húmeda

A partir de los resultados de secciones anteriores, se diseñó una columna de absorción húmeda (scrubber), basada en (Pérez Sánchez, Pérez Sánchez, & Segura Silva, 2016). Los flujos nominales calculados se muestran en la Tabla-R 7. Asimismo, la Figura-R 19 continúe los flujos molares nominales. Los resultados principales del diseño se recogieron en la Tabla-R 8.

Tabla-R 7: Flujos Nominales Columna de Absorción Húmeda. Fuente: Propia.

Parámetro	Entrada gas (ig)	Salida gas (og)	Entrada agua (iw)	Salida agua (ow)
n_{CH_4} (kmol/h)	78.3482	78.3482	0	0
n_{CO_2} (kmol/h)	8.7054	0.4353	0	8.2701
n_{H_2O} (kmol/h)	0	0	146.2953	146.2953
n_{total} (kmol/h)	87.0536	78.7835	146.2953	154.5654
x or y_{CH_4} (-)	0.9	0.995	0	0
x or y_{CO_2} (-)	0.1	0.005	0	0.0065
x or y_{H_2O} (-)	0	0	1	0.9935

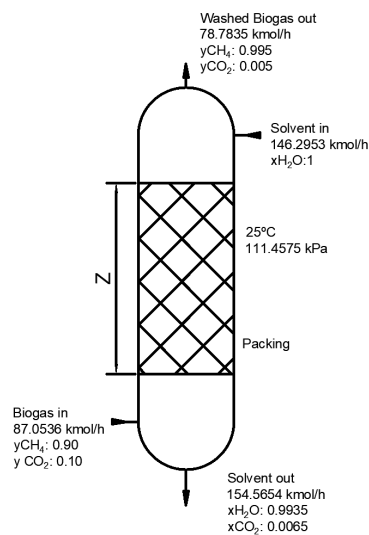


Figura-R 19: Flujos Nominales Columna de Absorción Húmeda. Fuente: Propia.

Tabla-R 8: Resultados Diseño Columna Húmeda. Fuente: Propia.

Parámetro	Valor
D (m)	0.6857
Z (m)	0.0288
$\Delta P/Z$ (Pa/m)	256.6111
K_{vG} (kmol/m ³ -s)	0.1144

Parámetro	Valor
K_{vL} (kmol/m ³ -s)	76.8123
K_m (kmol/m ³ -s)	0.1142
H_{iOG} (m)	0.5502
a_n (m ⁻¹)	111.7546

Conclusiones

Siguiendo una estructura similar al resto del resumen, esta sección presentará varias conclusiones de las distintas partes del proyecto, comenzando con las conclusiones experimentales y seguido de las obtenidas en los casos de aplicación presentados.

Conclusiones Experimentales

Conclusiones de los Ensayos BMP

La primera conclusión obtenida del estudio es la necesidad de realizar más ensayos para poder validar los hallazgos de este estudio. Los ensayos BMP mostraron resultados prometedores en lo referente a la producción de biogás y la calidad de este. Sin embargo, no se pudo asegurar estadísticamente que las nanopartículas afecten al proceso salvo a la desviación estándar del hidrógeno en fechas determinadas. Pese a esto, todas las muestras de ensayos BMP en las cuales se emplearon nanopartículas se consiguió una mejora en la producción de biogás y biometano frente a la monodigestión, llegando a picos de 23,2928 Nm³/grNP y 25,0605 Nm³/grNP, respectivamente.

Por último, la distribución bi-normal modelada con el biogás, metano e hidrógeno obtuvo modelos ajustados sin estructuras aparentes en los residuales y un R² aceptable para algunas regresiones. Sin embargo, modelados más refinados serían necesarios si se deseara hacer un estudio más detallado de los datos, junto con más grados de libertad obtenidos de realizar más ensayos BMP, idealmente más de cuarenta para asegurar que el teorema central del límite sea aplicable. Asimismo, aumentar los grados de libertad aseguraría un modelo más robusto en el cual se pudiesen identificar estructuras subyacentes. En estos casos se podría llegar a considerar el uso de técnicas avanzadas basadas en machine learning.

Conclusiones del Reactor Discontinuo

La conclusión más importante obtenida de los reactores de mayor tamaño es la necesidad de mejorar el diseño y construcción de estos, así como la tecnología de mezclado para prevenir la volatilización y descomposición de las nanopartículas, principalmente alrededor del eje de la pala. Este problema se intentó solucionar en ensayo posterior aplicando grasa de vacío en la parte externa del sello, aunque no se consiguió una mejora significativa.

Conclusiones del Reactor Semicontinuo

En primer lugar, se ha de mejorar la metodología de alimentación del reactor para facilitar esta actividad diaria. Se observó que la preparación de la mezcla agua-sustrato antes de su uso (1 o 2 días previos a su bombeo) crea una mezcla más homogénea mucho más fácil de inyectar en las botellas y succionar con la bomba peristáltica. También se debería realizar un estudio detallado de la semana final del ensayo (días 14 a 21) con un especial foco en el estudio de la concentración de los AGVs en la mezcla de codigestión. Asimismo, el contenido en nitrógeno sugiere la posibilidad de una modificación en la cinética del reactor, causando un aumento en su concentración, pudiendo afectar a la metanogénesis.

Conclusiones de las Aplicaciones

Pese a que el reactor sintético empleado como base para estos modelados no es realista, al obtenerse un biogás con una fracción molar del 90%, si que se ha demostrado la viabilidad del biogás como una fuente de energía viable para la cogeneración en casos de alta demanda térmica. En ambos casos, el VAN fue mayor de 27.500.000,00€, siendo el del biometano 27.953.327,42 € y el del escenario del biogás de 29.880.973,60€.

Referencias

- AENOR. (30 de june de 1999). UNE-EN ISO 11734:1999 Calidad del agua. Evaluación de la biodegradabilidad anaerobia "final" de los compuestos orgánicos con lodos en digestión. Método por medida de la producción de biogás. doi:EN ISO 11734:1998
- European Biogas Association. (2020). *BioLNG in Transport: Making Climate Neutrality a Reality*. Belgium: European Biogas Association. Obtenido de https://www.europeanbiogas.eu/wp-content/uploads/2020/11/BioLNG-in-Transport_Making-Climate-Neutrality-a-Reality.pdf
- European Commission. (29 de january de 2020). Commission Work Programme 2020. *The Official Journal of the European Union*, págs. 1-11. doi:COM*2020(37 final
- European Commission. (29 de november de 2021). *European Commission*. Obtenido de European Green Deal: https://ec.europa.eu/info/strategy/priorities-2019-2024/european-green-deal_es
- FCC. (28 de october de 2021). Valdemingomez biomethanisation plant field trip. Madrid, Madrid, Spain.
- Heidolph. (2022). *Hei-FLOW Ultimate 120 Multi*. (Heidolph) Recuperado el 13 de july de 2022, de <https://heidolph-instruments.com/en/products/Peristaltic-Pumps/Hei-FLOW-Ultimate-120-Multi~p1007>
- Linares Hurtado, J. I. (2021). Tema 5: Cogeneración, renovables y ciclos de potencia avanzados. Ejercicios de clase. En J. I. Linares Hurtado, *Ingeniería Energética* (pág. 5.2.14). Madrid: Universidad Pontificia Comillas-ICAI.
- Ministero para la Transición Ecológica y el Reto Demográfico. (2022). *Hoja de Ruta del Biogás*. Madrid: Ministerio para la Transición Ecológica y el Reto Demográfico. Obtenido de <https://drive.google.com/file/d/1Uw7iaML1Evh0e0nI91ZvNFWDCcwjprlN/view>
- Morales Polo, C. (2019). *Co-Digestión anaerobia y pretratamiento de residuos agroalimentarios con fangos UASB de depuradora*. Madrid: Universidad Pontificia Comillas-ICAI.
- Pacala, S., & Socolow, S. (13 de august de 2004). Stabilization Wedges: Solving the Climate Problem for the Next 50 Years with Current Technologies. *Science*, 968-972. doi:10.1126/science.1100103
- Pérez Sánchez, A., Pérez Sánchez, E. J., & Segura Silva, R. (12 de septiembre de 2016). Design of a packed-bed absorption column considering four packing types and applying Matlab. *Nexo Revista Científica*, 29(2), 83-. doi:<https://www.camjol.info/index.php/NEXO/article/view/4577>
- Rannard, G. (12 de november de 2021). COP 26: Coal compromise as leaders near climate deal. London, Greater London, United Kingdom. Obtenido de <https://www.bbc.com/news/science-environment-59221790>
- Romero Mora, J. C., & Tatay Nieto, J. (2020). What is the circular economy. En J. C. Romero Mora, & J. Tatay Nieto, *Sustainable Development Agenda- Apuntes de Clase* (págs. 5.1-5.53). Madrid: Universidad Pontificia Comillas-ICAI.
- Tran, T. (2017). *Standard Methods for the Examination of Water and Wastewater, 23rd edition*. Washington, DC.: American Public Health Association.
- United Nations. (29 de november de 2021). *UN Climate Change Conference UK 2021*. Obtenido de COP26: <https://ukcop26.org/>

ANAEROBIC CO-DIGESTION STUDY AND CHARACTERISATION OF DIFFERENT DIGESTERS TO MAXIMIZE BIOGAS GENERATION

Author: Victoria Rodríguez, Javier

Directors: María del Mar Cledera Castro and Carlos Morales Polo

Collaborating Institution: ICAI- Universidad Pontificia Comillas

PROJECT SUMMARY

Introduction

The main problem faced by our society today is the named Ecological Transition to a greener economy by reducing the impact humans have on the planet because of anthropogenic climate change. This part of the “Twin Transitions” (European Commission, 2020) is considered by the EU and its member states a pillar to define the direction in which Europe must lead the world, which resulted in the creation and approval of the European Green Deal (European Commission, 2021) to provide a response to ever increasing climatic anomalies & disasters caused by climate change.

To permit and direct the required effort and investment, both of public and private nature, the Climate Delegated Act was passed to direct and align the various key players and technologies. Among this key technologies, bioenergy, and particularly biogas and biomethane, were identified as “low-carbon gases” meant to replace natural gas, produced through anaerobic digestion (AD), in the energy and industrial sectors coupled with applications in heavy-duty transport (European Biogas Association, 2020).

The recent COP 26 held in Glasgow (United Nations, 2021) further emphasized the need for the global temperature increase to be limited to 1.5°C above pre-industrial levels. Therefore, global leaders reached a compromise to remove coal from their electrical generation mixes (Rannard, 2021), widely considered to be the most polluting of fossil fuels. Furthermore, the EU, the US as well as a hundred countries announced their intentions to reduce their methane emissions, particularly from natural gas leaks. Methane emissions have long been considered one of the 8 stabilization wedges required to prevent an increase in global temperatures (Pacala & Socolow, 2004).

On a national scale, the Ministry for Ecological Transition (MITECO) identified biogas as a new renewable energy source with the capability of preventing up to 2.1 million tonnes CO₂-eq. per year according to the Biogas National Plan (Ministero para la Transición Ecológica y el Reto Demográfico, 2022). The Plan highlights the minimal use of AD reactors, which produced 2.74 TWh of energy in 2020. Moreover, there are only five biomethane plants in the country, with the largest located in Valdemingomez, Madrid (FCC, 2021).

The last aspect of the context in which this research occurred pertains to the goal of achieving a circular economy in which waste is minimised and resources used to their full potential, extracting all the value contained within them before final disposal (Romero Mora & Tatay Nieto, 2020). AD proposes the transformation of sludge from a residue into a co-product to be used not only for energy generation, but also the upcycling of the obtained digestate as fertilizer. By considering the full life cycle of the sludge, eco-design of waste treatment processes can be expanded until a full cradle-to-cradle approach can be implemented. This advancements would reduce the energy intensity of water treatment facilities or similar industrial processes which require wastewater treatment plants to comply with regulations.

Methodology

All experiments had a common characteristic, their composition, as such, the calculations made to obtain the volumes required by each vessel are as shown below in Table-R 1 along with the formulae. In keeping with previous research, the sludge-feed proportion was set at a 3:1 ratio . Also, a 50% humidity was required (FCC, 2021), which set another constraint on the vessel composition. To create the substrate mixture, the pumpkin used as substrate.

$$V_{water}[l] = 0.5 * V_{Total}[ml]$$

$$V_{sludge}[l] = 0.375 * V_{Total}[ml]$$

$$V_{substrate}[l] = 0.125 * V_{Total}[ml]$$

Table-R 1: Co-Digestion Mixture Proportion. Source: Own

Variable	BMP	Reactor
V _{Total} (ml)	300.0	2000.0
V _{water} (ml)	150.0	1000.0
V _{sludge} (ml)	112.5	750.0
V _{substrate} (ml)	37.5	125.0

BMP Design & Set-Up

The first set of tests were BMP tests. These were performed as per the guidelines set in the norm ISO 11734:1999 (AENOR, 1999), employed in previous research which this project was based on. This Norm required the use of sealed 1-litre bottles in which 300ml of an AD- mixture was sampled for 21 days, collecting daily pressure readings. The bottles were closed using a septum and silicone paste.

Moreover, to replicate semi-continuous testing at a bottle scale, 2 BMP bottles were modified utilizing a cap with valves: the sampling port and the feeding port. Lastly, an incubator was used to agitate & maintain at a constant temperature up to nine bottles, limiting batches to said number. To maintain the mesophilic conditions, the target was set at 38.0°C. A batch BMP bottles is shown in Figure-R 1; an example of a semi-continuous bottle in Figure-R 2 and lastly the design diagram in Figure-R 3.



Figure-R 1: BMP Batch Bottle. Source: Own.



Figure-R 2: Semi-Continuous BMP Bottle. Source: Own.

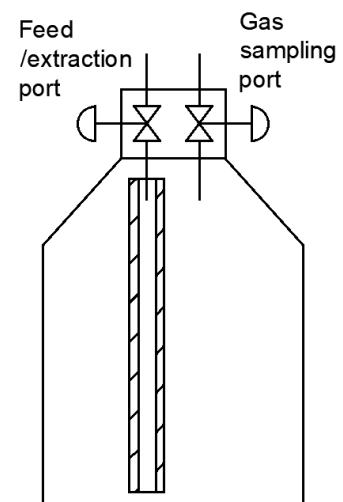


Figure-R 3: Semi-Continuous Bottle Diagram. Source: Own.

Batch Reactors Design & Set Up

The second set of experiments were performed in 2-litre batch reactors, which represent a larger version of the standard BMP tests. The larger vessel also required some changes in the design. The first and most relevant was that of temperature control and agitation. In this case external thermostats were employed to control temperature, requiring the use of a temperature probe inside the vessel.

Additional changes required were the use of external agitation, achieved by utilising a stirring rod with a welded paddle attachments to stir the digester mixture, moved by the Scharlau MiniReactor motor.

In addition, to connect the MilliGascounters, a three-way valve system was developed to permit biogas sampling and direct production measurement from the same outlet. In this case, the valve would be set to direct the flow to the counters, switching the active outlet to retrieve samples. The final reactor set-up can be seen in Figure-R 4. Also, all the components used are pictured in Figure-R 5.



Figure-R 4: Final Reactor Set-Up. Source: Own.

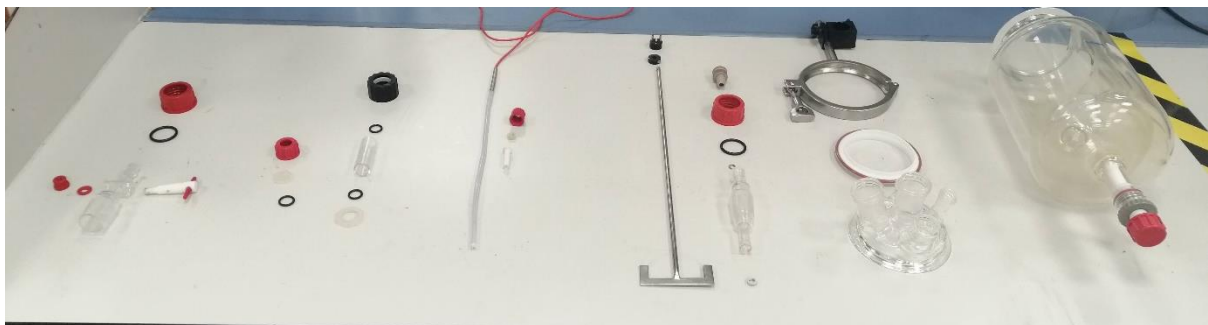


Figure-R 5: Reactor Components. Source: Own.

Semi-Continuous Reactor Design & Set Up

The last experiment to be performed was that of the semi-continuous reactor. Similar to the batch reactor, this test had its equivalent bottle, in this case the semi-continuous bottles previously designed.

The scaled reactor presented its unique characteristics and design challenges, primarily to accommodate the larger volume of AD-mixture as well as the support equipment, which was identical to that of the batch reactor with one exception. The previously unused port was replaced by a septum modified in a

similar way to that of the pH probe. This modified port was used to fit the feeding hose which extended from the substrate reservoir to the vessel through the Heidolph Hei-FLOW Precision 01 (Heidolph, 2022) peristaltic pump, which provided the hermetic seal. Lastly, to achieve the semi-continuous behaviour and control the digestate outlet, the reactor's bottom port received a spheric valve to extract the daily amount required. The design diagram appears in Figure-R 6.

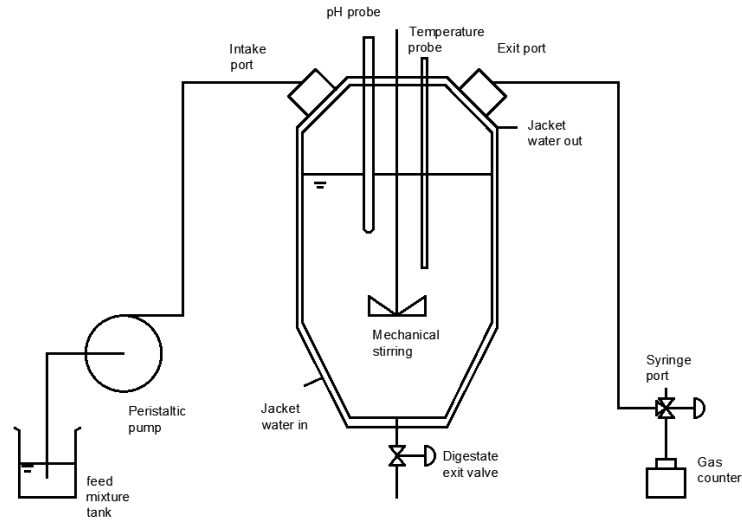


Figure-R 6: Semi-Continuous Reactor Design. Source: Own.

BMP Batch Bottles Pressure & Biogas Sampling

As previously stated, BMP tests are performed on sealed 1-litre bottles, allowing the biogas to build up inside them for collection and analysis. These bottles were sampled daily to indirectly measure the moles of biogas produced through the ideal gas law. In addition, the temperature inside the bottles was also controlled by the Ivymen orbital shaker incubator, which was set at 38°C, as previously explained. The following formula was used to obtain the moles of biogas produced:

$$[mol] = 0,041 * P[bar]$$

Reactor Biogas Production & Sampling

Similarly, to the bottles previously described, the measurement of biogas produced and the sampling of said gas was performed daily. The reactor design allowed for the direct measurement of biogas production through the MilliGascounters.

Volatile Fatty Acids Test

The first test performed on the supernatant from the extracted samples was a measurement of the alkalinity within the reactor. This test was a variation of (Tran, 2017). The first stage in the titration employed HCl to reduce the pH to 5.75 as per the norm. The volume and final pH were also recorded. The next step in the process was the final titration utilising the H₂SO₄ until the target of 4.3 was reached. These were V₁ and V₂, respectively. These measurements were then used to determine Partial (AP), Intermediate (AI) and Total Alkalinity (AT), using AI to measure VFA:

$$AP \left[\frac{mgCaCO_3}{l} \right] = \frac{V_{HCl} * N_{HCl} * 5000}{V_{sample}}$$

$$AI \left[\frac{mgCaCO_3}{l} \right] = \frac{V_{H_2SO_4} * N_{H_2SO_4} * 5000}{V_{sample}}$$

$$AT \left[\frac{mg_{CaCO_3}}{l} \right] = Ap + AI = \frac{(V_{H_2SO_4} * N_{H_2SO_4} + V_{HCl} * N_{HCl}) * 5000}{V_{sample}}$$

Gas Chromatography

Moreover, the daily extracted gas samples were analysed to determine the composition of the biogas produced. The method used within the chromatographer was designed in for this purpose. The temperature and flow graphs which determine the method are shown in Figure-R 7.

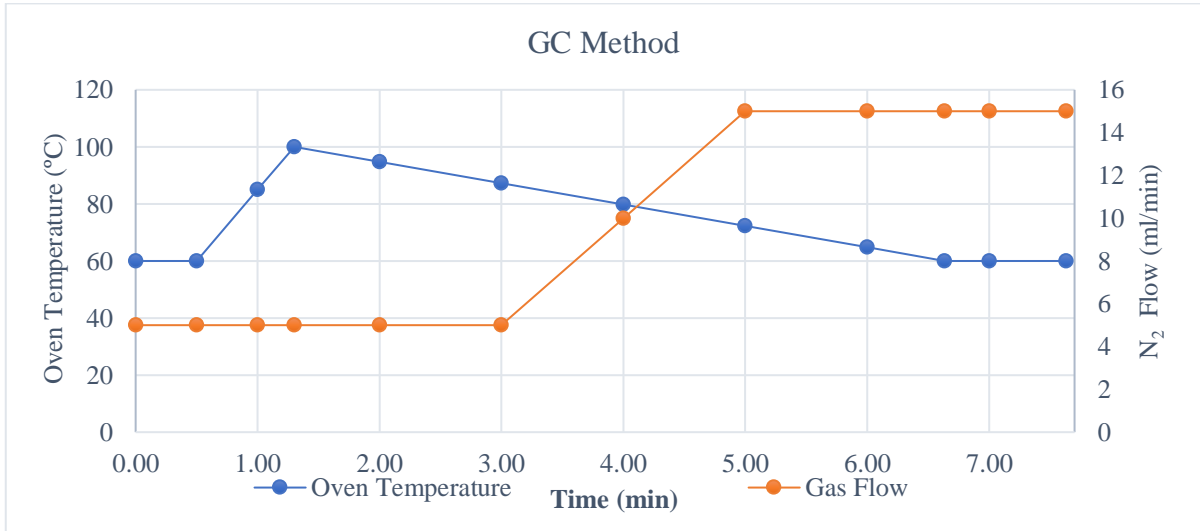


Figure-R 7: Gas Chromatography Method. Source: Own.

Results

BMP Bottle Results

Once data was collected, the average normalised production was calculated for each bottle type used. It must be noted that semi-continuous bottles were not included in the analysis because of their failure caused by the inhibition of the AD process on day 4. The accumulated production was compiled in Figure-R 8

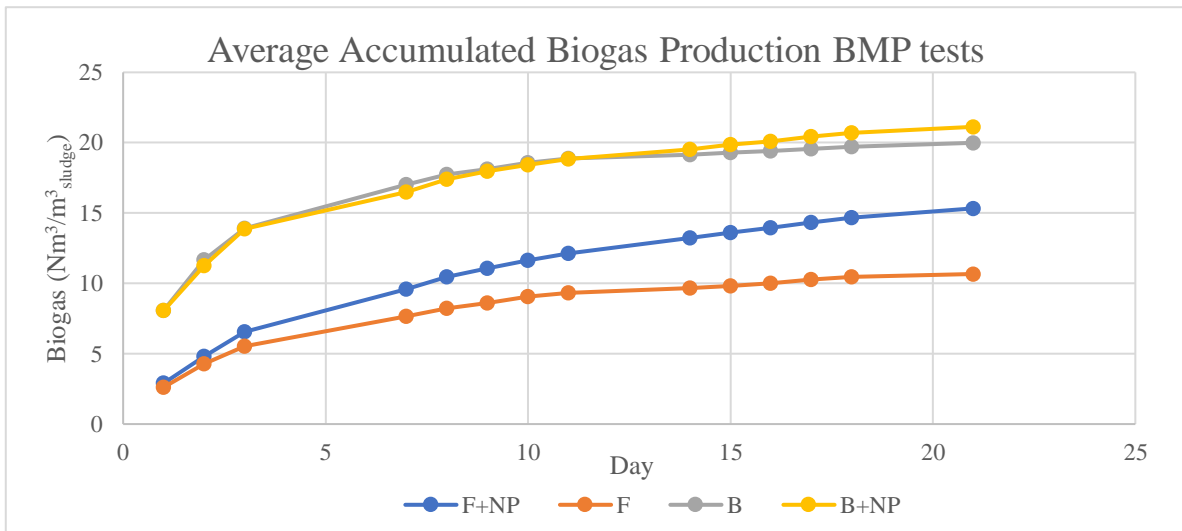


Figure-R 8: Accumulated Production by Bottle Type. Source: Own.

As evidenced in the above Figure, normalised biogas production was far superior in co-digestion tests when compared to the sludge (F) and sludge & nanoparticle (F+NP) baselines.

It must also be mentioned that the addition of nanoparticles did not increase biogas production significantly, which suggests that the main benefit of adding these into AD co-digestion reactors would be added process stability. To obtain a better analysis, B and B+NP data series were compared in Figure-R 9.

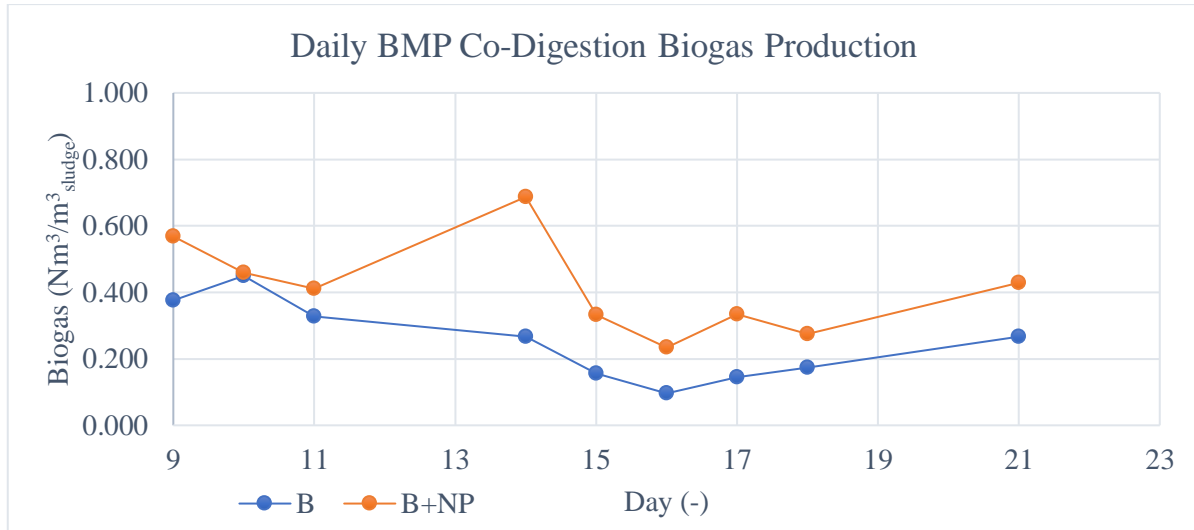


Figure-R 9: Detailed View of Daily Co-Digestion Biogas Production. Source: Own.

As opposed to Figure-R 8, it is apparent in the above graph that the nanoparticles do improve production by a small margin after day nine. Also, both curves follow a similar trend during the final days, although B+NP presents a sudden increase in production which could indicate that said nanoparticles accelerate the AD process.

To determine the effects of nanoparticles, both in the average production and in the variability of said data points, a Student's t-test was used to determine if both daily sample groups could have the same mean (assuming a confidence of 95% and that both populations follow a normal distributions). The null hypothesis used was that both means were equal.

Similarly, Snedecor's f-test was used to determine if the population's variance were equal (estimated using the sample variance corrected for skewing). In this test, the null hypothesis was that the variance of both populations was the same. Lastly, the significance was set at 5%.

Due to the various tests performed, the results for were combined into Table-R 2 and Table-R 3, containing t-tests and f-test, respectively. If the null hypothesis were accepted, the displayed result was zero, if it could not be accepted, the result shown was one. It must also be added that the results displayed for the f-test are the standard deviation.

B Binomial Distribution Modelling

Utilizing the above results, a binomial distribution for mean biogas without nanoparticles (sample B) was constructed. The resulting model is shown in the following equation and the statistics for its regression are shown in Figure-R 10.

$$\mu_B(t) \left[\frac{Nm^3}{m^3_{Sludge}} \right] = 4.1587 * e^{-0.192t} *; \quad t[day]$$

Number of observations: 14, Error degrees of freedom: 12
 Root Mean Squared Error: 0.579
 R-squared: 0.824, Adjusted R-Squared: 0.809
 F-statistic vs. constant model: 56.1, p-value = 7.33e-06

Figure-R 10: B-model Mean Modelling Statistics. Source: Own.

In addition, a polynomial model was fitted to the standard deviation, whose resulting formula is shown below. The statistics for said regression are shown in Figure-R 11.

$$\sigma_B(t) \left[\frac{Nm^3}{m^3_{Sludge}} \right] = 1.2177 - 0.012 * t^2 + 4.7875 * 10^{-4} * t^3; \quad t[day]$$

Number of observations: 14, Error degrees of freedom: 11
 Root Mean Squared Error: 0.461
 R-squared: 0.479, Adjusted R-Squared: 0.384
 F-statistic vs. constant model: 5.06, p-value = 0.0277

Figure-R 11: B-model Standard Deviation Modelling Statistics. Source: Own.

Once the mean and standard deviation were analysed, the binormal distribution was constructed, whose formula is shown below. In addition, the final distribution is shown in Figure-R 12.

$$n_{biogas} \left[\frac{Nm^3}{m^3_{Sludge}} \right] = N(4.1587 * e^{-0.192*t}, 1.2177 - 0.012 * t^2 + 4.7875 * 10^{-4} * t^3)$$

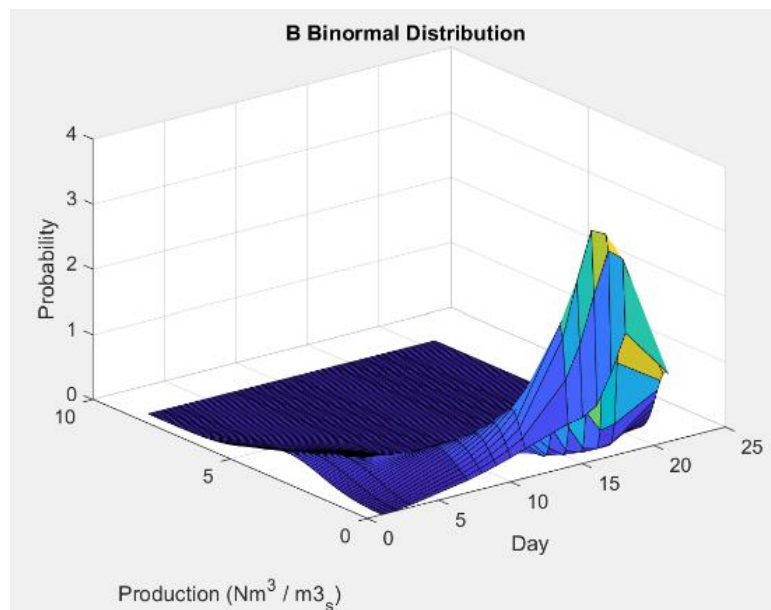


Figure-R 12: B-model Binominal Distribution. Source: Own.

B-NP Bottles Binomial Distribution Modelling

Similar to the previous modelling, the binormal distribution was divided into the mean and standard deviation modelling. In this case, the obtained model for samples B-NP is provided below, and its statistics were collected into Figure-R 13.

$$\mu_{B-NP}(t) \left[\frac{Nm^3}{m_{Sludge}^3} \right] = 4.1604 * e^{-0.1531*t}; \quad t[day]$$

Number of observations: 14, Error degrees of freedom: 12
 Root Mean Squared Error: 0.546
 R-squared: 0.769, Adjusted R-Squared: 0.75
 F-statistic vs. constant model: 40, p-value = 3.78e-05

Figure-R 13: B-NP-model Mean Modelling Statistics. Source: Own.

After modelling the mean for this sample, the standard deviation was also estimated employing the polynomial regression model. The resulting formula is shown below and the statistics in Figure-R 14.

$$\sigma_{B-NP}(t) \left[\frac{Nm^3}{m_{Sludge}^3} \right] = 0.8495 - 0.0741 * t^2 + 2.8246 * 10^{-4} * t^3; \quad t[day]$$

Number of observations: 14, Error degrees of freedom: 11
 Root Mean Squared Error: 0.409
 R-squared: 0.355, Adjusted R-Squared: 0.237
 F-statistic vs. constant model: 3.02, p-value = 0.09

Figure-R 14: B-NP-model Standard Deviation Modelling Statistics. Source: Own.

Once the mean and standard deviation were analysed, the binormal distribution was constructed, whose formula is shown below. In addition, the final distribution is shown in Figure-R 15

$$n_{biogas} \left[\frac{Nm^3}{m_{Sludge}^3} \right] = N(4.1604 * e^{-0.1531*t}, 0.8495 - 0.0741 * t^2 + 2.8246 * 10^{-4} * t^3)$$

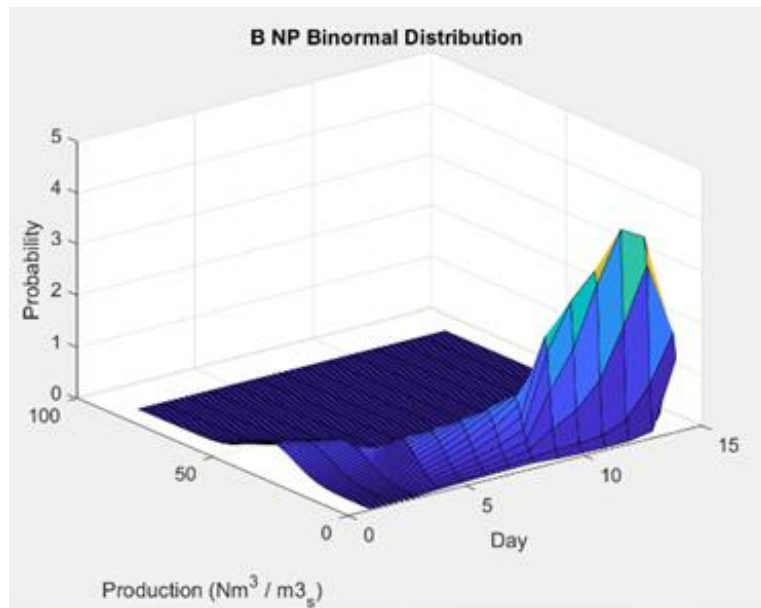


Figure-R 15: B-NP-model Binominal Distribution. Source: Own.

Batch Reactor Results

The batch reactor behaved similar to the Batch BMP bottles as it was a scaled-up version of the same test, with the aforementioned design change and requirements. An in depth analysis of the composition and the effect of nanoparticles was performed, although no statistical tests could be used. The most significant result is that of the methane and hydrogen gas behaviour, which is displayed in Figure-R 16.

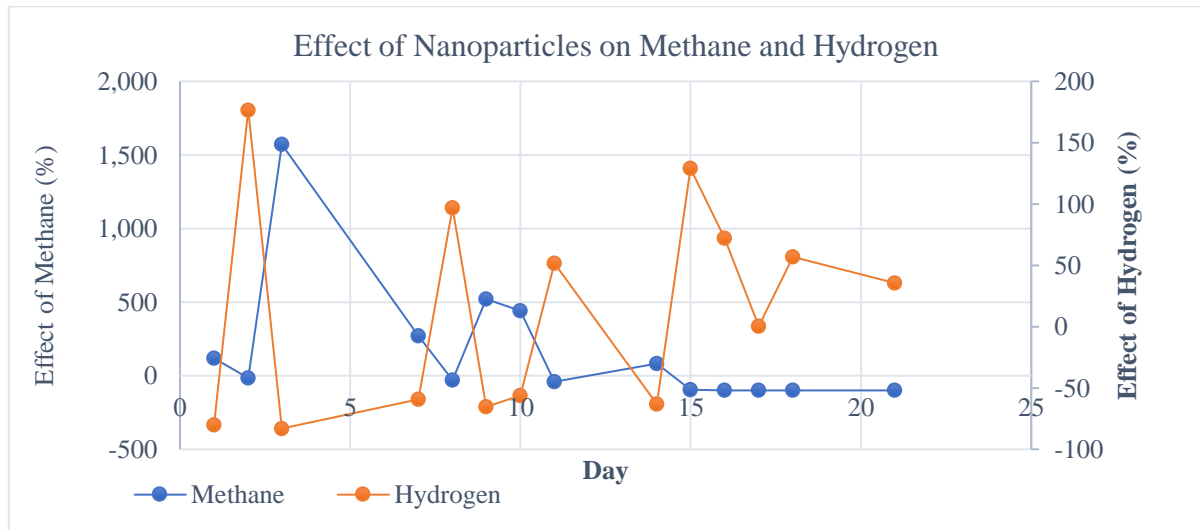


Figure-R 16: Effect of Nanoparticles on Methane and Hydrogen in Batch Reactor. Source: Own.

Semi-Continuous Reactor Results

The most relevant results obtained from the semi-continuous reactor were those pertaining to composition variation through time, which were collected into Figure-R 17.

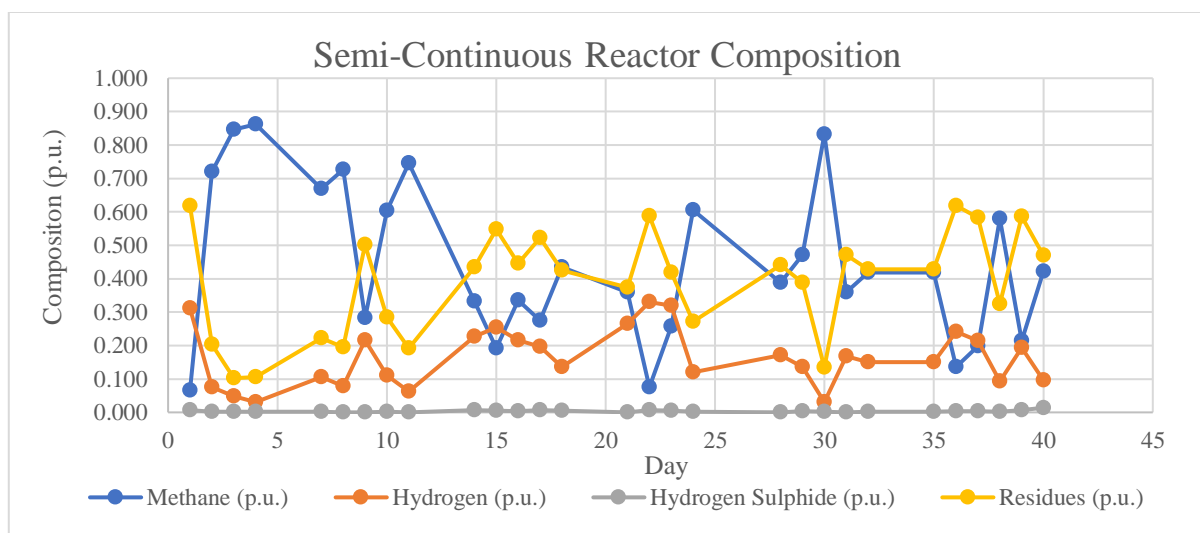


Figure-R 17: Semi-Continuous Reactor Composition. Source: Own.

In addition, other tests pertaining to VFA, and COD were performed. These showed an increase in concentration towards the final days of the experiment, which could inhibit methanogenesis if left unchecked.

Lastly, the C/N ratio was estimated using empiric data as well as methods identified in the State of the Art, but no consistent results were obtained.

Application Scenarios

The proposed scenario solved in this section was based on a heat demand from (Linares Hurtado, 2021). This demand was modelled using with the following formula & it is displayed in Figure-R 18.

$$\dot{V} (MW_T) = 20 * e^{\frac{-H}{5000}}$$

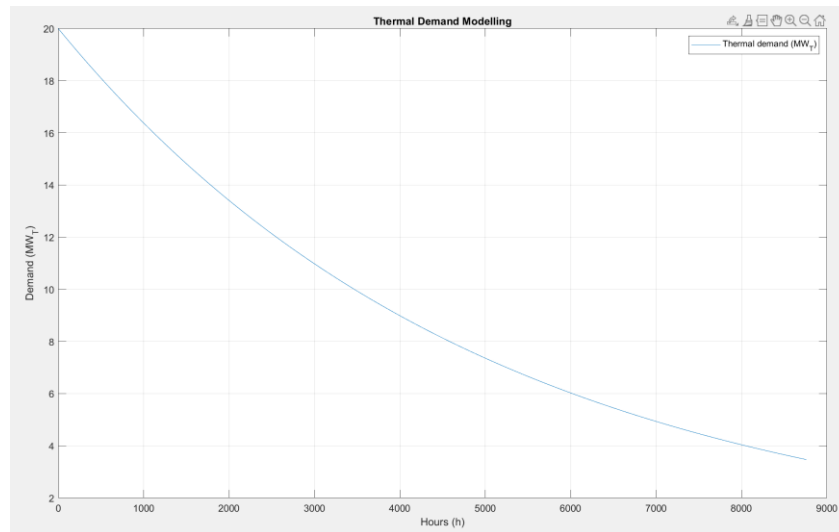


Figure-R 18: Annual Thermal Demand Modelling. Source: Own.

The reactor used to digest the substrate and produce the biogas used in each scenario was modelled through a synthetic reactor built from the BMP results, which were the most complete result set obtained. The daily production was recorded in Table-R 4.

Table-R 4: Synthetic Reactor Daily Production. Source: Own.

Day (-)	n_{CH_4} (Nm ³ / day-m ³ _s)	n_{H_2} (Nm ³ / day-m ³ _s)	n_{H_2S} (Nm ³ / day-m ³ _s)	n_{RES} (Nm ³ / day-m ³ _s)	N_{tot} (Nm ³ / day-m ³ _s)
Total	1.3601	0.0004	0.0007	0.1214	1.4826

This was then used to model the co-generation plant (CHT) required to satisfy demand. Two scenarios were considered. The first was based on direct biogas combustion, while the second scenario considered the upgrading of the produced biogas into biomethane. The results for each scenario were compounded into Table-R 5. Lastly, digester dimensions were calculated based on the biogas production and demand. A cylindrical reactor vessel was used as the basis.

Table-R 5: Application Scenarios Economic Results. Source: Own.

Parameter	Direct Biogas Use	Upgrading to Biomethane
H* (h)	5015.31	5016.36
Pe (MW _e)	7.32	7.08
NVA (EUR)	29,880,973.60€	27,953,327.42€
Q _{biogas} (m ³ /h)	3014.3115	1732.5979
V _{sludge} (m ³)	90.4240	60.9337
V _{substrate} (m ³)	30.1413	20.3112
V _{supernatant} (m ³)	120.5653	81.2449
V _{total} (m ³)	241.1306	162.4897
V _{reactor} (m ³)	337.5829	227.4856
D (m)	4.8866	4.0014
h (m)	4.5	4.5

Regarding the type of plant designed, the PES and EEE were also calculated. The fuel used is biogas. In addition, the plant was built after 2015, and therefore the reference electrical value is 0.42. The heat will be used to produce hot water, which requires the higher reference value at 0.7. The calculations are shown below in Table-R 6.

Table-R 6: PES & EEE for Application Scenarios. Source: Own.

Parameter	Direct Biogas Use	Upgrading to Biomethane
η_{ER} (-)	0.42	0.42
η_{VR} (-)	0.7	0.7
η_E (-)	0.427	0.426
η_V (-)	0.428	0.441
PES (-)	0.3858	0.3918
EEE (-)	1.0990	1.1514

Wet Absorption Column Design

Utilizing the results obtained in the study, a wet absorption column was designed based on (Pérez Sánchez, Pérez Sánchez, & Segura Silva, 2016). The nominal flows were calculated and are displayed in Table-R 7 below. A diagram of the nominal molar flow rates is provided in Figure-R 19. The main design parameters obtained are displayed in Table-R 8.

Table-R 7: Wet absorption Column Nominal Flows. Source: Own.

Parameter	Gas in (ig)	Gas out (og)	Water in (iw)	Water out (ow)
n_{CH_4} (kmol/h)	78.3482	78.3482	0	0
n_{CO_2} (kmol/h)	8.7054	0.4353	0	8.2701
n_{H_2O} (kmol/h)	0	0	146.2953	146.2953
n_{total} (kmol/h)	87.0536	78.7835	146.2953	154.5654
x or y $_{CH_4}$ (-)	0.9	0.995	0	0
x or y $_{CO_2}$ (-)	0.1	0.005	0	0.0065
x or y $_{H_2O}$ (-)	0	0	1	0.9935

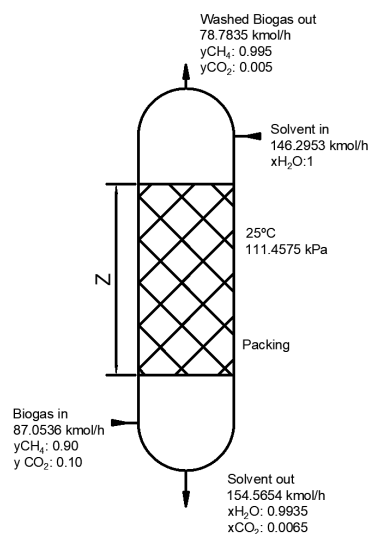


Figure-R 19: Wet absorption Column Nominal Flows. Source: Own.

Table-R 8: Wet Absorption Column Results. Source: Own.

Parameter	Value	Parameter	Value
D (m)	0.6857	K_{vL} (kmol/m ³ -s)	76.8123
Z (m)	0.0288	K_m (kmol/m ³ -s)	0.1142
$\Delta P/Z$ (Pa/m)	256.6111	H_{iOG} (m)	0.5502
K_{vG} (kmol/m ³ -s)	0.1144	a_h (m ⁻¹)	111.7546

Conclusions

Following a similar structure to that of the rest of the summary, this section will present the various conclusions from the various parts of the study, commencing with the experiment conclusions & followed by the conclusions drawn from the three applications previously presented.

Experiment Conclusions

BMP Test Conclusions

The first conclusion drawn from the study is that further experimental runs are required to validate the findings of this study. The various BMP tests displayed promising results in biogas production and quality. However, this study could not statistically determine that the C-Fe nanoparticles affect the daily production's mean or variance, except during certain dates and periods regarding the standard deviation of hydrogen. Despite the lack of statistical conclusions, all BMP samples in which the nanoparticles were used did achieve an increase biogas and biomethane production over the simple co-digestion samples, registering a peak of 23,2928 Nm³/grNP and 25,0605 Nm³/grNP, respectively.

Lastly, the binormal distribution modelling performed on the biogas, methane and hydrogen did provide well fitted models with no apparent residual structure and an acceptable R² value for certain models. However, a finely tuned model would require further analysis of the data as well as more degrees of freedom, obtained from performing additional BMP experiments to obtain over forty mean data points and thus ensure that the central limit theorem is fully applicable. Moreover, increasing the degrees of freedom will ensure a more robust model and permit the identification of underlying data structures. The use of advanced analysis techniques based on machine learning should also be considered.

Batch Reactor Conclusions

The most important conclusion obtained from the larger vessels was the need to further improve the set up and sealing techniques, as well as the stirring to prevent the volatilization and deposition of the nanoparticles, particularly on the stirring rod seal. This issue was addressed in a posterior run, which was not part of this project, by applying vacuum grease around the exterior side of the seal, although no clear improvement was made.

Semi-Continuous Reactor Conclusion

Firstly, a new and refined sample feeding methodology is recommended to facilitate this daily procedure. It was observed that by preparing the water-pumpkin feed slurry in advance (1 to 2 days), the resulting mash was easier to inject into the bottle and suctioned by the peristaltic pump used for the reactor. A detailed review of the final week. Also well, the nitrogen content suggests the possibility of a change in reactor dynamics as a result of the addition of the Fe-C nanoparticles, resulting in the build-up of these compounds, possibly affecting methanogenesis negatively.

Application Conclusions

Although the synthetic reactor utilised as the base for the modelling was no realistic, obtaining a biogas with a 90% methane molar fraction; the use of the biogas in cogeneration did prove to be a viable solution to satisfy a large thermal demand. In both cases the NVA was larger than EUR 27.5 Mn, with the biomethane reaching 27.953.327,42 € and the biogas scenario obtaining 29.880.973,60€.

References

- AENOR. (30 de june de 1999). UNE-EN ISO 11734:1999 Calidad del agua. Evaluación de la biodegradabilidad anaerobia "final" de los compuestos orgánicos con lodos en digestión. Método por medida de la producción de biogás. doi:EN ISO 11734:1998
- European Biogas Association. (2020). *BioLNG in Transport: Making Climate Neutrality a Reality*. Belgium: European Biogas Association. Obtenido de https://www.europeanbiogas.eu/wp-content/uploads/2020/11/BioLNG-in-Transport_Making-Climate-Neutrality-a-Reality.pdf
- European Commission. (29 de january de 2020). Commission Work Programme 2020. *The Official Journal of the European Union*, págs. 1-11. doi:COM*2020(37 final
- European Commission.
- FCC. (28 de october de 2021). Valdemingomez biomethanisation plant field trip. Madrid, Madrid, Spain.
- Heidolph. (2022). *Hei-FLOW Ultimate 120 Multi*. (Heidolph) Recuperado el 13 de july de 2022, de <https://heidolph-instruments.com/en/products/Peristaltic-Pumps/Hei-FLOW-Ultimate-120-Multi~p1007>
- Linares Hurtado, J. I. (2021). Tema 5: Cogeneración, renovables y ciclos de potencia avanzados. Ejercicios de clase. En J. I. Linares Hurtado, *Ingeniería Energética* (pág. 5.2.14). Madrid: Universidad Pontificia Comillas-ICAI.
- Ministero para la Transición Ecológica y el Reto Demográfico. (2022). *Hoja de Ruta del Biogás*. Madrid: Ministerio para la Transición Ecológica y el Reto Demográfico. Obtenido de <https://drive.google.com/file/d/1Uw7iaML1Evh0e0nI91ZvNFWDCcwjprlN/view>
- Morales Polo, C. (2019). *Co-Digestión anaerobia y pretratamiento de residuos agroalimentarios con fangos UASB de depuradora*. Madrid: Universidad Pontificia Comillas-ICAI.
- Pacala, S., & Socolow, S. (13 de august de 2004). Stabilization Wedges: Solving the Climate Problem for the Next 50 Years with Current Technologies. *Science*, 968-972. doi:10.1126/science.1100103
- Pérez Sánchez, A., Pérez Sánchez, E. J., & Segura Silva, R. (12 de septiembre de 2016). Design of a packed-bed absorption column considering four packing types and applying Matlab. *Nexo Revista Científica*, 29(2), 83-. doi:<https://www.camjol.info/index.php/NEXO/article/view/4577>
- Rannard, G. (12 de november de 2021). COP 26: Coal compromise as leaders near climate deal. London, Greater London, United Kingdom. Obtenido de <https://www.bbc.com/news/science-environment-59221790>
- Romero Mora, J. C., & Tatay Nieto, J. (2020). What is the circular economy. En J. C. Romero Mora, & J. Tatay Nieto, *Sustainable Development Agenda- Apuntes de Clase* (págs. 5.1-5.53). Madrid: Universidad Pontificia Comillas-ICAI.
- Tran, T. (2017). *Standard Methods for the Examination of Water and Wastewater, 23rd edition*. Washington, DC.: American Public Health Association.
- United Nations. /

THIS PROJECT CONTAINS THE FOLLOWING DOCUMENTS

DOCUMENT 1: MEMOIR

pages 1 to 225

Document 1

Memoir

Memoir Index

Chapter 1: Introduction	1
1.1. Introduction.....	1
1.2. State of the Art	3
1.2.1. Usable Substrates in Anaerobic Digestion Processes	3
1.2.2. Influence of Substrates in Biogas Production and Composition	4
1.2.3. Anaerobic Digestion Stages	6
1.2.4. Anaerobic Digestion Control Parameters	9
1.2.5. Anaerobic Co-digestion.....	12
1.3. Project Objectives	13
1.4. Motivation.....	14
Chapter 2: Methodology	15
2.1. Resources Required.....	15
2.2. BMP Batch Bottles Design & Set Up.....	18
2.3. Batch Reactors Design & Set Up	21
2.4. Semi-Continuous Reactor Design & Set Up	23
2.5. Nanoparticle Dosing and Addition.....	25
2.5.1. Nanoparticle Dosage Calculation	25
2.6. Daily Sampling & Reactor Feeding	28
2.6.1. BMP Bottles Generic Tests	28
2.6.2. Generic Reactor Tests	31
2.6.3. Semi-Continuous Tests	33
2.6.4. Gas Chromatography.....	36
2.6.5. Semi-Continuous Reactor & Bottle Feeding	37
2.7. MATLAB Chromatography Analysis	38
2.7.1. Chromatogram Image Treatment.....	38
2.7.2. Chromatogram Calculations	40
Chapter 3: Results.....	41
3.1. BMP Bottle Results.....	41
3.1.1. BMP Binormal distribution modelling	46
3.1.2. B Bottles Binomial Distribution Modelling.....	46
3.1.3. B-NP Bottles Binomial Distribution Modelling	48
3.2. Batch Reactor Results	51
3.3. Semi-Continuous Reactor Results.....	54
3.3.1. Composition Analysis	54
3.3.2. VFA Analysis.....	55
3.3.3. COD and NTK Analysis.....	56

3.3.4.	C/N Ratio Estimation and Analysis.....	58
3.4.	Synthetic Reactor Modelling.....	61
Chapter 4:	Biogas Application Scenarios.....	63
4.1.	System Description	63
4.2.	Cogeneration Equipment.....	66
4.2.1.	Biogas Motors	66
4.2.2.	Natural Gas Motors	67
4.3.	Direct Biogas Use Scenario.....	69
4.3.1.	AD Reactor LCOE Estimation	69
4.3.2.	Direct Biogas Use Economic Analysis.....	71
4.4.	Biogas Upgrading Scenario.....	73
4.4.1.	Biogas Upgrading LCOE Estimation	73
4.4.2.	Biogas Upgrading Economic Analysis	75
Chapter 5:	Biogas Upgrading Equipment Design	79
5.1.	Biogas Upgrading Technology Selection & Demand Sizing.....	79
5.2.	Packed-Bed Absorption Column Design.....	80
	Random Packing Selection	80
5.2.1.	Scrubber Minimum Boundary Conditions.....	82
5.2.2.	Gas Inlet Data.....	84
5.2.3.	Tower Diameter	86
5.2.4.	Pressure Drop	87
5.2.5.	Diffusion Coefficients	89
5.2.6.	Mass Transfer Coefficients	90
5.2.7.	Packing Height.....	90
5.2.8.	Design Results.....	93
Chapter 6:	Conclusions.....	95
6.1.	Experiment Conclusions	95
6.1.1.	BMP Test Conclusions.....	95
6.1.2.	Batch Reactor Conclusions	96
6.1.3.	Semi-Continuous Reactor Conclusion.....	96
6.2.	Application Conclusions	96
6.3.	Wet Absorption Column Design Conclusion	97
Chapter 7:	Anejos	99
7.1.	Anejo I: Sustainable Development Goals Alignment.....	99
7.2.	Anejo II: Initial Result Analysis.....	101
7.3.	Anejo III: Hannah HI 902 Potentiometric Titrator Manual	129
7.4.	Anejo IV: Chromatogram Manual.....	151

7.5. Anejo V: MATLAB Code.....	181
Chapter 8: References	217

Figure Index

Figure 1: NMOC Methane Percentage Composition. Source: (Morales Polo, Digestión Anaerobia, 2022) (van Lier, Mahmoud, & Zeeman, 2020).	4
Figure 2. Anaerobic Digestion Stages. Source: (Rabii, Aldin, Dahman, & Elbeshbishy, 2019).....	6
Figure 3: The dynamics of biogas production at different temperatures. Source: (Al Seadi, y otros, 2008).....	9
Figure 4. Biodegradability Table of Wastewater. Source: (Cledera Castro, 2022).....	10
Figure 5: Substrate and Technical Parameters Relation. Source: (Ministero para la Transición Ecológica y el Reto Demográfico, 2022).	12
Figure 6. BMP Batch Bottle Resealed with Silicone Paste. Source: Own.	15
Figure 7: Ivymen Incubator. Source: Own.	15
Figure 8: Custom-Built BMP Bottle Barometer. Source: Own.	15
Figure 10: TFT-200 Thermostat. Source: Own.	16
Figure 11: HeiFLOW 01 Peristaltic Pump. Source: Own.	16
Figure 12: Ritter MilliGascounters. Source: Own.....	16
Figure 13: XS pH70 pHmeter. Source: Own.....	16
Figure 14: Aglient 7820A Gas Chromatographer. Source: Own.....	17
Figure 15: Hannah HI902 Potentiometric Titrator. Source: Own.....	17
Figure 16: Spectroquant 100 Spectrometer. Source: Own.....	17
Figure 17: Initial Substrate Processing. Source: Own.	18
Figure 18: Sludge in Oven. Source: Own.....	18
Figure 19: Prepared BMP Bottle. Source: Own.	19
Figure 20: Sample BMP Bottle. Source: Own.	19
Figure 21: Prepared Semi-Continuous BMP Bottle. Source: Own.....	19
Figure 22: Sample Semi-Continuous BMP Bottle. Source: Own.....	19
Figure 23: Semi-Continuous Bottle Design. Source: Own.....	20
Figure 24: Optic Ivymen System's Orbital Shaker Incubator during testing. Source: Own.	20
Figure 25: Batch Reactor Components 1. Source: Own.....	21
Figure 26: Three-Way Sampling Valve. Source: Own.....	21
Figure 27: Batch Reactor Components 2. Source: Own.....	22
Figure 28: Batch Reactor Components 3. Source: Own.....	22
Figure 29: Batch Reactor Complete Components. Source: Own.....	22
Figure 30: Final Batch Reactor Set-up. Source: Own.	22
Figure 31: Detailed pH Port Fitting. Top View. Source: Own.	23
Figure 32: Detailed pH Port Fitting. Side View. Source: Own.	23
Figure 33: 250 mm pH Probe. Source: Own.	23
Figure 34: Final Semi-Continuous Reactor Set-Up. Source: Own.	24
Figure 35: Semi-Continuous Reactor Design Diagram. Source: Own.....	24
Figure 36: Sludge Filtering to Determine Density. Source: Own.....	25
Figure 37: Filtered Sludge Weighing. Source: Own.	25
Figure 38: Volumetric Flask Filling. Source: Own.	27
Figure 39: Transferred Distilled Water. Source: Own.....	27
Figure 40: Nanoparticle Measurement. Source: Own.	27
Figure 41: Nanoparticle Sonication. Source: Own.....	27
Figure 42: BMP Batch Bottle Septum Covered in Silicone Paste. Source: Own.....	29
Figure 43: Silicone Paste-B Used to Seal Septums. Source: Own.....	29
Figure 44: BMP Batch Bottle Pressure Measuring. Source: Own.....	29
Figure 45: Barometer Control Unit. Source: Own.	29
Figure 46: Biogas Sample Collection in BMP Batch Bottle. Source: Own.	30

Figure 47: Biogas Sample Collection during Collection from BMP Batch Bottle. Source: Own.....	30
Figure 48: Depressurization of BMP Batch Bottle. Source: Own.	30
Figure 49: BMP Batch Bottle Resealed with Silicone Paste. Source: Own.....	30
Figure 50: BMP Semi-Continuous Bottle Pressure Measuring. Source: Own.....	31
Figure 51: Biogas Sample Collection during Collection from BMP Semi-Continuous Bottle. Source: Own.	31
Figure 52:Depressurization of BMP Semi-Continuous Bottle. Source: Own.....	31
Figure 53: Milligasometer in Operation. Source: Own.	32
Figure 54: Batch Reactor pH Correction. Source: Own.	33
Figure 55: VFA Titration. Source: Own.	34
Figure 56: Acid Pumps Used during VFA Testing. Source: Own.....	34
Figure 57: Sludge Extraction from Semi-Continuous Bottle. Source: Own.	34
Figure 58: Cell Test Procedure 1. Source: Own.....	35
Figure 59: Cell Test Procedure 2. Source: Own.....	35
Figure 60: Treated Cell Tests. Source: Own.	35
Figure 61: Cell Test Digester. Source: Own.	35
Figure 62: Cell Test Spectrometer Analysis. Source: Own.	35
Figure 63:Injection Port Fitting. Source: Own.	36
Figure 64:Biogas Sample Injection Representation. Source: Own.....	36
Figure 65: Gas Chromatography Method. Source: Own.	36
Figure 66: Semi-Continuous Bottle Feed Injection 1. Source: Own.	37
Figure 67: Semi-Continuous Bottle Feed Injection 2. Source: Own.	37
Figure 68: Semi-Continuous Bottle Feed Injection 3. Source: Own.	37
Figure 69: B.1.1 Untreated Screen Capture. Source: Own.	38
Figure 70: B1.1 Chromatogram Cut Out from Screen Capture. Source: Own.....	39
Figure 71: B.1.1 Cleaned Chromatogram. Source: Own.	39
Figure 72: Chromatogram Obtained during Testing. Source: Own.....	42
Figure 73: Average Accumulated Biogas Production for each BMP test. Source: Own.	42
Figure 74: Daily BMP Co-Digestion Biogas Production. Source: Own.....	43
Figure 75: B Model Mean Stats. Source: Own.....	46
Figure 76: B Model Mean Residual Analysis. Source: Own.....	46
Figure 77: B Model Standard Deviation Stats. Source: Own.	47
Figure 78: B Model Standard Deviation Residual Analysis. Source: Own.	47
Figure 79: B Model Binormal Distribution. Source: Own.	48
Figure 80: B-NP Mean Model Stats. Source: Own.	49
Figure 81: B-NP Mean Residual Analysis. Source: Own.....	49
Figure 82: B NP Standard Deviation Model Stats. Source: Own.	49
Figure 83: B-NP Standard Deviation Residual Analysis. Source: Own.	50
Figure 84: B-NP Model Binormal Distribution. Source: Own.	50
Figure 85: Effect of Nanoparticles on Methane and Hydrogen in Batch Reactor. Source: Own.	53
Figure 86: Effect of Nanoparticles on Hydrogen Sulphide and Residues in Batch Reactor. Source: Own.	53
Figure 87: Semi-Continuous Reactor Composition. Source: Own.	55
Figure 88:Semi-Continuous Reactor Partial Alkalinity. Source: Own.	56
Figure 89: Semi-Continuous Reactor's COD. Source: Own.	57
Figure 90: Semi-Continuous Reactor's NTK. Source: Own.	58
Figure 91: NMOC Methane Percentage Composition. Source: (Morales Polo, Digestión Anaerobia, 2022) (van Lier, Mahmoud, & Zeeman, 2020).	59
Figure 92: Semi-Continuous Reactor TOC NMOC Estimation. Source: Own.....	60
Figure 93: : Semi-Continuous Reactor C/N NMOC Estimation, Source: Own.	60

Figure 94: Synthetic Reactor Cell Division. Source: Own.....	61
Figure 95: Annual Thermal Demand Modelling. Source: Own.....	63
Figure 96: Minimum EEE to Include CHT Plant in the Special Regime Registry. Source: (Linares Hurtado J. I., Tema 5: Cogeneración, Renovables y Ciclos de Potencia. Apuntes de Clase, 2021); ..	64
Figure 97: Harmonised Efficiency Reference values for Heat Generation. Source: (European Comission, 2011).....	64
Figure 98: Harmonised Efficiency Reference values for Electricity Generation. Source: (European Comission, 2011).....	64
Figure 99: Future Yearly Energy Prices. Source: (OMIP, 2022).....	65
Figure 100: Biogas Motor Price Modelling. Source: Own.....	66
Figure 101: Biogas Consumption Modelling. Source: Own.....	67
Figure 102: Natural Gas Motor Price Modelling. Source: Own.....	68
Figure 103: Natural Gas Consumption Modelling. Source: Own.....	68
Figure 104: Random Packing Material Ring Geometries. Source: (Crynes, Albright, & Tan, 2003)..	81
Figure 105: Minimum Operating Conditions for Packed Column. Source: Own.....	83
Figure 106: Nominal Operating Conditions for Packed Column. Source: Own.....	86
Figure 107: Molar Fraction Correlation in Gas & Liquid Phase. Source: Own.....	92

Table Index

Table 1: Theoretical Composition and Production of Biogas using the Buswell-Mueller and Boyle Formulae. Source: (Morales Polo, Co-Digestión anaerobia y pretratamiento de residuos agroalimentarios con fangos UASB de depuradora, 2019) (Verlag des Vereins Deutscher Ingenieure, 2006).....	5
Table 2: BMP Bottle Co-Digestion Mixture. Source: Own.....	18
Table 3: Batch Reactor Co-Digestion Mixture. Source: Own.	21
Table 4: Nanoparticle Addition Calculations. Source: Own.	26
Table 5: Nanoparticle Solution Calculations. Source: Own.	26
Table 6: Sonication Parameters. Source: Own.	27
Table 7: pH Calibration Table. Source: Own.	33
Table 8:Chromatogram Pixel Limits. Source: Own.	38
Table 9: BMP Bottle Pressure Readings. Source: Own.	41
Table 10: Student’s t-test on Mean Results. Source: Own.	44
Table 11: Snedecor’s f-test on Variance Results. Source: Own.	45
Table 12. Effects of Nanoparticles on Batch Reactor Methane Composition. Source: Own.	51
Table 13: Effects of Nanoparticles on Batch Reactor Hydrogen Composition. Source: Own.	51
Table 14: Effects of Nanoparticles on Batch Reactor Hydrogen Sulphide Composition. Source: Own.	52
Table 15:Effects of Nanoparticles on Batch Reactor Residue Composition. Source: Own.	52
Table 16: Semi-Continuous Reactor Composition, Days 1-21. Source: Own.	54
Table 17: Semi-Continuous Reactor Composition, Days 22-42. Source: Own.	54
Table 18: Semi-Continuous Reactor VFA Analysis, Days 1-21. Source: Own.....	55
Table 19: Semi-Continuous Reactor VFA Analysis, Days 22-42. Source: Own.....	56
Table 20: COD & NTK Cell Test Range Limits. Source: Own.	57
Table 21: Semi-Continuous Reactor NTK & COD Tess, Days 1-21. Source: Own.....	57
Table 22: Semi-Continuous Reactor NTK & COD Tess, Days 22-42. Source: Own.....	57
Table 23: Semi-Continuous Reactor TOC NMOC Estimation, Days 1-21. Source: Own.....	59
Table 24: Semi-Continuous Reactor TOC NMOC Estimation, Days 22-42. Source: Own.....	59
Table 25: Semi-Continuous Reactor C/N NMOC Estimation, Days 1-21. Source: Own.	60
Table 26: Semi-Continuous Reactor C/N NMOC Estimation, Days 22-42. Source: Own.	60
Table 27: Synthetic Reactor Construction. Source: Own.	62
Table 28: Synthetic Reactor Hourly Molar Production and Composition. Source: Own.	62
Table 29: Fuel Costs and Nominal Rate. Source: Own.	65
Table 30: O&M Costs and Nominal Rate. Source: Own.....	65
Table 31: Project Return Rate and Lifespan. Source: Own.	65
Table 32: Jenbacher Motor’s Efficiency. Source: (Zorg Biogas, 2022).	66
Table 33: Jenbacher Motor Catalogue. Source: (Zorg Biogas, 2022).....	66
Table 34: Enerblue Motor’s Efficiency. Source: (Zorg Biogas, 2022).....	67
Table 35: Enerblue Motor Catalogue. Source: (Zorg Biogas, 2022).	67
Table 36: WACC estimation. Source: (Fraunhofer ISE, 2018).	69
Table 37: Hypothesis for Reactor Cost and Operation. Source: (Fraunhofer ISE, 2018).	69
Table 38: Reactor Hypothesis Combination. Source: Own.	69
Table 39:Variable AD Reactor Costs & Rates. Source: (Fraunhofer ISE, 2018).	70
Table 40:Compounding and Annualization results. Source: Own.....	70
Table 41: LCOE Calculation per Scenario. Source: Own.	71
Table 42: LCOE of AD Reactor Adjusted for Inflation. Source: Own.....	71
Table 43:Compounding and Annualization results. Source: Own.....	71
Table 44: Biogas Scenario NVA. Source: Own.	72

Table 45:AD Reactor Sizing for Biogas Scenario. Source: Own.	72
Table 46: PES & EEE of Biomethane Scenario. Source: Own.	73
Table 47: Hypothesis for Scrubber Cost and Operation. Source: (Nguyen, Morrison, & Nelson, 2005).	74
Table 48: Scrubber Hypothesis Combination. Source: Own.	74
Table 49:Variable Scrubber Costs & Rates. Source: (Fraunhofer ISE, 2018).	74
Table 50:Compounding and Annualization results. Source: Own.....	74
Table 51: Scrubber LCOE Calculation per Scenario. Source: Own.	75
Table 52: LCOE of AD Reactor Adjusted for Inflation. Source: Own.....	75
Table 53:Compounding and Annualization results. Source: Own.....	76
Table 54: Biomethane Scenario NVA. Source: Own.	76
Table 55:AD Reactor Sizing for Biomethane Scenario. Source: Own.	77
Table 56: PES & EEE of Biomethane Scenario. Source: Own.	77
Table 57: Simplified Biogas Composition. Source: Own.....	79
Table 58: Biogas Demand to Upgrade. Source: Own.....	79
Table 59: Packing geometries characteristics. Source: (Kayode Coker, 2010).	80
Table 60: Packing material parameters. Source: (Benitez, Principles and modern applications of mass transfer operations, 2009).	81
Table 61: Sample Hydraulic & Mass-transfer parameters of packing material. Source: (Benitez, Principles and modern applications of mass transfer operations, 2009).	81
Table 62: Selected Pall Ring Parameters. Source: (Walcoom Corporation, 2022), (Pérez Sánchez, Pérez Sánchez, & Segura Silva, 2016).	81
Table 63: Packed Column Operating Conditions. Source: Own.	83
Table 64: Minimum Molar Flow Rates & Composition at Intakes and Outlets. Source: Own.	83
Table 65: Selection of Nominal Values. Source: Own.	84
Table 66: Nominal Inlet Conditions, Parameters and Constants. Source: Own.....	84
Table 67: Gas Inlet Data. Source: Own.....	85
Table 68: Nominal Design molar flows. Source: Own.....	85
Table 69: Tower Diameter Results. Source: Own.	87
Table 70: Pressure Drop Results. Source: Own.	88
Table 71: Diffusion Coefficients Results. Source: Own.....	90
Table 72: Mass Transfer Coefficients Results. Source: Own.	90
Table 73: Molar Fractions of CO ₂ in flows. Source: Own.	92
Table 74: Packing Height Results. Source: own.	92
Table 75: Main Packed Column Design Parameters. Source: Own.	93
Table 76: Full Design Parameters Results. Source: Own.	93

Ilustración Index

<i>Ilustración 1: Incubadora</i>	104
<i>Ilustración 2: Cromatógrafo de gases</i>	104
<i>Ilustración 3: Reactor Discontinuo</i>	104
<i>Ilustración 4: Ejemplo Cromatograma</i>	106
<i>Ilustración 5: Producción Acumulada de biogás</i>	107
<i>Ilustración 6: Detalle de la Producción Diaria de Biogás</i>	107
<i>Ilustración 7: Incremento Porcentual de la Producción Debido a las Nanopartículas</i>	108
<i>Ilustración 8: Mejora Específica Biogás</i>	110
<i>Ilustración 9: Efecto sobre sobre la media del Metano</i>	115
<i>Ilustración 10: Efecto sobre la media del Hidrógeno</i>	115
<i>Ilustración 11: Efecto sobre sobre la media del Ácido Sulfhídrico</i>	116
<i>Ilustración 12: Efecto sobre la media de los Residuos</i>	116
<i>Ilustración 13: Efecto sobre la desviación estándar del Metano</i>	121
<i>Ilustración 14: Efecto sobre la desviación estándar del Hidrógeno</i>	121
<i>Ilustración 15: Efecto sobre la desviación estándar del Ácido Sulfhídrico</i>	122
<i>Ilustración 16: Efecto sobre la desviación estándar de los Residuos</i>	122
<i>Ilustración 17: Efecto sobre la composición del Reactor (I)</i>	126
<i>Ilustración 18: Efecto sobre la composición del Reactor (II)</i>	126
<i>Ilustración 19: Componentes del equipo</i>	133
<i>Ilustración 20: Detalle Sondas</i>	133
<i>Ilustración 21: Detalle Conjunto Bureta</i>	133
<i>Ilustración 22: Detalle Botella y Pipeta</i>	133
<i>Ilustración 23: Pantalla de Ensayo</i>	135
<i>Ilustración 24: Panel de Control</i>	136
<i>Ilustración 25: Menú General</i>	136
<i>Ilustración 26: Menú Selección Método</i>	137
<i>Ilustración 27: Límites de dosado manual. Obtenido de (Laboquímica, 2022)</i>	138
<i>Ilustración 28: Menú Bureta</i>	138
<i>Ilustración 29: Menú Ver Método</i>	138
<i>Ilustración 30: Posición de las sondas en la muestra</i>	141
<i>Ilustración 31: Menú Ver Método, Detalle 1</i>	143
<i>Ilustración 32: Menú Ver Método, Detalle 2</i>	143
<i>Ilustración 33: Tipo de Análisis</i>	144
<i>Ilustración 34: Menú Tipo Dosificación</i>	145
<i>Ilustración 35: Menú Punto Final</i>	146
<i>Ilustración 36: Menú Modo Medición</i>	147
<i>Ilustración 37: Menú Estabilidad de la Señal</i>	147
<i>Ilustración 38: Opción de Blanco</i>	148
<i>Ilustración 39: Menú de Cálculos</i>	148
<i>Ilustración 40: Menú de Rango de Potencial</i>	149
<i>Ilustración 41: Cromatógrafo, balas de nitrógeno y ordenador</i>	154
<i>Ilustración 42: Componentes Principales del Equipo</i>	155
<i>Ilustración 43: Detalle de Inyección de Muestras</i>	155
<i>Ilustración 44: Detalle Balas de Nitrógeno</i>	155
<i>Ilustración 45: Detalle Manómetros de las Balas</i>	155
<i>Ilustración 46: Interior del Horno</i>	156
<i>Ilustración 47: Cromatograma de Bala de Calibración</i>	157
<i>Ilustración 48: Programas de control del Cromatógrafo</i>	158

<i>Ilustración 49: Pantalla de Inicio de GC7820A</i>	159
<i>Ilustración 50: Pestaña File</i>	160
<i>Ilustración 51: Pestaña Edit</i>	160
<i>Ilustración 52: Pestaña View</i>	161
<i>Ilustración 53: Pestaña Method</i>	161
<i>Ilustración 54: Pestaña Data</i>	162
<i>Ilustración 55: Pestaña Result Set</i>	162
<i>Ilustración 56: Pestaña Analysis</i>	163
<i>Ilustración 57: Pestaña Control</i>	163
<i>Ilustración 58: Pestaña Reports</i>	164
<i>Ilustración 59: Ventana Instrument Wizard</i>	164
<i>Ilustración 60: Icono Instrument Set Up</i>	165
<i>Ilustración 61: Icono Peak/ Group Tables</i>	165
<i>Ilustración 62: Eventos de Integración</i>	166
<i>Ilustración 63: Tabla de Integración Manual</i>	167
<i>Ilustración 64: Ventana de Secuencia de Ensayos</i>	167
<i>Ilustración 65: Ventana Analyze</i>	168
<i>Ilustración 66: Ventana Analyze Single Run</i>	168
<i>Ilustración 67: Ventana Single Run</i>	169
<i>Ilustración 68: Ventana del Result Path de un ensayo Single Run</i>	169
<i>Ilustración 69: Ventana Sequence Run</i>	170
<i>Ilustración 70: Ventana Run Queue</i>	170
<i>Ilustración 71: Ventana Instrument Wizard</i>	171
<i>Ilustración 72: OpenLAB Control Panel</i>	172
<i>Ilustración 73: 7820A Remote Control Panel</i>	173
<i>Ilustración 74: Gráfica del Método de Análisis de Muestras de Biogás</i>	175
<i>Ilustración 75: Inyección de muestra en el cromatógrafo desde jeringa</i>	178

Tabla Index

<i>Tabla 1: Medidas de presión (bar) recogidas</i>	106
<i>Tabla 2: Producción Acumulada de Biogás</i>	107
<i>Tabla 3: Mejora Porcentual de las Nanopartículas en la Producción Diaria</i>	108
<i>Tabla 4: Resultados test estadísticos producción de biogás bruto</i>	110
<i>Tabla 5: Análisis estadístico de la media de CH₄</i>	111
<i>Tabla 6: Análisis estadístico de la media de H₂</i>	112
<i>Tabla 7: Análisis estadístico de la media de H₂S</i>	113
<i>Tabla 8: Análisis estadístico de la media de RES</i>	114
<i>Tabla 9: Análisis estadístico de la varianza de CH₄</i>	117
<i>Tabla 10: Análisis estadístico de la varianza de H₂</i>	118
<i>Tabla 11: Análisis estadístico de la varianza de H₂S</i>	119
<i>Tabla 12: Análisis estadístico de la varianza de RES</i>	120
<i>Tabla 13: Composición del Metano en los Reactores</i>	123
<i>Tabla 14: Composición del Hidrógeno en los Reactores</i>	124
<i>Tabla 15: Composición del Ácido Sulfhídrico en los Reactores</i>	124
<i>Tabla 16: Composición de los Residuos en los Reactores</i>	125
<i>Tabla 17: Variables a recoger en el ensayo de AGVs</i>	140
<i>Tabla 18: Composición de la Bala de Calibración</i>	156
<i>Tabla 19: Variables a recoger en el ensayo de biogás</i>	177

Chapter 1: Introduction

1.1. Introduction

The main problem faced by our society today is the named Ecological Transition to a greener economy by reducing the impact humans have on the planet because of anthropogenic climate change. This part of the “Twin Transitions” (European Commission, 2020) is considered by the EU and its member states a pillar to define the direction in which Europe must lead the world, which resulted in the creation and approval of the European Green Deal (European Commission, 2021) to provide a response to ever increasing climatic anomalies & disasters caused by climate change.

To permit and direct the required effort and investment, both of public and private nature, the Climate Delegated Act was passed to direct and align the various key players and technologies. Among this key technologies, bioenergy, and particularly biogas and biomethane, were identified as “low-carbon gases” meant to replace natural gas, produced through anaerobic digestion (AD), in the energy and industrial sectors coupled with applications in heavy-duty transport (European Biogas Association, 2020).

The recent COP 26 held in Glasgow (United Nations, 2021) further emphasized the need for the global temperature increase to be limited to 1.5°C above pre-industrial levels. Therefore, global leaders reached a compromise to remove coal from their electrical generation mixes (Rannard, 2021), widely considered to be the most polluting of fossil fuels. Furthermore, the EU, the US as well as a hundred countries announced their intentions to reduce their methane emissions, particularly from natural gas leaks (BBC News, 2021). Methane emissions have long been considered one of the 8 stabilization wedges required to prevent an increase in global temperatures (Pacala & Socolow, 2004) due to its high global warming potential of 21 CO₂-eq (IPCC, 2018).

This new advancements in climate action will require substantial investments in infrastructure and research in new technologies to transition to a greener economy. To facilitate said change, the EU included renewable fuels and bioenergy as part of the 2020 SET Plan revision (European Commission, 2020). However, most projects are set to start by the 2022–2025-time frame once laboratory research is finalised and results can be used to design industrial applications.

On a national scale, the Ministry for Ecological Transition (MITECO) identified biogas as a new renewable energy source with the capability of preventing up to 2.1 million tonnes CO₂-eq. per year according to the Biogas National Plan (Ministero para la Transición Ecológica y el Reto Demográfico, 2022). The Plan highlights the minimal use of AD reactors, which produced 2.74 TWh of energy in 2020. The 146 operating plants are in landfills or wastewater treatment plants, with only thirteen used in commercial applications. Moreover, there are only five biomethane plants in the country, with the largest located in Valdemingomez, Madrid (FCC, 2021).

The last aspect of the context in which this research occurred pertains to the goal of achieving a circular economy in which waste is minimised and resources used to their full potential, extracting all the value contained within them before final disposal (Romero Mora & Tatay Nieto, 2020). AD proposes the transformation of sludge from a residue into a co-product to be used not only for energy generation, but also the upcycling of the obtained digestate as fertilizer. By considering the full life cycle of the sludge, eco-design of waste treatment processes can be expanded until a full cradle-to-cradle approach can be implemented. These advancements would reduce the energy intensity of water treatment facilities or similar industrial processes which require wastewater treatment plants to comply with regulations.

Another important aspect of AD is the capability of reducing environmental pollution resulting from mishandling of residues. These residues currently have become a major problem due to their impact in soil and water pollution as diffuse and punctual emission sources percolate into superficial and ground water (Palomar, 2020), altering their chemical balances and requiring additional treatment of raw water

before it is deemed potable. On the other hand, if said sludges are not effectively managed the environmental damage resulting from the addition of external bacteria leads to the eutrophication of superficial waters and all the related consequences.

1.2. State of the Art

Anaerobic digestion (AD) is a naturally occurring process in which complex organic matter is broken down in an oxygen-free environment, producing a homogenous gas mixture, known as biogas, and a mixture of mineralized nutrients and undigested matter known as digestate (Morales Polo, *Digestión Anaerobia*, 2022).

The digestion of organic matter occurs in four distinct steps, performed by four different microbial families with different environmental needs. This results in AD processes being unstable, especially if employed in continuous reactors, traditionally used in waste treatment processes with high organic pollution in dry (solid) or wet (liquid) form (Lampaya Nasarre, 2022).

It must also be added that the obtained products (biogas and digestate), will present different compositions and thus uses depending on the nature and source of the treated waste. As a result, both the biogas and specially the digestate require strict control when determining their final uses, as they may require processing and cleaning techniques.

1.2.1. Usable Substrates in Anaerobic Digestion Processes

AD only requires the use of a substrate containing organic matter; however, each type of substrate may have different characteristics which may result in variations in biogas production. To that end, the main substrates used are listed in this section (Morales Polo, *Residuos Rurales*, 2022).

Crop Residue: Also known as agricultural residue, this refers to leftover crop or parts of the plant which were harvested by later discarded such as grain husks and dried crop such as hay. It is characterized by its low humidity content, paired with a 10% lignin, which inhibits AD. However, winter crops present a high C/N ratio between 80 and 100.

Animal Manure & Slurry: Manure content and composition varies based on the animal which produced it. Animal waste requires treatment because of its high nitrogen content and biological contamination which may be harmful to the environment. Similarly, slurries also represent an environmental hazard if they percolate into aquifers, due to their basic pH and high organic and nitrogen loading. Manure is rich in solid matter as well as organic loading. As a result, they are usually mixed and treated as a liquid mixture.

Wastewater sludge: Wastewater sludge is a prime substrate, due to its biological composition, which contains all the necessary bacterial families necessary to perform the AD process. It must also be mentioned that the sludge is itself poor when used on its own, as it is produced from previously treated waste which results in a low C/N ration (Morales Polo, *Co-Digestión anaerobia y pretratamiento de residuos agroalimentarios con fangos UASB de depuradora*, 2019) (García Mingo, 2021). This in turn causes AD processes in wastewater treatment plants to not be self-sustaining energy wise, as they require more methane than they produce to maintain their operating conditions.

Organic Fraction of Municipal Solid Waste: Used as AD substrate in landfills, the OFMSW presents a high organic content as well as a high biodegradability but lacks any compound which may be used as a buffer for acidification. Another problem it faces is the presence of inorganic or inert waste which cannot be digested, requiring separation and screening prior to digestion (Lampaya Nasarre, 2022).

1.2.2. Influence of Substrates in Biogas Production and Composition

Due to the nature of the process in which organic waste is broken into simpler chemical compounds, the composition of said intake will influence the composition as well as the production rate of the biogas, with simpler and shorter organic compounds being digested at a faster rate, especially sugars (Morales Polo, Co-Digestión anaerobia y pretratamiento de residuos agroalimentarios con fangos UASB de depuradora, 2019).

On the other hand, lignin (a complex polymer which characterizes woody plants) which reduces biodegradability of organic compounds, considered to be a more representative indicator than the Volatile Solids in the waste being processed. As a result, the biodegradability can be estimated using equation 1 below (Morales Polo, Residuos Sólidos Urbanos, 2022). It must also be mentioned that biodegradability in AD tests can be measured using BMP tests (AENOR, 1999).

$$FB [p. u.] = 0.83 - 0.028 * lignin [\%_{db}]$$

Furthermore, the composition of said biogas can be estimated using de NMOC method, which employs the COD/TOC ratio (chemical oxygen demand/Total Organic Carbon), which can also be used to measure biodegradability, to estimate the methane composition in the produced biogas. The formula provided can be seen below in equation 2 and the related graph in Figure 1 (Morales Polo, Digestión Anaerobia, 2022) (van Lier, Mahmoud, & Zeeman, 2020).

$$CH_4[\%] = 18.75 * \frac{COD}{TOC}$$

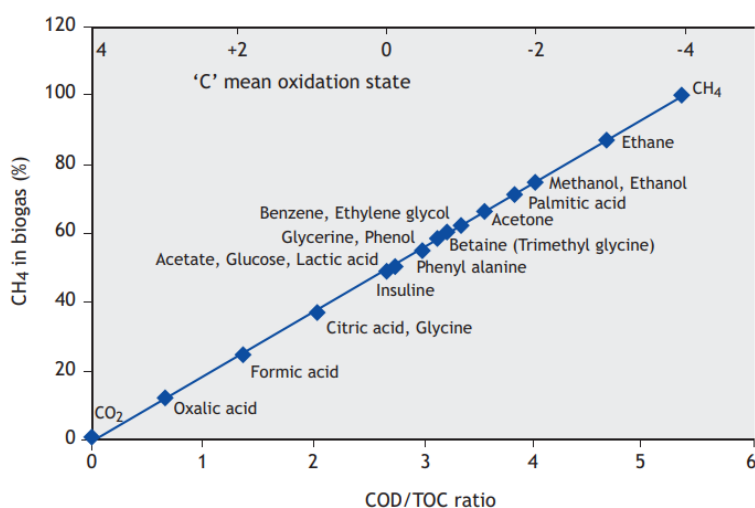


Figure 1: NMOC Methane Percentage Composition. Source: (Morales Polo, Digestión Anaerobia, 2022) (van Lier, Mahmoud, & Zeeman, 2020).

Similarly, several observations on the decomposition of lipids, proteins and carbohydrates were made in (Morales Polo, Co-Digestión anaerobia y pretratamiento de residuos agroalimentarios con fangos UASB de depuradora, 2019) and summarized in (Morales Polo, Digestión Anaerobia, 2022). Regarding lipids, these present a high carbon content, which will yield a larger biogas generation, with a higher content of methane. However, as it will be explained later, these long-chained compounds present a slower degradation and risk the acidification of the reaction medium.

Proteins, contain nitrogen and sulphur, which reduce the methane yield during degradation and may produce hydrogen sulphide and ammonia. These unwanted products require monitorization as they may inhibit methanogenesis.

The final compound to be analysed were carbohydrates, which produce low quantities of biogas, with a low methane content. Despite this, they present the highest degradation within the reactor and thus simplify the AD process. However, the fast decay may result in the acidification of the vessel if the simple sugars decompose into Volatile Fatty Acids and accumulate.

As previously stated, AD products will depend on the composition of the substrate, which can be a singular type (known as monodigestion) or a mixture of two or more different substrates, being thus referred to as co-digestion.

The biogas potential of each compound was also calculated in (Morales Polo, Co-Digestión anaerobia y pretratamiento de residuos agroalimentarios con fangos UASB de depuradora, 2019), whose results are compounded below in Table 1.

Table 1: Theoretical Composition and Production of Biogas using the Buswell-Mueller and Boyle Formulae. Source: (Morales Polo, Co-Digestión anaerobia y pretratamiento de residuos agroalimentarios con fangos UASB de depuradora, 2019) (Verlag des Vereins Deutscher Ingenieure, 2006).

	Theoretical biogas production	Theoretical Composition of biogas		Reference
	[L_N/kg-ST]	[% CH₄ vol.]	[% CO₂ vol.]	
Lipids	1390	72	28	(Verlag des Vereins Deutscher Ingenieure, 2006)
Proteins	800	60	40	
Carbohydrates	750	50	50	

Using the obtained data displayed throughout this section, the biogas production of various compounds can be estimated based on their lipids, protein, and carbohydrate content, although lignin and other inhibitors should also be considered when performing a detailed analysis of each substrate.

1.2.3. Anaerobic Digestion Stages

As previously stated, the digestion process consists of four distinct stages. These stages occur simultaneously, although the dominant phase varies during batch processes. In continuous processes however, the four processes occur in equilibrium during operation. These stages, along with the products are shown below in Figure 2. In addition, detailed reviews of the stages are provided below.

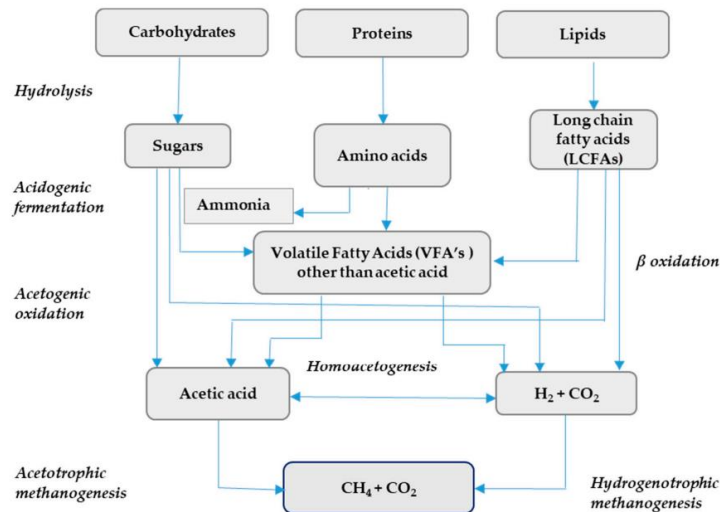
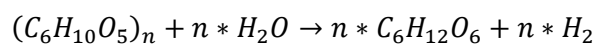


Figure 2. Anaerobic Digestion Stages. Source: (Rabii, Aldin, Dahman, & Elbeshbishy, 2019).

1.2.3.1. Hydrolysis

The first step in the AD process. This represents the critical stage of the digestion as well as the only extra-cellular phase using enzymes released into the digestion medium (Meegoda, 2018). The latter three occur inside the various microbes. During hydrolysis, long chain organic compounds, such as carbohydrates and proteins are broken down into simpler compounds such as acetate carbon dioxide and hydrogen gas.

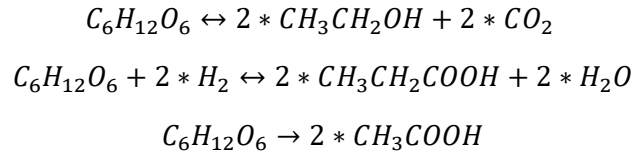
These simpler compounds can then be absorbed by acidogenic bacteria, responsible for the following step of the process. It must also be mentioned that different compounds will present a smaller decay rate during hydrolysis based on their complexity and the elements found in the monomers, with sugar and carbohydrates being processes faster than lipids and proteins (Vijayalakshmi Arelli, 2022). Lastly, the ideal pH at which the phase occurs is also of importance, with (Menzel, 2020) identifying said range between 5 and 6. A sample equation for the decomposition of a glucan polymer was provided by (Lefers, 2004) and is shown below.



1.2.3.2. Acidogenesis

Once the complex organic compounds have been broken down, acidogenic bacteria absorb said compounds through their cell membranes and release Volatile Fatty Acids (VFA). These intermediate acids include compounds such as the acetate, the main compound from which methane is eventually produced after further digestion. It must also be mentioned that VFA can cause the sludge to acidify, reducing the pH drastically and inhibiting further digestion by killing the bacteria responsible for acidogenesis and methanogenesis (Zhang C. , Su, Baeyens, & Tan, 2014). The pH range at which acidogenesis occurs is between 5 and 8 (Zhao, y otros, 2021).

This has led to developments in reactor design, which now propose the use of separate vessels for AD processes (Morales Polo, Digestión Anaerobia, 2022), connected through digitally controlled valve so that the first 2 stages occur in an acidic vessel, in their ideal conditions, while the remaining steps, which required a basic pH, may take place in the second vessel. However, this is currently being researched to assess viability and the complexity required to design the control system for the flow valve. Lastly, the acidogenic decomposition process is shown below, compiled in (eckson Kamusoko, 2022), which can occur through various reversible reactions.



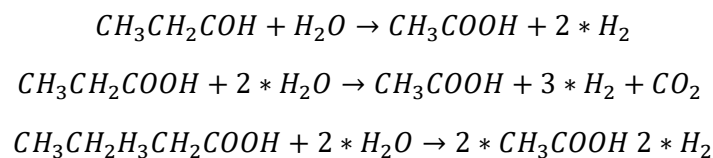
Lastly, it must also be mentioned that the decomposition of proteins releases nitrogen in the form of ammonia, which presents a buffer to prevent acidification of the reaction medium. However, a large ammonia concentration may also result in the suppression of methanogenesis, requiring a balance with the carbon content to maximize production (Yang, Wang, He, Zhang, & Liu, 2018).

1.2.3.3. *Acetogenesis*

Acetic acid is the main compound from which methane is produced. The mechanism used depends on the temperature at which the reaction takes place. At a thermophilic temperature (65-70°C), the dominant mechanism is hydrogenotrophic methanogenesis, which skips the stage currently being detailed and produces methane directly from acetate (Dong, Bu, Zhou, Khanal, & Xie, 2018).

However, most processes used occur at mesophilic (30-40°C) or psychrophilic (2-25°C) (Morales Polo, Digestión Anaerobia, 2022). At these temperature ranges, the dominant methanogenesis process is acetoclastic methanogenesis, which requires the production of acetic acid during the acetogenesis phase, with an ideal like that of acidogenesis, considering the production of acetic acid as a two-step process (Lorenzo Acosta & Obaya Abreu, 2005).

During said phase, the VFA as well as lighter compounds such as alcohols, previously produced are converted into acetic acid by the dehydrogenation of the acetate. Another reaction which produces acetic acid is the homoacetogenesis of H₂ and CH₄ previously released (Rabii, Aldin, Dahman, & Elbeshbishy, 2019). As with the previous processes, the decomposition of acetate into acetic acid is shown below 9 (Liu, y otros, 2021).

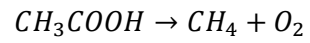
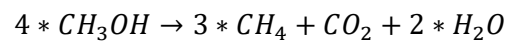
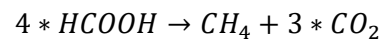
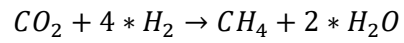


1.2.3.4. *Methanogenesis*

Once the acetic acid has been produced, it can then be converted into methane and carbon dioxide through acetoclastic methanogenesis as previously explained. Temperature has such a profound effect on the dominant mechanism that in thermophilic conditions, 90% methane is produced through the hydrogenotrophic process, while in mesophilic conditions around 66% of methane is produced via acetoclastic methanogenesis.

These bacteria, unlike the previous digesters, require a higher pH, between 6.5 and 7.6 (Ghaly, 2000). In addition, these bacteria are overly sensitive to pH changes, which can inhibit the process when it

reaches de 5.5 to 6.25 range (Staley, de los Reyes III, & Barlaz, 2011). Lastly, the equations for hydrogenotrophic methanogenesis are displayed below. The fourth equation represents acetoclastic methanogenesis.



1.2.4. Anaerobic Digestion Control Parameters

Certain parameters have been lightly mentioned throughout the previous subsections, such as the C/N ratio of the Volatile Fatty Acids. Due to their significance, they will be discussed in this subsection, as they represent the key metrics used to control and determine the state of the digester.

1.2.4.1. Temperature

As with all biological processes, temperature plays a key role in AD reactions, promoting or inhibiting the growth of certain microbial families which result in different compound decay rates and therefore methane production rates by changing the predominant methanogenesis mechanism from acetoclastic methanogenesis to hydrogenotrophic methanogenesis, as reviewed in subsection 2.2.4.

Temperature control is also a key element when performing AD experiments, as it was shown in (Kim & Oh, 2011) that a variation of 1°C/day may result in a process failure (Zhang C. , Su, Baeyens, & Tan, 2014). Lastly, the temperature ranges for AD: psychrophilic (2-25°C), mesophilic (20-40°C) and thermophilic (65-70°C) are displayed below along with their relative methane production in Figure 3 (Morales Polo, Digestión Anaerobia, 2022) (Al Seadi, y otros, 2008).

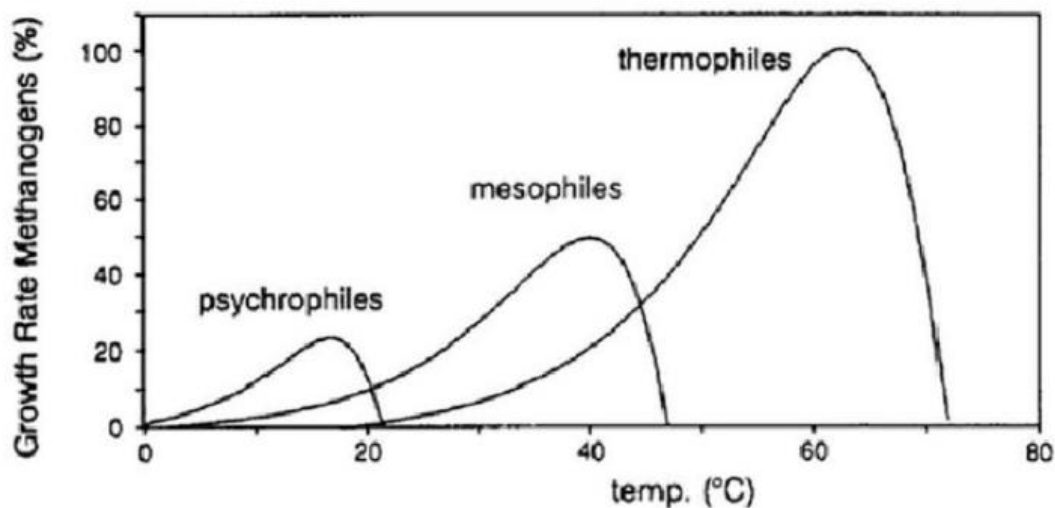


Figure 3: The dynamics of biogas production at different temperatures. Source: (Al Seadi, y otros, 2008).

1.2.4.2. pH and Volatile Fatty Acids

pH is an essential parameter which can have severe impacts on the AD process due to the acidity or alkalinity levels required for each phase of the digestion. Various studies such as (Zhang, Zhang, Zhang, Shi, & Cai, 2005) found that the ideal pH level is an intermediate value between the optimum for each phase, resulting in a final value of 7.

Within pH control, Volatile Fatty Acids (VFAs) represent the most significant contributing factor. These are simple intermediate compounds found in the AD process such as acetic, butyric, propionic and valeric acid (Zhang C. , Su, Baeyens, & Tan, 2014) (Morales Polo, Digestión Anaerobia, 2022).

To determine the VFA concentration within the reaction vessel, various methods have been developed, being (APHA, AWWA, WEF, 2012) among the most widespread as it does not require the use of a gas or liquid chromatographer. This procedure was adapted from (Morales Polo, Co-Digestión anaerobia y pretratamiento de residuos agroalimentarios con fangos UASB de depuradora, 2019). The proposed method employs a 2-stage titration to measure the intermediate, partial, and total alkalinity of a liquid sample. Of these, intermediate alkalinity is used to measure VFAs within the sample.

The performed titration requires the use of hydrochloric acid or sulphuric acid, preferably with standard normalities. The first titration stops when a pH of 5,75 is reached, while the second stage ends at a target value of 4.3. In both cases, the volume of titrant used (V_i) must be recorded. Lastly, the formulas used for total, partial and intermediate alkalinity are presented below.

$$AP \left[\frac{mg_{CaCO_3}}{l} \right] = \frac{V_{HCl} * N_{HCl} * 5000}{V_{sample}}$$

$$AI \left[\frac{mg_{CaCO_3}}{l} \right] = \frac{V_{H_2SO_4} * N_{H_2SO_4} * 5000}{V_{sample}}$$

$$AT \left[\frac{mg_{CaCO_3}}{l} \right] = Ap + AI = \frac{(V_{H_2SO_4} * N_{H_2SO_4} + V_{HCl} * N_{HCl}) * 5000}{V_{sample}}$$

1.2.4.3. Chemical Oxygen Demand

Two main parameters are used to measure the pollution in wastewater, as well as the biodegradability of said pollution. 5-day Biochemical Oxygen Demand (BOD₅) is used to measure the oxygen demand required by bacteria to digest and decompose biodegradable pollutants.

Similarly, Chemical Oxygen Demand (COD) measures the total demand of oxygen required to fully oxidise all organic contaminants found in the sample. In addition, the BOD₅/COD quotient is used to determine the biodegradability, with the qualitative categories shown below in Figure 4 (Cledera Castro, 2022).

DBO5/DQO	Biodegradabilidad del agua residual
0,4	Alta
0,2-0,4	Normal
0,2	Baja

Figure 4. Biodegradability Table of Wastewater. Source: (Cledera Castro, 2022).

Due to the anaerobic nature of AD processes, BOD₅ cannot be used to measure the pollutant loading of the various liquid samples, being an essential parameter in water treatment. However, COD is used to characterise said samples and as a proxy to estimate Total Organic Carbon through the NMOC method (van Lier, Mahmoud, & Zeeman, 2020) if the methane content of the biogas is known.

1.2.4.4. Total Organic Carbon

Total Organic Carbon (TOC) represents the most widely used method to determine the total carbon found in organic compounds in the sample (Whitehead, 2021). As such, it represents the carbon susceptible of being digested in the AD process, permitting the calculation of the C/N ratio.

It is also considered a more direct measurement to determine the organic content of wastewater with smaller environmental impacts, as it does not require the use of chrome compounds, unlike COD. As a result, it is currently under review to use as a substitute in industrial water treatment processes (Marin Galvín, 2017).

1.2.4.5. *Total Nitrogen*

As previously mentioned, nitrogen plays a key role in AD, specifically nitrogen found as ammonia (Morozova, Nikulina, Oechsner, Krümpel, & Lemmer, 2020). Ammonia dissolved in the digestion medium can have a positive or negative effect based on the concentration levels. At low concentrations, ammonia presents a buffer against acidification caused by VFA and promotes bacterial growth (Zhang C. , Su, Baeyens, & Tan, 2014).

However, higher concentrations of ammonia (AN) may result in the inhibition of the acetoclastic methanogenesis due to their higher sensitivity.

The remaining nitrogen can be found in various organic compounds such as proteins and amino acids, being thus referred to as organic nitrogen (ON). To facilitate measuring, the total nitrogen (NTK) and used as part of the C/N ratio which governs AD (Morales Polo, Co-Digestión anaerobia y pretratamiento de residuos agroalimentarios con fangos UASB de depuradora, 2019).

1.2.4.6. *C/N Ratio*

Proven to be the governing parameter in anaerobic digestion, it is the quotient between TOC and NTK. This ratio represents the balance required to promote bacterial growth and thus biogas generation. The optimal value varies depends on the substrate and the feed used, although the consensus is that the optimal range is [20-30] (Zhang C. , Su, Baeyens, & Tan, 2014) or [25-35] (Akratos, Tekerlekopoulou, Vasiliadou, & Vayenas, 2017).

It must also be mentioned that the C and N are obtained from different elements, as substrates (particularly sludges) are typically rich in organic matter but poor in nitrogen content because of water treatment processes, which presents a restrictive limit on nitrogen emissions.

On the contrary, feeds used in co-digestion such as purines and food waste present high N content.

1.2.4.7. *Density*

Residue density represents one of the primary characteristics of a residue, along with the aforementioned biodegradability. Its importance resides on its classifying nature and therefore impacts the types of treatments used.

Regarding AD processes, (Caicedo, et al., 2017) analysed the effect of density on the digestion of Municipal Solid Waste (MSW). They determined that sludges and mixes with a higher density than that of water (around 1000 kg/m³) may inhibit methanogenesis, indicating an inverse relation between both variables. This results backs previous studies such as (Petchsri, Towprayoon, Chairasert, & Nopharatana, 2004), which estimated optimum methane production with a density of 600 kg/m³.

The impact of density was also shown to be most significant during the first 30 days of the process, increasing the importance of controlling said variable in short-lived reactors.

Lastly, density also affects VFA and TOC variation within the reactor's mixture. The results showed that an increase in density decreases percolation within the sludge and therefore decreases the concentration of TOC within.

1.2.5. Anaerobic Co-digestion

AD processes can be used to treat different substrates individually, in which case it is known as anaerobic monodigestion. These can also be treated in a substrate mixture of two or more components in a process known as anaerobic co-digestion. This is the AD process studied in this project.

During co-digestion processes, a substrate-feed mixture is used to generate biogas. These must complement each other, depending on the composition of each. In the case of this study, the mixture used was Municipal Solid Waste (MSW) and wastewater treatment sludge.

Contrary to mono digestion processes, co-digestion presents several advantages which make it a viable alternative as well as the designated process to be used in biomethane generation according to the National Energy and Climate Plan (Ministerio para la Transición Ecológica y el Reto Demográfico, 2020) (Ministero para la Transición Ecológica y el Reto Demográfico, 2022). These official documents also include an illustration displaying the viability of different AD substrate as well as that of a mixture, shown below in Figure 5.

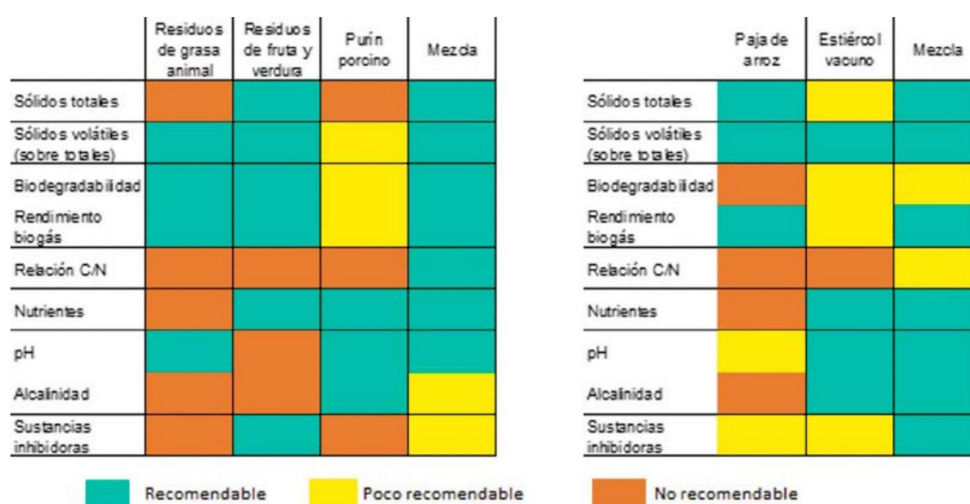


Figure 5: Substrate and Technical Parameters Relation. Source: (Ministero para la Transición Ecológica y el Reto Demográfico, 2022).

A mixture of the various MSW, rural waste (animal fat and animal slurry) and wastewater sludge is shown to be the best substrate to use in AD processes, having the preferred characteristics for all technical criteria save for alkalinity due to organic MSW and rural waste and inhibitors from rural waste (both sources).

Another mixture utilizing animal slurry and agricultural waste (rice crop residue) would not be preferable based solely on biodegradability from the lignin content of found in the rice crop and the C/N ratio as animal slurry has a remarkably high nitrogen content.

By mixing different residues, their compositions may be used to complement each other by increasing the carbon content in the final mixture to a preferable level or by diluting inhibitors such as the volatile fatty acids. In addition, this allows for the centralization of the treatment facilities and processes.

Also, utilizing a mixture compensates for the seasonal variations found in different residues and their compositions, especially in MSW, whose organic content varies significantly between summer and winter (Morales Polo, Residuos Sólidos Urbanos, 2022). The possibility to increase biogas generation by using otherwise spent substrate is still being researched.

1.3. Project Objectives

To achieve valid results & determine real world applications, the project will be divided into 2 distinct areas, pertaining the co-digestion study & application designs, respectively. Therefore, the following objectives were determined:

1. Sludge characterization: Sludge composition varies between digesters from different reactors, depending on the nature of the treated residual water. Furthermore, this will also affect the doses of nanoparticles used, as certain components may inhibit bacterial growth & negatively affect the digester.
2. Characterization of nanoparticles: The nanoparticles must be analysed to determine their elemental composition. Approximate estimates provided by the manufacturer suggest a 55% C content & 45% Fe content. However, an analysis must be performed to determine the exact Fe content.
3. BMP tests: The first set of tests required to assess the effects of the aforementioned nanoparticles is the standardized BMP tests. These will be used to determine the initial biomethane & hydrogen generation in small batches. Due to their nature, the generated biogas will be sampled with a syringe through a septum and the volume produced will be measured indirectly.
4. Batch reactor tests: Once the sludge & feed mixture has been characterized through the previous tests, the reactor tests can be performed. These will maintain the same ratios used in the BMP tests. However, the volume measurement will be continuous through the use of gasometers. Several tests will be performed to determine the optimal nanoparticle dosage.
5. Continuous reactor tests: The last set of tests to be performed will take place in a custom built 5 litre reactor to determine the sludge's behaviour & viability in continuous operation aimed at resembling industrial anaerobic digestions. As a side requirement, the appropriate equipment not found in the Chemistry Lab must be procured.

These objectives finalise the lab tests to be performed in the study. The remaining objectives will focus on the analysis of the results as well as the possible applications of anaerobic co-digestion.

6. Assess the viability of biomethane as a substitute for natural gas: As mentioned in previous sections, biogas is a potential substitute for natural gas. In order to qualify as such, it must fulfil certain criteria based on European legislation (European Parliament, European Council, 2018). Consequently, a comparative LCA study will be performed to determine said possibility. The details of said study will be expanded upon when more primary source data has been collected to avoid the over reliance on existing databases. Improving the modelling, as the process will be represented in a more faithful manner. It must be pointed out that due to scheduling issues, this objective could not be met.
7. Design biogas plants: The last objective focuses on the real-world applications of the biogas, in keeping with the Chair's focus. Due to the versatility of biogas, two scenarios will be analysed from an economic & an energetic perspective. The first design will focus on a co-generation plant based on an internal combustion engine. The second option will consider a co-generation plant with upgrading to obtain biomethane. In both cases, tri-generation may be considered if the analysis permits further energy recovery and time permits it. It must also be added that in both cases they design will be based on the guidelines set in the existing legislation (Ministerio de Industria, Energía y Turismo, 2014).

1.4. Motivation

As seen in the previous sections, AD research has seen great advancement in recent years in various directions. However, anaerobic co-digestion has been identified as a viable alternative to turn AD reactors into self-sufficient processes.

Within the University and particularly as part of the Rafael Mariño Chair in New Energy Technologies (Universidad Pontificia Comillas-ICAI, 2021) there has been extensive research in anaerobic co-digestion, which peaked with (Morales Polo, Co-Digestión anaerobia y pretratamiento de residuos agroalimentarios con fangos UASB de depuradora, 2019) as a doctoral thesis. Further research has also been performed to move from the BMP & FW analysis to bigger reactors in the Chemistry & Environment Laboratory at the University with the ultimate goal of creating a small-scale continuous pilot plant. AD can also be boosted through the use of new materials such as nanoparticles to increase biogas production, although more research is needed to determine their possible contributions.

Furthermore, as previously stated the increasing importance of decarbonisation to combat climate change requires the development of new technologies capable of replacing fossil fuels in general, and methane in particular, which has become one of the pillars to drastically reduce yearly emissions in developed regions such as the EU & US.

AD also present the capability of producing either biomethane or green hydrogen, depending on the plant designed downstream from the reaction. This new hydrogen production technique is a natural replacement for current H₂ processes, which obtained it by reforming methane (Linares Hurtado J. , 2021). To adapt said existing chemical plants biogas would need to be upgraded before entering the plant. Otherwise, no other major modifications would be required.

In addition, AD can also be used to serve as a local waste treatment solution to reduce polluting emissions, particularly those affecting superficial & ground water. The biogas can be used in co-generation plants to produce heat and electricity, reducing resource intensity & primary energy usage within the industrial sector.

The impulse which biogas has been receiving recently through European and national initiatives as part of the European Green Deal and the Biogas National Plan previously describe represent an opportunity to start research in a nascent field with critical importance by 2030, not only in energy generation and waste treatment, but also as a tool capable of furthering the transformation into a circular economy.

As a result, AD is currently a field in which much research is required to create new solutions to the ecological transition by 2030, with increasing support from institutions which has resulted in the creation of dedicated research networks and collaborations between universities. Moreover, the University has a stablished background on this topic, which can be drawn upon and eventually expanded by developing standardised methodology for current and future projects as well as evaluating the viability of proposed technologies such as the aforementioned nanoparticles.

Chapter 2: Methodology

This research Project aims to determine the effects of C-Fe nanoparticles on anaerobic digestion reactors. Therefore, a stablished methodology will be followed where stablished, and a new one will be developed if there are none available to ensure results are consistent & reliable.

2.1. Resources Required

The study was performed in the Chemistry & Environment Laboratory located in ICAI's first floor. As a result, the equipment found in the lab was used to perform the study. Certain components had to be ordered, namely the semi-continuous reactor's original 5-litre jacketed vessel and its supporting equipment, although due to a delay in shipment it could not be utilised in the experimental runs.

Firstly, all reactions were performed in sealed reactors or bottles, depending on the research stage. The first experiments were those performed to assess the sludge's BMP using the existing 1-litre, 10-bar bottles used in (Morales Polo, Co-Digestión anaerobia y pretratamiento de residuos agroalimentarios con fangos UASB de depuradora, 2019) with their respective caps and septums, which can be seen below in Figure 6. The samples were incubated in the Optic Ivymen System's Orbital Shaker Incubator (Comecta, 2022). This incubator was be used to agitate & maintain a constant temperature, up to 9 bottles, limiting batches to said number. The Orbital Incubator can be seen below in Figure 7. The pressure inside the BMP bottles was measured using an in-house custom-built barometer with a range of 0-2 bar with a needle to pierce the septum shown in

Figure 8: Custom-Built BMP Bottle Barometer. Source: Own. Figure 8



Figure 6. BMP Batch Bottle Resealed with Silicone Paste. Source: Own.



Figure 7: Ivymen Incubator. Source: Own.



Figure 8: Custom-Built BMP Bottle Barometer. Source: Own.

The remaining experiments were performed in sleeved reactors 2-litre (Scharlab, 2021). Furthermore, both the batch & the semi-continuous reactors required auxiliary equipment for operation & sampling. Due to their size, temperature inside the reactors will be maintained using Digiterm-TFT-200 (J.P. Selecta, 2021) immersion circulator along with their thermal set inside the reactor, pictured below in Figure 9. The reactors were also be equipped with paddle attachments to stir the digester mixture, moved by the Scharlau MiniReactor motor, provided with the 2-litre vessels. Lastly, the semi-continuous reactor also required the use of the Hei-FLOW Precision 01 peristaltic pump to ensure feed supply during operation, shown in Figure 10.



Figure 9: TFT-200 Thermostat. Source: Own.



Figure 10: HeiFLOW 01 Peristaltic Pump. Source: Own.

As previously mentioned, reactor tests will have live, direct biogas production measuring as opposed to the indirect method used for the BMP tests. Therefore, 2 Ritter MilliGascounters (Ritter, 2022) were be employed. These were attached to the sampling port through a three-way valve which will also be used to obtain biogas samples. Lastly, the reactor's pH will be measured using the XS pH70 pHmeter (Scharlab, 2022) as well as its 130mm long probes found in the lab & the ordered 250mm probe. The MilliGascounters can be seen below in Figure 11 and the pHmeter in Figure 12.



Figure 11: Ritter MilliGascounters. Source: Own.



Figure 12: XS pH70 pHmeter. Source: Own.

Gas samples were analysed with the Agilent 7820A gas chromatographer (Agilent Technologies, 2011) with nitrogen gas (N_2) as the carrier, shown in Figure 13. Samples were retrieved using the syringe provided with the chromatographer. Lastly, supernatant samples were tested using the HANNA HI 902 Potentiometric Titrator (Laboquímica, 2022) to determine their VFA content, seen below in Figure 14. Similarly, other properties such as the total nitrogen and the COD will be obtained using the Spectroquant Prove 100 spectrometer (Merck, 2022) also found in the Chemistry lab.



Figure 13: Agilent 7820A Gas Chromatograph. Source: Own.



Figure 14: Hannah HI902 Potentiometric Titrator. Source: Own.



Figure 15: Spectroquant 100 Spectrometer. Source: Own.

Lastly, numerical analysis will be based on MATLAB (MathWorks, 2021) scripts.

2.2. BMP Batch Bottles Design & Set Up

The first set of tests were BMP tests. These were performed as per the guidelines set in the norm ISO 11734:1999 (AENOR, 1999), employed in previous research (Morales Polo, Co-Digestión anaerobia y pretratamiento de residuos agroalimentarios con fangos UASB de depuradora, 2019) which this project was based on. This Norm required the use of sealed 1-litre bottles in which 300ml of a sludge-substrate mixture was sampled for 21 days, collecting daily pressure readings and releasing said pressure after the sampling process had finished. The bottles were closed using a septum and silicone paste.

To create said bottles, these were first cleaned to prevent sample contamination. Once cleaned, they were filled with the required volumes of substrate, sludge, and water in the proportions required.

Prior to sealing each bottle, the air contained inside was replaced with N_2 . In keeping with previous research, the sludge-feed proportion was set at a 3:1 ratio (Morales Polo, Co-Digestión anaerobia y pretratamiento de residuos agroalimentarios con fangos UASB de depuradora, 2019). Also, a 50% humidity was required (FCC, 2021), which set another constraint on the vessel composition. The final proportions were calculated using the following formulae. The results were collected in Table 2. It must also be mentioned that the sludge was stabilised for a week in an oven prior to use, as seen in REF.

$$V_{water}[l] = 0.5 * V_{Total}[ml]$$

$$V_{sludge}[l] = 0.375 * V_{Total}[ml]$$

$$V_{substrate}[l] = 0.125 * V_{Total}[ml]$$

Table 2: BMP Bottle Co-Digestion Mixture. Source: Own.

Variable	Value
V_{Total} (ml)	300.0
V_{water} (ml)	150.0
V_{sludge} (ml)	112.5
$V_{substrate}$ (ml)	37.5

To create the substrate mixture, the pumpkin used as substrate was first cut into 1 cm cubes and processed in a food processor without the addition of liquid to reduce their size to about 3 mm pieces. The process can be seen below in Figure 16. It must be noted that the pumpkin was cored but not peeled.

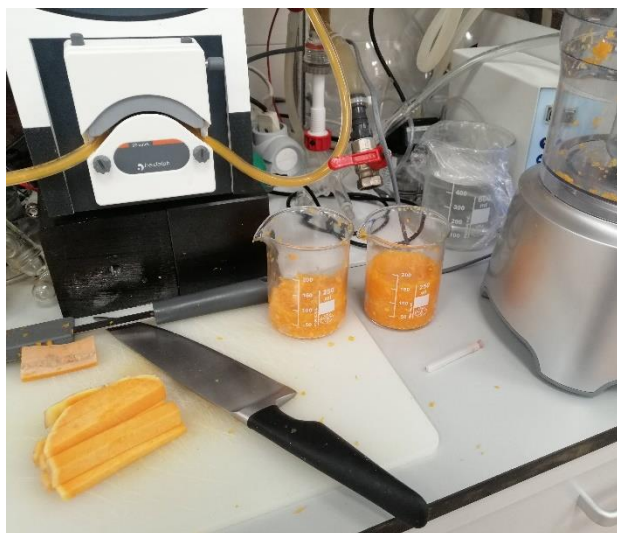


Figure 16: Initial Substrate Processing. Source: Own.



Figure 17: Sludge in Oven. Source: Own.

Once the samples were prepared, nitrogen gas was injected on top of the mixture for 5 minutes to remove the air inside the bottle, replacing it with an inert gas which would not interfere or affect the AD process. Lastly, bottles were sealed with their respective septum and silicone paste was added to reinforce the seal. Two images of said BMP bottles are provided in Figure 18 and Figure 19.



Figure 18: Prepared BMP Bottle. Source: Own.



Figure 19: Sample BMP Bottle. Source: Own.

Moreover, to replicate semi-continuous testing at a bottle scale, 2 BMP bottles were modified utilizing a cap with valves to permit the replicate the sampling port and the feeding port. To that end, the feeding port's inner adapter was fitted with a tube to facilitate feeding and sample extraction. The final bottles along with the are shown in Figure 20 and Figure 21. The design diagram is shown in Figure 22.



Figure 20: Prepared Semi-Continuous BMP Bottle.
Source: Own.

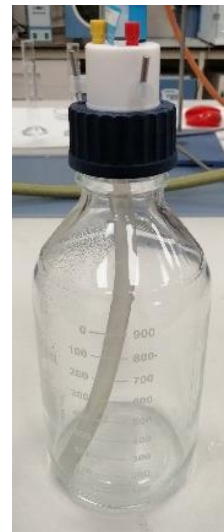


Figure 21: Sample Semi-Continuous BMP Bottle. Source:
Own.

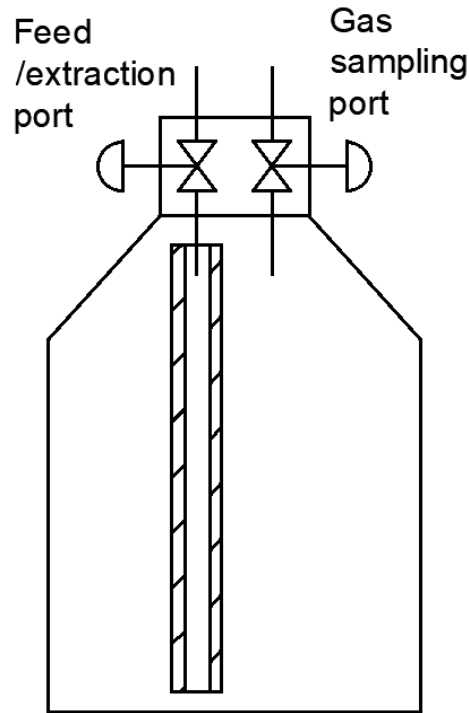


Figure 22: Semi-Continuous Bottle Design. Source: Own.

Lastly, it must be mentioned that the semi-continuous bottles require refinement for future tests as all samples were inhibited early in the run. As a result, no useful data could be extracted from said bottles.

To incubate the samples during testing, the Optic Ivymen System's Orbital Shaker Incubator (Comecta, 2022). This incubator can be used to agitate & maintain at a constant temperature up to nine bottles, limiting batches to said number. To maintain the mesophilic temperature range, the target was set at 38.0°C. The incubator can be seen in Figure 23.



Figure 23: Optic Ivymen System's Orbital Shaker Incubator during testing. Source: Own.

2.3. Batch Reactors Design & Set Up

The second set of experiments were the Batch Reactors, which represent a larger version of the standard BMP tests. As a result, the same formulae were applied to determine the volumes required in the 2-litre jacketed reactors. The results are shown below in Table 3.

Table 3: Batch Reactor Co-Digestion Mixture. Source: Own.

Variable	Value
V_{Total} (ml)	2000.0
V_{water} (ml)	1000.0
V_{sludge} (ml)	750.0
$V_{\text{substrate}}$ (ml)	125.0

The larger vessel also required some changes in the design. The first and most relevant was that of temperature control and agitation. The BMP bottles were kept at 38°C through the use of the incubator. In this case, the reactors were jacketed, which permitted the use of external Digiterm TFT-200 thermostats to control temperature (J.P. Selecta, 2021), which included an immersion pump to circulate the heated water. These baths required the use of a temperature probe inserted into the reactor.

Additional changes required were the use of external agitation, achieved by utilising a stirring rod with a welded paddle attachments to stir the digester mixture, moved by the Scharlau MiniReactor motor provided with the reactor. The thermal probe & the stirring pale and its fitting are shown in Figure 24.

In addition, to connect the previously mentioned Ritter MilliGascounters (Ritter, 2022), a three-way valve system was developed to permit biogas sampling and direct production measurement from the same outlet. In this case, the valve would be set to direct the flow to the MilliGascounters, only switching the active outlet to obtain samples with the syringe. The construct is shown in Figure 25.



Figure 24: Batch Reactor Components I. Source: Own.



Figure 25: Three-Way Sampling Valve. Source: Own.

It should also be noted that the lid permitted the insertion of the pH probe. In the case of the Batch Reactors, the 130 mm probe was used. It was fitted through a glass sleeve with 2 O-rings to ensure an airtight seal. The sleeve itself was fitted to the black cap shown in Figure 26. The remaining port was used to feed the mixture into the reactor and remained sealed throughout the experiment, shown on the left side of Figure 26. It must also be mentioned that all the fittings in the reactor were sealed with Teflon and vacuum grease on their threads. The frosted adapters on the keys were also sleeved with Teflon. This created hermetic seals throughout the reactor, except for the stirring rod which could not be sealed.



Figure 26: Batch Reactor Components 2. Source: Own.



Figure 27: Batch Reactor Components 3. Source: Own.

Lastly, the vessel was secured to its stand with the use of a neck clamp which also doubled as the seal between the body and the lid, these are shown in Figure 27. All the reactor components are shown in Figure 28 and the final set up in Figure 29.

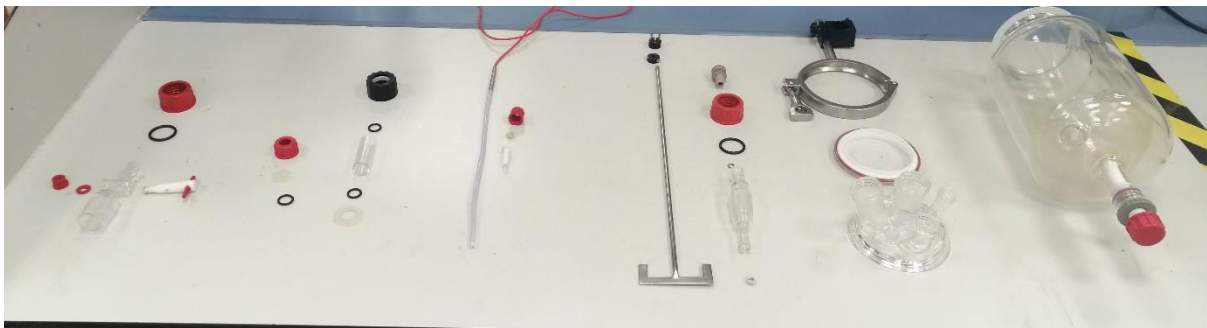


Figure 28: Batch Reactor Complete Components. Source: Own.



Figure 29: Final Batch Reactor Set-up. Source: Own.

2.4. Semi-Continuous Reactor Design & Set Up

The last experiment to be performed was that of the semi-continuous reactor. Similar to the Batch Reactor, this test had its equivalent bottle, in this case the semi-continuous bottles previously designed.

In addition, the scaled reactor presented its unique characteristics and design challenges, primarily to accommodate the larger volume of AD-mixture as well as the support equipment, which was identical to that of the Batch Reactor with one exception. The previously unused port was replaced by a septum modified in a similar way to that of the pH probe. This modified port was used to fit the feeding hose which extended from the substrate reservoir to the vessel through the Heidolph Hei-FLOW Precision 01 (Heidolph, 2022) peristaltic pump, which provided the hermetic seal. A detailed view of the modified pH port can be seen in Figure 30 and Figure 31. The red inlet port was modified in an identical way.



Figure 30: Detailed pH Port Fitting. Top View. Source: Own.



Figure 31: Detailed pH Port Fitting. Side View. Source: Own.

Lastly, to achieve the semi-continuous behaviour and control the digestate outlet, the reactor's bottom port received a spheric valve to extract the daily amount required. The design diagram appears in Figure 34. Also, the reactor was fitted with the 250 mm probe seen in Figure 32. The final set-up can also be seen in Figure 33.



Figure 32: 250 mm pH Probe. Source: Own.



Figure 33: Final Semi-Continuous Reactor Set-Up. Source: Own.

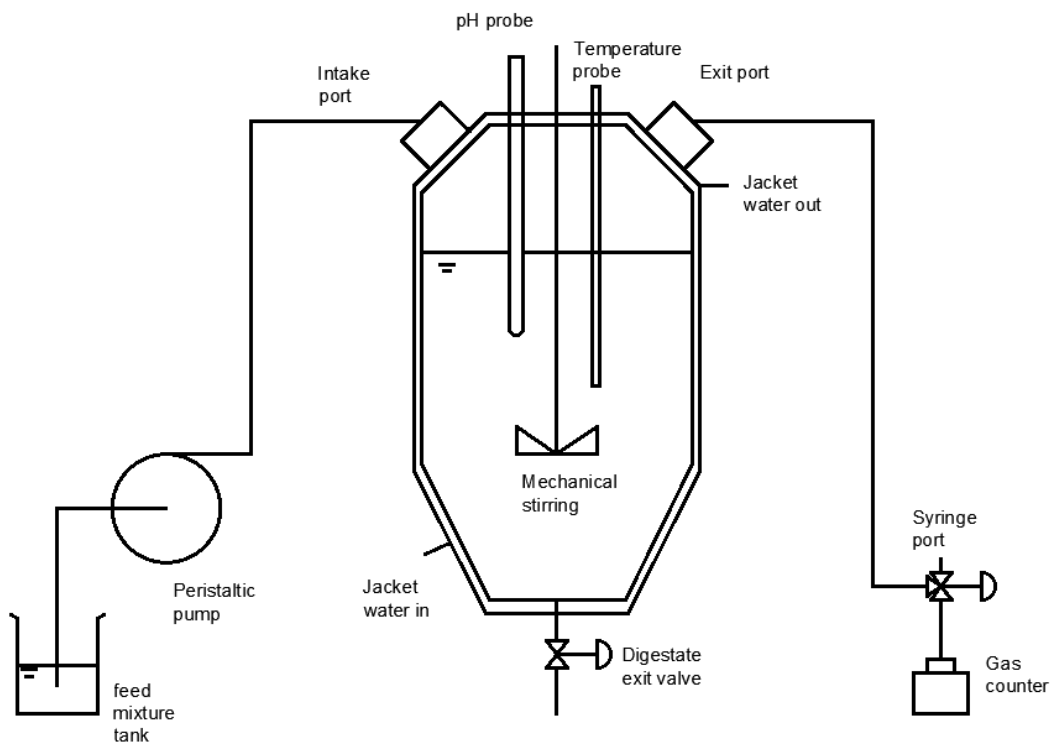


Figure 34: Semi-Continuous Reactor Design Diagram. Source: Own.

2.5. Nanoparticle Dosing and Addition

2.5.1. Nanoparticle Dosage Calculation

To determine the required dosage of nanoparticles and administer those to the appropriate samples, an analytical procedure was developed to ensure consistency and prevent error. The process consisted of several steps explained in this section.

Firstly, the sludge had been analysed to obtain the percentage of volatile solids found within it. These were calculated as a percentage of the total sludge mass inserted (Morales Polo, Co-Digestión anaerobia y pretratamiento de residuos agroalimentarios con fangos UASB de depuradora, 2019):

$$SV [\%] = \frac{m_{SV}}{m_{total}}$$

Therefore, before measuring the required mass of nanoparticles, the sludge mass inserted into each vessel had to be determined. As the process is based on added volumes, the density was estimated during the initial set up. To do so, 100ml of sludge were sieved to remove free liquid, shown in Figure 35.



Figure 35: Sludge Filtering to Determine Density. Source: Own.

Once the total measured volume was acquired, the sample was weighed to determine its mass and therefore its density, as shown in Figure 36.



Figure 36: Filtered Sludge Weighing. Source: Own.

With both datapoints collected, the sludge's density could be used to determine the mass of sludge inside each vessel type along with the total volatile solids in them. Similarly, the recommended dosage of nanoparticles was 2grNP/2kgsSV, permitting the calculation of the required nanoparticles.

$$\rho_{sludge} \left[\frac{kg}{m^3} \right] = \frac{m_{sludge} [gr]}{100ml} * \frac{10^6 ml}{1m^3} * \frac{1kg}{1000 gr}$$

$$m_{sludge} (kg) = V_{vessel} [l] * 12.5\% * \rho_{sludge} \left[\frac{kg}{m^3} \right] * \frac{1m^3}{1000 l}$$

$$m_{sludge_{SV}} (kg_{SV}) = m_{sludge} (kg) * SV$$

$$m_{NP} [gr_{NP}] = 2 \frac{gr_{NP}}{kg_{SV}} * m_{sludge_{SV}}$$

The results for each vessel type are shown below in Table 4.

Table 4: Nanoparticle Addition Calculations. Source: Own.

Variable	Value
V _{sludge} (ml)	100
m _{sludge} (gr)	100.68
ρ _{sludge} (kg/m ³)	1006.8
SV (%)	6.1403
V _{BMP} (l)	0.3
V _{reactor} (l)	2.0
m _{BMP} (kg)	0.0378
m _{reactor} (kg _{SV})	0.2517
m _{SVBMP} (kg _{SV})	2.318*10 ⁻³
m _{SVreactor} (kg)	15.4551*10 ⁻³
m _{NPBMP} (gr _{NP})	4.6365*10 ⁻³
m _{NPreactor} (gr _{NP})	30.9103*10 ⁻³

2.5.2. Nanoparticle Addition Method

Once the required dosages were determined, the addition method was developed, as nanoparticles did not form a persistent solution in water and precipitated to the bottom of the container. It was decided that the best method to solve this issue was to forcibly dissolve the required nanoparticles into pure water utilizing the sonicator found in the laboratory.

Therefore, the first step in the process was to determine the nanoparticle concentration within the solutions to facilitate injection. After certain consideration, it was decided that a concentration of 1gr_{NP}/l would be the most useful, as it would simplify the solution volume measurement when injecting. The resulting volumes required are shown below in Table 5.

$$V_{solution} [ml_{sol}] = m_{SV} [gr_{NP}] * \frac{1l}{1gr_{NP}} * \frac{1000ml}{1l}$$

Table 5: Nanoparticle Solution Calculations. Source: Own.

Variable	Value
m _{NPBMP} (gr _{NP})	4.6365*10 ⁻³
m _{NPreactor} (gr _{NP})	30.9103*10 ⁻³
V _{BMPsol} (ml _{sol})	4.6365
V _{reactorsol} (ml _{sol})	30.9103

Proceeding with the solution; the first step was to fill a 1-litre precision volumetric flask to its line with distilled water, measuring thus the required volume and transferring said volume into a graduated cylinder to facilitate sonication, as shown in Figure 37 and Figure 38 respectively.



Figure 37: Volumetric Flask Filling. Source: Own.

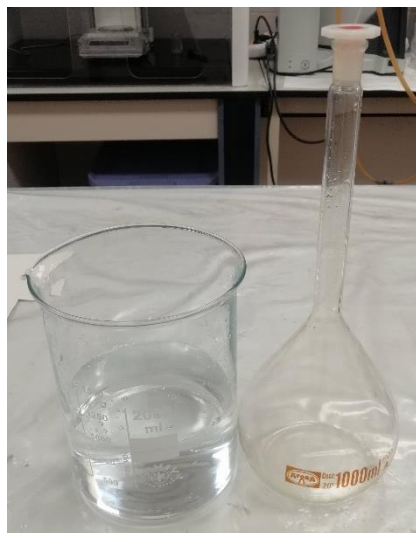


Figure 38: Transferred Distilled Water. Source: Own.

The following step was to measure the required mass of nanoparticles, which was performed with the use of a precision scale, as displayed in Figure 39. Once the required mass of 1 gram was measured, it was added to the graduated cylinder. Finally, the mixture was sonicated with the following parameters shown below in Figure 40. After sonication, the solution was degassed in a sonic bath for 10 minutes. The calculations are shown in Table 6.



Figure 39: Nanoparticle Measurement. Source: Own.



Figure 40: Nanoparticle Sonication. Source: Own.

Table 6: Sonication Parameters. Source: Own.

Variable	Value
t_{Total} (min)	15
t_{ON} (sec)	30
t_{OFF} (sec)	10
Amplitude (%)	50%
t_{degas} (min)	10

Lastly, the required solution volume was added into the preparation of the substrate mixture.

2.6. Daily Sampling & Reactor Feeding

Once the various reactors and bottle were prepared, the experiments were initiated on a Monday, as previously stated. Therefore, this Section focuses on the methodology and procedures used to sample the various vessels used for the experiments, as well as the equipment used to perform it. It must also be noted that the vast majority of said test were performed on the reactors and BMP bottles, although those that required liquid from the reaction vessel were performed primarily on the semi/continuous reactor, which was the only one designed to allow for extraction during operation.

It is also important to note that the experiments were started on a Monday to ensure that the start-up and stabilization process, which lasted from days 1 to 3 was continually monitored. Not doing so could have resulted in anomalous results or the loss of a bottle due to overpressure.

2.6.1. BMP Bottles Generic Tests

The BMP bottles, both the semi-continuous & batch experiments required daily measurements of their internal pressure and the composition of the biogas produced. In addition, the semi-continuous bottles also required daily sampling of their Volatile Fatty Acid concentration. The process is described in the Semi-Continuous Vessel Tests Section along with several other tests which were performed daily on the semi-continuous reactor.

2.6.1.1. BMP Batch Bottles Pressure & Biogas Sampling

As previously stated, BMP tests are performed on sealed 1-litre bottles, allowing the biogas to build up inside them for collection and analysis. These bottles were sampled daily to indirectly measure the moles of biogas produced through the ideal gas law (ChemTalk, 2022).

This was possible because the conditions inside the bottles were known, as well as the free volume inside them was measured beforehand to be 1.370,50 ml. Furthermore, as the volume of the sludge-feed mixture was measured to be 300 ml, the free volume inside the bottle was known (1.007,50 ml). In addition, the temperature inside the bottles was also controlled by the Ivymen orbital shaker incubator, which was set at 38°C, as previously explained. As a result, the following formula can be used to obtain the moles of biogas produced:

$$P * V = n * R * T \rightarrow n = \frac{P * V}{R * T} \rightarrow n [mol] = \frac{1,0075 * 10^{-6} * P [Pa]}{8,314 * (273,15 + 38)} \rightarrow$$

$$n[mol] = \frac{1,0075 * 10^{-6} * 10^5 * P[bar]}{8,314 * (273,15 + 38)} \rightarrow n [mol] = 0,041 * P[bar]$$

To obtain the pressure, the method employed in (Morales Polo, Co-Digestión Anaerobia y Pretratamientos de Residuos Agroalimentarios con Fangos UASB de Depuradora, 2019) was followed. The pressure inside the BMP bottles will be measured using an in-house custom-built digital barometer with a range of 0-2 bar with a needle to pierce the septum of the BMP bottles. Before sampling, the bottle's septum was wiped to remove the silicone paste used to secure the septum's hermetic seal once pierced, shown in Figure 41 below. This was a critical step as the paste was viscous enough to block the needle, preventing the pressure from being recorded or a gas sample retrieved. The silicone paste can be seen below in Figure 42.

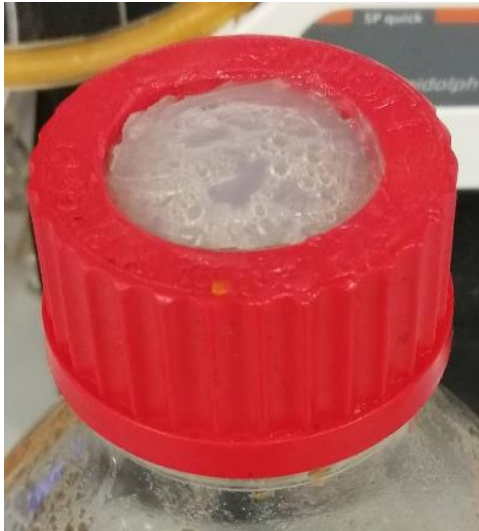


Figure 41: BMP Batch Bottle Septum Covered in Silicone Paste. Source: Own.

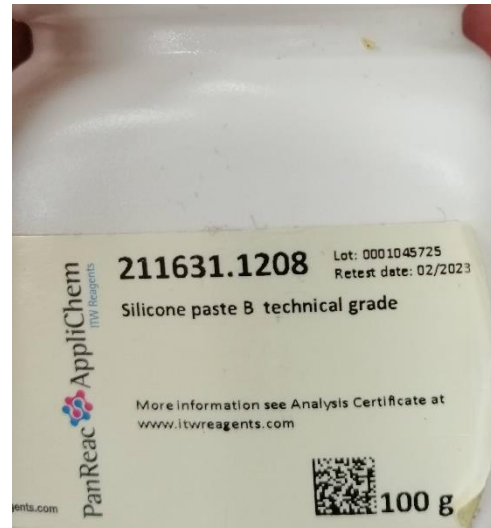


Figure 42: Silicone Paste-B Used to Seal Septums. Source: Own.

Once the septum had been cleaned, the sampling procedure was as follows: Firstly, the barometer was fitted with a 14-gauge needle, and the instrument started. The needle was installed before initiating the device to ensure that the calibration was accurate as in practice runs the needle fitting could change the pressure read. Once fitted, the needle was inserted into the bottle vertically to avoid hitting the sides of the bottle, as shown in Figure 43.

It must also be noted that the barometer had an external control unit with 2 switches used to turn on the device. The barometer's control unit is shown below in Figure 44.



Figure 43: BMP Batch Bottle Pressure Measuring. Source: Own.



Figure 44: Barometer Control Unit. Source: Own.

Once the pressure had stabilised, the reading was recorded, and the barometer removed. To allow for the retrieval of a gas sample. To obtain said sample, the chromatogram's syringe was also fitted beforehand with another 14-gauge needle.

Similarly, the septum was also pierced with said needle and the plunger in the syringe drawn to extract a gas sample. It must also be noted that in cases where the pressure exceeded around 0,150 bar, the force exerted on the plunger was enough to move it without external help. This process is shown in Figure 45 and Figure 46, before and during the biogas collection process.

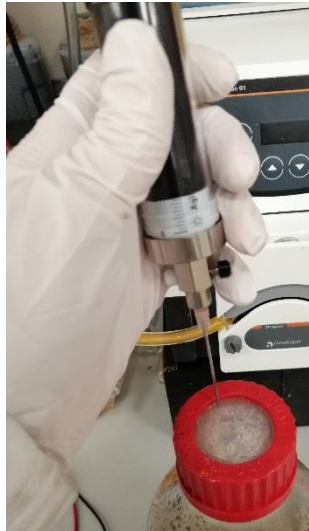


Figure 45: Biogas Sample Collection in BMP Batch Bottle.
Source: Own.



Figure 46: Biogas Sample Collection during Collection from BMP Batch Bottle. Source: Own.

Lastly, once the sample had been collected, a third needle was used to relieve the pressure inside the BMP bottles, allowing the gas to escape. Finally, the bottles were resealed with the silicone paste and placed inside the orbital incubator. These processes are shown below in Figure 47 and Figure 48, respectively.

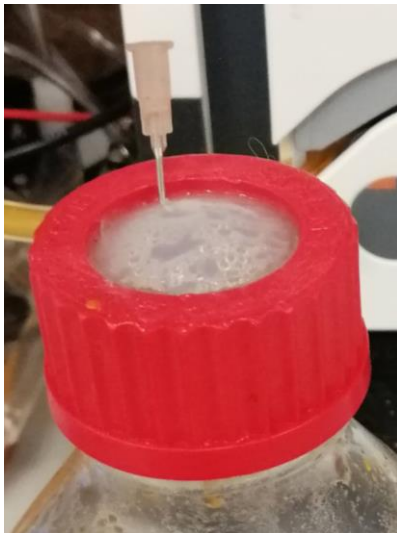


Figure 47: Depressurization of BMP Batch Bottle. Source: Own.



Figure 48: BMP Batch Bottle Resealed with Silicone Paste. Source: Own.

2.6.1.2. Semi-Continuous Bottles Pressure & Biogas Sampling

As previously stated, 2 experimental semi-continuous bottles were designed and used during the second batch of testing to obtain results which could be scaled to the 2-litre semi-continuous reactor in the same way BMP batch bottles could represent a smaller scale of the 2-litre batch reactor.

Due to their semi-continuous nature and resulting design, the process was nearly identical to the previously described sampling methodology, although simpler due to the valves which replaced the septum. It must also be noted that the bottles used were identical to those employed in the BMP tests.

With regards to the sampling methodology, the steps followed were similar to those previously described. Firstly, the bottle's pressure was measured using the barometer through the right port, following the design specifications previously described.

Additionally, the port was fitted with a threaded adapter which ensured a hermetic seal, with the barometer and the chromatogram's syringe. The pressure reading and biogas collection processes are shown below in Figure 49 & Figure 50.



Figure 49: BMP Semi-Continuous Bottle Pressure Measuring. Source: Own.



Figure 50: Biogas Sample Collection during Collection from BMP Semi-Continuous Bottle. Source: Own.

Lastly, the excess pressure was relieved through the right port prior to the bottle was replaced inside the incubator. This process can be seen in Figure 51.



Figure 51: Depressurization of BMP Semi-Continuous Bottle. Source: Own.

These were the daily measurements and samples collected from the BMP experiments. However, the semi-continuous bottles were also fed daily with a feed and nanoparticle mixture, which is described in the Semi-Continuous Reactor & Bottle-Feeding Section.

2.6.2. Generic Reactor Tests

As previously stated, sample collection and measurement of the various control variables was performed daily in all the vessels, including the reactors. In this case, the batch reactor required only a biogas production and biogas sampling, while the semi-continuous reactor required additional tests, as previously stated, detailed in other sections.

2.6.2.1. *Reactor Biogas Production & Sampling*

Similarly, to the bottles previously described, the measurement of biogas produced and the sampling of said gas was performed daily. The reactor design allowed for the direct measurement of biogas production, as opposed to the BMP bottle tests, which required the use of the indirect method.

Therefore, the exit port previously described was fitted with a 3-way valve to permit said processes. It must also be noted that the Ritter milligasometer used functioned correctly during the first few days through it.

However, the milligasometers stopped recording the volume of biogas produced due to the head losses resulting from the length and diameter of the tube connecting the device to the valve paired with the decrease in biogas production as the vessels stabilised.

As per the manufacturer's specifications, a 1-metre-long tube with an internal diameter of 4mm was used. The length of the tube was preestablished by the manufacturer to allow for the biogas to cool down to room temperature. The milligasometer can be seen in operation below in Figure 52



Figure 52: Milligasometer in Operation. Source: Own.

This problem has been thoroughly reviewed and improvements have been proposed in the Conclusions Section of this document to solve this issue which had such a profound effect on the experiment that it prevented any modelling and use of the vessel results, as production rate could not be established. This issue is further discussed in the Results Section of the document.

Biogas sampling was performed through the 3-way valve by setting the exit port to the one without the plastic tube fittings. To procure a sample, the syringe was fitted into the port exit and a sealed was ensured. After the port was opened, 75ml of gas was extracted as a purge to prevent any cross contamination from outside air, closing the valve between the 3 purges. Once the purging process was completed, the syringe was again inserted, and the sample collected.

2.6.2.2. *Reactor pH Measurement*

In addition to gas related tests, the reactors were fitted with pH probes to record its evolution throughout the experiment and to use it as an indicator of possible acidification. It is also worth mentioning that only 1 pHmeter was available while 2 probes were required. As a result, the meter was calibrated to the longer 250 mm probe, inserted into the semi-continuous reactor, while the shorter 130 mm probe required a linear adjustment. The reference values for said adjustment in both batch reactor can be found below in Table 7 and graphically in Figure 53.

Table 7: pH Calibration Table. Source: Own.

Parameter	Value
pH 7 RB reading (-)	7.32
pH 4 RB reading (-)	4.35
pH 7 RNP reading (-)	7.34
pH 4 RNP reading (-)	4.42
pH 7 target (-)	7.00
pH 4 target (-)	4.01

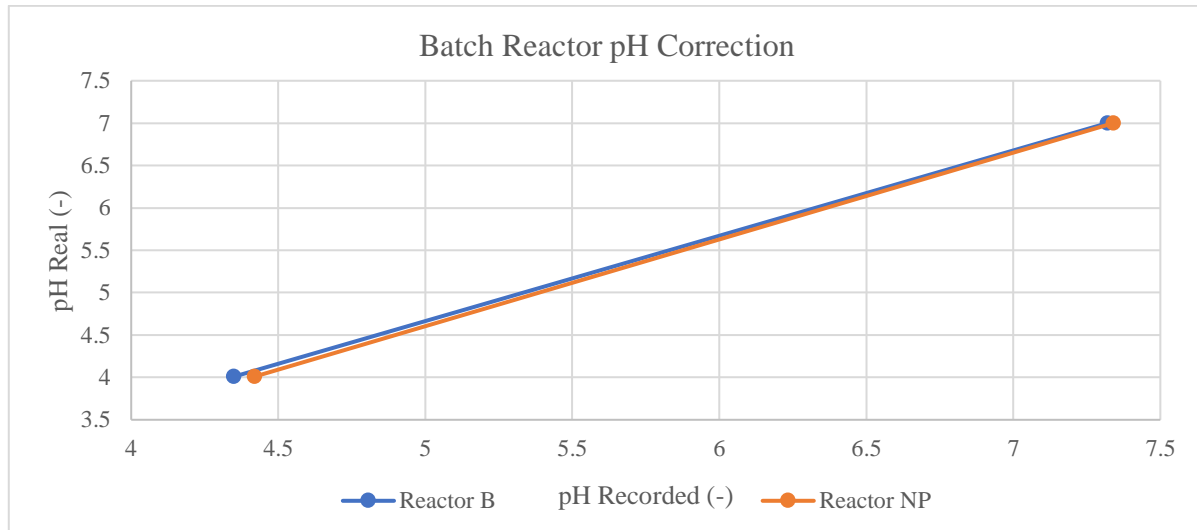


Figure 53: Batch Reactor pH Correction. Source: Own.

2.6.3. Semi-Continuous Tests

In addition to tests performed on all experiments, semi continuous reactors also permitted other tests to be performed on their extracted volumes. These tests consisted of the analysis of VFA within the extracted volume as well as the COD and NTK of said vessels. As semi-continuous test required a 21-day residence time, maintaining the original experiment duration. This required the daily extraction and later injection of 95,24 ml of digestate and feed mixture.

2.6.3.1. Volatile Fatty Acids Test

The first test performed on the supernatant from the extracted samples was a measurement of the alkalinity within the reactor. As previously stated, this test was found in (Morales Polo, Co-Digestión anaerobia y pretratamiento de residuos agroalimentarios con fangos UASB de depuradora, 2019) as a variation of (Tran, 2017). This method is based on a two-stage titration which can be performed using 2 different acids. HCl and H₂SO₄ were employed with 0.05 N and 0.1 N, respectively.

The first stage in the titration employed HCl to reduce the pH to 5.75 as per the norm. The volume and final pH were also recorded. The next step in the process was the final titration utilising the H₂SO₄ until the target of 4.3 was reached. These were V₁ and V₂, respectively. These measurements were then used to determine Partial (AP), Intermediate (AI) and Total Alkalinity (AT), using AI to measure VFA:

$$AP \left[\frac{mgCaCO_3}{l} \right] = \frac{V_{HCl} * N_{HCl} * 5000}{V_{sample}}$$

$$AI \left[\frac{mgCaCO_3}{l} \right] = \frac{V_{H_2SO_4} * N_{H_2SO_4} * 5000}{V_{sample}}$$

$$AT \left[\frac{mg_{CaCO_3}}{l} \right] = Ap + AI = \frac{(V_{H_2SO_4} * N_{H_2SO_4} + V_{HCl} * N_{HCl}) * 5000}{V_{sample}}$$

The procedure to produce the samples was as follows: 25ml of the filtered supernatant were collected with a pipette and diluted into 25ml of distilled water to facilitate titration. This was accounted for in the formulae by only considering the 25 ml of recovered sample. Once correctly mixed, the titration process was initiated by pressing the “Start button,” having selected the correct method and acid pump. A sample of supernatant during testing can be seen in Figure 54, while Figure 55 shows the acid pumps. A detailed guide on can be found in Anejo III: Hannah HI 902 Potentiometric Titrator Manual.

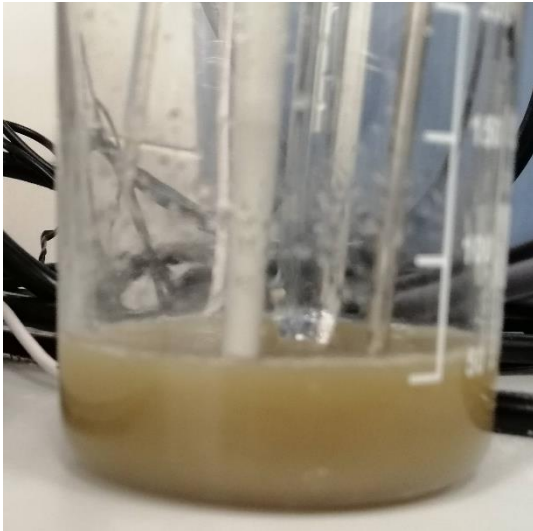


Figure 54: VFA Titration. Source: Own.



Figure 55: Acid Pumps Used during VFA Testing. Source: Own.

Another aspect worth mentioning is that the semi-continuous bottles required a more complex method to extract the daily sample. In their case, a syringe was fitted to the sampling port and used to suction the required dosage, as shown in Figure 56.



Figure 56: Sludge Extraction from Semi-Continuous Bottle. Source: Own.

2.6.3.2. Chemical Oxygen Demand & Total Nitrogen Cell Tests

Due to the materials required to perform COD and NTK tests, these were performed using cell test kits, which contained 25 vials per box. As such, these were spread throughout testing to ensure a good coverage. This is the reason the tests were performed bi-daily. The tests used were all provided with their own reagents and material required. As such, the described process was followed. This process can be seen below in Figure 57, Figure 58 and Figure 59. It must be noted that samples required the use of a digester to permit the oxidation of compounds at high temperatures. Once treated, they were analysed in the spectrometer. These last two processes can be seen in Figure 60 and Figure 61.

The cell kits used were the 1145410001 COD Cell Test, with a range of 25-1500 mg/l (Merck, 2022) and the 114537001 Nitrogen (total) Cell Test, with a range of 0.5-15 mg/l (Merck, 2022).



Figure 57: Cell Test Procedure 1. Source: Own.



Figure 58: Cell Test Procedure 2. Source: Own



Figure 59: Treated Cell Tests. Source: Own.



Figure 60: Cell Test Digester. Source: Own



Figure 61: Cell Test Spectrometer Analysis. Source: Own.

2.6.4. Gas Chromatography

The retrieved gas samples were injected into the chromatographer through the intake port, shown in Figure 62. This fitting was attached to the apparatus to ensure an airtight connection, avoiding the samples from being contaminated with outside air from the laboratory. To inject the sample, the syringe was connected to the Injection port and the plunger pressed, as seen in Figure 63.

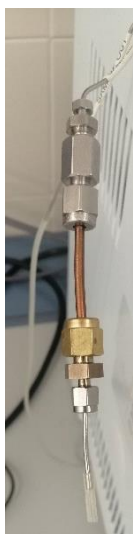


Figure 62: Injection Port Fitting. Source: Own.



Figure 63: Biogas Sample Injection Representation. Source: Own.

Moreover, the daily extracted gas samples were analysed to determine the composition of the biogas produced. The method used within the chromatographer was designed in (Morales Polo, Co-Digestión anaerobia y pretratamiento de residuos agroalimentarios con fangos UASB de depuradora, 2019) for this purpose. The temperature and flow graphs which determine the method are shown in Figure 64.



Figure 64: Gas Chromatography Method. Source: Own.

Lastly, it must be pointed out that a detailed guide on the use of the chromatogram was produced and can be found in Anejo IV: Chromatogram Manual.

2.6.5. Semi-Continuous Reactor & Bottle Feeding

To create the semi-continuous AD process within the reactor and the designed bottles, these had to be fed daily a mixture of substrate (pumpkin) mixed with the nanoparticle solution (if applicable) as well as the water utilised to maintain the solid-liquid proportion of 50% within the vessel. The substrate mixture was prepared in the same way as explained in BMP Batch Bottles Design & Set Up.

The mixture was then placed in a cylinder which served as reservoir for the hydraulic system. To feed it, the HeiFLOW was turned on and the programmed volume pumped.

Regarding the semi-continuous bottle feeding, the process proved to be more complex. To prevent false results during VFA analysis, the sludge sample was extracted using a syringe prior to injection. The feed mixture was placed inside a syringe and the air inside it removed, Figure 65. Lastly, the syringe was fitted, and the plunger pressed to inject the Figure 66 and Figure 67.



Figure 65: Semi-Continuous Bottle Feed Injection 1. Source: Own.



Figure 66: Semi-Continuous Bottle Feed Injection 2. Source: Own.



Figure 67: Semi-Continuous Bottle Feed Injection 3. Source: Own.

2.7. MATLAB Chromatography Analysis

2.7.1. Chromatogram Image Treatment

As previously stated, the software required to analyse the chromatograms as program files was not available within the laboratory's office suite. To permit the subsequent analysis and modelling found in the following sections, it was decided to perform a graphical analysis.

This graphical analysis was performed on the chromatograms obtained, treated as images and the use of MATLAB to treat the screenshots as RGB matrices once loaded. The first hurdle was encountered when designing the analytical procedure, as chromatograms could be obtained in varying pixel sizes, based on the capture and window size.

To remove this uncertainty, all images were captured as maximized windows. Furthermore, the whole screen was captured to ensure that all images were the same size and thus had the same pixel length and chromatogram position. One of these screenshots can be seen below in Figure 68.

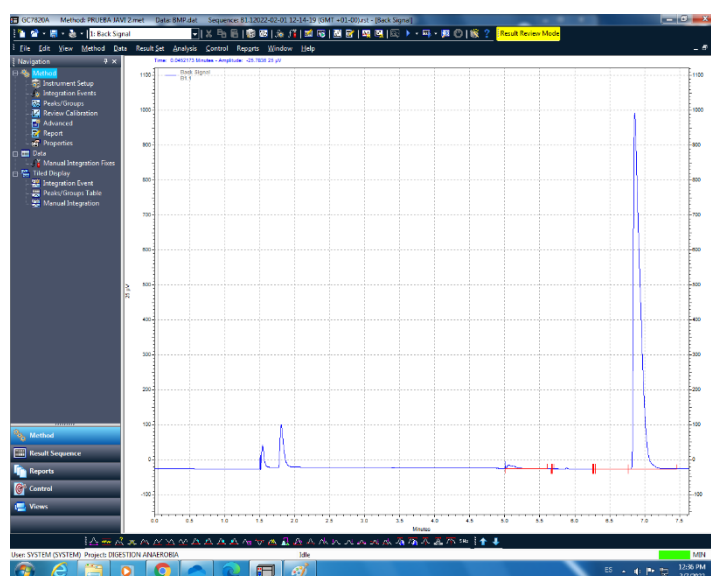


Figure 68: B.1.1 Untreated Screen Capture. Source: Own.

Once all the chromatograms were retrieved, an ad-hoc MATLAB code was developed to clean and analyse the peaks registered within each one. To do this, the first step was to cut the chromatogram from the screenshot to reduce pixel size and facilitate the computing of all the samples. The original image size along with the coordinates to perform the cuts were collected below in Table 8.

Table 8: Chromatogram Pixel Limits. Source: Own.

Parameter	Value
x_o (pixel)	1024
y_o (pixel)	1280
$x_{GCstart}$ (pixel)	121
x_{GCend} (pixel)	902
$y_{GCstart}$ (pixel)	262
y_{GCend} (pixel)	1224

In addition, the cut chromatogram can be seen below in Figure 69.

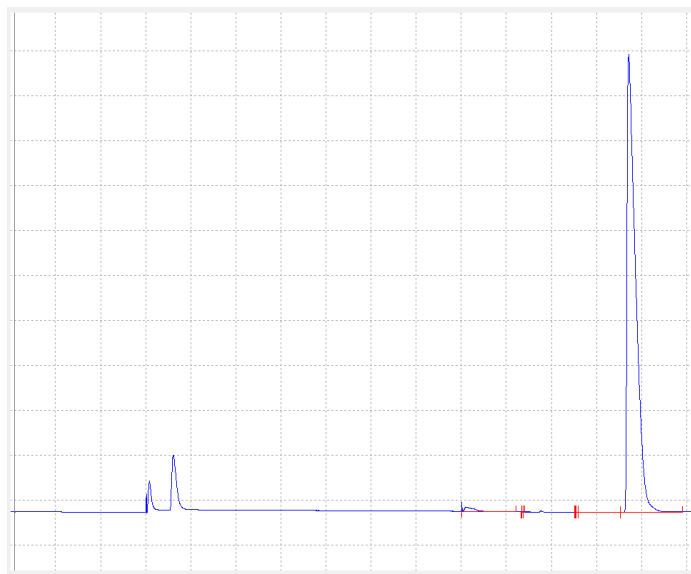


Figure 69: B.1.1 Chromatogram Cut Out from Screen Capture. Source: Own.

As a result of this capture and load procedure, all chromatograms had the same pixel size. Furthermore, as a result of maintaining the same GC Method throughout the project, the x axis, which displayed the time steps within the process, all chromatograms have the same x-axis scale, with the y-axis varying based on peak sizes.

This varying y-scale inhibits the possibility of performing a comparative analysis between the raw images, requiring a pixel step approach to determine concentration. To do so images were firstly cleaned of the grid and cursor vertical line, as shown in Figure 70.

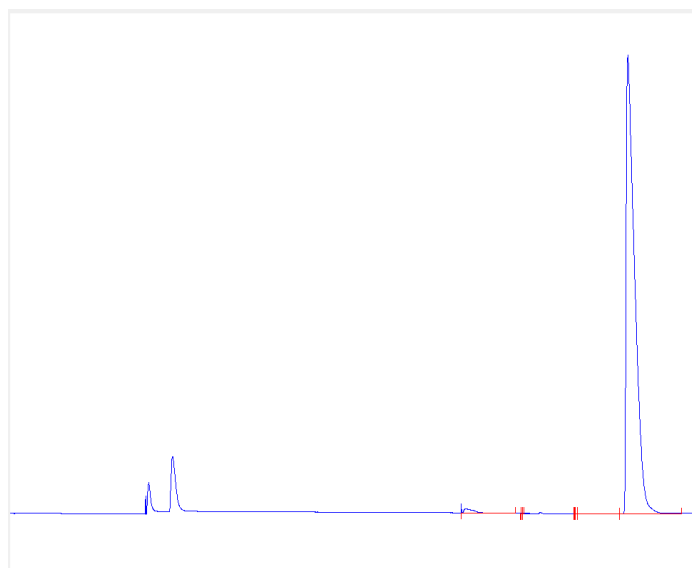


Figure 70: B.1.1 Cleaned Chromatogram. Source: Own.

The red line which appears throughout the previously explained Figures could not be removed as it is overlaid on top of the chromatogram. The grid previously removed was placed behind the blue diagram and could therefore be treated without losing information. The black cursor line, on the other hand, crossed the blue chromatogram on a single pixel. To remove it, the line was converted to white and the pixel on which it crossed turned blue, ensuring continuity. This marked the end of the image treatment, with the remaining process focusing on retrieving the molar fraction of each analysed compound.

2.7.2. Chromatogram Calculations

In order to obtain the previously mentioned molar fraction estimations, the integration baseline was established. This line, commonly placed around $-25\mu\text{V}$ represents the sensor base reading, established during prior to the first valve opening within the method. To do this, two possibilities were considered, the use of the median or the use of the mode. To determine which one was more representative, several chromatograms were analysed, without showing significant variation between them when large peaks were registered (less than 0.25-pixel difference).

However, chromatograms with smaller peaks experienced larger noise when determining the baseline employing the median, which did not reflect on the mode. As such, the baseline was established as:

$$y_{base} = mode[y(t = base_{start}), y(t = base_{end})]$$

Once the baseline was established, each species to be analysed was assigned a start and end pixels. These were in turn employed in the for loop which calculated the area between the chromatogram and the previously defined baseline. It must also be mentioned that the residues analysed had 2 peaks, corresponding to the 2 valve commands given during the method and thus required 2 integration intervals. The formula utilised also accounted for the possibility of the area being negative, in which case it was saturated down to 0 to prevent anomalous results. Thus, the equation employed in each pixel column, for each species is provided below:

$$A_{CH_4}(i) = \begin{cases} A_{CH_4}(i-1) + y_{chrom}(i) - y_{base} & \text{if } i \in [x_{CH_4o}; x_{CH_4f}] \\ 0 & \text{if } i \text{ not contained } [x_{CH_4o}; x_{CH_4f}] \end{cases}$$

$$A_{H_2}(i) = \begin{cases} A_{H_2}(i-1) + y_{chrom}(i) - y_{base} & \text{if } i \in [x_{H_2o}; x_{H_2f}] \\ 0 & \text{if } i \text{ not contained } [x_{H_2o}; x_{H_2f}] \end{cases}$$

$$A_{H_2S}(i) = \begin{cases} A_{H_2S}(i-1) + y_{chrom}(i) - y_{base} & \text{if } i \in [x_{H_2So}; x_{H_2Sf}] \\ 0 & \text{if } i \text{ not contained } [x_{H_2So}; x_{H_2Sf}] \end{cases}$$

$$A_{RES}(i) = \begin{cases} A_{CH_4}(i-1) + y_{chrom}(i) - y_{base} & \text{if } i \in [x_{RES1o}; x_{RES1f}] \mid i \in [x_{RES2o}; x_{RES2f}] \\ 0 & \text{if } i \in [x_{RES1o}; x_{RES1f}] \mid i \in [x_{RES2o}; x_{RES2f}] \end{cases}$$

Finally, to determine the concentration of each species in a chromatogram, the total integrated area was used as the denominator for each species, obtaining the molar fraction:

$$A_T = A_{CH_4} + A_{H_2} + A_{H_2S} + A_{RES}$$

$$y_{CH_4} = \frac{A_{CH_4}}{A_T} \quad y_{H_2} = \frac{A_{H_2}}{A_T}$$

$$y_{H_2S} = \frac{A_{H_2S}}{A_T} \quad y_{RES} = \frac{A_{RES}}{A_T}$$

Lastly, the full MATLAB code can be found in Anejo V: MATLAB Code.

Chapter 3: Results

In this section the results from the various experiments performed were presented and analysed, as such, it will be divided into sections pertaining to the three tests. Before proceeding, it must be mentioned that during the second round of experiments, day four coincided with a bank holiday and therefore no data could be collected that day. To facilitate data treatment and clarity, data was grouped with that obtained during the next sampling. It must also be pointed out that initial results were analysed in a report which can be found in Anejo II: Initial Result Analysis

It must also be added that the reactor results were affected by the volatilization of the nanoparticles, which deposited on the stir rod and its seal.

3.1. BMP Bottle Results

Firstly, it must be mentioned that only the data obtained from BMP bottles will be analysed, as the semi-continuous bottles presented difficulties and were inhibited early into the study, as previously mentioned.

Raw pressure data was obtained daily using the barometer, as previously stated. In addition, the gaseous samples were also analysed in the chromatographer, producing chromatograms which could be later graphically analysed using a MATLAB (MatWorks, 2022) code developed to graphically obtain the composition of each analysed sample. A sample of an obtained chromatogram is shown Figure 71. In addition, pressure readings were recorded in Table 9.

From the obtained data, the normalised production by volume of sludge using the following equation, was calculated an aggregated to obtain the average accumulated biogas production. This graph is displayed in Figure 72. In said graph, F stands for sludge, F+NP sludge with nanoparticles, B: BMP bottle and B+NP signifies BMP bottle with nanoparticles.

$$n_{biogas} \left[\frac{Nm^3}{day} \right] = 0.9269 * P_{bottle}[bar]$$

Table 9: BMP Bottle Pressure Readings. Source: Own.

Day	1	2	3	7	8	9	10	11	14	15	16	17	18	21
F1	0.469	0.309	0.282	0.489	0.143	0.101	0.091	0.078	0.18	0.062	0.052	0.065	0.051	0.109
FN	0.423	0.27	0.205	0.342	0.092	0.061	0.072	0.042	0.056	0.028	0.031	0.04	0.03	0.034
B1	0.979	0.259	0.284	0.187	0.147	0.018	0.015	0.006	0.002	0	0	0	0	0
B2	0.947	0.606	0.21	0.122	0.097	0.085	0.109	0.077	0.056	0.045	0.039	0.039	0.054	0.109
B3	0.979	0.044	0.045	0.006	0.023	0.006	0.012	0.045	0.111	0.039	0.024	0.033	0.03	0.05
B4	1	0.524	0.512	0.408	0.17	0.093	0.101	0.085	0	0	0	0	0.026	0
B5	0.979	0.087	0.269	0.045	0.019	0.015	0.01	0.043	0.038	0.038	0	0.018	0	0
B6	0.979	0.452	0.388	0.108	0.046	0.045	0.057	0.055	0.07	0.025	0.027	0.043	0.041	0.082
B7	0.979	0.597	0.344	0.262	0.158	0.105	0.126	0.01	0.008	0	0	0.016	0.024	0.024
B8	0.979	0.618	0.001	0	0	0	0	0	0	0	0	0.003	0	0
B9	1	0.728	0.41	0.373	0.127	0.043	0.062	0.037	0.006	0.024	0.015	0.006	0.015	0.027
BNP1	0.975	0.464	0.366	0.295	0.129	0.086	0.064	0.035	0.04	0.029	0.026	0.046	0.048	0.046
BNP2	0.979	0.526	0.37	0.543	0.132	0.076	0.077	0.067	0.149	0.056	0.033	0.045	0.031	0.037
BNP3	0.979	0.417	0.421	0.234	0.093	0.056	0.059	0.05	0.101	0.049	0.026	0.032	0.023	0.058
BNP4	0.979	0.102	0.111	0.13	0.102	0.122	0.07	0.068	0.127	0.051	0.031	0.043	0.03	0.095
BNP5	0.979	0.436	0.325	0.371	0.097	0.005	0.009	0.03	0	0.017	0.026	0.037	0.035	0.024

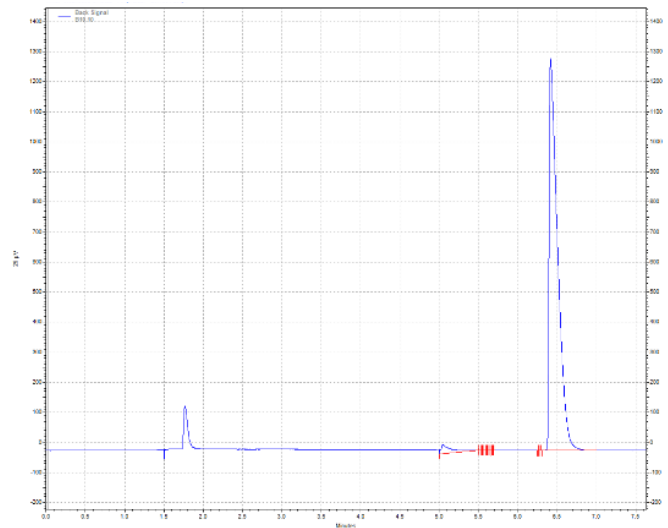


Figure 71: Chromatogram Obtained during Testing. Source: Own.

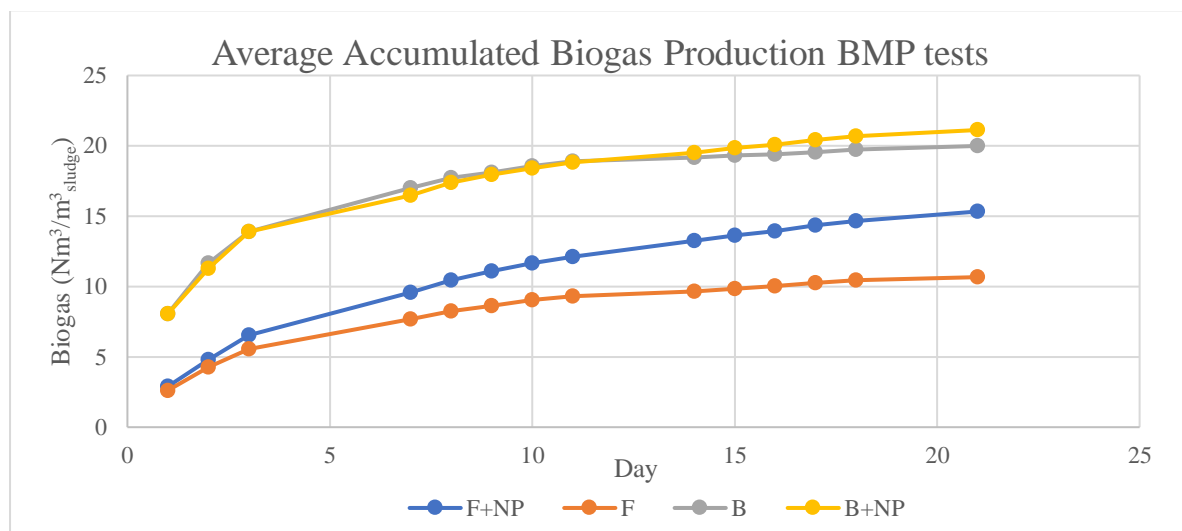


Figure 72: Average Accumulated Biogas Production for each BMP test. Source: Own.

As evidenced in the above figure, normalised biogas production was far superior in co-digestion tests when compared to the sludge and sludge & nanoparticle baselines. However, no further analysis could be made until a statistical analysis was performed on the data.

It must also be mentioned that the addition of nanoparticles did not increase biogas production significantly, which suggests that the main benefit of adding these into AD co-digestion reactors would be added process stability, based on the data dispersion that can be seen in Table 2. To obtain a better analysis, B and B+NP data series were compared in Figure 73.

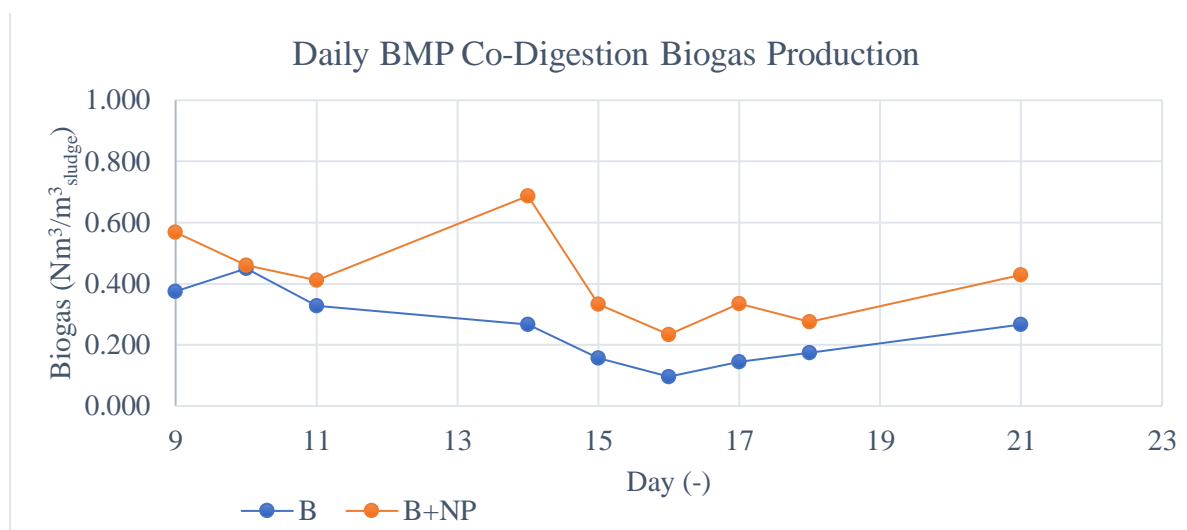


Figure 73: Daily BMP Co-Digestion Biogas Production. Source: Own.

As opposed to Figure 19, it is apparent in the above graph that the nanoparticles do improve production by a small margin after day nine. Also, both curves follow a similar trend during the final days, although B+NP presents a sudden increase in production which could indicate that said nanoparticles accelerate the AD process.

To determine the effects of nano particles, both in the average production and in the variability of said data points, a Student's t-test (Statistics How To, 2022) was used to determine if both daily sample groups could have the same mean (assuming a confidence of 95% and that both populations follow a normal distributions). The null hypothesis used was that both means were equal.

Similarly, Snedecor's f-test was used to determine if the population's variance (estimated using the sample variance corrected for skewing). In this test, the null hypothesis was that the variance of both populations was the same. Lastly, the significance was set at 5%. Due to the various tests performed, the results for were combined into Table 10 and Table 11, containing t-tests and f-test, respectively. If the null hypothesis were accepted, the displayed result was zero, if it could not be accepted, the result shown was one. It must also be added that the results displayed for the f-test are the standard deviation.

As it can be appreciated in Table 10, the null hypothesis can only be rejected sparingly, primarily during the final days of methanogenesis in hydrogen composition. Regarding methane, the nanoparticles do not have a significant effect in the mean, as the null hypothesis is not rejected. This could be improved if a larger sample is obtained by performing more BMP tests.

Pertaining to the hydrogen sulphide, the null hypothesis must be accepted always, save for the central days of methanogenesis, like the hydrogen. In addition, the H₂S displays a sudden increase in both production and composition in day eleven, being the only day where it presents a relevant change. Further study would be advised to analyse the effects of the nanoparticles on this chemical compound.

Lastly, the residuals behave statistically identical in both cases, as the hypothesis is always accepted in composition and production. Focusing on the composition, the nanoparticles do cause a small change, although not significant enough. Regarding production, the effects are more significant, as in certain cases the production doubles. Also, residue production is always higher in samples containing the nanoparticles except for three distinct days.

Table 10: Student's t-test on Mean Results. Source: Own.

Day	1	2	3	7	8	9	10	11	14	15	16	17	18	21
Methane Production														
Prod B (p.u.)	7.297	3.297	2.088	1.292	0.670	0.349	0.418	0.303	0.248	0.145	0.089	0.135	0.162	0.254
Prod. BN (p.u.)	7.318	2.932	2.408	2.392	0.782	0.529	0.429	0.381	0.639	0.310	0.218	0.312	0.256	0.400
H	0	0	1	1	0	0	0	0	0	0	0	0	0	1
Methane Composition														
Comp. B (p.u.)	0.904	0.921	0.927	0.931	0.927	0.927	0.929	0.926	0.929	0.927	0.929	0.930	0.935	0.947
Comp. BN (p.u.)	0.908	0.917	0.918	0.922	0.848	0.924	0.929	0.923	0.930	0.929	0.932	0.932	0.930	0.934
H	0	0	1	1	0	0	0	0	0	0	0	0	0	1
Hydrogen Production														
Prod B (p.u.)	0.005	0.002	0.001	0.000	0.001	0.000	0.000	0.000	0.000	0.000	0.000	0.000	0.000	0.000
Prod. BN (p.u.)	0.003	0.002	0.000	0.000	0.001	0.000	0.000	0.000	0.000	0.000	0.000	0.000	0.000	0.000
H	0	0	0	0	0	0	0	0	0	0	0	0	0	0
Hydrogen Composition														
Comp. B (p.u.)	0.001	0.000	0.000	0.001	0.001	0.002	0.000	0.001	0.001	0.001	0.001	0.001	0.001	0.000
Comp. BN (p.u.)	0.000	0.001	0.000	0.000	0.001	0.000	0.000	0.001	0.000	0.000	0.000	0.000	0.000	0.000
H	0	0	0	0	0	0	0	0	0	1	1	1	0	0
Hydrogen Sulphide Production														
Prod B (p.u.)	0.008	0.002	0.001	0.001	0.000	0.000	0.000	0.000	0.000	0.000	0.000	0.000	0.000	0.000
Prod. BN (p.u.)	0.006	0.003	0.001	0.001	0.001	0.000	0.000	0.000	0.000	0.000	0.000	0.000	0.000	0.000
H	0	0	0	0	0	0	0	0	0	0	0	0	0	0
Hydrogen Sulphide Composition														
Comp. B (p.u.)	0.001	0.001	0.000	0.001	0.000	0.000	0.000	0.001	0.000	0.000	0.000	0.000	0.000	0.000
Comp. BN (p.u.)	0.001	0.001	0.000	0.000	0.001	0.000	0.000	0.001	0.000	0.000	0.000	0.000	0.000	0.000
H	0	0	0	0	0	0	0	0	0	1	1	1	0	0
Residue Production														
Prod B (p.u.)	0.765	0.282	0.166	0.091	0.049	0.026	0.032	0.024	0.018	0.011	0.007	0.010	0.011	0.013
Prod. BN (p.u.)	0.734	0.268	0.215	0.198	0.128	0.040	0.031	0.031	0.048	0.023	0.016	0.023	0.019	0.028
H	0	0	0	0	0	0	0	0	0	0	0	0	0	0
Residue Composition														
Comp. B (p.u.)	0.095	0.078	0.072	0.068	0.071	0.071	0.070	0.073	0.069	0.072	0.070	0.069	0.064	0.053
Comp. BN (p.u.)	0.091	0.081	0.082	0.078	0.150	0.075	0.070	0.076	0.070	0.070	0.068	0.068	0.070	0.066
H	0	0	0	0	0	0	0	0	0	0	0	0	0	0

Table 11: Snedecor's *f*-test on Variance Results. Source: Own.

Day	1	2	3	7	8	9	10	11	14	15	16	17	18	21
Methane Production														
Prod B (p.u.)	0.131	1.878	1.279	1.171	0.511	0.307	0.370	0.231	0.303	0.147	0.116	0.130	0.147	0.316
Prod. BN (p.u.)	0.148	1.247	0.914	1.188	0.237	0.333	0.209	0.136	0.474	0.129	0.026	0.046	0.071	0.208
H	0	0	0	0	0	0	0	0	0	0	1	0	0	0
Methane Composition														
Comp. B (p.u.)	0.008	0.008	0.008	0.005	0.007	0.009	0.008	0.007	0.008	0.005	0.004	0.005	0.008	0.008
Comp. BN (p.u.)	0.019	0.013	0.006	0.003	0.177	0.011	0.011	0.006	0.004	0.005	0.003	0.002	0.003	0.005
H	1	0	0	0	1	0	0	0	0	0	0	0	0	0
Hydrogen Production														
Prod B (p.u.)	0.007	0.004	0.002	0.001	0.001	0.000	0.000	0.001	0.000	0.000	0.000	0.000	0.000	0.000
Prod. BN (p.u.)	0.003	0.003	0.001	0.001	0.000	0.000	0.000	0.000	0.000	0.000	0.000	0.000	0.000	0.000
H	0	0	0	0	0	1	0	0	0	1	0	1	1	1
Hydrogen Composition														
Comp. B (p.u.)	0.001	0.001	0.001	0.001	0.001	0.002	0.001	0.002	0.002	0.001	0.001	0.001	0.001	0.000
Comp. BN (p.u.)	0.000	0.001	0.000	0.001	0.000	0.001	0.001	0.001	0.000	0.000	0.000	0.000	0.000	0.000
H	0	0	0	0	1	0	0	0	1	1	1	1	1	1
Hydrogen Sulphide Production														
Prod B (p.u.)	0.008	0.003	0.001	0.001	0.001	0.000	0.001	0.000	0.000	0.000	0.000	0.000	0.000	0.000
Prod. BN (p.u.)	0.007	0.003	0.002	0.001	0.002	0.000	0.000	0.000	0.000	0.000	0.000	0.000	0.000	0.000
H	0	0	0	0	0	0	1	0	0	0	1	1	0	0
Hydrogen Sulphide Composition														
Comp. B (p.u.)	0.001	0.001	0.001	0.001	0.001	0.000	0.001	0.001	0.000	0.001	0.001	0.001	0.001	0.001
Comp. BN (p.u.)	0.001	0.001	0.001	0.000	0.002	0.000	0.001	0.001	0.000	0.000	0.000	0.000	0.000	0.000
H	0	0	0	0	0	0	0	0	0	0	1	1	0	0
Residue Production														
Prod B (p.u.)	0.057	0.156	0.101	0.079	0.036	0.021	0.028	0.018	0.022	0.011	0.009	0.010	0.011	0.015
Prod. BN (p.u.)	0.142	0.120	0.084	0.091	0.136	0.022	0.014	0.009	0.036	0.009	0.001	0.003	0.005	0.015
H	1	0	0	0	1	0	0	0	0	0	1	1	0	0
Residue Composition														
Comp. B (p.u.)	0.007	0.007	0.007	0.004	0.006	0.008	0.007	0.005	0.007	0.004	0.003	0.004	0.008	0.008
Comp. BN (p.u.)	0.018	0.012	0.006	0.003	0.175	0.010	0.010	0.005	0.003	0.005	0.003	0.002	0.003	0.005
H	1	0	0	0	1	0	0	0	0	0	0	0	0	0

3.1.1. BMP Binormal distribution modelling

The data collected was used to model the binormal distribution of various species as well as the overall biogas production. This modelling was performed separately for the samples with and without nanoparticles. The only models with significant results, with no structured residuals and an acceptable R^2 were those for raw biogas production, which are presented below.

In both cases an exponential decay function was obtained using linear regression models for the mean, while a polynomial regression model up to t^3 was employed to model the standard deviation. The models utilised for each variable modelled can be seen in the following two formulae.

$$\mu_s(t) \left[\frac{Nm^3}{m_{Studge}^3} \right] = A_{om} * e^{-A_{1m} * t}; \quad t[day]; \quad Variables: A_{om}; A_{1m}$$

$$\sigma_{ss}(t) \left[\frac{Nm^3}{m_{Studge}^3} \right] = A_{os} + A_{1s} * t + A_{2s} * t^2 + A_{3s} * t^3; \quad t[day]; \quad Variables: A_{os}; A_{1s}; A_{2s}; A_{3s}$$

3.1.2. B Bottles Binomial Distribution Modelling

The obtained model for mean biogas without nanoparticles (sample B) is shown below.

$$\mu_B(t) \left[\frac{Nm^3}{m_{Studge}^3} \right] = 4.1587 * e^{-0.192t}; \quad t[day]$$

In addition, the residual model parameters and the residual analysis are shown in Figure 79 for the exponential regression of the mean value, its residuals in Figure 75.

Number of observations: 14, Error degrees of freedom: 12
 Root Mean Squared Error: 0.579
 R-squared: 0.824, Adjusted R-Squared: 0.809
 F-statistic vs. constant model: 56.1, p-value = 7.33e-06

Figure 74: B Model Mean Stats. Source: Own.

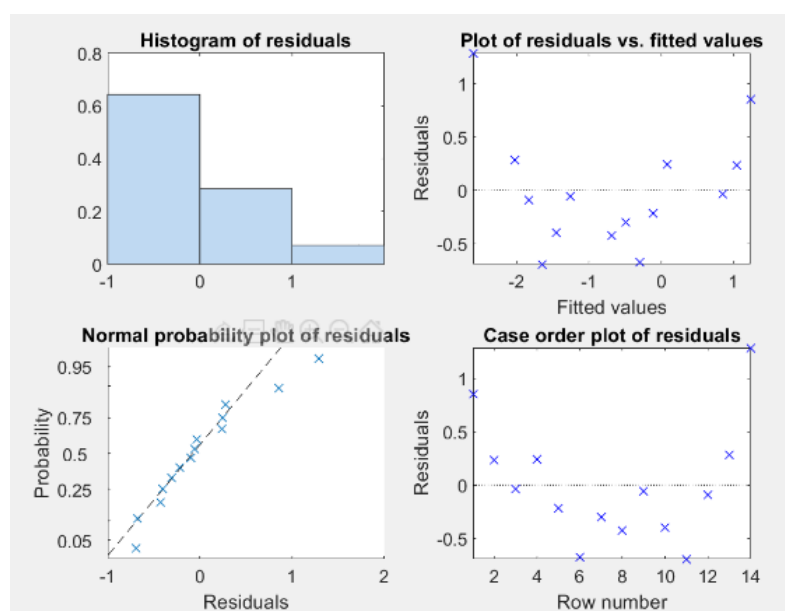


Figure 75: B Model Mean Residual Analysis. Source: Own.

Analysing the Figure presented above; there are not enough data points to determine the presence of patterns or structures in the data. However, the obtained residuals appear to follow a normal distribution throughout, although the tails deviate from this. It must also be added that the residuals do appear to be predominantly negative when compared with their fitted values, pointing to an accuracy deviation, although dispersion of data is contained within ± 0.5 . Regarding the R^2 , the fitted model has a value of 0.824, above the 0.8 considered to be the soft limit to obtain a representative model. Furthermore, the p-value to reject the null hypothesis of a constant model is well below the 5% confidence interval.

In addition, to the exponential regression of the mean, a polynomial model was fitted to the standard deviation, whose resulting formula is shown below:

$$\sigma_B(t) \left[\frac{Nm^3}{m_{Studge}^3} \right] = 1.2177 - 0.012 * t^2 + 4.7875 * 10^{-4} * t^3; \quad t[day]$$

As with the previous modelling, the residual model parameters and model evaluation were displayed in Figure 76 below. The residual analysis is provided in Figure 77.

Number of observations: 14, Error degrees of freedom: 11
 Root Mean Squared Error: 0.461
 R-squared: 0.479, Adjusted R-Squared: 0.384
 F-statistic vs. constant model: 5.06, p-value = 0.0277

Figure 76: B Model Standard Deviation Stats. Source: Own.

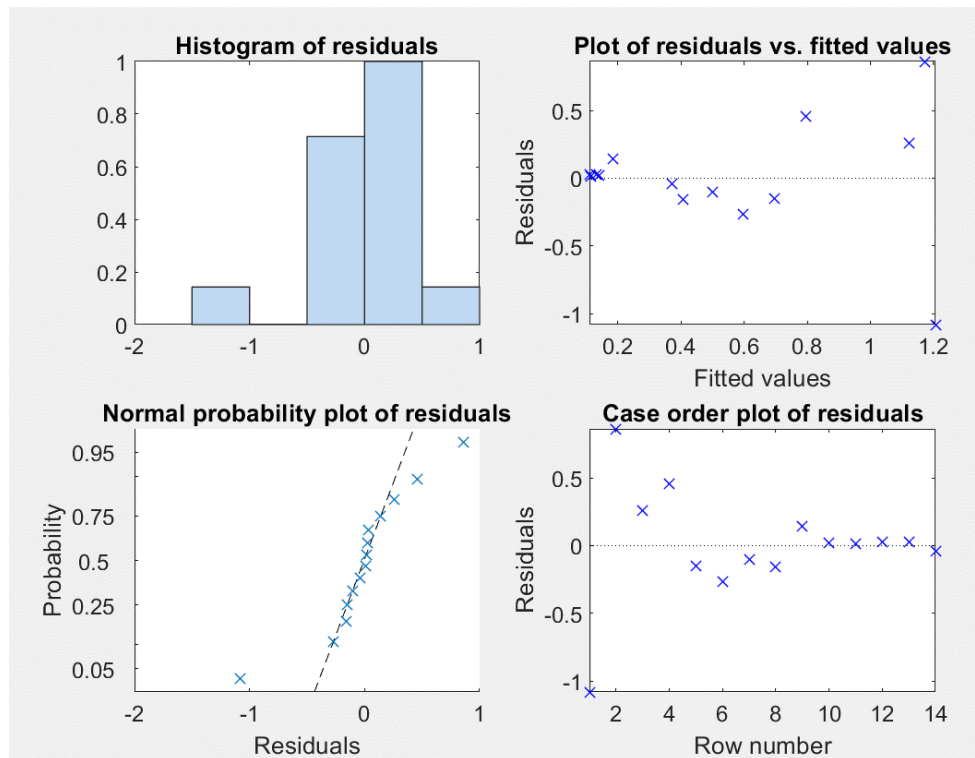


Figure 77: B Model Standard Deviation Residual Analysis. Source: Own.

Similar to the previous analysis, the residual distribution appears to follow a normal distribution with a smaller deviation on both tails, which supports the modelling hypothesis. Furthermore, residuals do not appear to have any structure, although error amplitude does decrease with time, thus suggesting that there is an underlying structure which will be revealed once more data is collected.

Regarding the p-value, it can be rejected with a 5% confidence interval, although a lower value would be preferred to ensure the model is robust. This will therefore require further data collection and analysis.

Once the mean and standard deviation were analysed, the binormal distribution was constructed, whose formula is shown below. In addition, the final distribution is shown in Figure 78

$$n_{biogas} \left[\frac{Nm^3}{m_{Sludge}^3} \right] = N(4.1587 * e^{-0.192*t}, 1.2177 - 0.012 * t^2 + 4.7875 * 10^{-4} * t^3)$$

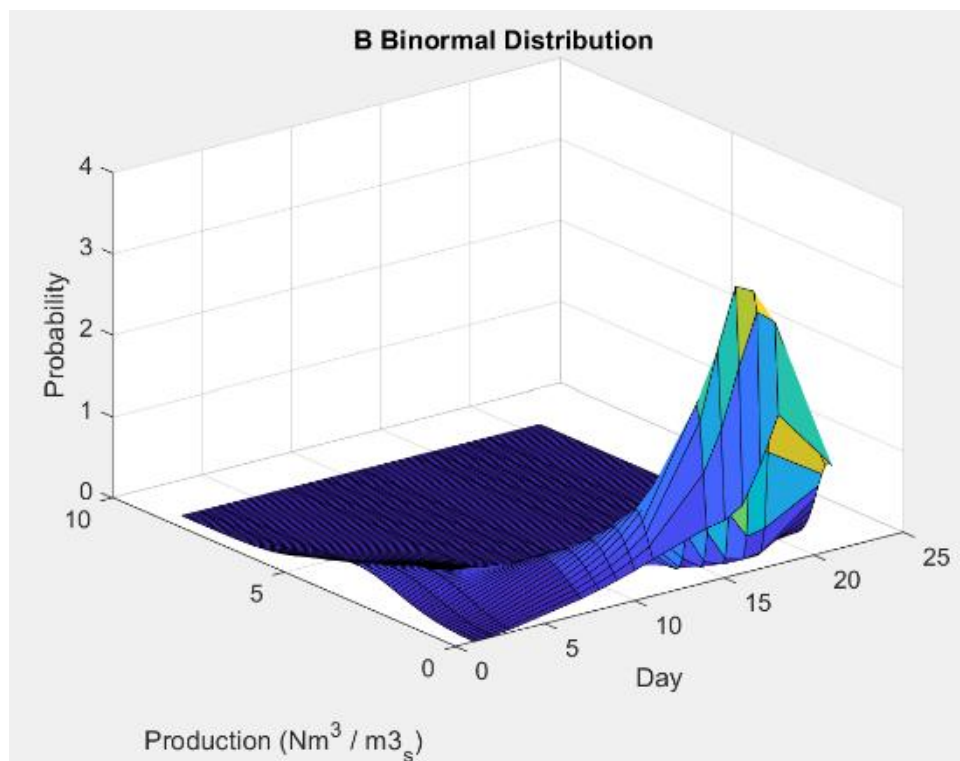


Figure 78: B Model Binormal Distribution. Source: Own.

3.1.3. B-NP Bottles Binomial Distribution Modelling

Similar to the previous section, the modelling of the binormal distribution utilised was divided into the mean and standard deviation modelling. In this case, the obtained model for samples B-NP was:

$$\mu_{B-NP}(t) \left[\frac{Nm^3}{m_{Sludge}^3} \right] = 4.1604 * e^{-0.1531*t}; \quad t[day]$$

The residual model stats are shown in Figure 79. The residual analysis performed is included in Figure 80.

Number of observations: 14, Error degrees of freedom: 12
 Root Mean Squared Error: 0.546
 R-squared: 0.769, Adjusted R-Squared: 0.75
 F-statistic vs. constant model: 40, p-value = 3.78e-05

Figure 79: B-NP Mean Model Stats. Source: Own.

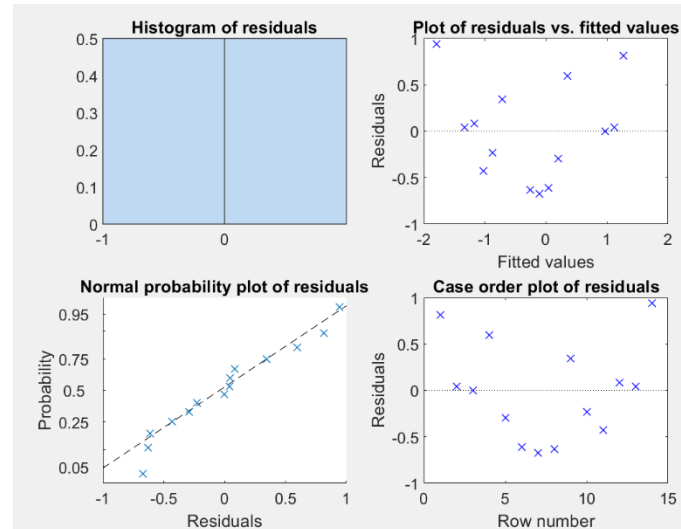


Figure 80: B-NP Mean Residual Analysis. Source: Own.

Similar to previous modelling, the low number of data points and therefore degrees of freedom, the model appears to follow a normal distribution, although residuals display poor accuracy. They also display a quadratic structure. Regarding the R^2 , it is close to the 0.8 limit, and the null hypothesis can be rejected thanks to the low p-value.

After modelling the mean for this sample, the standard deviation was also estimated employing the aforementioned polynomial regression model. The resulting formula is shown below:

$$\sigma_{B-NP}(t) \left[\frac{Nm^3}{m_{sludge}^3} \right] = 0.8495 - 0.0741 * t^2 + 2.8246 * 10^{-4} * t^3; \quad t[day]$$

As with the previous modelling, the residual model parameters and model evaluation were displayed in Figure 81 Figure 76below. The residual analysis is provided in Figure 82.

Number of observations: 14, Error degrees of freedom: 11
 Root Mean Squared Error: 0.409
 R-squared: 0.355, Adjusted R-Squared: 0.237
 F-statistic vs. constant model: 3.02, p-value = 0.09

Figure 81: B NP Standard Deviation Model Stats. Source: Own.

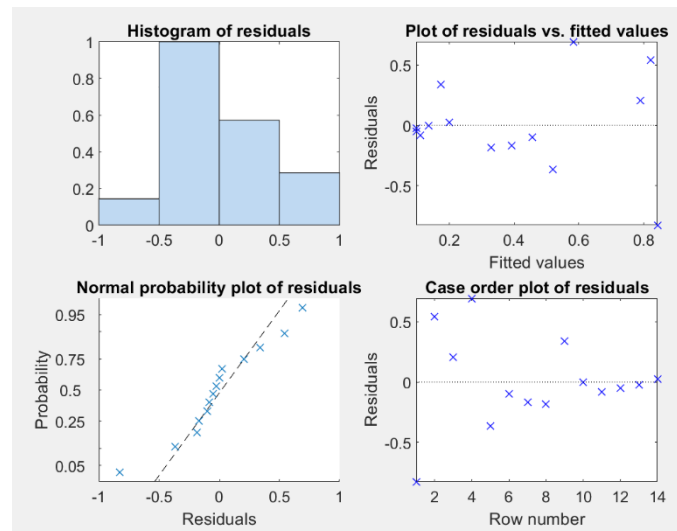


Figure 82: B-NP Standard Deviation Residual Analysis. Source: Own.

Standard deviation has been shown in previous modelling to contain underlying structures, also present in the NP bottles. As a result, the R^2 of the model is considerably lower than the previous exercises. In addition, the p-value is high, meaning that the null hypothesis could not be rejected with a low confidence interval, although it was rejected in this exercise to model the binormal curve.

Moreover, the underlying structure and poor R^2 cause the residuals to not follow the normality curve, as shown in the above Figure, both in the distribution's tails and the middle.

Once the mean and standard deviation were analysed, the binormal distribution was constructed, whose formula is shown below. In addition, the final distribution is shown in Figure 83

$$n_{biogas} \left[\frac{Nm^3}{m^3_{Studge}} \right] = N(4.1604 * e^{-0.1531*t}, 0.8495 - 0.0741 * t^2 + 2.8246 * 10^{-4} * t^3)$$

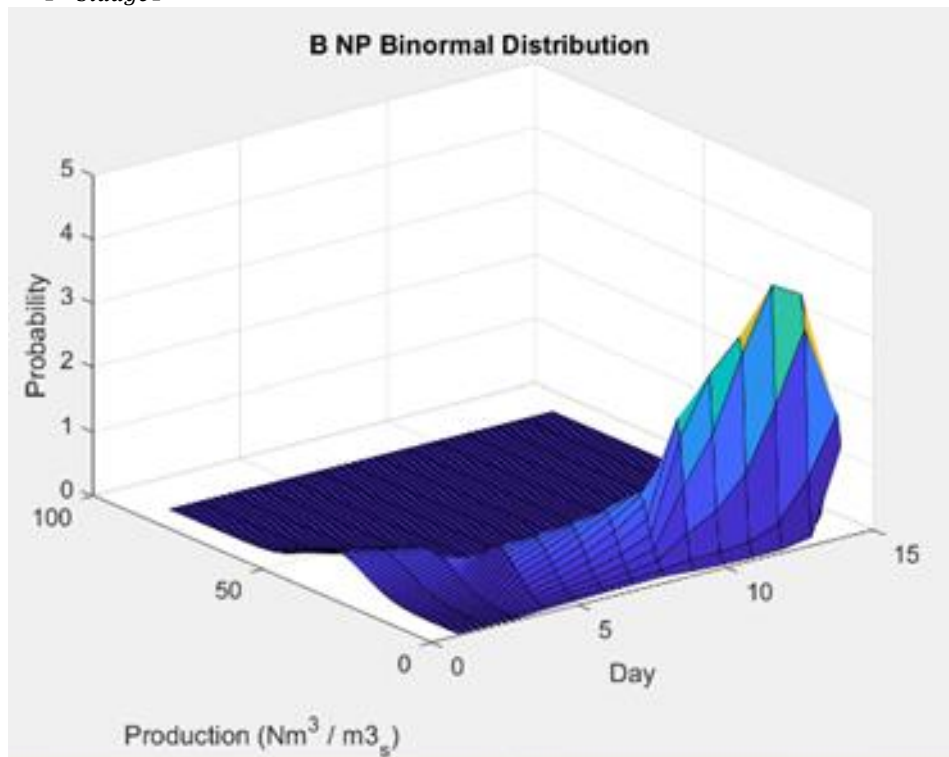


Figure 83: B-NP Model Binormal Distribution. Source: Own.

3.2. Batch Reactor Results

As previously stated, both reactors presented problems when measuring production after day three of the experiment. Therefore, only the composition could be analysed in this section. It must also be added that, due to the low number of runs, no statistical analysis or modelling could be obtained.

Firstly, the composition of both reactors was determined using the MATLAB code previously mentioned. The results were divided by analysed species in the following order: methane, hydrogen, hydrogen sulphide and residues. These results were presented in Table 12, Table 13, Table 14 and Table 15, respectively.

It is apparent that the nanoparticles had a positive contribution between days 9 and 14, whose effects were larger than those observed in the bottles, which suggests a magnifying effect caused by the vessel volume.

However, methane production, and therefore methanogenesis, stops by day fifteen, which indicates that the reactor is spent or the inhibition of the reactions. Production measurements would be required for a detailed analysis, although this behaviour is in line with the lower decay rate observed in the BMP bottles.

Moving on to hydrogen sulphide, the larger reaction vessel magnifies the observed effects on the BMP bottles, namely the sudden peak by day eleven before becoming a residual species.

Table 12. Effects of Nanoparticles on Batch Reactor Methane Composition. Source: Own.

Day	1	2	3	7	8	9	10	11	14	15	16	17	18	21
Comp R (p.u.)	0.379	0.821	0.044	0.174	0.727	0.099	0.109	0.571	0.341	0.397	0.432	0.053	0.387	0.508
Comp RN (p.u.)	0.827	0.681	0.734	0.642	0.516	0.616	0.586	0.346	0.620	0.012	0.000	0.000	0.000	0.000
NP Effect (-)	+	-	+	+	-	+	+	-	+	-	-	-	-	-
Specific Effect (p.u./g _{NP})	3.998	-1.247	6.157	4.181	-1.886	4.610	4.265	-2.007	2.487	-3.442	-3.856	-0.474	-3.456	-4.537

It is apparent that the nanoparticles had a positive contribution between days 9 and 14, whose effects were larger than those observed in the bottles, which suggests a magnifying effect caused by the vessel volume.

However, methane production, and therefore methanogenesis, stops by day fifteen, which indicates that the reactor is spent or the inhibition of the reactions. Production measurements would be required for a detailed analysis, although this behaviour is in line with the lower decay rate observed in the BMP bottles.

Table 13: Effects of Nanoparticles on Batch Reactor Hydrogen Composition. Source: Own.

Day	1	2	3	7	8	9	10	11	14	15	16	17	18	21
Comp R (p.u.)	0.253	0.042	0.436	0.271	0.065	0.290	0.262	0.112	0.249	0.161	0.171	0.279	0.167	0.168
Comp RN (p.u.)	0.050	0.116	0.074	0.110	0.127	0.100	0.115	0.169	0.092	0.368	0.293	0.280	0.262	0.227
NP Effect (-)	-	+	-	-	+	-	-	+	-	+	+	+	+	+
Specific Effect (p.u./g _{NP})	-1.81	0.662	-3.231	-1.431	0.560	-1.693	-1.314	0.514	-1.398	1.852	1.095	0.013	0.846	0.529

Pertaining to hydrogen composition, this species behaves inversely to methane, having opposing trends on most days, as shown in Figure 84. This persistent inversion suggests the existence of an overall observable and impactful interaction between them. This could be caused by the increased methane production, which causes the population of methane producing bacteria to oscillate.

It must also be pointed out that the hydrogen is positively impacted by the nanoparticles, which drastically increases production during the early stages of the AD process.

Table 14: Effects of Nanoparticles on Batch Reactor Hydrogen Sulphide Composition. Source: Own.

Day	1	2	3	7	8	9	10	11	14	15	16	17	18	21
Comp R (p.u.)	0.000	0.002	0.001	0.000	0.002	0.003	0.000	0.004	0.000	0.005	0.000	0.003	0.002	0.004
Comp RN (p.u.)	0.001	0.000	0.001	0.000	0.003	0.001	0.001	0.000	0.002	0.002	0.003	0.000	0.002	0.002
NP Effect (-)	+	-	-	-	+	-	+	-	+	-	+	-	-	-
Specific Effect (p.u./g _{NP})	0.010	-0.020	-0.010	0.000	0.014	-0.027	0.005	-0.037	0.017	-0.026	0.029	-0.024	-0.004	-0.024

Moving on to hydrogen sulphide, the larger reaction vessel magnifies the observed effects on the BMP bottles, namely the sudden peak by day eleven before becoming a residual species.

Table 15: Effects of Nanoparticles on Batch Reactor Residue Composition. Source: Own.

Day	1	2	3	7	8	9	10	11	14	15	16	17	18	21
Comp R (p.u.)	0.368	0.135	0.519	0.556	0.206	0.607	0.630	0.313	0.410	0.437	0.398	0.666	0.444	0.320
Comp RN (p.u.)	0.122	0.203	0.192	0.248	0.353	0.284	0.299	0.485	0.287	0.618	0.704	0.720	0.736	0.771
NP Effect (-)	-	+	-	-	+	-	-	+	-	+	+	+	+	+
Specific Effect (p.u./g _{NP})	-2.202	0.605	-2.915	4.181	-2.750	1.312	-2.890	-2.956	1.529	-1.105	1.616	2.732	0.485	2.614

Lastly, the weight of residues in the biogas composition displayed a similar behaviour as in the BMP bottles by reducing their appearance until day seven. They also present a sudden peak in day eleven which reached 48.5% of the composition, coinciding with the peak in H₂S. As the data varies significantly, the specific effect caused is displayed in Figure 84 and Figure 85.

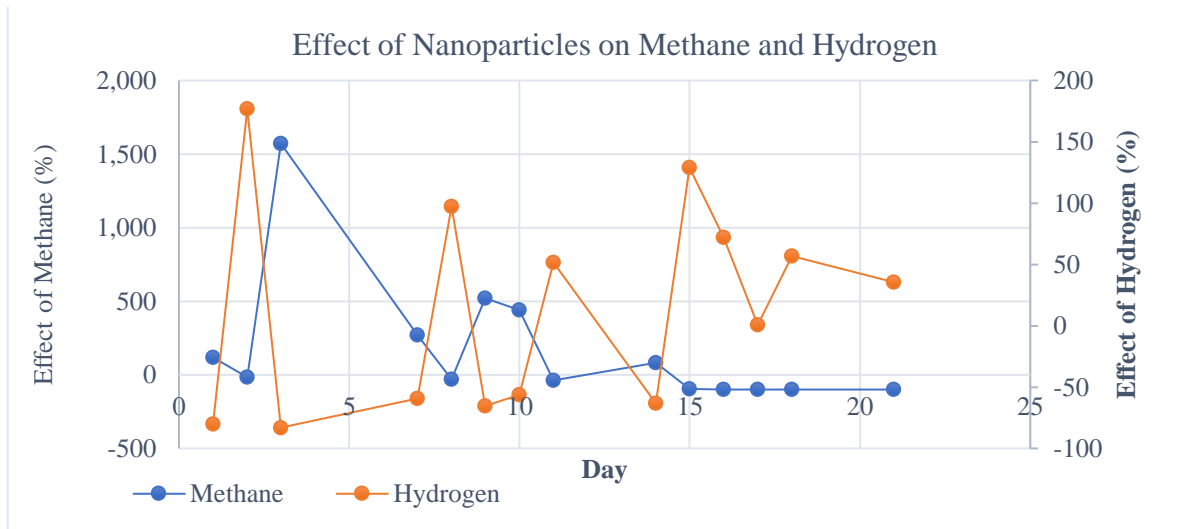


Figure 84: Effect of Nanoparticles on Methane and Hydrogen in Batch Reactor. Source: Own.

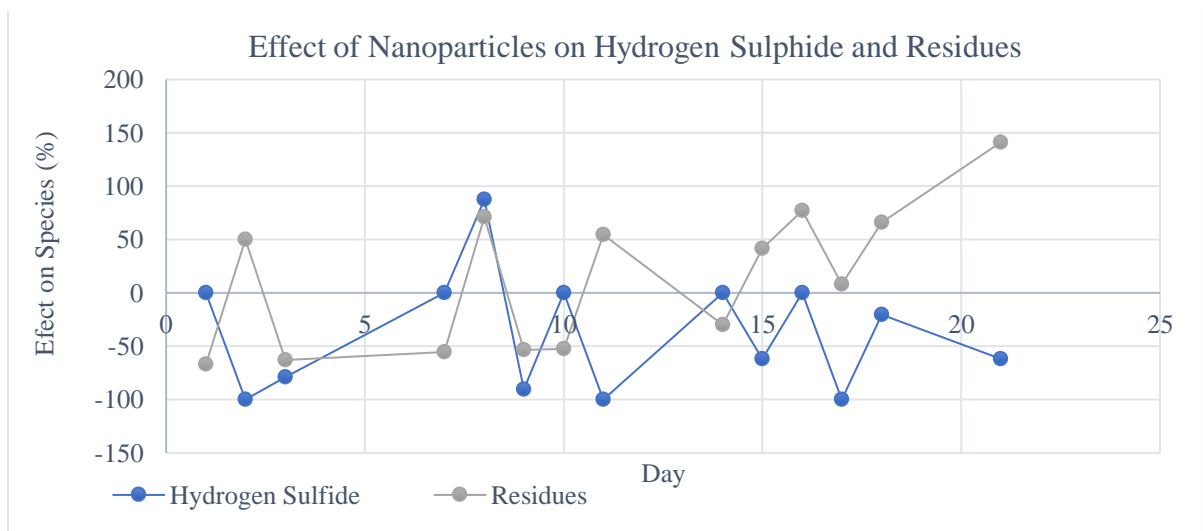


Figure 85: Effect of Nanoparticles on Hydrogen Sulphide and Residues in Batch Reactor. Source: Own.

As previously stated, these figures reinforce the notion of a CH₄-H₂ as well as an increase in reaction speed which suggests that the residence time could be reduced significantly.

3.3. Semi-Continuous Reactor Results

Due to the nature of the reactor, it operated continuously for 42 days, the length of the two sets of runs made. During this time, the reactor operated the first 21 days without nanoparticles, which were added the 22nd day of operation. This dosage included the daily injection as well as the initial dose required.

3.3.1. Composition Analysis

The results obtained are not comparable to any of the previously presented, as the continuous bottles failed. Therefore, the only possible analysis is that of the composition, which is shown split in Table 16 for days 1 to 21 and Table 17 for days 22 to 42. It must also be pointed out that the missing day in this case is not day four, but day twenty-five, as the bank holiday occurred during the second round of tests.

Table 16: Semi-Continuous Reactor Composition, Days 1-21. Source: Own.

Day	1	2	3	4	7	8	9	10	11	14	15	16	17	18	21
Methane (p.u.)	0.065	0.720	0.847	0.862	0.669	0.726	0.283	0.603	0.746	0.332	0.192	0.335	0.275	0.434	0.360
Hydrogen (p.u.)	0.311	0.075	0.048	0.031	0.106	0.078	0.216	0.110	0.062	0.227	0.254	0.216	0.196	0.137	0.266
Hydrogen Sulphide (p.u.)	0.006	0.002	0.003	0.002	0.002	0.000	0.000	0.002	0.000	0.007	0.005	0.004	0.006	0.005	0.000
Residues (p.u.)	0.617	0.203	0.102	0.105	0.223	0.195	0.501	0.285	0.191	0.435	0.548	0.446	0.523	0.425	0.374

Table 17: Semi-Continuous Reactor Composition, Days 22-42. Source: Own.

Day	22	23	24	28	29	30	31	32	35	36	37	38	39	42
Methane (p.u.)	0.065	0.720	0.847	0.862	0.669	0.726	0.283	0.603	0.746	0.332	0.192	0.335	0.275	0.434
Hydrogen (p.u.)	0.311	0.075	0.048	0.031	0.106	0.078	0.216	0.110	0.062	0.227	0.254	0.216	0.196	0.137
Hydrogen Sulphide (p.u.)	0.006	0.002	0.003	0.002	0.002	0.000	0.000	0.002	0.000	0.007	0.005	0.004	0.006	0.005
Residues (p.u.)	0.617	0.203	0.102	0.105	0.223	0.195	0.501	0.285	0.191	0.435	0.548	0.446	0.523	0.425

When performing a qualitative analysis of the presented data, it is apparent that the weight of methane in the composition varies from the first section of the study (pre day 21) to the second. Regarding the first 21 days, similar behaviours to that of the BMP bottles can be seen, such as de peak in secondary species found on day nine. However, this peak is mitigated but the semi-continuous nature of the reactor. This semi continuous nature also contributes to achieve a baseline in hydrogen production throughout the study, due to hydrolysis being the first stage of the AD process. Focusing on the methane, the addition of the nanoparticles on day twenty-one has a visible impact on methane production, causing an increase from 0.36 p.u. to 0.72 in day twenty-three.

Lastly, it can be determined that the hydrogen sulphide is not a significant species when in continuous operation, as it never exceeds a 0,7% weight. However, residues found in the gas samples do increase drastically, being the dominant compound in certain days, stablishing two operating ranges for the four analysed compounds: The higher range in which residues and methane can be found and the lower range which contains the hydrogen and hydrogen sulphide are found. The cut off for these ranges appears to be around 30%. To facilitate the analysis, the results are also shown below in Figure 86.

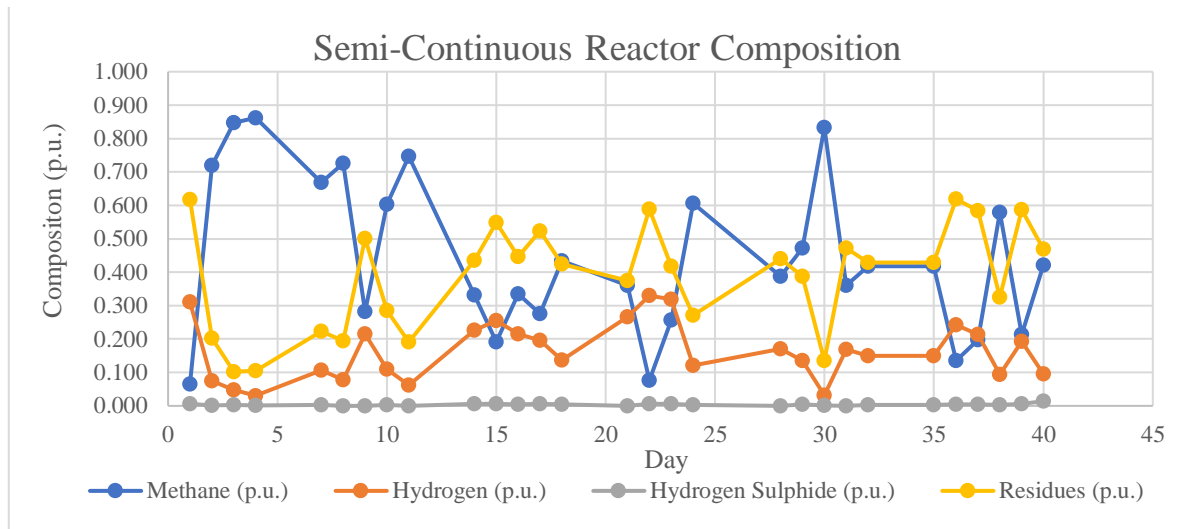


Figure 86: Semi-Continuous Reactor Composition. Source: Own.

3.3.2. VFA Analysis

Another aspect which was monitored daily was the VFA concentration to if the reactor had become too acidic and therefore inhibited methanogenesis. As it was previously explained, a two-stage valorisation of the supernatant extracted from the reactor was performed. The sample was diluted at a 50:50 (25ml of supernatant and 25 ml of distilled water) ratio with distilled water prior to performing the analysis. In addition, temperature was also recorded with the HI 902 titrator. Similar to the previous section, the results were divided into Table 18 and Table 19 for days 1 to 21 and 22 to 42. Results obtained were used to determine the partial (AP, measured in $\text{mg}_{\text{CaCO}_3}/\text{l}$), intermediate (AI, $\text{mg}_{\text{CaCO}_3}/\text{l}$) and total alkalinity (AT, $\text{mg}_{\text{CaCO}_3}/\text{l}$), utilizing (APHA, AWWA, WEF, 2012):

$$AP \left[\frac{\text{mg}_{\text{CaCO}_3}}{\text{l}} \right] = \frac{V_{\text{HCl}} * N_{\text{HCl}} * 5000}{V_{\text{sample}}} \quad AI \left[\frac{\text{mg}_{\text{CaCO}_3}}{\text{l}} \right] = \frac{V_{\text{H}_2\text{SO}_4} * N_{\text{H}_2\text{SO}_4} * 5000}{V_{\text{sample}}}$$

$$AT \left[\frac{\text{mg}_{\text{CaCO}_3}}{\text{l}} \right] = Ap + AI = \frac{(V_{\text{H}_2\text{SO}_4} * N_{\text{H}_2\text{SO}_4} + V_{\text{HCl}} * N_{\text{HCl}}) * 5000}{V_{\text{sample}}}$$

Table 18: Semi-Continuous Reactor VFA Analysis, Days 1-21. Source: Own.

Day	1	2	3	4	7	8	9	10	11	14	15	16	17	18	21
T (°C)	20.8	20.2	21.3	22.7	22.5	23.3	23.8	23.8	22.1	22.2	23.1	23.7	23.6	24.8	23.7
pH _o (-)	7.11	7.72	7.55	7.48	7.11	7.43	7.67	7.53	7.57	7.61	7.68	7.56	7.47	7.52	7.53
pH _i (-)	5.74	5.77	5.77	5.78	5.75	5.77	5.78	5.77	5.76	5.76	5.76	5.78	5.77	5.76	5.77
pH _f (-)	3.98	4.19	3.61	3.35	4.43	4.23	4.12	3.98	4.02	4.27	4.4	3.85	4.3	4.31	4.36
V _{HCl} (ml)	18.294	18.697	25.209	24.165	23.959	25.288	25.754	25.899	18.481	28.415	27.1	27.202	27.175	28.229	26.889
V _{H₂SO₄} (ml)	0.086	0.172	0.419	0.98	0.145	0.185	0.184	0.171	0.125	0.179	0.195	0.3	0.218	0.234	0.231
AP (mg _{CaCO₃} /l)	182.94	186.97	252.09	241.65	239.59	252.88	257.54	258.99	184.81	284.15	271	272.02	271.75	282.29	268.89
AI (mg _{CaCO₃} /l)	1.72	3.44	8.38	19.6	2.9	3.7	3.68	3.42	2.5	3.58	3.9	6	4.36	4.68	4.62
AT (mg _{CaCO₃} /l)	184.66	190.41	260.47	261.25	242.49	256.58	261.22	262.41	187.31	287.73	274.9	278.02	276.11	286.97	273.51

Table 19: Semi-Continuous Reactor VFA Analysis, Days 22-42. Source: Own.

Day	22	23	24	28	29	30	31	32	35	36	37	38	39	42
T (°C)	23.2	22	23.4	23.2	21.7	23.6	22.4	24.1	23	22.2	22.3	22.7	23.9	24
pH _o (-)	7.65	7.66	7.69	7.73	7.79	7.35	7.51	7.37	7.59	7.69	7.81	7.42	7.18	7.04
pH _i (-)	5.75	5.76	5.76	5.76	5.76	5.75	5.77	5.76	5.77	5.76	5.77	5.76	5.76	5.76
pH _f (-)	4.19	4.25	4.36	4.32	3.63	4.29	4.38	4.31	4.36	3.72	4.32	4.28	4.24	4.29
V _{HCl} (ml)	27.738	26.47	25.399	24.978	22.582	21.025	26.568	22.015	21.234	25.166	17.106	11.65	18.109	14.279
V _{H2SO4} (ml)	0.186	0.092	2.08	0.209	0.155	0.267	0.391	0.335	0.34	0.214	5.7	0.562	1.042	0.961
AP (mgCaCO ₃ /l)	277.38	264.7	253.99	249.78	225.82	210.25	265.68	220.15	212.34	251.66	171.06	116.5	181.09	142.79
AI (mgCaCO ₃ /l)	3.72	1.84	41.64	4.18	3.1	5.34	7.82	6.7	6.8	4.28	114	11.24	20.84	19.22
AT (mgCaCO ₃ /l)	281.1	266.54	295.63	253.96	228.92	215.59	273.5	226.85	219.14	255.94	285.06	127.74	201.93	162.01

As is apparent, initially the initial pH was lightly basic, consistently between 7 and 8, considered within the ideal range for anaerobic digestion. However, a more detailed analysis on the pH was performed in a later section, as it varies within the reactor based on height and therefore a gradient appears within it.

Furthermore, intermediate alkalinity was stable generally stable throughout the process, although certain peaks were recorded during operation. The first peak recorded occurred on day 4 of the study, at the end of the stabilization period and therefore it could not be considered representative. Once the nanoparticles were added however, an initial peak on day 24 was registered. This build-up points to the possibility that the addition of nanoparticles accelerated the AD process as VFA content increased.

Lastly, intermediate alkalinity rose during the final days of the study, even when disregarding day 37, which was a measurement error. The acidification of the reactor towards the final days should be further analysed to determine the cause, to determine if the reactor could be sustainable in stationary operation. The results were displayed in Figure 87 below.

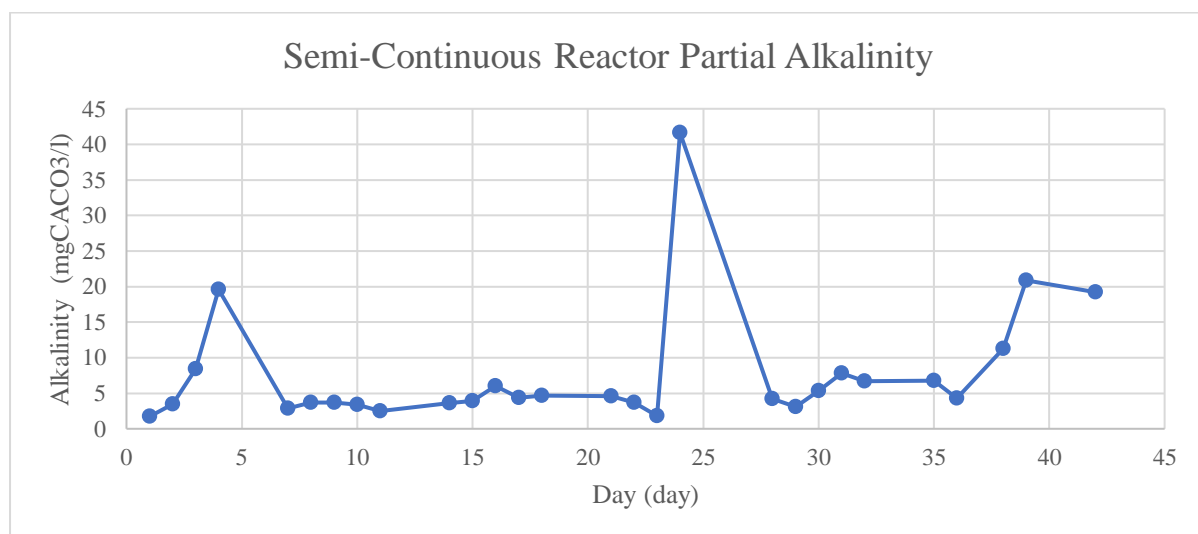


Figure 87: Semi-Continuous Reactor Partial Alkalinity. Source: Own.

3.3.3. COD and NTK Analysis

Proceeding with the final reactor variables to be measured and recorded, the COD and NTK were used jointly to analyse their behaviour through the experiment. These were measured every two days.

It must also be added that due to the measuring range of the cell tests used, NTK samples were concentrated when treating the samples while COD samples were diluted with distilled water. This is noted as it may have altered the real values. Also, the measurements presented below in Table 21 and Table 22 were already adjusted for dilution and concentration. However, because of the changing COD and NTK levels, certain values could not be recorded due to them exceeding the range of each test. Said range limits are presented below in Table 20. HI indicates that the reading exceeded the upper limit, while LO indicates that the concentration was too low to be measured.

Table 20: COD & NTK Cell Test Range Limits. Source: Own.

Cell Test	Lower Limit	Upper Limit
COD (mgO ₂ /l)	0	15000
NTK (mgN/l)	0.5	15

Table 21: Semi-Continuous Reactor NTK & COD Tess, Days 1-21. Source: Own.

Day	1	2	3	4	7	8	9	10	11	14	15	16	17	18	21
COD (mgO ₂ /l)	-	HI	-	8050	8120	ERR	-	6980	-	7970	-	6830	-	7470	5180
NTK (mgN/l)	-	2.4	-	0.4	13.2	2.5	-	1.5	-	3.3	-	3.3	-	4.9	2

Table 22: Semi-Continuous Reactor NTK & COD Tess, Days 22-42. Source: Own

Day	22	23	24	28	29	30	31	32	35	36	37	38	39	42
COD (mgO ₂ /l)	3500	-	4480	2220	-	7040	-	5990	3290	-	-	12240	-	9690
NTK (mgN/l)	13.2	-	15	2.35	-	1	-	18.5	12.5	-	-	47	-	67.5

Moreover, these series were independently plotted in Figure 88 and Figure 89 for COD and NTK, respectively. It must be noted that an error occurred when processing the sample retrieved on day 8, which failed during the digestion period.

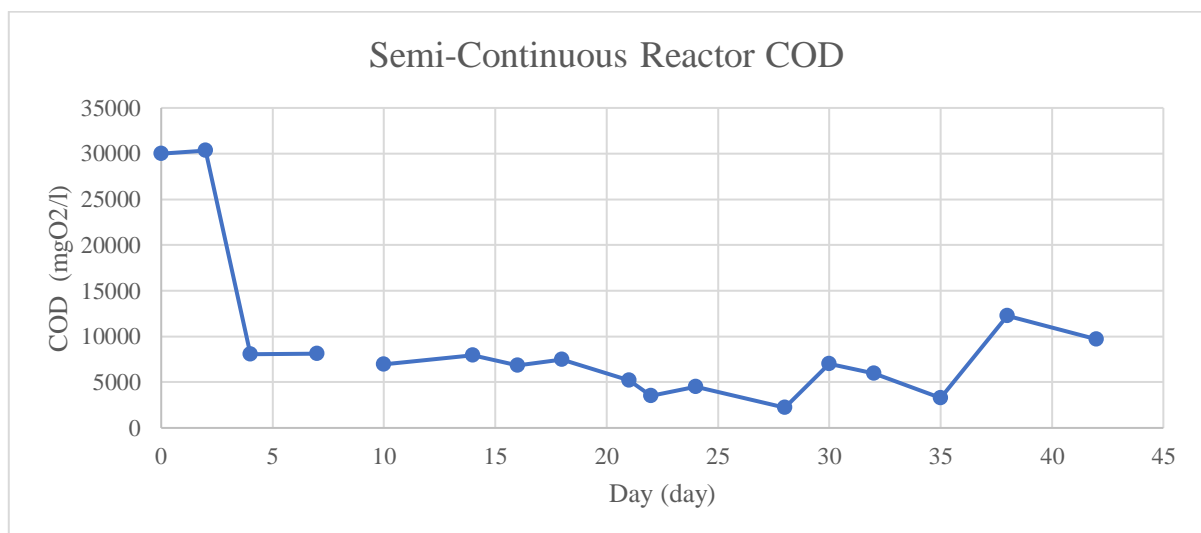


Figure 88: Semi-Continuous Reactor's COD. Source: Own.

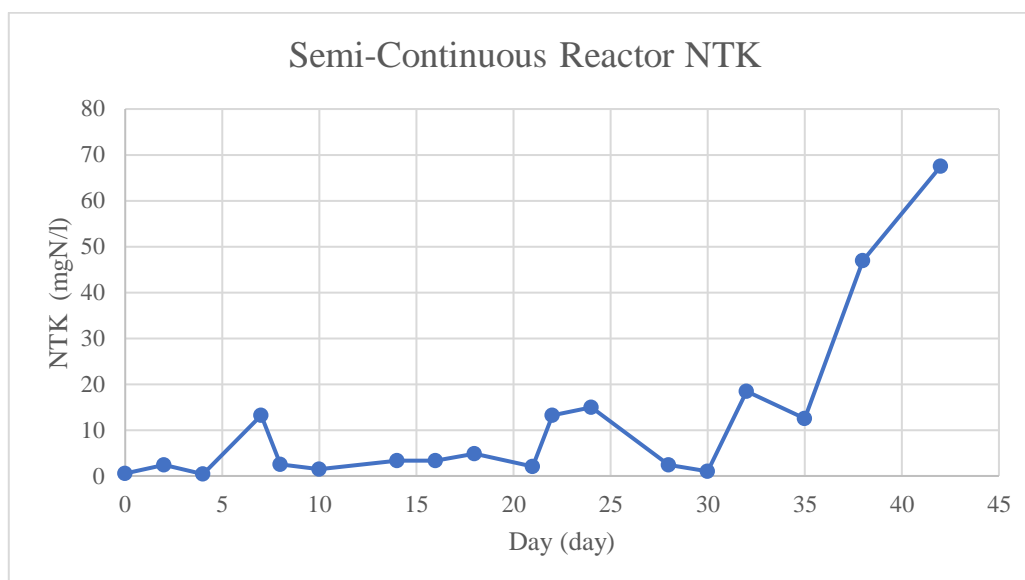


Figure 89: Semi-Continuous Reactor's NTK. Source: Own.

Analysing both Figures, it is apparent that COD remains approximately constant throughout the experiment once it has entered a stable phase at around 7000 mgO₂/l. However, there are signs that the total contamination decreases as the initial sludge is replaced by the substrate and supernatant mixture. This trend is reversed around day 28, when it increases and reaches around 9690 mgO₂/l the final day of the experiment. This accumulation of pollution within the reactor coincides with the increase in alkalinity, suggesting that the reactor's behaviour changed as a result of the addition of nanoparticles.

NTK also displayed the opposite behaviour during the first half of the study, with low N levels (the sludge was analysed, and nitrogen was found only in trace amounts) which steadily increased as substrate was added. However, nitrogen accumulation increases drastically the final days of the experiment, like COD and VFA. This could be caused by an increase in ammonia or nitrate production, although further testing is required to determine the type of nitrous compound produced. Lastly, the combination of COD and NTK could be used to estimate the C/N ratio within the reactor.

3.3.4. C/N Ratio Estimation and Analysis

In the State of the Art Section, the NMOC method was presented and explained. Used in its direct manner, it allows the estimation of the methane fraction within the produced biogas. This requires the use of the COD/TOC ratio. Therefore, if the molar fraction of CH₄ is known, along with the previously analysed COD, the TOC can be estimated. However, the estimation must be deemed consistent and reliable to validate its use. The NMOC method is shown below in Figure 90. Both the Figure and the formula were retrieved from (Morales Polo, Digestión Anaerobia, 2022) (van Lier, Mahmoud, & Zeeman, 2020).

$$CH_4[\%] = 18.75 * \frac{COD}{TOC}$$

In addition, the necessary data along with the results was compounded into Table 23 and Table 24.

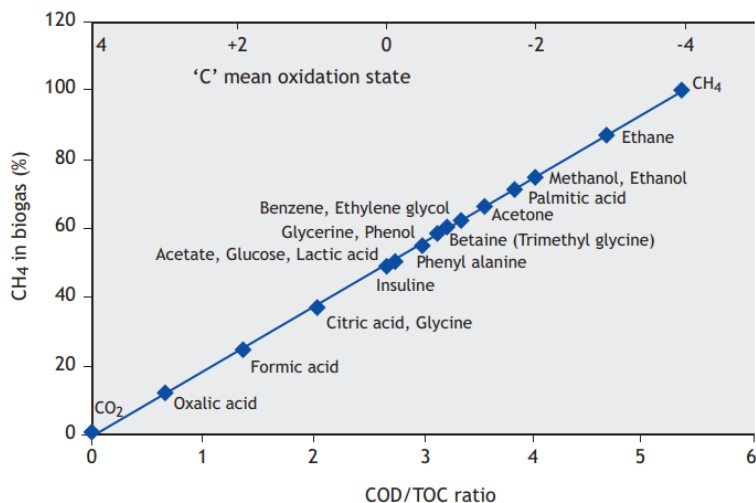


Figure 90: NMOc Methane Percentage Composition. Source: (Morales Polo, Digestión Anaerobia, 2022) (van Lier, Mahmoud, & Zeeman, 2020).

Table 23: Semi-Continuous Reactor TOC NMOc Estimation, Days 1-21. Source: Own.

Day	1	2	3	4	7	8	9	10	11	14	15	16	17	18	21
COD (mgO ₂ /l)	-	HI	-	8050	8120	ERR	-	6980	-	7970	-	6830	-	7470	5180
Methane (p.u.)	0.065	0.720	0.847	0.862	0.669	0.726	0.283	0.603	0.746	0.332	0.192	0.335	0.275	0.434	0.360
TOC (mg/l)	-	-	-	1751	2276	.	.	2171	.	4506	.	3824	.	3227	2697

Table 24: Semi-Continuous Reactor TOC NMOc Estimation, Days 22-42. Source: Own.

Day	22	23	24	28	29	30	31	32	35	36	37	38	39	42
COD (mgO ₂ /l)	3500	-	4480	2220	-	7040	-	5990	3290	-	-	12240	-	9690
Methane (p.u.)	0.065	0.720	0.847	0.862	0.669	0.726	0.283	0.603	0.746	0.332	0.192	0.335	0.275	0.434
TOC (mg/l)	8649	-	1387	1072	-	1585	-	2685	1475	-	-	3959	-	4309

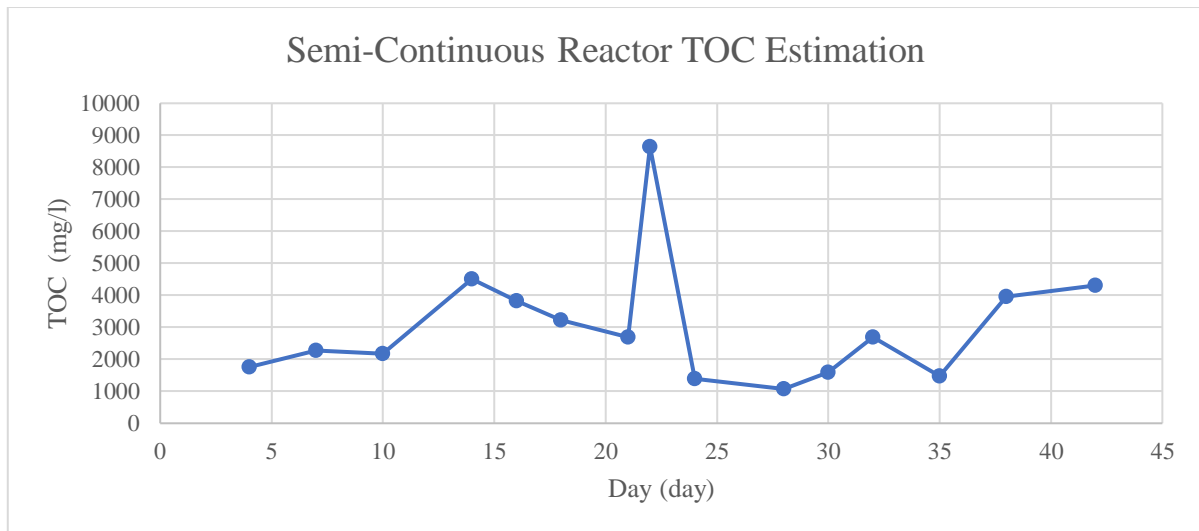


Figure 91: Semi-Continuous Reactor TOC NMOC Estimation. Source: Own.

It is apparent that the NMOC estimation does not represent a reliable method to determine the TOC within the reactor, as the formula employed inversely causes large variations due to the dilution of the COD samples. However, to finalise the analysis presented in this Section, the estimated C/N ratio was calculated and is shown in Table 25 and Table 26. The variation through time is also shown in Figure 92 below.

Table 25: Semi-Continuous Reactor C/N NMOC Estimation, Days 1-21. Source: Own.

Day	1	2	3	4	7	8	9	10	11	14	15	16	17	18	21
C/N (-)	-	-	-	4377	172	-	-	1448	-	1366	-	1159	-	659	1348

Table 26: Semi-Continuous Reactor C/N NMOC Estimation, Days 22-42. Source: Own.

Day	22	23	24	28	29	30	31	32	35	36	37	38	39	42
C/N (-)	655	-	-	456	-	1585	-	145	118	-	-	84	-	64

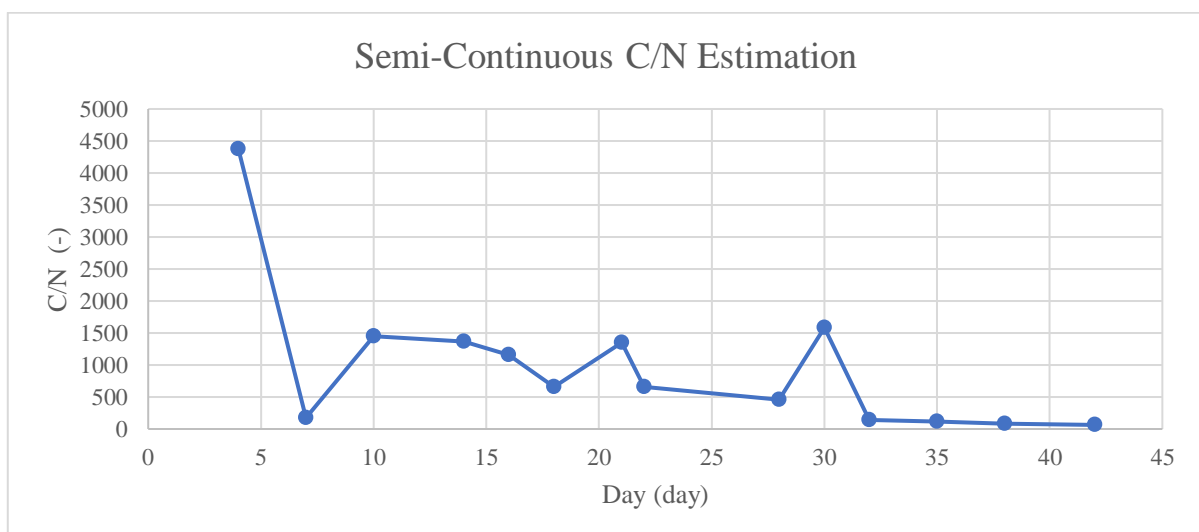


Figure 92: : Semi-Continuous Reactor C/N NMOC Estimation, Source: Own.

3.4. Synthetic Reactor Modelling

As it was previously explained, the continuous reactor did not yield reliable results due to a variety of factors and problems which arose during the testing period. To that end, a sample, synthetic reactor will be modelled utilizing the data obtained from the BMP tests.

This construct, defined as the synthetic reactor, was created on assumptions deemed compatible with the reactor designed. This reactor was based on the assumption that the residence time is maintained constant at 21 days. In addition, it was assumed that the reactor could be divided into a number of sections equal to the residence time of the reactor.

Furthermore, these sections maintain an equal and constant volume. Their sum equals the reactor's capacity. It must also be mentioned that these cells are themselves isolated, not permitting exchanges between them, but allowing stirring within each cell.

The creation of isolated cells permits the use of BMP data to simulate its behaviour, as the uncommunicated cell, which presents the same composition and age as a BMP sample, is assumed to behave in the same way. Through this model, the synthetic reactor is assumed to behave as the sum of as many BMP bottles as the residence time (in days). However, to ensure the aging and consumption of the co-digestion mixture behaves in a stationary manner, each cell must maintain its conditions while allowing sludge extraction and feeding injection.

When the feeding process is performed, the bottom most cell is extracted from the reactor, causing the remaining cells to move down 1 position. The missing cell is replaced by the added feeding mixture inserted through the top. This modelling permits the creation of a semi-continuous behaviour, in which the daily feeding doses added sink into the reactor and age, accordingly, leaving the reactor when their age is that of the residence time. It must also be mentioned that the cells must be stacked vertically to simulate the natural flow of sludge and substrate caused by the reactor design. This process was illustrated in Figure 93. It must also be pointed out that for the days in which production was not recorded (8; 9; 12; 13; 19 and 20), the production was assumed to be that of the next recorded day. On the other hand, day 4's production was assumed to be that of the previous day.

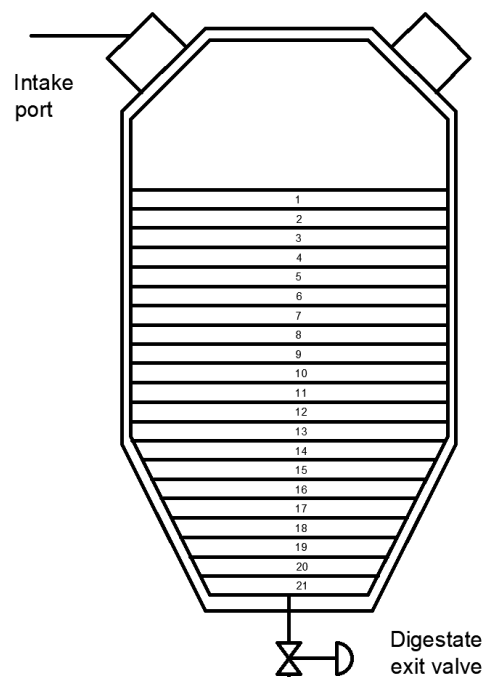


Figure 93: Synthetic Reactor Cell Division. Source: Own.

In addition, the governing equations of the reactor are as follows:

$$V_{cell_i} = \frac{V_{tot}}{t_R}; \quad i \in [1, t_R]$$

$$n_{CH_4} = \frac{1}{V_R} * \sum_{i=1}^{t_R} V_{cell_i} * n_{BMP_{CH_4}_i} \quad n_{H_2} = \frac{1}{V_R} * \sum_{i=1}^{t_R} V_{cell_i} * n_{BMP_{H_2}_i}$$

$$n_{H_2S} = \frac{1}{V_R} * \sum_{i=1}^{t_R} V_{cell_i} * n_{BMP_{H_2S}_i} \quad n_{RES} = \frac{1}{V_R} * \sum_{i=1}^{t_R} V_{cell_i} * n_{BMP_{RES}_i}$$

As a result, employing the mean daily production for each day of the BMP test the composition and production of the reactor can be determined, displayed below in Table 27.

Table 27: Synthetic Reactor Construction. Source: Own.

Day (-)	V _{cell} (V _R)	n _{CH₄} (Nm ³ / day-m ³ _s)	n _{H₂} (Nm ³ / day-m ³ _s)	n _{H₂S} (Nm ³ / day-m ³ _s)	n _{RES} (Nm ³ / day-m ³ _s)	N _{tot} (Nm ³ / day-m ³ _s)
1	1/21	7.3176	0.0030	0.0055	0.7338	8.0599
2	1/21	2.9322	0.0020	0.0030	0.2679	3.2052
3	1/21	2.4084	0.0004	0.0010	0.2154	2.6251
4	1/21	2.4084	0.0004	0.0010	0.2154	2.6251
5	1/21	2.3924	0.0005	0.0008	0.1985	2.5922
6	1/21	2.3924	0.0005	0.0008	0.1985	2.5922
7	1/21	2.3924	0.0005	0.0008	0.1985	2.5922
8	1/21	0.7817	0.0005	0.0007	0.1283	0.9113
9	1/21	0.5286	0.0001	0.0001	0.0398	0.5685
10	1/21	0.4286	0.0001	0.0001	0.0310	0.4598
11	1/21	0.3807	0.0002	0.0002	0.0309	0.4120
12	1/21	0.6393	0.0000	0.0001	0.0477	0.6872
13	1/21	0.6393	0.0000	0.0001	0.0477	0.6872
14	1/21	0.6393	0.0000	0.0001	0.0477	0.6872
15	1/21	0.3098	0.0000	0.0000	0.0230	0.3329
16	1/21	0.2180	0.0000	0.0000	0.0159	0.2340
17	1/21	0.3119	0.0000	0.0000	0.0226	0.3345
18	1/21	0.2560	0.0000	0.0001	0.0191	0.2752
19	1/21	0.4000	0.0000	0.0001	0.0284	0.4285
20	1/21	0.4000	0.0000	0.0001	0.0284	0.4285
21	1/21	0.4000	0.0000	0.0001	0.0284	0.4285
Total	1	1.3601	0.0004	0.0007	0.1214	1.4826

Furthermore, the composition and hourly production was also determined and is shown in Table 28.

Table 28: Synthetic Reactor Hourly Molar Production and Composition. Source: Own.

Parameter	CH ₄	H ₂	H ₂ S	RES	Total
n (kmol/h-m ³ _s)	1.2694	0.0004	0.0007	0.1133	1.3837
y (-)	0.9174	0.0003	0.0005	0.0819	1

This synthetic reactor was used in the following Chapter as the model biogas reactor when analysing its viability in cogeneration and hydrogen production applications.

Chapter 4: Biogas Application Scenarios

4.1. System Description

The proposed scenario solved in this section was based on a heat demand retrieved from (Linares Hurtado J. I., Tema 5: Cogeneración, renovables y ciclos de potencia avanzados. Ejercicios de clase, 2021). This demand was modelled using an exponential equation with the following formula. The graph is also displayed in Figure 94.

$$\dot{V} (MW_T) = 20 * e^{\frac{-H}{5000}}$$

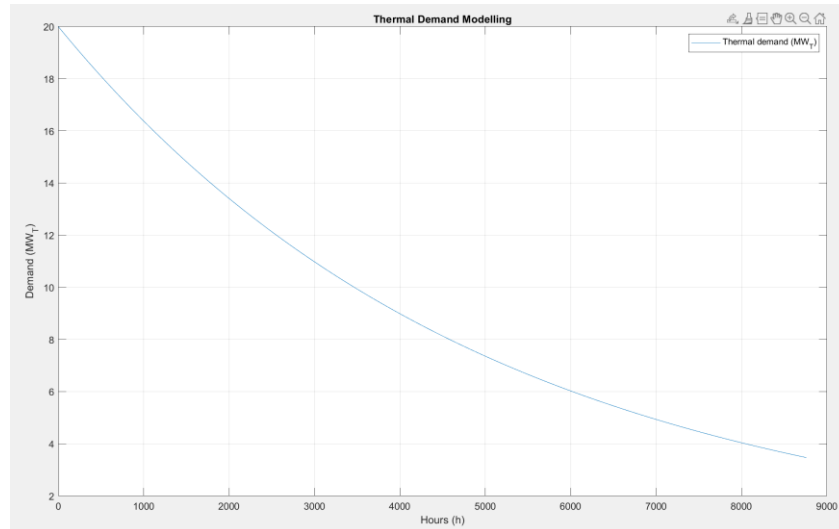


Figure 94: Annual Thermal Demand Modelling. Source: Own.

Furthermore, the problem statement provides additional information required to perform the cogeneration exercise. As such, the current installation meant to be replaced currently supplies the demand employing natural gas boilers with an 85% efficiency, referred to the LHV.

In addition, there are several required parameters to finalize the economic analysis as well as determine the type of cogeneration and its regime. These were determined utilizing the Primary Energy Savings (PES) and the Equivalent Electrical Efficiency (EEE) (Linares Hurtado J. I., Tema 5: Cogeneración, Renovables y Ciclos de Potencia. Apuntes de Clase, 2021) and are as follows:

$$PES = 1 - \frac{Q}{\frac{E}{\eta_{ER}} + \frac{V}{\eta_{VR}}} = 1 - \frac{1}{\frac{\eta_E}{\eta_{ER}} + \frac{\eta_V}{\eta_{VR}}}$$

$$EEE = \frac{E}{Q - \frac{V}{\eta_{VR}}} = \frac{\eta_E}{1 - \frac{\eta_V}{\eta_{VR}}}$$

The PES formula was developed by the European Union and transposed Spanish law through (Ministerio de Industria, Energía y Turismo, 2014), requiring sizing and analysis to be based on thermal demand, as electrical demand sizing, lead to oversized CHT (Combined Heat and Power) plants.

Legislation also establishes the requirement for systems with an electrical power higher than 1 MWe to have a PES>10% to be considered high-efficiency systems. PES evaluates the energy savings of producing heat and power jointly as opposed to producing the same power employing separate equipment with reference efficiencies. On the other hand, EEE sized based on electrical demand.

This parameter calculates the electrical generation efficiency from the waste heat (produced and not consumed by thermal demand), covered using reference technologies. In addition, the EEE is used to include the CHT plant in the special regime of the generation registry, based on data found in (Ministerio de Industria, Turismo y Comercio, 2013). The table is shown below in REF.

Combustible	Potencia eléctrica \leq 1 MW	Potencia eléctrica \wedge 1 MW
Gas natural y GLP en motores térmicos	49,5	55
Gas natural y GLP en turbinas de gas	53,1	59
Combustibles líquidos en centrales con calderas	44,1	49
Combustibles líquidos en motores térmicos	50,4	56
Biomasa agraria, forestal o industrial	27	30
Biogas, estiércol o biocarburantes	45	50
Otros combustibles	53,1	59

Figure 95: Minimum EEE to Include CHT Plant in the Special Regime Registry. Source: (Linares Hurtado J. I., Tema 5: Cogeneración, Renovables y Ciclos de Potencia. Apuntes de Clase, 2021);

Furthermore, the reference efficiencies to be used in the formulae depend on the intended use of the heat as well as the fuel used in CHT. The tables with these reference values can be seen below in Figure 96 and Figure 97 for the thermal and electrical efficiencies, respectively (European Commission, 2011).

	Type of fuel	Steam/hot water	Direct use of exhaust gases (*)
Solids	Hard coal/coke	88	80
	Lignite/lignite briquettes	86	78
	Peat/peat briquettes	86	78
	Wood fuels	86	78
	Agricultural biomass	80	72
	Biodegradable (municipal) waste	80	72
	Non-renewable (municipal and industrial) waste	80	72
	Oil shale	86	78
Liquids	Oil (gas oil + residual fuel oil), LPG	89	81
	Bio-fuels	89	81
	Biodegradable waste	80	72
	Non-renewable waste	80	72
Gaseous	Natural gas	90	82
	Refinery gas/hydrogen	89	81
	Biogas	70	62
	Coke oven gas, blast furnace gas, other waste gases, recovered waste heat	80	72

(*) Values for direct heat should be used if the temperature is 250 °C or higher.

Figure 96: Harmonised Efficiency Reference values for Heat Generation. Source: (European Commission, 2011).

	Year of construction: Type of fuel	2001 and before	2002	2003	2004	2005	2006-2011	2012-2015
Solids	Hard coal/coke	42,7	43,1	43,5	43,8	44,0	44,2	44,2
	Lignite/lignite briquettes	40,3	40,7	41,1	41,4	41,6	41,8	41,8
	Peat/peat briquettes	38,1	38,4	38,6	38,8	38,9	39,0	39,0
	Wood fuels	30,4	31,1	31,7	32,2	32,6	33,0	33,0
	Agricultural biomass	23,1	23,5	24,0	24,4	24,7	25,0	25,0
	Biodegradable (municipal) waste	23,1	23,5	24,0	24,4	24,7	25,0	25,0
	Non-renewable (municipal and industrial) waste	23,1	23,5	24,0	24,4	24,7	25,0	25,0
	Oil shale	38,9	38,9	38,9	38,9	38,9	39,0	39,0
Liquids	Oil (gas oil + residual fuel oil), LPG	42,7	43,1	43,5	43,8	44,0	44,2	44,2
	Biofuels	42,7	43,1	43,5	43,8	44,0	44,2	44,2
	Biodegradable waste	23,1	23,5	24,0	24,4	24,7	25,0	25,0
	Non-renewable waste	23,1	23,5	24,0	24,4	24,7	25,0	25,0
Gaseous	Natural gas	51,7	51,9	52,1	52,3	52,4	52,5	52,5
	Refinery gas/hydrogen	42,7	43,1	43,5	43,8	44,0	44,2	44,2
	Biogas	40,1	40,6	41,0	41,4	41,7	42,0	42,0
	Coke oven gas, blast furnace gas, other waste gases, recovered waste heat	35	35	35	35	35	35	35

Figure 97: Harmonised Efficiency Reference values for Electricity Generation. Source: (European Commission, 2011).

Along with the PES and EEE, the sizing must be performed such that the NVA of the project is maximized. As the NVA is composed of the yearly cashflows and the initial investment, these must be established prior to optimizing said value. To do this, costs for fuel, O&M and electricity were estimated. In the case of electricity and fuel (natural gas), the cost was calculated as the average value of future yearly markets, retrieved from OMIP (OMIP, 2022) in both cases. OMIP prices are shown for both in Figure 98. The mean energy prices are displayed in Figure 98. It must also be added that the relation between HHV and LHV of natural gas is 1.11. Both were assumed to have a 5% nominal rate, a standard value.

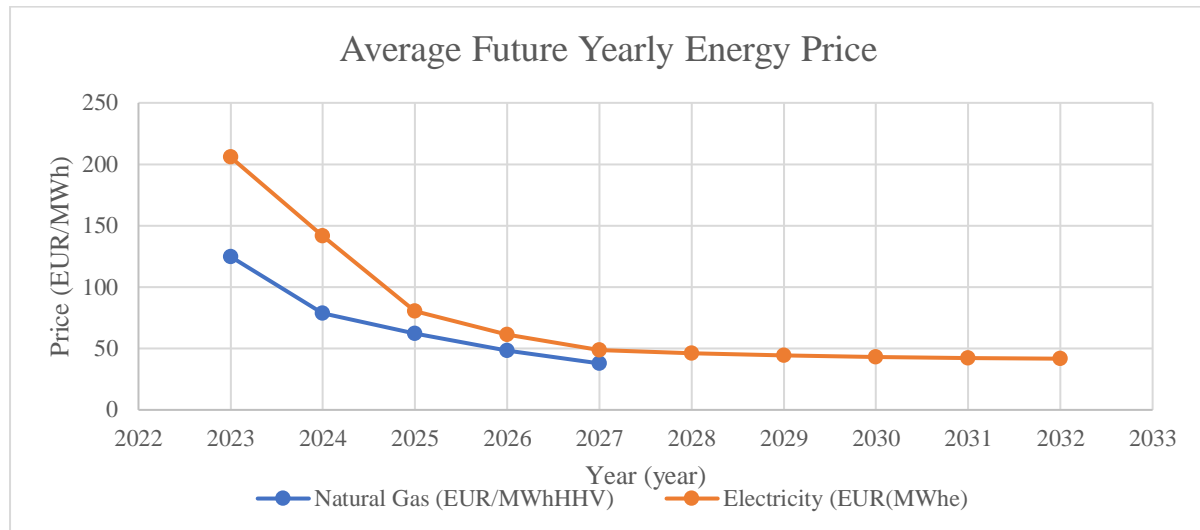


Figure 98: Future Yearly Energy Prices. Source: (OMIP, 2022).

Table 29: Fuel Costs and Nominal Rate. Source: Own.

Parameter	Value
T_{GN} (EUR/MWh _{HHV})	75.55
T_E (EUR/MWh _e)	70.33
HHV/LHV (-)	1.11
t_{fuel} (%)	5.0%

Furthermore, O&M was also considered as part of the analysis. However, as no sources or estimated were found, the data provided in (Linares Hurtado J. I., Tema 5: Cogeneración, renovables y ciclos de potencia avanzados. Ejercicios de clase, 2021). The data required for O&M is provided in Table 30.

Table 30: O&M Costs and Nominal Rate. Source: Own.

Parameter	Value
T_{OM} (EUR/MWh _e)	10
t_{OM} (%)	2.5%

Lastly, both projects were assigned a required return rate of 10%, a typical value (Linares Hurtado J. I., Tema 1: Introducción, 2021). The project was assumed to have a 25-year lifespan. These details are collected in Table 31.

Table 31: Project Return Rate and Lifespan. Source: Own.

Parameter	Value
i (%)	10.0%
N (years)	25

4.2. Cogeneration Equipment

4.2.1. Biogas Motors

The biogas cogeneration motors selected were obtained from the Jenbacher product line found in (Zorg Biogas, 2022). These provided the electrical power, their consumption, and efficiencies. The data is provided in Table 32 and Table 33 below. The cost was estimated using smaller cogeneration groups found in the site and scaled.

Table 32: Jenbacher Motor's Efficiency. Source: (Zorg Biogas, 2022).

Parameter	Value
η_V (-)	0.428
η_T (-)	0.427
η_{boiler} (-)	0.85

Table 33: Jenbacher Motor Catalogue. Source: (Zorg Biogas, 2022).

Nominal power (MWe)	Price (EUR)	Consumption (m ³ /h)
1.501	405,671.91€	642.4
1.202	385,277.91€	518
1.067	374,340.64€	476
0.901	358,816.33€	389
0.851	353,574.89€	382

A logarithmic and a linear regression were made on the group's price and biogas consumption, using electrical power as the input. Both graphs are shown below in Figure 99 and Figure 100, respectively.

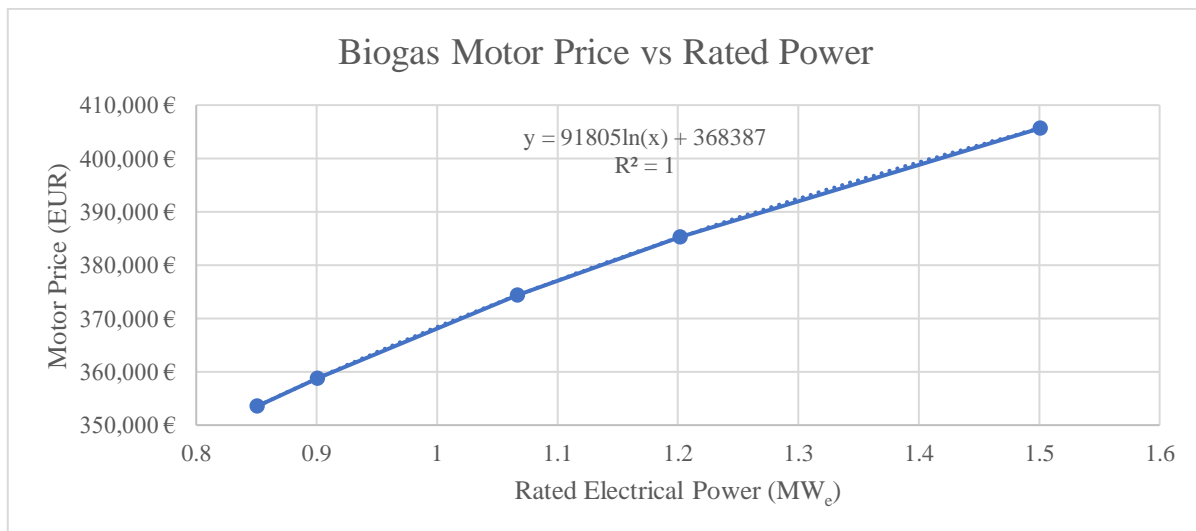


Figure 99: Biogas Motor Price Modelling. Source: Own.

$$\text{Price [EUR]} = 91805 * \ln(P_e [MWe]) + 368387; \quad R^2 = 1$$

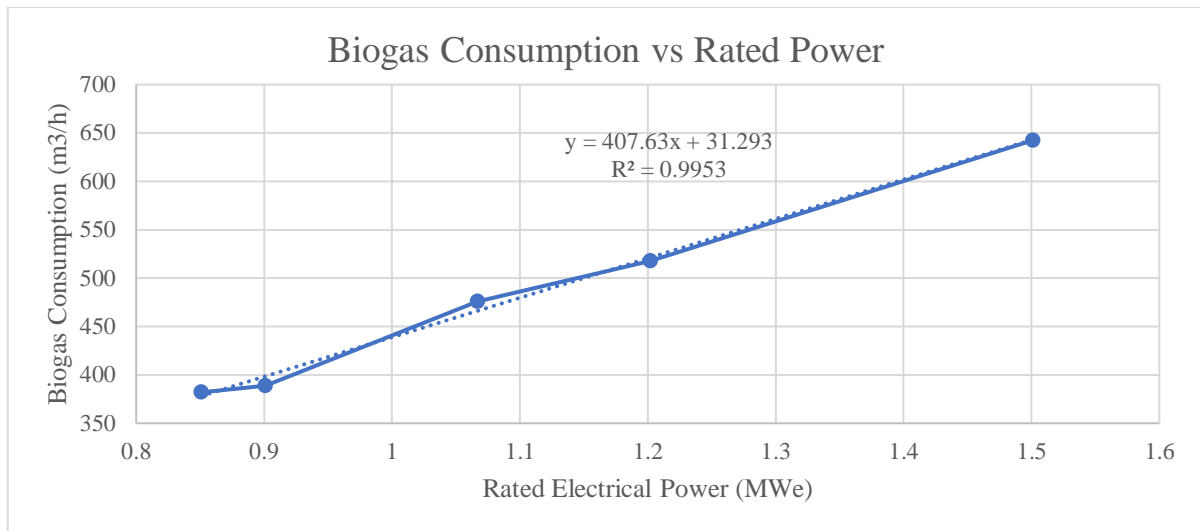


Figure 100: Biogas Consumption Modelling. Source: Own.

$$Q_G \left[\frac{m^3}{h} \right] = 407.63 * P_e [MWe] + 31.293; \quad R^2 = 0.9953$$

4.2.2. Natural Gas Motors

As in the previous equipment selection, a catalogue of CHT motors was used to model power and consumption curves. However, in this case the motors operate with natural gas, which can be substituted with biomethane once the impurities in biogas are removed along with the CO₂ through an upgrading process. These motors were retrieved from (Enerblue Cogeneration, 2019). To maintain a similar structure and modelling, the motors obtained from the catalogue, along with their efficiencies can be found in Table 34 and Table 35 below. It must also be added that the regression obtained when modelling the price was reused in this section as it was not provided.

Table 34: Enerblue Motor's Efficiency. Source: (Zorg Biogas, 2022).

Parameter	Value
η_V (-)	0.441
η_T (-)	0.426

Table 35: Enerblue Motor Catalogue. Source: (Zorg Biogas, 2022).

Nominal power (MWe)	Price (EUR)	Consumption (m³/h)
2	432,021.38€	489.6
1.56	409,211.38€	385.4
1.2	385,125.03€	294.2
1.013	369,572.77€	250.1
0.8	347,901.31€	197.1

As with the previous section, the graphs and formulae for price and consumption can be found below in Figure 101 and Figure 102, respectively.

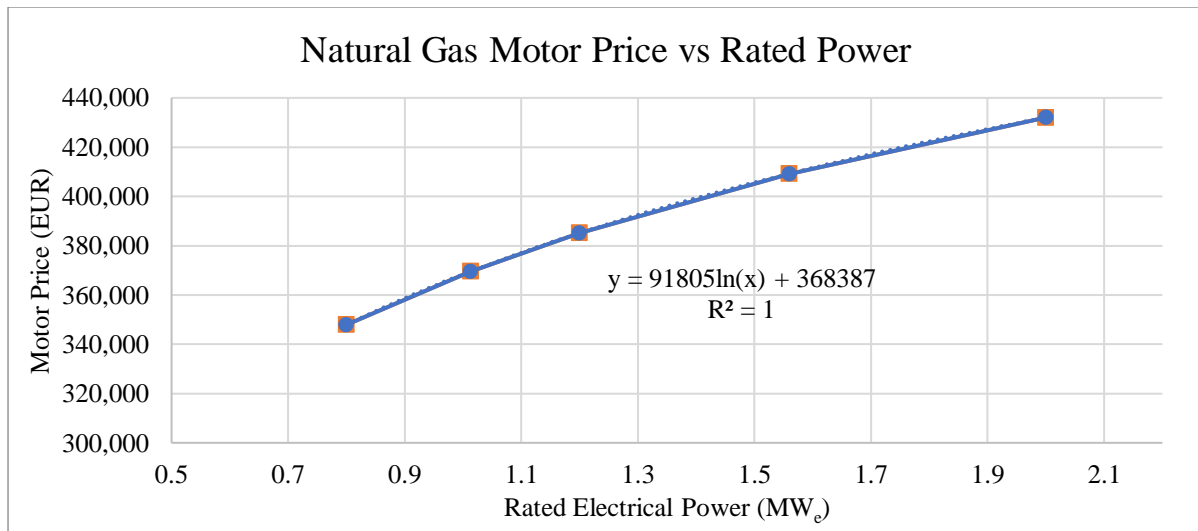


Figure 101: Natural Gas Motor Price Modelling. Source: Own.

$$\text{Price [EUR]} = 91805 * \ln(P_e [MW_e]) + 368387; \quad R^2 = 1$$

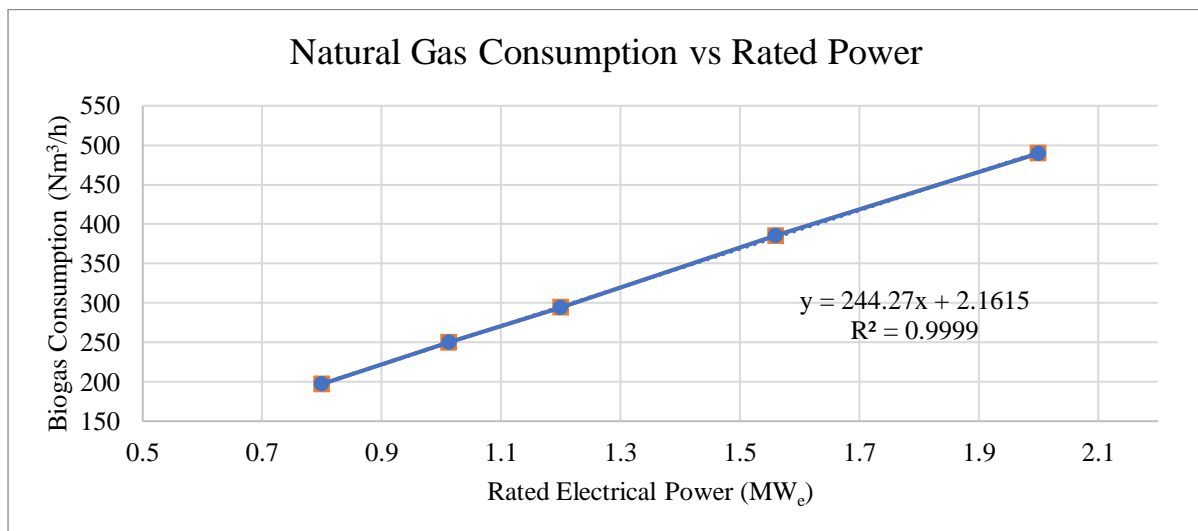


Figure 102: Natural Gas Consumption Modelling. Source: Own.

$$Q_G \left[\frac{Nm^3}{h} \right] = 244.27 * P_e [MW_e] + 2.1615; \quad R^2 = 0.9999$$

Comparing both applications; it is evident that natural gas motors present a lower consumption for a given nominal power. This is due to the similarity of the combustion technologies, as both engines oxidise the methane present in the intake gas.

The difference resides in the composition of the fuel gas. Raw biogas contains much higher impurities when compared to natural gas, which is almost pure methane.

4.3. Direct Biogas Use Scenario

In this scenario, the biogas produced by the reactor, which was calculated once the NVA was optimised, is used directly in cogeneration motors, without upgrading or treating. Furthermore, was calculated using the following formula (Linares Hurtado J. I., Tema 1: Introducción, 2021):

$$NVA = VE * f_{\Sigma}^{VE} + ER * f_{\Sigma}^{ER} - OM * f_{\Sigma}^{OM} - F * f_{\Sigma}^F - INV_0$$

The provided fields correspond to Energy Sale (VE, referred to the electricity generate); Recovered Energy (ER, referred to the natural gas previously used in the boilers); O&M (OM, operation & maintenance); Fuel Cost (F, in this case referred to the biogas) and lastly the Initial Investment INV_0 . Prior to continuing with the modelling and optimization, the cost for the biogas reactor was determined, which can be approximated as the LCOE.

4.3.1. AD Reactor LCOE Estimation

There has been ample research into the LCOE (levelized Cost of Energy) of established renewable technologies such as PV and wind power. However, the cost of biogas production has rarely been studied on its own for electricity generation. However, (Fraunhofer ISE, 2018) does analyse the use of biogas for energy generation, without upgrading. As such, the data collected during their research can be used to estimate the LCOE to produce raw biogas. It must also be noted that the study was published in 2018, and therefore the result must be adjusted for inflation.

The report collects several data points as well as 2 hypotheses for operation and investment required. They first data collected referred to the financing structure of the project to estimate the WACC. However, to maintain consistency the aforementioned 10% nominal rate was used as the resulting WACC was deemed too low. The WACC results can be seen in Table 36.

$$WACC = (1 - Tax) * \%_{Debt} * i_{Debt} + \%_{Equity} * ROE$$

Table 36: WACC estimation. Source: (Fraunhofer ISE, 2018).

Parameter	Value
Tax (%)	30%
Debt (%)	80%
Equity (%)	20%
i_{Debt} (%)	3.5%
ROE (%)	8%
WACC (%)	3.56%

As previously explained, two hypotheses were made regarding operation and investment (fixed costs), which can be found in Table 37. The possible combinations are presented in Table 38.

Table 37: Hypothesis for Reactor Cost and Operation. Source: (Fraunhofer ISE, 2018).

Parameter	Low Value	High Value
Investment (EUR/MW)	2500000	5000000
Operation (h/year)	4000	7000

Table 38: Reactor Hypothesis Combination. Source: Own.

Parameter	Scenario 1	Scenario 2	Scenario 3	Scenario 4
Investment (EUR/MW)	5000000	5000000	2500000	2500000
Operation (h/year)	7000	4000	7000	4000

Once the various scenarios were presented, the variable costs pertaining to the production of biogas were compiled. These include the cost of the substrate, labelled as fuel (F, in EUR/MW) as well as O&M. In this case, O&M was further divided into “fixed O&M,” which depends on the plant’s nominal power (OM_f , as a percentage of the fixed cost investment) and “variable O&M” which depends on energy produced (OM_v , in EUR/MWh). In addition, these maintain the nominal rates for fuel and O&M previously presented. The values, along with the rates can be found below in Table 39.

Table 39: Variable AD Reactor Costs & Rates. Source: (Fraunhofer ISE, 2018).

Parameter	Value
F (EUR/MW)	38.4
OM_f (% _{INV})	4%
OM_v (EUR/MWh)	4
t_F (%)	5%
t_{OM} (%)	2.5%
i (%)	10.0%
N (years)	25

Finally, employing all the accumulation factors (f_Σ) along with the annualization factor (f_a) can be established using the following formulae retrieved from (Linares Hurtado J. I., Tema 1: Introducción, 2021). The results are shown in Table 40.

$$k_f = \frac{1 + t_f}{1 + i} \quad k_{OM} = \frac{1 + t_{OM}}{1 + i}$$

$$f_\Sigma^f = \frac{k_f * (1 - k_f^N)}{1 - k_f} \quad f_\Sigma^{OM} = \frac{k_{OM} * (1 - k_{OM}^N)}{1 - k_{OM}}$$

$$f_a = \frac{i * (1 + i)^N}{(1 + i)^N - 1}$$

Table 40: Compounding and Annualization results. Source: Own.

Parameter	Value
k_f (-)	0.955
k_{OM} (-)	0.9318
f_f (-)	14.4365
f_{OM} (-)	11.3281
f_a (-)	0.0611

Lastly, the LCOE to produce the biogas was determined using the following formula which compounds all the costs to Year 0 and annualises them.

$$LCOE \left[\frac{\text{€}}{\text{MWh}} \right] = \frac{OM * f_\Sigma^{OM} + F * f_\Sigma^F + INV_0}{h} * f_a$$

The final LCOE results per scenario are shown in Table 41 below.

Table 41: LCOE Calculation per Scenario. Source: Own.

Parameter	Scenario 1	Scenario 2	Scenario 3	Scenario 4
Investment (EUR/MW)	5,000,000.00€	5,000,000.00€	2,500,000.00€	2,500,000.00€
Operation (h/year)	7000	4000€	7000	4000
OM _f (EUR/MW)	200,000.00€	200,000.00€	100,000.00€	100,000.00€
OM _v (EUR/MWh)	28,000.00€	16,000.00€	28,000.00€	16,000.00€
F (EUR/MW)	268,800.00€	153,600.00€	268,800.00€	153,600.00€
Cumulative Cost (EUR/MW)	11,463,350.83€	9,664,326.86€	7,830,536.71€	6,031,512.74€
Annualized Cost (EUR/MW)	700,064.45€	590,198.43€	478,209.25€	368,343.23€
LCOE (EUR/MWh)	100.01€	147.55€	68.32€	92.09€

As it can be appreciated, LCOE varies greatly depending on the scenario. Therefore, the mean LCOE was selected as a representative value. Lastly, the cost was adjusted for inflation, which was 13.97% from 2018 to 2022 (CPI Inflation Calculator, 2022). The final LCOE is provided in Table 42.

Table 42: LCOE of AD Reactor Adjusted for Inflation. Source: Own.

Parameter	Value
Mean LCOE ₂₀₁₈ (EUR/MWh)	101.99€
Inflation (%)	13.97%
Mean LCOE ₂₀₂₂ (EUR/MWh)	116.24€

4.3.2. Direct Biogas Use Economic Analysis

Proceeding with the final section of the design, the compounding factor for fuel and O&M were obtained using the previous formulae retrieved from (Linares Hurtado J. I., Tema 1: Introducción, 2021). The results are shown in Table 43.

$$k_f = \frac{1 + t_f}{1 + i} \quad k_{OM} = \frac{1 + t_{OM}}{1 + i}$$

$$f_{\Sigma}^f = \frac{k_f * (1 - k_f^N)}{1 - k_f} \quad f_{\Sigma}^{OM} = \frac{k_{OM} * (1 - k_{OM}^N)}{1 - k_{OM}}$$

Table 43: Compounding and Annualization results. Source: Own.

Parameter	Value
k _f (-)	0.955
k _{OM} (-)	0.9318
f _f (-)	14.4365
f _{OM} (-)	11.3281

The remaining step is to calculate the various cashflows, which will depend on the electrical power and the hours of operation:

$$\eta_e = \frac{\dot{W}}{\dot{Q}} \quad \eta_v = \frac{\dot{V}}{\dot{Q}}$$

$$W(\dot{h}) = \frac{\eta_e}{\eta_v} * V(\dot{h}) \rightarrow W(\dot{h}) = \frac{\eta_e}{\eta_v} * 20 * e^{\frac{-h}{5000}}$$

$$\begin{aligned} \dot{Q} &= \frac{1}{\eta_V} * V(\dot{h}) \rightarrow \frac{1}{\eta_V} * 20 * e^{\frac{-h}{5000}} \\ VE &= W(\dot{h}) * T_e * h \rightarrow \frac{\eta_e}{\eta_V} * 20 * e^{\frac{-h}{5000}} * T_e * h \\ ER &= Q(\dot{h}) * T_{GN} * \frac{HHV}{LHV} * h \rightarrow \frac{1}{\eta_V} * 20 * e^{\frac{-h}{5000}} * T_{GN} * h \\ F &= \frac{1}{\eta_V} * V(\dot{h}) * LCOE_{biogas} * h \rightarrow \frac{1}{\eta_V} * 20 * e^{\frac{-h}{5000}} * LCOE_{biogas} * h \\ OM &= W(h) * T_{OM} * h \rightarrow OM = \frac{\eta_e}{\eta_V} * 20 * e^{\frac{-h}{5000}} * T_{OM} * h \\ INV_o &= 36387 + 91805 * \ln\left(\frac{\eta_e}{\eta_V} * 20 * e^{\frac{-h}{5000}}\right) \end{aligned}$$

Therefore, the NVA can be constructed, as follows:

$$\begin{aligned} NVA &= VE * f_{\Sigma}^{VE} + ER * f_{\Sigma}^{ER} - OM * f_{\Sigma}^{OM} - F * f_{\Sigma}^F - INV_o \\ NVA &= \frac{\eta_e}{\eta_V} * 20 * e^{\frac{-h}{5000}} * T_e * h * f_{\Sigma}^{VE} + \frac{1}{\eta_V} * 20 * e^{\frac{-h}{5000}} * f_{\Sigma}^{ER} - \frac{\eta_e}{\eta_V} * 20 * e^{\frac{-h}{5000}} * T_{OM} * h * f_{\Sigma}^{OM} \\ &\quad - \frac{1}{\eta_V} * 20 * e^{\frac{-h}{5000}} * LCOE_{biogas} * h * f_{\Sigma}^F - 36387 - 91805 * \ln\left(\frac{\eta_e}{\eta_V} * 20 * e^{\frac{-h}{5000}}\right) \end{aligned}$$

Due to the nature of the investment formula, the optimization had to be solved numerically. The results are shown below in Table 44.

Table 44: Biogas Scenario NVA. Source: Own.

Parameter	Value
H* (h)	5015.31
Pe (MW _e)	7.32
NVA (EUR)	29,880,973.60€
Q _{biogas} (m ³ /h)	3014.3115

Lastly, the Reactor dimensions were calculated based on the biogas production of the synthetic reactor. The results are shown in Table 45. A cylindrical reactor vessel was used as the basis:

$$V_{total} = \pi * \frac{D^2}{4} * h$$

Table 45:AD Reactor Sizing for Biogas Scenario. Source: Own.

Parameter	Value
V _{sludge} (m ³)	90.4240
V _{substrate} (m ³)	30.1413
V _{supernatant} (m ³)	120.5653
V _{total} (m ³)	241.1306
V _{reactor} (m ³)	337.5829
D (m)	4.8866
h (m)	4.5

Regarding the type of plant designed, the PES and EEE were calculated. This plant utilizes biogas as the fuel source. In addition, the plant was built after 2015, and therefore the reference electrical value is 0.42. The heat will be used to produce hot water, which requires the higher reference value at 0.7. The calculations are shown below in Table 46.

Table 46: PES & EEE of Biomethane Scenario. Source: Own.

Parameter	Value
η_{ER} (-)	0.42
η_{VR} (-)	0.7
η_E (-)	0.427
η_V (-)	0.428
PES (-)	0.3858
EEE (-)	1.0990

As it can be seen, the biogas plant would be considered a high-efficiency plant and would be inscribed in the special regime. It is also worth noting that the EEE is higher than 100%, which is not impossible, but uncommon.

4.4. Biogas Upgrading Scenario

In this scenario, the biogas produced by the reactor, which was calculated once the NVA was optimised, is used directly in cogeneration motors, without upgrading or treating. Furthermore, was calculated using the following formula (Linares Hurtado J. I., Tema 1: Introducción, 2021):

$$NVA = VE * f_{\Sigma}^{VE} + ER * f_{\Sigma}^{ER} - OM * f_{\Sigma}^{OM} - F * f_{\Sigma}^F - INV_o$$

The provided fields correspond to Energy Sale (VE, referred to the electricity generate); Recovered Energy (ER, referred to the natural gas previously used in the boilers); O&M (OM, operation & maintenance); Fuel Cost (F, in this case referred to the biogas) and lastly the Initial Investment INV_o . Prior to continuing with the modelling and optimization, the cost for the biogas scrubbing technology is required, as that of the biogas reactor was previously determined.

4.4.1. Biogas Upgrading LCOE Estimation

To maintain a similar structure to the previous Scenario, the LCOE of the scrubber will be modelled and treated as part of the fuel cost, resulting in:

$$T_f \left(\frac{\text{€}}{\text{MWh}} \right) = LCOE_{biogas} + LCOE_{upgrading} = LCOE_{bg+sc}$$

However, before the LCOE could be calculated, the upgrading technology had to be selected. To do this, several technologies were researched (Angelidaki, et al., 2019). These were based primarily on the absorption of CO_2 from the biogas, which proved a more the most effective principle. As a result, the gas-liquid packing column system was selected to be used as the upgrading technology.

To determine the LCOE of biogas, previous estimations were used as a basis, including the fixed O&M as well as the 2 operation hours previously employed. The data was retrieved from (Nguyen, Morrison, & Nelson, 2005), considering a new scrubber employing the FGD (flue-gas desulphurization), which are wet scrubbers. The nominal rates were considered equal to those of the previous section. The information is displayed in Table 47 and the scenarios in Table 48. It must also be mentioned that the report contains information from 2005, and will therefore require adjusting for inflation and conversion into EUR.

Table 47: Hypothesis for Scrubber Cost and Operation. Source: (Nguyen, Morrison, & Nelson, 2005).

Parameter	Low Value	High Value
Investment (AUD/MW)	130000	380000
O&M (AUD/MWh)	1.1	22.6
Operation (h/year)	4000	7000

Table 48: Scrubber Hypothesis Combination. Source: Own.

Parameter	Sc 1	Sc 2	Sc 3	Sc 4	Sc 5	Sc 6	Sc 7	Sc 8
INV (AUD/MW)	130000	130000	130000	130000	380000	380000	380000	380000
O&M (AUD/MWh)	1.1	1.1	22.6	22.6	1.1	1.1	22.6	22.6
Oper. (h/year)	4000	7000	4000	7000	4000	7000	4000	7000

Once the various scenarios were presented, the variable costs pertaining to the production of biogas were compiled. These include the O&M. In this case, O&M was further divided into “fixed O&M,” which depends on the plant’s nominal power (OM_f , as a percentage of the fixed cost investment) and “variable O&M” which depends on energy produced (OM_v , in AUD/MWh). In addition, these maintain the nominal rates for fuel and O&M previously presented. The values, along with the rates can be found below in Table 49.

Table 49: Variable Scrubber Costs & Rates. Source: (Fraunhofer ISE, 2018).

Parameter	Value
OM_f (%INV)	4%
t_{OM} (%)	2.5%
i (%)	10.0%
N (years)	25

Finally, employing all the accumulation factors (f_Σ) along with the annualization factor (f_a) can be established using the following formulae retrieved from (Linares Hurtado J. I., Tema 1: Introducción, 2021). The results are shown in Table 50.

$$k_{OM} = \frac{1 + t_{OM}}{1 + i}$$

$$f_\Sigma^{OM} = \frac{k_{OM} * (1 - k_{OM}^N)}{1 - k_{OM}}$$

$$f_a = \frac{i * (1 + i)^N}{(1 + i)^N - 1}$$

Table 50: Compounding and Annualization results. Source: Own.

Parameter	Value
k_f (-)	0.955
k_{OM} (-)	0.9318
f_f (-)	14.4365
f_{OM} (-)	11.3281
f_a (-)	0.0611

Lastly, the LCOE to produce the biogas was determined using the following formula which compounds all the costs to Year 0 and annualises them.

$$LCOE \left[\frac{\text{€}}{\text{MWh}} \right] = \frac{OM * f_{\Sigma}^{OM} + F * f_{\Sigma}^F + INV_0}{h} * f_a$$

The final LCOE results per scenario are shown in Table 51 below.

Table 51: Scrubber LCOE Calculation per Scenario. Source: Own.

Parameter	Sc 1	Sc 2	Sc 3	Sc 4	Sc 5	Sc 6	Sc 7	Sc 8
Investment (AUD /MW)	\$130,000.00	\$130,000.00	\$130,000.00	\$130,000.00	\$380,000.00	\$380,000.00	\$380,000.00	\$380,000.00
Operation (h/year)	4000	7000	4000	7000	4000	7000	4000	7000
OM _f (AUD /MW)	\$5,200.00	\$5,200.00	\$5,200.00	\$5,200.00	\$15,200.00	\$15,200.00	\$15,200.00	\$15,200.00
OM _v (AUD /MWh)	\$4,400.00	\$7,700.00	\$90,400.00	\$158,200.00	\$4,400.00	\$7,700.00	\$90,400.00	\$158,200.00
Cumm. Cost (AUD /MW)	\$238,750.16	\$276,133.02	\$1,212,970.30	\$1,981,018.27	\$602,031.57	\$639,414.43	\$1,576,251.71	\$2,344,299.68
Ann. Cost (AUD/MW)	\$14,580.42	\$16,863.39	\$74,075.84	\$120,980.37	\$36,765.94	\$39,048.91	\$96,261.36	\$143,165.89
LCOE (AUD/MWh)	\$3.65	\$2.41	\$18.52	\$17.28	\$9.19	\$5.58	\$24.07	\$20.45

As it can be appreciated, LCOE varies depending on the scenario. Therefore, the mean LCOE was selected as a representative value. Lastly, the cost was adjusted for inflation, which was 39.62% from 2005 to 2022 (CPI Inflation Calculator, 2022). The final LCOE is provided in Table 52. The conversion rate provided was obtained from (European Central Bank, 2022).

Table 52: LCOE of AD Reactor Adjusted for Inflation. Source: Own.

Parameter	Value
Mean LCOE ₂₀₂₅ (AUD/MWh)	12.64€
Inflation (%)	39.62%
Mean LCOE ₂₀₂₂ (AUD/MWh)	\$17.6521
Conversion rate (AUD/EUR)	1.5478
Mean LCOE ₂₀₂₂ (EUR/MWh)	11.4046€
LCOE _{bg+sc} (EUR/MWh)	127.6427€

4.4.2. Biogas Upgrading Economic Analysis

Proceeding with the final section of the design, the compounding factor for fuel and O&M were obtained using the previous formulae retrieved from (Linares Hurtado J. I., Tema 1: Introducción, 2021). The results are shown in Table 57Table 53.

$$k_f = \frac{1 + t_f}{1 + i} \quad k_{OM} = \frac{1 + t_{OM}}{1 + i}$$

$$f_{\Sigma}^f = \frac{k_f * (1 - k_f^N)}{1 - k_f} \quad f_{\Sigma}^{OM} = \frac{k_{OM} * (1 - k_{OM}^N)}{1 - k_{OM}}$$

Table 53: Compounding and Annualization results. Source: Own.

Parameter	Value
k_f (-)	0.955
k_{OM} (-)	0.9318
f_f (-)	14.4365
f_{OM} (-)	11.3281

The remaining step is to calculate the various cashflows, which will depend on the electrical power and the hours of operation:

$$\eta_e = \frac{\dot{W}}{\dot{Q}} \quad \eta_V = \frac{\dot{V}}{\dot{Q}}$$

$$W(h) = \frac{\eta_e}{\eta_V} * V(h) \rightarrow W(h) = \frac{\eta_e}{\eta_V} * 20 * e^{\frac{-h}{5000}}$$

$$\dot{Q} = \frac{1}{\eta_V} * V(h) \rightarrow \frac{1}{\eta_V} * 20 * e^{\frac{-h}{5000}}$$

$$VE = W(h) * T_e * h \rightarrow \frac{\eta_e}{\eta_V} * 20 * e^{\frac{-h}{5000}} * T_e * h$$

$$ER = Q(h) * T_{GN} * \frac{HHV}{LHV} * h \rightarrow \frac{1}{\eta_V} * 20 * e^{\frac{-h}{5000}} * T_{GN} * h$$

$$F = \frac{1}{\eta_V} * V(h) * LCOE_{biogas} * h \rightarrow \frac{1}{\eta_V} * 20 * e^{\frac{-h}{5000}} * LCOE_{bb+sc} * h$$

$$OM = W(h) * T_{OM} * h \rightarrow OM = \frac{\eta_e}{\eta_V} * 20 * e^{\frac{-h}{5000}} * T_{OM} * h$$

$$INV_o = 36387 + 91805 * \ln\left(\frac{\eta_e}{\eta_V} * 20 * e^{\frac{-h}{5000}}\right)$$

Therefore, the NVA can be constructed, as follows:

$$NVA = VE * f_{\Sigma}^{VE} + ER * f_{\Sigma}^{ER} - OM * f_{\Sigma}^{OM} - F * f_{\Sigma}^F - INV_o$$

$$NVA = \frac{\eta_e}{\eta_V} * 20 * e^{\frac{-h}{5000}} * T_e * h * f_{\Sigma}^{VE} + \frac{1}{\eta_V} * 20 * e^{\frac{-h}{5000}} * f_{\Sigma}^{ER} - \frac{\eta_e}{\eta_V} * 20 * e^{\frac{-h}{5000}} * T_{OM} * h * f_{\Sigma}^{OM}$$

$$- \frac{1}{\eta_V} * 20 * e^{\frac{-h}{5000}} * (LCOE_{bg+sc}) * h * f_{\Sigma}^F - 36387 - 91805 * \ln\left(\frac{\eta_e}{\eta_V} * 20 * e^{\frac{-h}{5000}}\right)$$

Due to the nature of the investment formula, the optimization had to be solved numerically. The results are shown below in Table 54.

Table 54: Biomethane Scenario NVA. Source: Own.

Parameter	Value
H^* (h)	5016.36
Pe (MW _e)	7.08
NVA (EUR)	27,953,327.42€
$Q_{biomethane}$ (m ³ /h)	1732.5979

Lastly, the Reactor dimensions were calculated based on the biogas production of the synthetic reactor. The results are shown in Table 55. A cylindrical reactor vessel was used as the basis:

$$V_{total} = \pi * \frac{D^2}{4} * h$$

Table 55: AD Reactor Sizing for Biomethane Scenario. Source: Own.

Parameter	Value
V _{sludge} (m ³)	60.9337
V _{substrate} (m ³)	20.3112
V _{supernatant} (m ³)	81.2449
V _{total} (m ³)	162.4897
V _{reactor} (m ³)	227.4856
D (m)	4.0014
h (m)	4.5

Regarding the type of plant designed, the PES and EEE were calculated. Similar to the previous Scenario, this plant utilizes biogas as the fuel source. In addition, the plant was built after 2015, and therefore the reference electrical value is 0.42. The heat will be used to produce hot water, which requires the higher reference value at 0.7. The calculations are shown below in Table 56.

Table 56: PES & EEE of Biomethane Scenario. Source: Own.

Parameter	Value
η _{ER} (-)	0.42
η _{VR} (-)	0.7
η _E (-)	0.426
η _V (-)	0.441
PES (-)	0.3918
EEE (-)	1.1514

As it can be seen, the biogas plant would be considered a high-efficiency plant and would be inscribed in the special regime. It is also worth noting that the EEE is higher than 100%, which is not impossible, but uncommon.

Chapter 5: Biogas Upgrading Equipment Design

5.1. Biogas Upgrading Technology Selection & Demand Sizing

As previously stated, this scenario required the use of upgrading equipment to remove CO₂ and other impurities present in the biogas produced in the synthetic reactor modelled. To facilitate the design process, the biogas was simplified into a methane and carbon dioxide mixture by maintaining the methane percentage weight and assuming the remaining was CO₂. As a result, the H₂S found in the biogas would not be considered in the design as it accounts for 0.05% of the daily molar production. However, this was partly mitigated through material selection. The composition of the synthetic reactor's biogas and the simplified biogas are provided below in Table 57.

Table 57: Simplified Biogas Composition. Source: Own.

Species	Molar Fraction Synthetic Biogas (%)	Molar Fraction Simplified Biogas (% _{mol})
CH ₄	91.74%	91.74%
H ₂	0.03%	---
H ₂ S	0.05%	---
Residues	8.19%	---
CO ₂	---	8.26%
Total	100%	100%

In addition, the biogas production rate was also determined based on the heat demand curve used as the base for the application case. Once the system requirements were determined, a feasible upgrading technology was selected.

Moving to demand sizing it was decided that to maintain this project's consistency, the demand employed would be that of the second application scenario analysed, in which a packed absorption column was selected as the upgrading technology as a result of its feasibility and widespread use, as it does not require extensive or complex support equipment.

As a result, the demand requirements for the biogas reactor were collected in Table 58.

Table 58: Biogas Demand to Upgrade. Source: Own.

Parameter	Value
Methane Demand (Nm ³ /h)	1732.5979
Biogas Demand (Nm ³ /h)	1888.1359
Methane Demand (kmol/h)	77.3481
Biogas Demand (kmol/h)	84.3156
V _{supernatant} (m ³)	81.2449
V _{sludge} (m ³)	60.9337
V _{substrate} (m ³)	20.3112
V _{total} (m ³)	227.4856

5.2. Packed-Bed Absorption Column Design

Upgrading technologies based on absorption, particularly gas-liquid absorption represents the most cost-effective method to obtain biomethane as a result of their low operating requirements, permitting their use in domestic settings without the use of complex machinery, as evidenced by (Olugasa & Oyesule, 2015).

Despite this, the industrial-sized demand and therefore digester require a finer design procedure. As a result, the methodology proposed in (Pérez Sánchez, Pérez Sánchez, & Segura Silva, 2016). The scrubber designed in this paper absorbed ethanol mixed with carbon dioxide.

However, the governing principles remain those of liquid-gas absorption, permitting the use of the design procedure to design a suitable biogas upgrading process, which is itself divided into various sections pertaining to different aspects of the column.

Random Packing Selection

The first aspect to consider during design is the selection of packing material, as the geometry and material used have a significant impact on the set up and column design as a result of the pressure drop and mass transfer capabilities.

Generally, packing material is made using plastic or ceramic materials, depending on the chemical compound which must be removed. In this case, the upgrading process requires the removal of the CO₂ found in the gas mixture, which requires the use of ceramic rings, as described in (Walcoom Corporation, 2022). In addition, the use of ceramic rings eliminates traces of acid gases, removing H₂S from the real gas mixture.

Furthermore, there has been extensive research on ceramic materials to improve CO₂ removal, which has led to the development of iron (Fe 3+) doped MgO as a catalyst coated on ceramic rings to further increase hydrogen sulphide degradation during the scrubbing process, as shown in (Rakmak & Wiyaratn, 2010).

Once the material has been selected, the packing geometry must also be defined prior to proceeding with the remaining sections. Each ring type presents different technical parameters, primarily their void fraction, packing factor and mass transfer coefficient.

To facilitate design, the geometry selected was that of a Pall ring. This is the second generation of packing material, which improve on the Rasching ring, the first type of random packing, which provide medium mass transfer capacity, as well as a medium pressure drop, avoiding the use of high-pressure equipment which would drastically increase the cost of the packing column. Geometry characteristics were summarized below in (Kayode Coker, 2010).

Table 59: Packing geometries characteristics. Source: (Kayode Coker, 2010).

Packing	Mass Transfer	Pressure Drop	Capacity
Hiflow	High	Low-Medium	Medium-High
Pall	Medium	Medium	Medium
Top Pak	High	Low	High
VSP	High	Medium	High

In addition, Pall rings are the most widely used packing material in packed-bed absorption columns, (Walcoom Corporation, 2022). To provide a graphic representation, various ring geometries are shown below in Figure 103 (Crynes, Albright, & Tan, 2003). Hydraulic parameters of certain geometries were collected in Table 61 (Benitez, Principles and modern applications of mass transfer operations, 2009). Their names, symbols and units are shown in Table 60 (Pérez Sánchez, Pérez Sánchez, & Segura Silva, 2016).

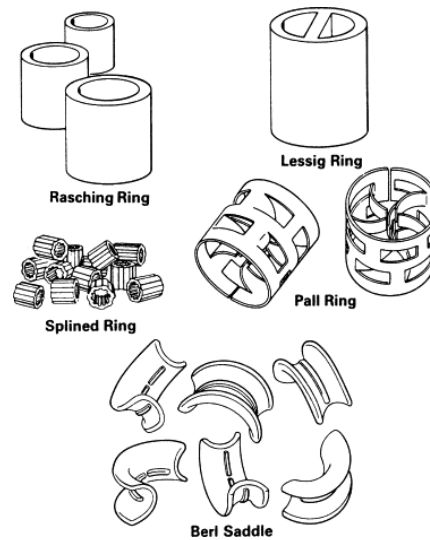


Figure 103: Random Packing Material Ring Geometries. Source: (Crynes, Albright, & Tan, 2003).

Table 60: Packing material parameters. Source: (Benitez, Principles and modern applications of mass transfer operations, 2009).

Symbol	Parameter	Unit
a	Mass-transfer surface area per volume	m ⁻¹
ε	Void fraction	-
Ch	Hydraulic factor	-
C _P	Hydraulic factor	-
F _P	Packing factor	ft ⁻¹
C _L	Mass-transfer factor	-
C _V	Mass-transfer factor	-

Table 61: Sample Hydraulic & Mass-transfer parameters of packing material. Source: (Benitez, Principles and modern applications of mass transfer operations, 2009).

Packing type	Hydraulic Parameters					Mass-transfer parameters	
	a (m ⁻¹)	ε (-)	Ch (-)	C _P (-)	F _P (ft ⁻¹)	C _L (-)	C _V (-)
50mm Metal Hiflow ring	92.0	0.977	0.876	0.421	52	1.168	0.408
50mm Ceramic Pall ring	121.0	0.783	1.335	0.662	142	1.227	0.415
50mm Metal Top Pak ring	75.0	0.98	0.881	0.604	46	1.326	0.389
25mm Metal VSP rings	205.0	0.97	1.369	0.782	105	1.376	0.405

As the material used in the packing rings causes changes in the characteristics of said packing material, especially the packing factor and void fraction due to the change in the ring's compressibility. The parameters used in this design are shown in Table 62 and correspond to a ceramic Pall-ring.

Table 62: Selected Pall Ring Parameters. Source: (Walcoom Corporation, 2022), (Pérez Sánchez, Pérez Sánchez, & Segura Silva, 2016).

Packing type	Hydraulic Parameters					Mass-transfer parameters	
	a (m ⁻¹)	ε (-)	Ch (-)	C _P (-)	F _P (ft ⁻¹)	C _L (-)	C _V (-)
MPR-04	121.0	0.78	1.335	0.662	131	1.227	0.415

Before proceeding, boundary conditions and design limits must be set, as well as species data, collected in the following section.

5.2.1. Scrubber Minimum Boundary Conditions

As mentioned, the operating conditions and other boundary conditions must be set. These represent not only safety parameters such as maximum pressure drop or flooding factor, but also those pertaining to CO₂ solubility in water and the required mass flow to absorb it.

Therefore, the first step is to determine the required water flow using the maximum solubility of CO₂ in water (S_{\max}), which varies with temperature (B10NUMB3R5, 2022). In this case, a temperature of 25°C (298,15K), which was also selected as the operating pressure (T_{op}).

The maximum absolute pressure drop ($\Delta PZ/m$) was also established at 350 Pa/m, within the 200-400Pa/m, although the maximum permittable pressure drop ($\Delta PZ_{\text{per}}/m$) was set using a 1.25 safety coefficient, resulting in 280 Pa/m.

Another design parameter needed were the operation pressure (P_{op}), set to 111.4575 kPa (1.1atm). Lastly, the columns efficiency (η) was also established at 95%. It must also be added that the flooding factor (f_{flood}), which estimates the percentage of the scrubber completely flooded in liquid was set to 70%, as per (Pérez Sánchez, Pérez Sánchez, & Segura Silva, 2016). Thus, the equations were:

$$\begin{aligned}
 n_{CH_4_{ig}} \dot{V} &= n_{CH_4_{og}} \dot{V} \\
 n_{H_2O_{iw}} \dot{V} &= n_{H_2O_{ow}} \dot{V} \\
 n_{CO_2_{ig}} \dot{V} &= n_{CO_2_{og}} \dot{V} + n_{CO_2_{ow}} \dot{V} \\
 n_{CO_2_{ow}} \dot{V} &= \eta * n_{CO_2_{og}} \dot{V} \\
 n_{CO_2_{og}} \dot{V} &= (1 - \eta) * n_{CO_2_{ig}} \dot{V} \\
 n_{CO_2_{ow}} \dot{V} &= S_{\max} * n_{H_2O_{iw}} \dot{V} \\
 y_{CH_4_{ig}} &= \frac{n_{CH_4_{ig}} \dot{V}}{n_{CH_4_{ig}} \dot{V} + n_{CO_2_{ig}} \dot{V}} & y_{CH_4_{og}} &= \frac{n_{CH_4_{og}} \dot{V}}{n_{CH_4_{og}} \dot{V} + n_{CO_2_{og}} \dot{V}} \\
 x_{CH_4_{iw}} &= 0 & x_{CH_4_{ow}} &= 0 \\
 y_{CO_2_{ig}} &= \frac{n_{CO_2_{ig}} \dot{V}}{n_{CH_4_{ig}} \dot{V} + n_{CO_2_{ig}} \dot{V}} & y_{CO_2_{og}} &= \frac{n_{CO_2_{og}} \dot{V}}{n_{CH_4_{og}} \dot{V} + n_{CO_2_{og}} \dot{V}} \\
 x_{CO_2_{iw}} &= 0 & x_{CO_2_{ow}} &= \frac{n_{CO_2_{ow}} \dot{V}}{n_{H_2O_{ow}} \dot{V} + n_{CO_2_{ow}} \dot{V}} \\
 y_{H_2O_{ig}} &= 0 & y_{H_2O_{og}} &= 0 \\
 x_{H_2O_{iw}} &= 1 & x_{H_2O_{ow}} &= \frac{n_{H_2O_{ow}} \dot{V}}{n_{H_2O_{ow}} \dot{V} + n_{CO_2_{ow}} \dot{V}}
 \end{aligned}$$

The parameters obtained from the synthetic reactor, along with the research data were used to dimension the inlet and outlet flows, compounded below into Table 63 and Table 64, respectively.

Table 63: Packed Column Operating Conditions. Source: Own.

Parameter	Value
S_{\max} (kmol _{CO2} /kmol _{H2O})	0.0568
η (-)	0.95
f_{flood} (-)	0.7
T_{op} (K)	298.15
P_{op} (kPa)	111.4575

Table 64: Minimum Molar Flow Rates & Composition at Intakes and Outlets. Source: Own.

Parameter	Gas in (ig)	Gas out (og)	Water in (iw)	Water out (ow)
n_{CH_4} (kmol/h)	77.3481	77.3481	0	0
n_{CO_2} (kmol/h)	6.9053	0.3183	0	6.5780
$n_{\text{H}_2\text{O}}$ (kmol/h)	0	0	116.0412	116.0412
n_{total} (kmol/h)	84.2535	77.6664	116.0412	122.6283
x or y_{CH_4} (-)	0.9180	0.9959	0	0
x or y_{CO_2} (-)	0.0820	0.0041	0	0.0567
x or $y_{\text{H}_2\text{O}}$ (-)	0	0	1	0.9432

A diagram of the minimum operating conditions and molar flow rates is provided in Figure 104.

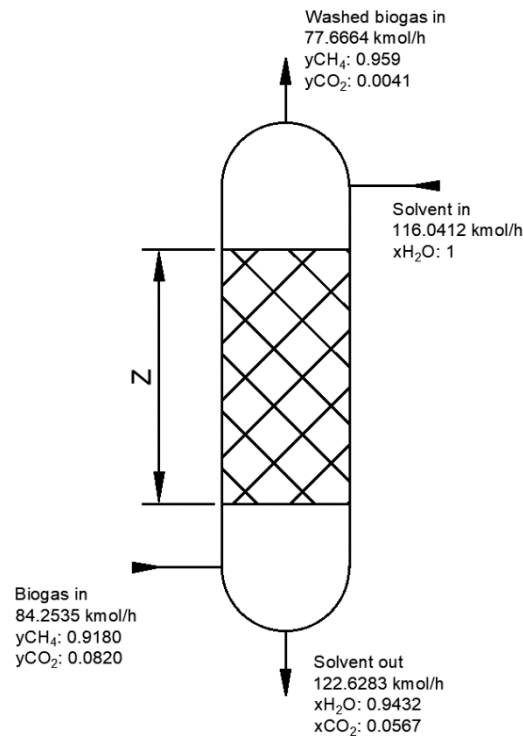


Figure 104: Minimum Operating Conditions for Packed Column. Source: Own.

After establishing the minimum operating conditions, gas composition and molecular data was collected to continue with the tower design.

5.2.2. Gas Inlet Data

To ensure that the scrubber can operate with a certain margin, the nominal gas inflow (Q_G), CO_2 composition and water inflow (m_{H_2O}) were upscaled, as shown in Table 65. The water flow required to achieve nominal conditions was determined employing the formulas previously stated.

Table 65: Selection of Nominal Values. Source: Own.

Parameter	Minimum Value	Nominal Value
Q_G (Nm ³ /h)	1888.1359	1950
N_G (kmol/h)	84.2535	87.0535
y_{CO_2} (-)	0.0820	0.1
N_{H_2O} (kmol/h)	116.0412	146.3336
m_{H_2O} (kg/h)	2091.0630	2636.2416
N_{CO_2r} (kmol/h)	6.5871	8.2701
m_{CO_2r} (kg/h)	303.8924	363.96663

To perform a correct design, specific data from the gas and the water was required. These were: molar mass (M , in kmol/kg) as well as the viscosity and density (ρ and μ , respectively) of the solvent, in this case, water as well as that of methane and carbon dioxide.

Another required parameter was the molar volume of CO_2 (m³/kmol). Furthermore, the collision diameter of both gas species was required (σ , in Å), which measures the minimum distance between two molecules of the type when these collide. This depends on the mass of said molecule, as larger molecules will present a larger molecular radius and therefore a larger collision diameter. The second molecular parameter required is the Lennard-Jonnes potential of both gases (ϵ/k , measured in K), which establishes the potential energy between two molecules depending on their separation and charge (Chemistry LibreTexts, 2015).

Lastly, the Henry constant for CO_2 in water (H , measured in kPa) along with the distribution coefficient, resulting from dividing H by the pressure within the column (ϕ , non-dimensional). The nominal inlet conditions are provided in Table 66. The gas data required in shown in Table 67.

Table 66: Nominal Inlet Conditions, Parameters and Constants. Source: Own.

Parameter	Value	Source
Q_g (Nm ³ /h)	1950	Own
y_{CO_2} (-)	0.1	Own
m_{H_2O} (kg/h)	2636.2416	Own
η (-)	0.95	Own
f_{flood} (-)	0.7	Own
T_{op} (K)	298.15	Own
P_{op} (kPa)	111.4575	Own
R (kJ/kmol-K)	8.314	(Chesmitry LibreTexts, 2021)
$\Delta P/Z$ (Pa/m)	250	Own
$\Delta P/Z_{per}$ (Pa/m)	200	Own
a (m ⁻¹)	121.0	Own
ϵ (-)	0.78	Own
Ch (-)	1.335	Own
C_P (-)	0.662	Own
F_P (ft ⁻¹)	131	Own
C_L (-)	1.227	Own
C_V (-)	0.415	Own
g (m/s ²)	9.81	(The Engineering Toolbox, 2022)

Table 67: Gas Inlet Data. Source: Own.

Parameter	Value	Source
M_{CH_4} (kg/kmol)	16.04	(The Engineering Toolbox, 2022)
M_{CO_2} (kg/kmol)	44.01	(The Engineering Toolbox, 2022)
M_{H_2O} (kg/kmol)	18.02	(The Engineering Toolbox, 2022)
ρ_{CH_4g} (kg/m ³)	0.668	(The Engineering Toolbox, 2022)
ρ_{CO_2g} (kg/m ³)	1.842	(The Engineering Toolbox, 2022)
ρ_{H_2O} (kg/m ³)	997.047	(The Engineering Toolbox, 2022)
μ_{CH_4g} (Pa*s)	1.115*10 ⁻⁵	(The Engineering ToolBox, 2022)
μ_{CO_2g} (Pa*s)	1.493*10 ⁻⁵	(The Engineering ToolBox, 2022)
μ_{H_2O} (Pa*s)	89*10 ⁻⁵	(The Engineering Toolbox, 2022)
V_{MCO_2g} (m ³ /kmol)	0.034	(Pérez Sánchez, Pérez Sánchez, & Segura Silva, 2016)
σ_{CH_4} (Å)	3.8	(Memon, Li, Wencheng, & Tian, 2019)
σ_{CO_2} (Å)	3.3	(Memon, Li, Wencheng, & Tian, 2019)
e/k_{CH_4g} (K)	148.99	(Li, Yu, Zheng, & Li, 2012)
e/k_{CO_2g} (K)	257.8	(Li, Yu, Zheng, & Li, 2012)
H_{pxCO_2} (Pa)	162770	(Sander, 2015)
ϕ (-)	1.4604	Own

In addition, the various nominal flows were calculated and are displayed in Table 68 below.

Table 68: Nominal Design molar flows. Source: Own.

Parameter	Gas in (ig)	Gas out (og)	Water in (iw)	Water out (ow)
n_{CH_4} (kmol/h)	78.3482	78.3482	0	0
n_{CO_2} (kmol/h)	8.7054	0.4353	0	8.2701
n_{H_2O} (kmol/h)	0	0	146.2953	146.2953
n_{total} (kmol/h)	87.0536	78.7835	146.2953	154.5654
x or y $_{CH_4}$ (-)	0.9	0.995	0	0
x or y $_{CO_2}$ (-)	0.1	0.005	0	0.0065
x or y $_{H_2O}$ (-)	0	0	1	0.9935

A diagram of the nominal molar flow rates is provided in Figure 105.

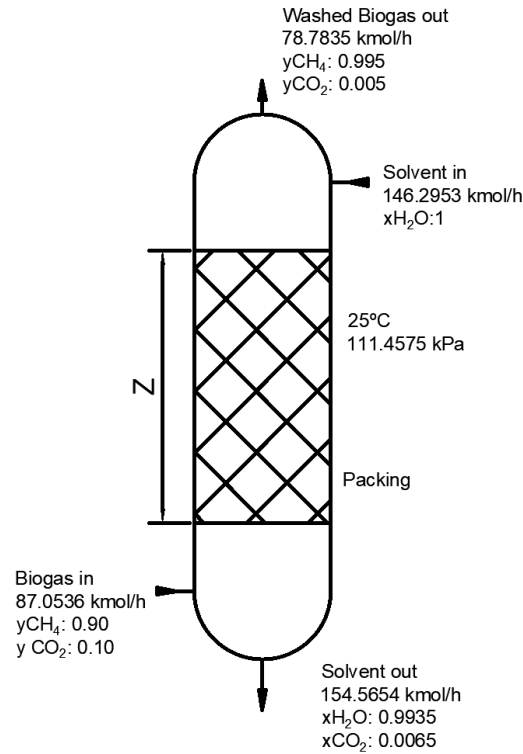


Figure 105: Nominal Operating Conditions for Packed Column. Source: Own.

5.2.3. Tower Diameter

To determine the tower diameter, several previous gas mixture properties must be obtained. The first property to be determined was the molar mass of the gas mixture, using the molecular composition:

$$M_G = y_{CH_4ig} * M_{CH_4} + y_{CO_2ig} * M_{CO_2}$$

Furthermore, the viscosity of said mixture was also required and was obtained through (Pavlov, 1981).

$$\mu_G = \left(\frac{M_G}{\left(\frac{y_{CH_4ig} * M_{CH_4}}{\mu_{CH_4}} \right) + \left(\frac{y_{CO_2ig} * M_{CO_2}}{\mu_{CO_2}} \right)} \right)$$

Once these have been obtained, the total CO_2 absorbed in the column can be determined, along with the exiting water flow:

$$\rho_G = \frac{M_G * P_{op}}{T_{op} * R}$$

$$m_{CO_2ow} = \frac{Q_G * \rho_G}{M_G} * y_{CO_2gi} * \eta * M_{CO_2}$$

$$m_{ow} = m_{iw} + m_{CO_2wo}$$

In addition, the flow parameter (X , non-dimensional), pressure drop parameter under flooding conditions (Y_{flood} , non-dimensional) along with the C_s in flooding conditions (C_{sflood} , non-dimensional) were also calculated with the methodology provided. These are the parameters values in the flooded section of the column. Lastly, the velocity of the gas mixture in flooding conditions

($v_{Gflooding}$, measured in m/s) was employed to calculate the gas velocity (v_G , m/s). Lastly, the tower diameter can be obtained.

$$X = \frac{m_{ow}}{Q_G * \rho_G} * \left(\frac{\rho_G}{\rho_{H_2O}} \right)^{0.5}$$

$$\ln Y_{flood} = \ln -(3.5021 + 1.028 * \ln X + 0.11093 * (\ln X)^2)$$

$$C_{Sflood} = \left(\frac{Y_{flood}}{F_P * \mu_{H_2O}^{0.1}} \right)^{0.5}$$

$$v_{Gflood} = \frac{C_{Sflood}}{\left(\frac{\rho_G}{\rho_{H_2O} - \rho_G} \right)^{0.5}}$$

$$v_G = v_{Gflood} * f_{flood}$$

$$D = \left(\frac{4 * Q_G}{3600 * v_G * \pi} \right)^{0.5}$$

The results pertaining to this section are shown below in Table 69.

Table 69: Tower Diameter Results. Source: Own.

Parameter	Value
M_G (kg/kmol)	18.3352
μ_G (Pa*s)	$6.2200 * 10^{-5}$
ρ_G (kg/m ³)	0.8244
m_{CO_2ow} (kg/h)	366.5845
m_{ow} (kg/h)	3002.8260
X (-)	0.0537
Y_{flood} (-)	0.2358
C_{Sflood} (-)	0.603
v_{Gflood} (m/s)	2.0956
D (m)	0.6857

5.2.4. Pressure Drop

Although a maximum operating pressure drop was established at 200 Pa/m, the solvent retained in the column causes a significant variation of said value in the dry section ($\Delta P/Z_o$, in Pa/m). To obtain said value, the effective particle diameter (d_p , in metres), wall factor (K_w , non-dimensional), the gas mixture Reynolds number (Re_G , non-dimensional) and dry packing resistance (Ψ_o , non-dimensional) were required.

$$d_p = 6 * \frac{1 - \varepsilon}{a}$$

$$K_w = \left(1 + \frac{2}{3} * \left(\frac{1}{1 - \varepsilon} \right) * \frac{d_p}{D} \right)^{-1}$$

$$Re_G = \frac{v_G * d_p * \rho_G * K_w}{(1 - \varepsilon) * \mu_G}$$

In turn, several calculations pertaining to the solvent can be determined such as the liquid mass velocity (G_{H_2O} , measured in kg/m²-s) and the solvent velocity (v_{H_2O} , in m/s). Utilizing said values, the solvent

Reynold's number (Re_{H_2O}) and Froude number (Fr_{H_2O} , non-dimensional) were inputted into the a_h/a ratio (non-dimensional) to be multiplied, obtaining the effective specific surface area of packing (a_h , m^{-1}), which governs liquid holdup (h_L , non-dimensional).

$$\Psi_o = C_P * \left(\frac{64}{Re_G} + \frac{1.8}{Re_G^{0.08}} \right)$$

$$G_L = \frac{4 * m_{H_2O_{iw}}}{3600 * D^2 * \pi}$$

$$v_L = \frac{G_L}{\rho_{H_2O}}$$

$$Re_L = \frac{v_L * \rho_{H_2O}}{a * \mu_{H_2O}}$$

$$Fr_L = \frac{v_L^2 * a}{g}$$

$$\frac{a_h}{a} = \begin{cases} C_h * Re_L^{0.5} * Fr_L^{0.1} & \text{if } Re_L < 5 \\ 0.85 * C_h * Re_L^{0.25} * Fr_L^{0.1} & \text{if } Re_L \geq 5 \end{cases}$$

$$a_h = \left(\frac{a_h}{a} \right) * a$$

$$h_L = \left(12 * \frac{Fr_L}{Re_L} * \left(\frac{a_h}{a} \right)^2 \right)^{\frac{1}{3}}$$

The calculated values were then introduced into the following formulas to obtain $\Delta P/Z_o$ and $\Delta P/Z$:

$$\frac{\Delta P_o}{Z} = \frac{\Psi_o * a * \rho_G * v_G^2}{2 * \varepsilon^3 * K_w}$$

$$\frac{\Delta P}{Z} = \frac{\Delta P_o}{Z} * \left(\left(\frac{\varepsilon}{\varepsilon - h_L} \right)^{1.5} * e^{\frac{Re_L}{200}} \right)$$

The next section of the design focused on the diffusion of the gas and liquid. As with the previous formulae, the results are shown below in Table 70.

Table 70: Pressure Drop Results. Source: Own.

Parameter	Value
d_p (m)	0.0025
K_w	0.9540
Re_G (-)	213.2187
Ψ_o (-)	0.9746
G_L (kg/m ² -s)	2.2589
v_L (m/s)	0.0023
Re_L (-)	20.9761
Fr_L (-)	0.0001
a_h/a (-)	0.9236
a_h (m ⁻¹)	111.7546
h_L (-)	0.0000
$\Delta P_o/Z$ (Pa/m)	231.0598
$\Delta P/Z$ (Pa/m)	256.6111

5.2.5. Diffusion Coefficients

The diffusion of the CO₂ from the biogas mixture into the water used as solvent is governed by the chemical phenomenon which have been studied to varying degrees of development. The process can further be divided into gaseous and aqueous diffusion, pertaining to the gas-phase and liquid-phase, respectively.

Gas-phase diffusion has been thoroughly studied in recent years, resulting in the gas-phase diffusion coefficient (D_G , in m²/s) utilizing the Wilkie & Lee correlation (Benitez, Principles and Modern Applications of Mass Transfer Operations, 2016). This is based on the collision parameter of the species (σ_{AB} , in Å) and the result of the collision integral for the species being studied (Ω_D , non-dimensional), assuming a binary and elastic collision, allowing the intermolecular forces to only act along the centre line (Mostinsky, 2022).

Supplementary calculations must also be made to determine the equations, including the molecular mass parameter of the collision (M_{AB} , in kmol/kg) as well as the ratio between the reactor temperature and the e/k of the collision (T^* , non-dimensional).

$$D_G = 0.0001 * \frac{10^{-3} * T^{\frac{3}{2}} * \left(3.03 - \frac{0.98}{M_{AB}^{0.5}}\right)}{P * M_{AB}^{0.5} * \sigma_{AB}^2 * \Omega_D}$$

$$M_{AB} = 2 * \left(\frac{1}{M_{CO_2}} + \frac{1}{M_{CH_4}}\right)^{-1}$$

$$\sigma_{AB} = \frac{\sigma_{CO_2} + \sigma_{CH_4}}{2}$$

$$\Omega_D = \frac{1.06036}{(T^*)^{0.15610}} + \frac{0.193}{e^{0.47635 * T^*}} + \frac{1.03587}{e^{1.52996 * T^*}} + \frac{1.76474}{e^{3.89411 * T^*}}$$

$$T^* = \frac{T}{\left(\frac{e}{k_{CH_4}} * \frac{e}{k_{CO_2}}\right)^{0.5}}$$

On the other hand, liquid phase diffusion (D_L , in m²/s) has not seen enough advancements to achieve the same level and accuracy obtained in gas diffusion. This is a consequence of the complexity of a liquid's molecular behaviour, specially related to its viscosity, which affects the diffusivity of molecules with in. This phenomenon was modelled through the Hayuk and Minhas correlation (Benitez, Principles and modern applications of mass transfer operations, 2009). This correlation requires the molar volume (V_{MCO_2} , in m³/kmol) as well as the viscosity of the solvent (μ_{H_2O} , in Pa*s) at the operation temperature, selected to be 25°C (298,15 K). As such, the equations used were:

$$D_L = \frac{1.25 * 10^{-8} * \left((V_{MCO_2} * 1000)^{-0.19} - 0.292\right) * T^{1.52} * (\mu_{H_2O} * 1000)^n}{10000}$$

$$n = \frac{9.58}{V_{MCO_2} * 1000} - 1.12$$

Proceeding with the design, the next section will focus on the mass transfer which occurs in the cleaning process. The diffusion results are compiled in Table 71.

Table 71: Diffusion Coefficients Results. Source: Own.

Parameter	Value
D_G (m ² /s)	$1.8163 \cdot 10^{-5}$
M_{AB} (kg/kmol)	23.5143
σ_{AB} (Å)	3.5500
Ω_D (-)	1.1924
T^* (-)	1.5213
D_L (m ² /s)	$0.0002 \cdot 10^{-5}$
n (-)	-0.8382

5.2.6. Mass Transfer Coefficients

Similar to the previous section, mass transfer was divided into gas and liquid phase transfers. However, in this case both phases have been extensively studied, with the equations used being retrieved from (Billet, 1989) for both.

Starting with the gas phase mass transfer, the process is determined by the convective mass transfer coefficient (k_G , non-dimensional). This requires the calculation of the gas' Schmidt number (Sc_G , non-dimensional).

$$Sc_G = \frac{\mu_G}{\rho_G * D_G}$$

$$k_G = 0.1304 * C_V * \frac{D_G * P_{op}}{R * T_{op}} * \frac{a}{(\varepsilon * (\varepsilon - h_L))^{0.5}} * \left(\frac{Re_G}{K_w}\right)^{\frac{3}{4}} * Sc_G^{\frac{2}{3}}$$

Proceeding with the liquid phase mass transfer, the parameter depends exclusively on previous calculations, given by the following formula (k_L , non-dimensional):

$$k_L = 0.757 * C_L * \left(\frac{D_L * a * v_L}{\varepsilon * h_L}\right)^{0.5}$$

Lastly, all the parameters calculated throughout the design permit the sizing of the packing height. It must also be mentioned that from this section it can be inferred that the mass transfer coefficients, C_V & C_L correspond to the gaseous (vaporous) and liquid phases, respectively. Mass transfer results can be found in Table 72 below.

Table 72: Mass Transfer Coefficients Results. Source: Own.

Parameter	Value
Sc_G (-)	4.1540
K_G (kmol/m ² -s)	0.0010
K_L (kmol/m ² -s)	0.0124

5.2.7. Packing Height

In order to clean the biogas, the transfer unit method can be employed. This method is used to determine the required number of transfers units (N_{tOG} , non-dimensional) between the liquid and gaseous phases as well as the height required per transfer unit (H_{tOG} , measured in metres). As such, the packing height of the column was solved as:

$$Z = H_{tOG} * N_{tOG}$$

However, several molar parameters such as the inlet (G_{Mig} , in kmol/m²s) and outlet (G_{Mog2} , in kmol/m²s) gas molar velocity. These will in turn determine the average molar gas velocity (G_{Mg} , in kmol/m²s).

$$G_{Mig} = \frac{4 * N_G}{3600 * \pi * D^2}$$

$$G_{Mog} = \frac{4 * (N_G - N_{CO_2r})}{3600 * \pi * D^2}$$

$$G_{MG} = \frac{G_{Mig} + G_{Mog}}{2}$$

The molar velocities of the solvent at its entry (G_{Miw} , in kmol/m²s) and exit points (G_{Mow} , in kmol/m²s) were also required to determine the absorption factor at the top (A_t , non-dimensional). and bottom of the column (A_b , non-dimensional). The average for both parameters was also calculated.

$$G_{Miw} = \frac{4 * N_{H_2O}}{3600 * \pi * D^2}$$

$$G_{Mow} = \frac{4 * (N_{H_2O} + N_{CO_2r})}{3600 * \pi * D^2}$$

$$G_{ML} = \frac{G_{Miw} + G_{Mow}}{2}$$

$$A_b = \frac{G_{Mow}}{G_{Mig} * \phi}$$

$$A_t = \frac{G_{Miw}}{G_{Mog} * \phi}$$

$$A = \frac{A_t + A_b}{2}$$

To continue with the design, the methodology requires the calculation of the weight of CO₂ in the cleaned gas (y_{CO_2og} , non-dimensional) as well as the volumetric gas phase (K_{vG} , measured in kmol/m³-s) and liquid phase (K_{vL} , measured in kmol/m³-s) volumetric mass transfer coefficients, used to determine their average (K_m , measured in kmol/m³-s). The last step in the design is the determination of the equilibrium line.

$$y_{CO_2og} = (1 - \eta) * y_{CO_2ig}$$

$$x_{CO_2iw} = 0$$

$$K_{vG} = k_G * a_h$$

$$K_{vL} = k_L * a_h * \frac{\rho_L}{M_w}$$

$$K_m = \frac{1}{\frac{1}{K_{vG}} + \frac{\phi}{K_{vL}}}$$

$$H_{tOG} = \frac{G_{MG}}{K_m}$$

$$N_{tOG} = \frac{\ln \left(\frac{y_{CO_2ig} - \phi * x_{CO_2iw}}{y_{CO_2og} - \phi * x_{CO_2iw}} * \left(1 - \frac{1}{A} \right) + \frac{1}{A} \right)}{1 - \frac{1}{A}}$$

$$y^* = \phi * x$$

This line provides the molar concentration of carbon dioxide in the gaseous phase, and as such operates between the following limits shown in Table 73. Also, the linear correlation of CO₂ in the gas & liquid phases is shown in Figure 106.

Table 73: Molar Fractions of CO₂ in flows. Source: Own.

Molar Fraction	Inlet	Outlet
y _{CO2} (-), gas	0.1	0.005
x _{CO2} (-), liquid	0	0.0065

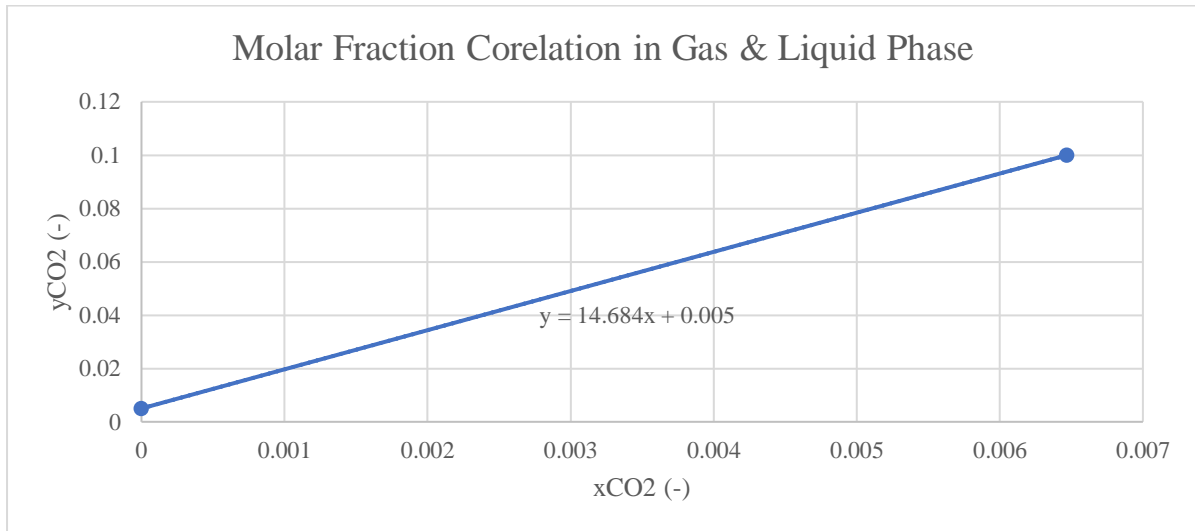


Figure 106: Molar Fraction Correlation in Gas & Liquid Phase. Source: Own.

Table 74: Packing Height Results. Source: own.

Parameter	Value
G _{Mig} (kmol/m ² -s)	0.660
G _{Mog} (kmol/m ² -s)	0.0597
G _{MG} (kmol/m ² -s)	0.0628
G _{Miw} (kmol/m ² -s)	0.1101
G _{Mow} (kmol/m ² -s)	0.1163
G _{ML} (kmol/m ² -s)	0.1132
A _b (-)	1.2076
A _t (-)	1.2625
A (-)	1.2350
K _{vG} (kmol/m ³ -s)	0.1144
K _{vL} (kmol/m ³ -s)	76.8123
H _{iOG} (m)	0.5502
K _m (kmol/m ³ -s)	0.1142
H _{iOG} (m)	0.5502
N _{iOG} (-)	0.0524
Z (m)	0.0288

5.2.8. Design Results

The main design parameters obtained are displayed in Table 75 below.

Table 75: Main Packed Column Design Parameters. Source: Own.

Parameter	Value
D (m)	0.6857
Z (m)	0.0288
$\Delta P/Z$ (Pa/m)	256.6111
K_{vG} (kmol/m ³ -s)	0.1144
K_{vL} (kmol/m ³ -s)	76.8123
K_m (kmol/m ³ -s)	0.1142
H_{tOG} (m)	0.5502
a_h (m ⁻¹)	111.7546

The full result list is provided in Table 76 below.

Table 76: Full Design Parameters Results. Source: Own.

Parameter	Value	Parameter	Value
M_G (kg/kmol)	18.3352	D_G (m ² /s)	$1.8163 \cdot 10^{-5}$
μ_G (Pa*s)	$6.2200 \cdot 10^{-5}$	M_{AB} (kg/kmol)	23.5143
ρ_G (kg/m ³)	0.8244	σ_{AB} (Å)	3.5500
m_{CO2ow} (kg/h)	366.5845	Ω_D (-)	1.1924
m_{ow} (kg/h)	3002.8260	T^* (-)	1.5213
X (-)	0.0537	D_L (m ² /s)	$0.0002 \cdot 10^{-5}$
Y_{flood} (-)	0.2358	n (-)	-0.8382
C_{Sflood} (-)	0.603	Sc_G (-)	4.1540
v_{Gflood} (m/s)	2.0956	K_G (kmol/m ² -s)	0.0010
D (m)	0.6857	K_L (kmol/m ² -s)	0.0124
d_p (m)	0.0025	G_{Mig} (kmol/m ² -s)	0.660
K_w	0.9540	G_{Mog} (kmol/m ² -s)	0.0597
Re_G (-)	213.2187	G_{MG} (kmol/m ² -s)	0.0628
Ψ_o (-)	0.9746	G_{Miw} (kmol/m ² -s)	0.1101
G_L (kg/m ² -s)	2.2589	G_{Mow} (kmol/m ² -s)	0.1163
v_L (m/s)	0.0023	G_{ML} (kmol/m ² -s)	0.1132
Re_L (-)	20.9761	A_b (-)	1.2076
Fr_L (-)	0.0001	A_t (-)	1.2625
a_h/a (-)	0.9236	A (-)	1.2350
a_h (m ⁻¹)	111.7546	K_{vG} (kmol/m ³ -s)	0.1144
h_L (-)	0.0000	K_{vL} (kmol/m ³ -s)	76.8123
$\Delta P_o/Z$ (Pa/m)	231.0598	H_{tOG} (m)	0.5502
$\Delta P/Z$ (Pa/m)	256.6111	K_m (kmol/m ³ -s)	0.1142
		H_{tOG} (m)	0.5502
		N_{tOG} (-)	0.0524
		Z (m)	0.0288

Chapter 6: Conclusions

Following a similar structure to that of the rest of the memoir, this section will present the various conclusions from the various parts of the study, commencing with the experiment conclusions & followed by the conclusions drawn from the three applications previously presented.

6.1. Experiment Conclusions

Once the various experiments, modelling and analysis were completed, conclusions could be made based on the findings of the present study. Due to the varied nature of the experiments performed, as well as the complications of larger reactor tests, this section will focus on the BMP test results.

6.1.1. BMP Test Conclusions

The first conclusion drawn from the study is that further experimental runs are required to validate the findings of this study. The various BMP tests displayed promising results in biogas production and quality. However, this study could not statistically determine that the C-Fe nanoparticles affect the daily production's mean or variance, except during certain dates and periods regarding the standard deviation of hydrogen.

Despite the lack of statistical conclusions, all BMP samples in which the nanoparticles were used did achieve an increase biogas and biomethane production over the simple co-digestion samples, registering a peak of 23,2928 Nm³/grNP and 25,0605 Nm³/grNP, respectively.

Another conclusion drawn from the data is the decrease in digestion speed of the sludge-feed mixture, reflected in the lower decay rate of the samples with nanoparticles. As was previously discussed. As a result of this, a new line of research resulting from this project could be the study, design, and operation of anaerobic digestion reactors with a short residence time.

It should also be mentioned that the nanoparticles reduce the percentage of biomethane while increasing that of the hydrogen sulphide and the various residues and unidentified components during the hydrolysis and acidogenesis stages of the AD process. To achieve a more detailed analysis by separating other compounds of significant interest such as CO₂, a new chromatography method should be developed in the future.

Regarding the effects of the nanoparticles on the hydrogen mole concentration, the most significant finding is the CH₄ and H₂ cyclical correlation observed, consistent with previous research in the use of hydrogen as an indicator of the digestion process.

Focusing on the H₂S, its weight decreases during the second half of the experiment, from day nine onwards, as evidenced by the 78,92% peak registered during the eighth day, followed by a reduction by three orders of magnitude, becoming a residual compound. It must also be mentioned that this reduction also affects the standard deviation, which was reduced by around 50%. To fully determine the effects of the nanoparticles on the compound, a detailed analysis on the acidogenesis process would be required and result into a new research line pertaining the interactions between the particles with the various microorganisms predominant during each stage of the AD stages.

The residual compounds were positively impacted by the nanoparticles, reducing their appearance both in the composition and overall generation when comparing both sets of bottles. In addition, their sharp increase during the final days of the methanogenesis stage further reinforce the previously drawn conclusion on reaction speed. Finally, the nanoparticles also reduced their variability from day ten onwards, achieving a drop of 83,73% in the daily variance change.

Lastly, the binormal distribution modelling performed on the biogas, methane and hydrogen did provide well fitted models with no apparent residual structure and an acceptable R² value for certain models. However, a finely tuned model would require further analysis of the data as well as more degrees of

freedom, obtained from performing additional BMP experiments to obtain over forty mean data points and thus ensure that the central limit theorem is fully applicable. Moreover, increasing the degrees of freedom will ensure a more robust model and permit the identification of underlying data structures. The use of advanced analysis techniques based on machine learning should also be considered once enough samples have been collected.

6.1.2. Batch Reactor Conclusions

Firstly, batch reactors showed a similar behaviour to the BMP tests, as the experiment performed on these was identical, barring the volume change resulting from using a 2-litre vessel. Furthermore, the increase in volume magnified the tendencies previously mentioned such as the CH₄ and H₂ interaction as well as the faster reaction speed, displaying a clear decrease in methane generation during the sixteenth day, proposing this as the initial residence time for future research on this.

Another important conclusion obtained from the larger vessels was the need to further improve the set up and sealing techniques, as well as the stirring to prevent the volatilization and deposition of the nanoparticles, particularly on the stirring rod seal. This issue was addressed in a posterior run, which was not part of this project, by applying vacuum grease around the exterior side of the seal, although no clear improvement was made.

Further improvements required would require a new method to measure biogas production once biogas production decreases significantly once the vessels have stabilised after the start-up process, preventing the biogas from having sufficient energy to overcome the head loss resulting from the use of the Ritter milli gasometer. To address this problem, the use of a differential pressure water column has been suggested and its viability will be assessed in a future project.

6.1.3. Semi-Continuous Reactor Conclusion

Firstly, a new and refined sample feeding methodology is recommended to facilitate this daily procedure. As previously mentioned, it was observed that by preparing the water-pumpkin feed slurry in advance (1 to 2 days), the resulting mash was easier to inject into the bottle and suctioned by the peristaltic pump used for the reactor.

Therefore, it is proposed that the feeding be prepared and allowed to soften before use; this will have the added benefit of obtaining a feed which more closely resembles the OFMSW.

Another aspect which must be discussed is the difficulty encountered when performing the reverse TOC analysis, which did not produce realistic or useful results. As such, future experiments will also require adding a bi-daily recording of TOC in order to correctly determine the C/N ratio within the AD reactor.

Lastly, a detailed review of the final week (days 14 to 21) would also require further study as the VFA content within the co-digestion mixture as well as the nitrogen content suggest the possibility of a change in reactor dynamics as a result of the addition of the Fe-C nanoparticles, resulting in the build-up of these compounds, possibly affecting methanogenesis negatively.

6.2. Application Conclusions

Although the synthetic reactor utilised as the base for the modelling was no realistic, obtaining a biogas with a 90% methane molar fraction; the use of the biogas in cogeneration did prove to be a viable solution to satisfy a large thermal demand. In both cases the NVA was larger than 27.500.000,00€, with the biomethane reaching 27.953.327,42 € and the biogas scenario obtaining 29.880.973,60€.

These large values indicate that biogas upgrading is not a desirable process when employing the biogas produced in cogeneration due to the added CAPEX and OPEX required to install and operate the wet absorption column, although the use of biomethane as opposed to biogas would reduce the O&M costs as well as prolong the motor's lifespan. To reach a final decision, detailed economic analysis on each scenario, as well as the corresponding sensitivity analysis should be performed.

6.3. Wet Absorption Column Design Conclusion

The final exercise performed within the project was the design of an absorption column to clean and upgrade the biogas into biomethane. This modelling proved to be complex and time consuming, but relatively easy to follow and thus can be easily replicated. The low solubility of carbon dioxide in the selected solvent (water) demands a large volume of said liquid to ensure proper cleaning. This may warrant the study of different solvents to reduce volume required.

Another aspect which must be mentioned is the small size of the column, being a space-efficient solution, which could see widespread use if the solvent issue is properly addressed. Other aspects which could be improved upon would be the packing material selection as well as a simulation of the column to ensure that the theoretical results are backed, and the design could move forward into detailed design and eventually production.

Chapter 7: Anejos

7.1. Anejo I: Sustainable Development Goals Alignment

Sustainability has been typically portrayed as the intersection of three distinct areas: Social; Economic & Environmental. Therefore, a sustainable project must seek to make substantial contributions either directly or indirectly, to all 3 areas. In order to achieve it, this Project will be aligned with Sustainable Development Goals. It must be pointed out that due to the reduced nature of this descriptive memoir, only the 3 main SDGs tackled will be discussed.

As the Project focuses on the production of biogas to use as an alternative primary resource, the first and most evident SDG is number 13: Climate Action (United Nations, 2015). The main goal of the study is to further develop an existing carbon neutral alternative to natural gas (Fumey, 2021) to be used in electricity or heat generation or in industrial processes which require methane or hydrogen, which can be obtained through reforming (Doan Pham Minh, 2018), which can further contribute to this Goal through the use of carbon-capture technology (Antonini, et al., 2020). Specific applications of the biogas produced pertaining SDG 13 would focus on the substitution of natural gas in energy generation & in industrial applications, which represent 38% & 33% of US demand, respectively (Energy Information Agency, 2021). These applications will directly contribute towards Target 13.2, which focuses on climate change measures, which includes the energy generation applications of this research as previously stated. Similarly, if applied in developing countries & funded through the UN's Climate Change Framework, it will permit its inclusion in Target 13.a to reduce the impact of developing economies, promoting economic growth without damaging the planet.

The proposed study will also contribute to the fulfilment of SDG 9: Industry, Innovation, and Infrastructure (United Nations, 2015) through the applications of the research as anaerobic digestion is used for sludge treatment in large water treatment plants. Retrofitting said plants with reactors and upgrading existing ones to incorporate the feed mechanisms, will enable industries to generate their own biogas to be used in house or have said gas upgraded through various methods and injected into the natural supply network as biomethane or green hydrogen, depending on future developments, directly contributing towards Target 9.4. Furthermore, biogas generation can be easily implemented in wastewater treatment plants, which can be used to create isolated electrical power systems in isolated regions with water treatment facilities around which small scale industrial businesses could originate. This will directly contribute to the fulfilment of Target 9.2, which focuses on promoting and creating an inclusive and sustainable industrialization. It must also be pointed out that the very nature of this project can be included within Target 9.5 as this is a research project aimed at developing new technologies

Lastly, this research project is also aligned with SDG 11: Sustainable Cities and Communities (United Nations, 2015). This goal focuses on improving cities by making them more sustainable. This is of special importance in developing countries, whose economies are based on agriculture to achieve economic growth (Food and Agriculture Organization, 2002). The increase in agriculture results in the increase of water, air & soil pollution if residues are not correctly managed. As previously explained, anaerobic digestion processes can operate with a variety of organic waste, utilizing residues to reduce waste, utilizing residues to produce both energy & fertilizer through the digestate, contributing towards Target 11.6 to reduce the environmental impact of cities. This will also improve the transition towards a circular economy. In addition, the use of this technology will also facilitate developing reliable infrastructure by minimizing and simplifying operating requirements in treatment plants. This will improve the implementation of Target 11.4 by helping safeguard the world's natural heritage through the reduction in resource intensity.

7.2. Anejo II: Initial Result Analysis



MÁSTER UNIVERSITARIO EN INGENIERÍA INDUSTRIAL

Informe de Resultados Iniciales
Empresa Colaboradora

Madrid

Enero 2022

1. Introducción

El objeto de este informe es el análisis de los resultados preliminares obtenidos del muestreo diario en el ensayo de codigestión anaerobia realizado a lo largo del curso 2021-2022 en la Universidad Pontificia Comillas-ICAI.

Estos ensayos se realizaron en colaboración con una empresa colaboradora a fin de determinar el efecto de sus nanopartículas Fe-C en la producción de biogás, así como la composición de este, como se explica más adelante en la metodología.

Para ello, se realizaron ensayos BMP estandarizados (AENOR, 1999) en el Laboratorio de Química y Medio Ambiente de la Universidad, empleándose la incubadora y el cromatógrafo de gases, los cuales se muestran en las Ilustraciones 1 y 2, respectivamente. Además, se realizó el mismo ensayo en reactores de 2 litros como siguiente paso en la escalabilidad del proceso, cuya imagen se muestra en la Ilustración 3.



Ilustración 1: Incubadora.



Ilustración 2: Cromatógrafo de gases



*Ilustración 3: Reactor
Discontinuo*

2. Metodología

Al realizarse ensayos normalizados, se siguió el procedimiento y composición de botellas recogido en la norma UNE-EN ISO 11734:1999. Estos ensayos requieren el uso de botellas normalizadas de 1L, las cuales se llenaron hasta los 300ml con una composición próxima a la empleada en reactores anaerobios industriales (FCC, 2021), a la vez que se mantenía la proporción fango-residuo de ensayos anteriores. Para ello, se empleó calabaza cruda a modo de sustrato al ser este el residuo que mejor caracteriza la mezcla de residuos de la FORSU (Morales Polo, Co-Digestión anaerobia y pretratamiento de residuos agroalimentarios con fangos UASB de depuradora, 2019).

Además, en las muestras en las que se añadieron las nanopartículas estas se disolvieron en agua destilada mediante sonicación. De acuerdo con los datos obtenidos del análisis del fango, se añadió la solución hasta llegar a la concentración de 2 g/kg_{SV} sugerida por la empresa colaboradora. También, se prepararon 2 botellas de fango con y sin nanopartículas a fin de usar estas lecturas como línea base del análisis. Finalmente, las muestras preparadas se incubaron durante 21 días a 38°C (rango mesofílico).

Durante el transcurso del ensayo, las botellas eran muestreadas a diario, registrando su presión a fin de obtener de manera indirecta el biogás producido. El gas liberado tras la medición se empleaba en el cromatógrafo de gases para determinar su composición.

Asimismo, este ensayo se realizó en reactores discontinuos con 2L de mezcla, con la misma mezcla de fango, residuo y sobrenadante a fin de determinar cambios significativos al aumentar el volumen de este. Se ha de señalar que durante estos ensayos hubo dificultades a la hora de medir la producción bruta de biogás debido a la pérdida de carga en la manguera que conectaba el puerto de salida del reactor con el gasómetro empleado, por lo que en este informe solo se incluye el análisis de la composición de este.

3. Lecturas Recogidas en Botellas

En esta sección se recogen las lecturas obtenidas con el presostato de cada botella durante cada día del ensayo. Se ha de indicar que, en la segunda tanda de ensayos, el día 4 fue festivo, motivo por el cual no se recogieron medidas. Los datos se muestran en la Tabla 1; así como un ejemplo de cromatograma en la Ilustración 3.

Tabla 1: Medidas de presión (bar) recogidas

Día	1	2	3	4	7	8	9	10	11	14	15	16	17	18	21
F1	0.469	0.309	0.282		0.489	0.143	0.101	0.091	0.078	0.18	0.062	0.052	0.065	0.051	0.109
FN	0.423	0.27	0.205		0.342	0.092	0.061	0.072	0.042	0.056	0.028	0.031	0.04	0.03	0.034
B1	0.979	0.259	0.284	0.208	0.187	0.147	0.018	0.015	0.006	0.002	0	0	0	0	0
B2	0.947	0.606	0.21	0.196	0.122	0.097	0.085	0.109	0.077	0.056	0.045	0.039	0.039	0.054	0.109
B3	0.979	0.044	0.045	0.054	0.006	0.023	0.006	0.012	0.045	0.111	0.039	0.024	0.033	0.03	0.05
B4	1	0.524	0.512	0.362	0.408	0.17	0.093	0.101	0.085	0	0	0	0	0.026	0
B5	0.979	0.087	0.269	0.176	0.045	0.019	0.015	0.01	0.043	0.038	0.038	0	0.018	0	0
B6	0.979	0.452	0.388	0.159	0.108	0.046	0.045	0.057	0.055	0.07	0.025	0.027	0.043	0.041	0.082
B7	0.979	0.597	0.344	0.352	0.262	0.158	0.105	0.126	0.01	0.008	0	0	0.016	0.024	0.024
B8	0.979	0.618	0.001	0	0	0	0	0	0	0	0	0	0.003	0	0
B9	1	0.728	0.41	0.366	0.373	0.127	0.043	0.062	0.037	0.006	0.024	0.015	0.006	0.015	0.027
BN1	0.975	0.464	0.366		0.295	0.129	0.086	0.064	0.035	0.04	0.029	0.026	0.046	0.048	0.046
BN2	0.979	0.526	0.37		0.543	0.132	0.076	0.077	0.067	0.149	0.056	0.033	0.045	0.031	0.037
BN3	0.979	0.417	0.421		0.234	0.093	0.056	0.059	0.05	0.101	0.049	0.026	0.032	0.023	0.058
BN4	0.979	0.102	0.111		0.13	0.102	0.122	0.07	0.068	0.127	0.051	0.031	0.043	0.03	0.095
BN5	0.979	0.436	0.325		0.371	0.097	0.005	0.009	0.03	0	0.017	0.026	0.037	0.035	0.024

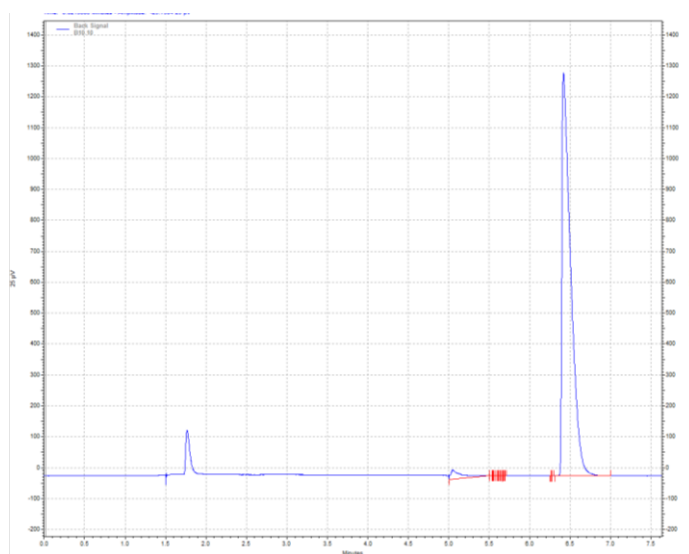


Ilustración 4: Ejemplo Cromatograma

A partir de los resultados recogidos se obtuvo producción normalizada por litro de fango, convirtiéndose la presión en el volumen producido en condiciones normales (Nm^3). Asimismo, la producción acumulada se muestra en la Tabla 2.

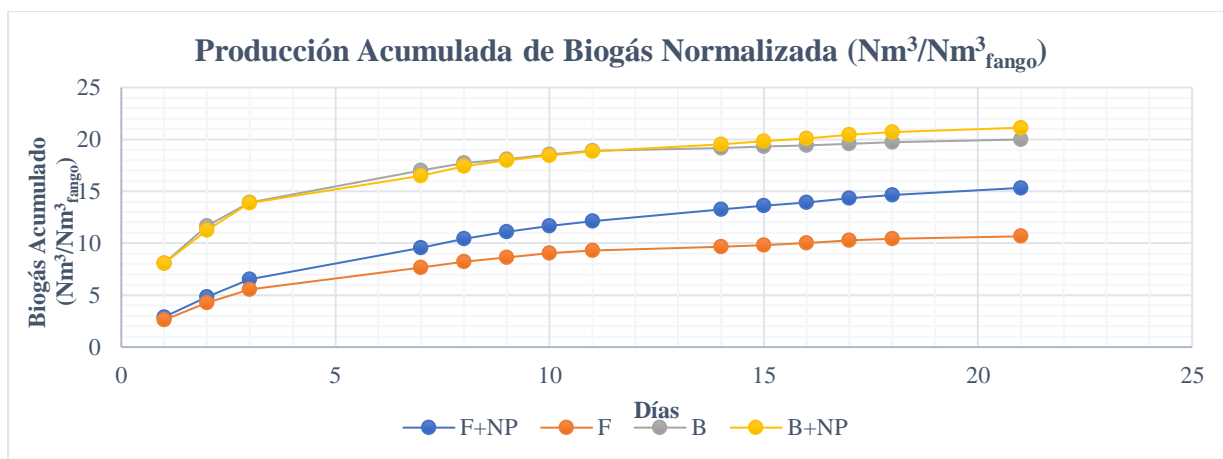


Ilustración 5: Producción Acumulada de biogás

Tabla 2: Producción Acumulada de Biogás

Día	1	2	3	4	7	8	9	10	11	14	15	16	17	18	21
Prod F+NP (Nm³/Nm³ _f)	2.90	4.81	6.55	6.55	9.57	10.46	11.08	11.64	12.12	13.24	13.62	13.94	14.34	14.66	15.33
Prod F (Nm³/Nm³ _f)	2.61	4.28	5.55	5.55	7.66	8.23	8.61	9.05	9.31	9.66	9.83	10.02	10.27	10.46	10.67
Prod B (Nm³/Nm³ _f)	8.08	11.66	13.91	15.63	17.01	17.73	18.11	18.56	18.89	19.15	19.31	19.41	19.55	19.72	19.99
Prod B+NP (Nm³/Nm³ _f)	8.06	11.27	13.89	13.89	16.48	17.39	17.96	18.42	18.83	19.52	19.85	20.09	20.42	20.70	21.13

Como puede apreciarse, la producción normalizada de biogás durante el transcurso del experimento fue ligeramente superior con nanopartículas que, sin ellas, siendo la diferencia de 1,14Nm³. Se habrá de realizar un análisis estadístico de la media para poder determinar si las muestras permiten decir que estas son rechazadas. Sin embargo, en ambos casos se comprueba el efecto de la codigestión en la producción frente al blanco (muestra F; únicamente fango) y frente a la muestra F+NP, la cual produjo más biogás que la base, en menor cantidad que la media de las botellas en codigestión.

En lo que respecta a la producción media bruta, el efecto de las nanopartículas se concentra en la metanogénesis, siendo apreciable a partir del día 14 en la producción acumulada. Esto sugiere que el efecto positivo de estas comienza antes en el proceso a fin de cubrir el déficit frente a la codigestión de la serie B. Para ello, se muestra a continuación en la Ilustración 6 el detalle de la producción diaria.

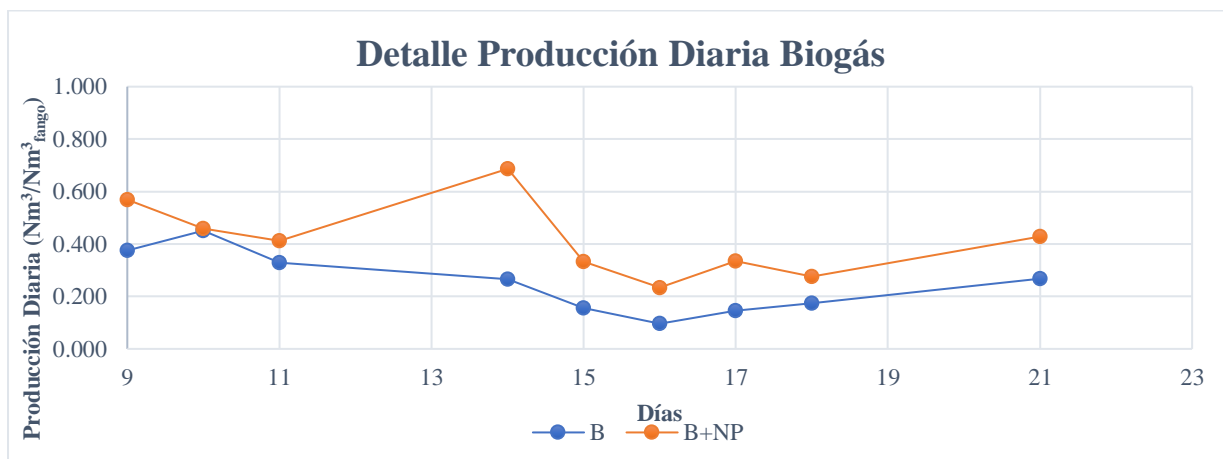


Ilustración 6: Detalle de la Producción Diaria de Biogás

Como se puede observar, los resultados corroboran lo expuesto previamente, causando las nanopartículas un efecto muy significativo en la producción de biogás tras el periodo de inicio del ensayo (días 1 a 4), con un especial impacto en el periodo de metanogénesis. Asimismo, la Ilustración 7 muestra la mejora porcentual de las nanopartículas sobre la codigestión.

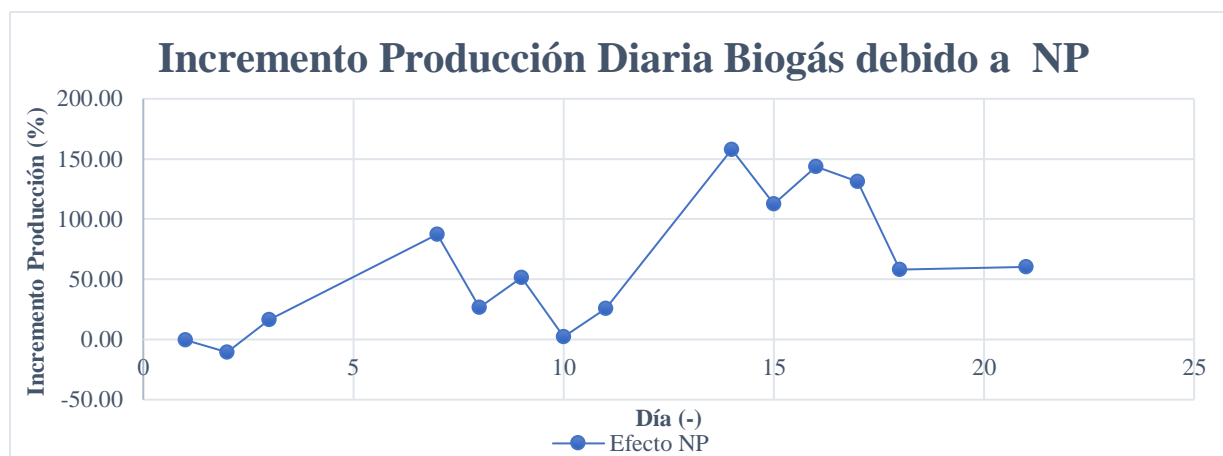


Ilustración 7: Incremento Porcentual de la Producción Debido a las Nanopartículas

Despreciando el día 4, como se ha mencionado previamente, las partículas presentan una mejora de hasta el 160% sobre las botellas sin ellas, centradas en torno al día 15 tras reducirse su efecto de manera puntual en el día 10. Asimismo, en los días finales la mejora es ligeramente superior al 60% de producción adicional. Los resultados numéricos se muestran a continuación en la Tabla 3.

Tabla 3: Mejora Porcentual de las Nanopartículas en la Producción Diaria

Día	1	2	3	4	7	8	9	10	11	14	15	16	17	18	21
Prod B (Nm ³ /Nm ³ t)	8.076	3.584	2.255	1.715	1.383	0.721	0.375	0.450	0.328	0.266	0.157	0.096	0.145	0.174	0.267
Prod BN (Nm ³ /Nm ³ t)	8.060	3.205	2.625	0.000	2.592	0.911	0.569	0.460	0.412	0.687	0.333	0.234	0.335	0.275	0.428
Cambio Producción (%)	-0.19	-10.57	16.42	-100	87.39	26.48	51.46	2.07	25.70	157.9	112.6	143.4	131.3	58.21	60.27

Los resultados muestran que las nanopartículas mejoran de manera significativa el proceso de codigestión a partir del día 3 o 7 del proceso, debido a la falta de medida del día 4. Por tanto, podemos concluir que tras la estabilización posterior al arranque siempre mejoran la producción bruta, con un pico del 157%. Además, durante el periodo de arranque solo presentan un efecto negativo en el día 2, en el cual reducen la producción diaria en un 10,57%, lo cual no debe tenerse en especial consideración al ser el arranque del ensayo y por tanto un periodo de estabilización del ensayo.

Por último, es de interés indicar la mejora de la producción acumulada del proceso de monodigestión con nanopartículas (F+NP) frente al proceso blanco (F), en el cual se producen 4,66Nm³ más, pese a no ser este el objeto del estudio e informe, son resultados prometedores.

3. Análisis de Resultados de las Botellas

Tras obtener todas las medidas y composiciones de las botellas, los datos fueron tratados para obtener una medida normalizada, como se ha explicado anteriormente. Además, se obtuvo la producción media de biogás para cada grupo de muestras obtenidas, así como la varianza muestral, a partir de la cual se estimará la poblacional en ambos casos y se comparará entre ellas.

Al tratarse de un experimento en el cual se ha recogido tanto la producción como composición de las muestras, se requiere un análisis de cada variable por separado, así como de la interacción entre estas para poder determinar los efectos globales que las nanopartículas tienen sobre el proceso de codigestión. A tal fin, en primer lugar, se analizará la producción bruta de biogás. Tras este, se analizarán cada uno de los componentes del biogás de acuerdo con la información extraída de los cromatogramas. Finalmente, la producción de cada componente (la interacción), se estudió de la misma manera.

Para poder determinar los efectos de las nanopartículas en el proceso se decidió analizar la mejora en producción y composición de cada componente, lo que requiere el uso de la producción media de cada grupo como indicador. Asimismo, se decidió evaluar el efecto de estas sobre la variabilidad y estabilidad del proceso, para lo que se decidió emplear la varianza como indicador de la dispersión de los resultados.

Al tratarse de un estudio comparativo entre 2 grupos en cada caso, se emplearon el contraste de hipótesis de la t de Student, bajo el supuesto de poblaciones normales con varianzas distintas y desconocidas; siendo la hipótesis nula la igualdad de medias. El contraste de hipótesis se muestra a continuación. S empleó un nivel de significación del 5% (95% de confianza).

Hipótesis nula	Estadístico de contraste	Región crítica
$H_0: \mu_1 = \mu_2$ $\sigma_1^2 \neq \sigma_2^2$ desconocidos	$t_o = \frac{\bar{x}_1 - \bar{x}_2}{\sqrt{\frac{s_1^2}{m} + \frac{s_2^2}{n}}}$	$H_1: \mu_1 \neq \mu_2 \rightarrow t_o > t_{k,\alpha/2}$ $H_1: \mu_1 > \mu_2 \rightarrow t_o > t_{k,\alpha}$ $H_1: \mu_1 < \mu_2 \rightarrow t_o < -t_{k,\alpha}$

El estadístico empleado para comprobar la diferencia de varianzas entre las muestras con nanopartículas y las muestras sin ellas, se empleó el contraste de hipótesis de la f de Snedecor, siendo la hipótesis nula la igualdad de varianzas bajo el supuesto de poblaciones normales. El contraste de hipótesis se muestra a continuación. S empleó un nivel de significación del 5% (95% de confianza).

Hipótesis nula	Estadístico de contraste	Región crítica
$H_0: \sigma_1^2 = \sigma_2^2$	$f_o = \frac{s_1^2}{s_2^2}$	$H_1: \sigma_1^2 \neq \sigma_2^2 \rightarrow f_o > F_{\frac{\alpha}{2}}(m-1, n-1)$ $H_1: \sigma_1^2 \neq \sigma_2^2 \rightarrow f_o < F_{1-\frac{\alpha}{2}}(m-1, n-1)$ $H_1: \sigma_1^2 > \sigma_2^2 \rightarrow f_o > F_{\alpha}(m-1, n-1)$

Del mismo modo, los efectos de las nanopartículas se cuantificaron en todos los casos, tanto en medidas absolutas como porcentuales, ya que son resultados de utilidad incluso si se rechaza la hipótesis nula, ya que en ese caso indicarán la tendencia de los conjuntos de datos y permitirán su contraste con futuros estudios con mayores muestras. Por último, es pertinente explicar el proceso de cálculo del efecto de las nanopartículas tras las comprobaciones de hipótesis

$$\text{Delta [Uds]} = \text{BN [Uds]} - \text{B [Uds]}$$

$$\text{Cambio (\%)} = \frac{\text{Delta [Uds]}}{\text{B [Uds]}} * 100\%$$

$$\text{Mejora Específica} = \frac{\text{Delta [Uds]}}{m_{NP}[\text{gr}_{NP}]}$$

a. Producción de Biogás de las Botellas

Como se ha mencionado anteriormente, en primer lugar, se analizó la producción de biogás a partir de los datos diarios recogidos por el presostato. Los resultados de ambos contrastes de hipótesis se muestran en la Tabla 4. Debido al orden de magnitud, se muestra la desviación estándar (STD).

Tabla 4: Resultados test estadísticos producción de biogás bruto

Medias															
Día	1	2	3	4	7	8	9	10	11	14	15	16	17	18	21
Prod B (Nm ³ /m ³ f)	8.0757	3.5842	2.2549	1.7147	1.3833	0.7205	0.3754	0.4504	0.3278	0.2664	0.1566	0.0961	0.1446	0.1739	0.2673
Prod BN (Nm ³ /m ³ f)	8.0599	3.2052	2.6251	0.0000	2.5922	0.9113	0.5685	0.4598	0.4120	0.6872	0.3329	0.2340	0.3345	0.2752	0.4285
Hipótesis Nula	ACEPT	ACEPT	ACPET	RECH	ACEPT	ACEPT	ACEPT	ACEPT	ACEPT	ACEPT	ACEPT	RECH	RECH	ACEPT	ACEPT
Efecto NP	Negativo	Negativo	Positivo	Negativo	Positivo	Positivo	Positivo	Positivo	Positivo	Positivo	Positivo	Positivo	Positivo	Positivo	Positivo
Delta Prod (Nm ³ /m ³ f)	-0.0157	-0.3790	0.3702	-1.7147	1.2088	0.1908	0.1932	0.0093	0.0842	0.4208	0.1763	0.1379	0.1899	0.1013	0.1611
Cambio Prod (%)	-0.19	-10.57	16.42	-100.00	87.39	26.48	51.46	2.07	25.70	157.94	112.63	143.43	131.27	58.21	60.27
Mejora Específica (Nm ³ /gr _{NP})	-0.9379	-22.5740	22.0506	-102.129	71.9970	11.3634	11.5051	0.5562	5.0165	25.0605	10.5018	8.2117	11.3088	6.0307	9.5967

Varianza															
Día	1	2	3	4	7	8	9	10	11	14	15	16	17	18	21
STD B (Nm ³ /m ³ f)	0.1268	2.0350	1.3794	1.0899	1.2500	0.5465	0.3280	0.3976	0.2492	0.3256	0.1580	0.1245	0.1400	0.1586	0.3313
STD BN (Nm ³ /m ³ f)	0.0147	1.3649	0.9966	0.0000	1.2785	0.1522	0.3547	0.2226	0.1450	0.5105	0.1371	0.0277	0.0490	0.0761	0.2230
Hipótesis Nula	RECH	ACEPT	ACEPT	RECH	ACEPT	RECH	ACEPT	ACEPT	ACEPT	ACEPT	ACEPT	RECH	ACEPT	ACEPT	ACEPT
Efecto NP	Positivo	Positivo	Positivo	Positivo	Negativo	Positivo	Negativo	Positivo	Positivo	Negativo	Positivo	Positivo	Positivo	Positivo	Positivo
Delta STD (Nm ³ /m ³ f)	-0.1121	-0.6701	-0.3829	-1.0899	0.0284	-0.3943	0.0266	-0.1750	-0.1042	0.1848	-0.0209	-0.0968	-0.0911	-0.0825	-0.1083
Mejora STD (%)	-88.38	-32.93	-27.76	-100.00	2.28	-72.15	8.12	-44.01	-41.83	56.76	-13.24	-77.75	-65.04	-52.01	-32.70
Mejora Biogás/gr NP (Nm ³ /gr _{NP})	-6.6748	-39.9134	-22.804	-64.9107	1.6942	-23.485	1.5871	-10.422	-6.2085	11.0082	-1.2462	-5.7644	-5.4237	-4.9118	-6.4520

Como se puede observar, no se aprecia un impacto significativo de las nanopartículas en la producción bruta de biogás, al no rechazarse la hipótesis nula en la media salvo los días 16 y 17, ya que el día 4 no se puede evaluar. Sin embargo, se aprecia una mejora significativa en la desviación estándar del proceso al reducirse esta en todos los días muestreados salvo los días 7 y 14, los cuales representan el efecto acumulado del fin de semana. Estos cambios se muestran en la Ilustración 8.

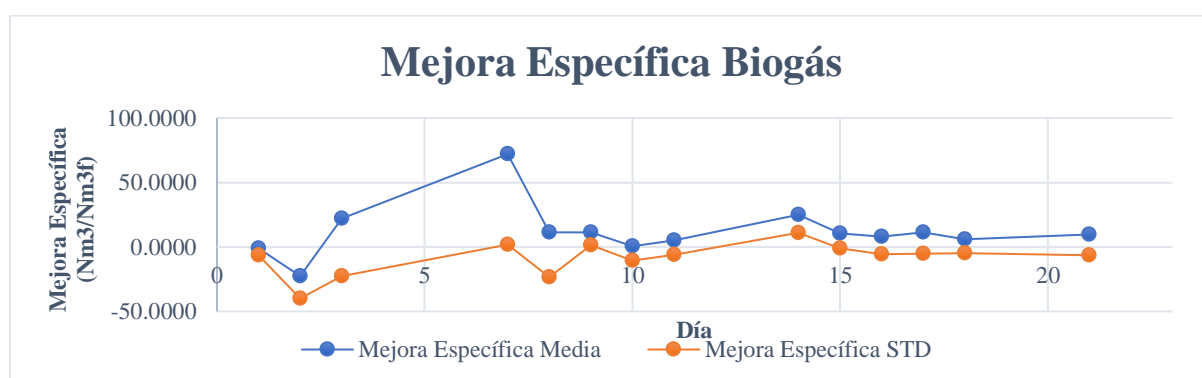


Ilustración 8: Mejora Específica Biogás

b. Análisis de Producción Media Diaria de las Botellas

Tras el análisis del biogás bruto, se decidió analizar la composición de este, así como la interacción de esta con el biogás diario, lo cual se ha denotado como la producción de cada componente. El orden de análisis es metano (CH_4), hidrógeno (H_2), ácido sulfhídrico (H_2S) y residuos (RES), cuyos resultados se muestran de la Tabla 5 a la Tabla 8, respectivamente.

Análisis de la Producción Media Diaria del Metano de las Botellas

Tabla 5: Análisis estadístico de la media de CH_4

Producción CH_4															
Día	1	2	3	4	7	8	9	10	11	14	15	16	17	18	21
Prod B (Nm^3/m^3_f)	7.2974	3.2975	2.0875	1.5915	1.2916	0.6703	0.3494	0.4179	0.3030	0.2482	0.1455	0.0895	0.1346	0.1623	0.2543
Prod BN (Nm^3/m^3_f)	7.3176	2.9322	2.4084	0.0000	2.3924	0.7817	0.5286	0.4286	0.3807	0.6393	0.3098	0.2180	0.3119	0.2560	0.4000
Hipótesis Nula	ACEPT	ACEPT	RECH	RECH	RECH	ACEPT	ACEPT	ACEPT	ACEPT	ACEPT	ACEPT	ACEPT	ACEPT	ACEPT	RECH
Efecto NP	Positivo	Negativo	Positivo	Negativo	Positivo	Positivo	Positivo	Positivo	Positivo	Positivo	Positivo	Positivo	Positivo	Positivo	Positivo
Delta Prod (Nm^3/m^3_f)	0.0202	-0.3653	0.3208	-1.5915	1.1008	0.1114	0.1792	0.0107	0.0776	0.3911	0.1643	0.1286	0.1774	0.0937	0.1457
Cambio Prod (%)	0.28	-11.08	15.37	-100.00	85.23	16.62	51.28	2.56	25.62	157.55	112.98	143.74	131.78	57.77	57.27
Mejora Específica ($\text{Nm}^3/\text{gr}_{\text{NP}}$)	1.2043	-21.7548	19.1088	-94.7873	65.5650	6.6368	10.6717	0.6364	4.6242	23.2928	9.7874	7.6581	10.5633	5.5835	8.6749

Composición CH_4															
Día	1	2	3	4	7	8	9	10	11	14	15	16	17	18	21
Comp B (p.u.)	0.9036	0.9206	0.9274	0.9271	0.9309	0.9270	0.9268	0.9290	0.9256	0.9295	0.9272	0.9290	0.9303	0.9349	0.9467
Comp BN (p.u.)	0.9079	0.9175	0.9179	0.9217	0.9217	0.8482	0.9244	0.9293	0.9227	0.9301	0.9293	0.9315	0.9323	0.9299	0.9336
Hipótesis Nula	ACEPT	ACEPT	RECH	ACEPT	RECH	ACEPT	ACEPT	ACEPT	ACEPT	ACEPT	ACEPT	ACEPT	ACEPT	ACEPT	RECH
Efecto NP	Positivo	Negativo	Negativo	Negativo	Negativo	Negativo	Negativo	Positivo	Negativo	Positivo	Positivo	Positivo	Positivo	Negativo	Negativo
Delta Comp (p.u.)	0.0043	-0.0031	-0.0096	-0.0054	-0.0092	-0.0788	-0.0024	0.0002	-0.0029	0.0006	0.0021	0.0026	0.0020	-0.0050	-0.0131
Cambio Comp (%)	0.47	-0.34	-1.03	-0.58	-0.99	-8.50	-0.26	0.03	-0.32	0.07	0.23	0.28	0.22	-0.54	-1.39
Mejora Específica (p.u./ gr_{NP})	0.2549	-0.1874	-0.5700	-0.3202	-0.5489	-4.6920	-0.1414	0.0143	-0.1748	0.0379	0.1265	0.1526	0.1192	-0.3000	-0.7829

Como se puede observar en la Tabla 5, no se puede rechazar la hipótesis nula salvo en los días 3, 7 y 21, tanto en la composición como en la producción de metano (el producto de composición y producción bruta). Pese a ello, se puede apreciar que las nanopartículas tienen un ligero efecto negativo en la composición, reduciendo el porcentaje de metano en la mezcla, siendo la mayor diferencia de 0.0788 p.u. (7,88%) entre ambas muestras en el día 8, una variación del 8,5% sobre las botellas de control.

En cambio, se puede observar el efecto contrario en la producción de metano, debido al incremento de producción de biogás bruto previamente analizado, llegando a presentar mejoras por encima del 100% (dobra la producción) entre los días 14 y 17, siendo estos los días centrales de la metanogénesis. Esta proporción decae hacia el final del ensayo debido al agotamiento de la muestra, en la cual presenta una mejora del 57,77%.

Por último, esto se ve reflejado en la mejora específica de la producción presentando efectos positivos salvo el día 2, y estando la mayoría de los días por encima de $10 \text{ Nm}^3/\text{gr}_{\text{NP}}$. Este efecto no se puede observar en la composición debido al efecto magnificador de los pequeños órdenes de magnitud. Además, estos efectos se muestran al final de la sección en la Ilustración 9.

Análisis de la Producción Media Diaria del Hidrógeno de las Botellas

En este apartado se procederá del mismo modo que en el anterior, analizándose la composición de la especie estudiada, así como la interacción que presenta con la producción bruta de biogás del apartado 4.1. de este documento. En este caso, se estudia los efectos de las nanopartículas sobre la producción media del hidrógeno.

Tabla 6: Análisis estadístico de la media de H₂

Producción H ₂															
Día	1	2	3	4	7	8	9	10	11	14	15	16	17	18	21
Prod B (Nm ³ /m ³ f)	0.0054	0.0021	0.0006	0.0004	0.0004	0.0006	0.0004	0.0002	0.0003	0.0001	0.0001	0.0000	0.0001	0.0001	0.0000
Prod BN (Nm ³ /m ³ f)	0.0030	0.0020	0.0004	0.0000	0.0005	0.0005	0.0001	0.0001	0.0002	0.0000	0.0000	0.0000	0.0000	0.0000	0.0000
Hipótesis Nula	ACEPT	ACEPT	ACEPT	ACEPT	ACEPT	ACEPT	ACEPT	ACEPT	ACEPT	ACEPT	ACEPT	ACEPT	ACEPT	ACEPT	ACEPT
Efecto NP	Negativo	Negativo	Negativo	Negativo	Positivo	Negativo	Negativo	Negativo	Negativo	Negativo	Negativo	Negativo	Negativo	Negativo	Negativo
Delta Prod (Nm ³ /m ³ f)	-0.0025	-0.0001	-0.0002	-0.0004	0.0001	0.0000	-0.0003	-0.0001	-0.0001	0.0000	-0.0001	0.0000	-0.0001	-0.0001	0.0000
Cambio Prod (%)	-45.53	-3.96	-35.88	-100.00	21.48	-2.40	-86.32	-32.78	-30.23	-39.92	-79.71	-57.09	-100.00	-100.00	-100.00
Mejora Específica (Nm ³ /grNP)	-0.1478	-0.0050	-0.0126	-0.0235	0.0048	-0.0008	-0.0208	-0.0031	-0.0054	-0.0016	-0.0040	-0.0009	-0.0045	-0.0040	-0.0003

Composición H ₂															
Día	1	2	3	4	7	8	9	10	11	14	15	16	17	18	21
Comp B (p.u.)	0.0007	0.0005	0.0003	0.0006	0.0007	0.0012	0.0017	0.0004	0.0009	0.0013	0.0008	0.0010	0.0010	0.0005	0.0002
Comp BN (p.u.)	0.0004	0.0006	0.0001	0.0004	0.0004	0.0006	0.0005	0.0005	0.0007	0.0002	0.0001	0.0000	0.0000	0.0000	0.0000
Hipótesis Nula	ACEPT	ACEPT	ACEPT	ACEPT	ACEPT	ACEPT	ACEPT	ACEPT	ACEPT	ACEPT	RECH	RECH	RECH	ACEPT	ACEPT
Efecto NP	Negativo	Positivo	Negativo	Negativo	Negativo	Negativo	Negativo	Positivo	Negativo	Negativo	Negativo	Negativo	Negativo	Negativo	Negativo
Delta Comp (p.u.)	-0.0003	0.0001	-0.0002	-0.0002	-0.0003	-0.0006	-0.0012	0.0000	-0.0002	-0.0012	-0.0007	-0.0009	-0.0010	-0.0005	-0.0002
Cambio Comp (%)	-45.17	24.73	-59.64	-29.77	-44.93	-52.45	-72.41	8.93	-23.34	-88.58	-88.38	-94.84	-100.00	-100.00	-100.00
Mejora Específica (p.u./grNP)	-0.0181	0.0070	-0.0124	-0.0100	-0.0193	-0.0374	-0.0721	0.0022	-0.0121	-0.0701	-0.0445	-0.0537	-0.0571	-0.0307	-0.0109

Como se puede observar en la Tabla 6, no se puede rechazar la hipótesis nula salvo en la composición del hidrógeno entre los días 15 y 17, debido a que la composición porcentual de este es por lo menos 8 veces mayor en el caso de las botellas BN frente a las botellas de control.

Pese a ello, la tendencia de las variaciones específicas, así como las deltas no presentan cambios positivos, y por tanto reducen la producción del hidrógeno. Esto se puede deber a la poca producción de hidrógeno, lo cual causa que el error de medición del aparato tenga un mayor efecto; o debido a la mayor producción de metano, lo cual reduce la cantidad de hidrógeno libre en los recipientes al consumirse este en la metanogénesis.

Se ha de añadir que, si se comparan los resultados del metano con los de esta especie, se comprueba de manera empírica que estos parecen ser similares si bien desfasados en el tiempo, lo cual sugiere que entre ellos existe una dependencia; lo cual es de esperar al ser el hidrógeno un producto intermedio del proceso de la digestión anaerobia. Por tanto, se producirá mayor cantidad de este cuando se ralentizan los procesos de metanogénesis y viceversa, reduciéndose su presencia en el gas muestreado al fomentarse la metanogénesis, la cual consume el H₂ presente, permitiendo determinar la etapa del proceso de digestión si se conoce la composición del gas y el tiempo transcurrido. Finalmente, estos efectos se muestran al final de la sección en la Ilustración 10.

Análisis de la Producción Media Diaria del Ácido Sulhídrico de las Botellas

En este apartado se procederá del mismo modo que en el anterior, analizándose la composición de la especie estudiada, así como la interacción que presenta con la producción bruta de biogás del apartado 4.1. de este documento. En este caso, se estudia los efectos de las nanopartículas sobre la producción media del ácido sulhídrico.

Tabla 7: Análisis estadístico de la media de H₂S

Producción H ₂ S															
Día	1	2	3	4	7	8	9	10	11	14	15	16	17	18	21
Prod B (Nm ³ /m ³)	0.00757	0.00247	0.00100	0.00072	0.00071	0.00030	0.00004	0.00027	0.00036	0.00007	0.00008	0.00004	0.00005	0.00013	0.00006
Prod BN (Nm ³ /m ³)	0.00552	0.00301	0.00099	0.00000	0.00082	0.00069	0.00010	0.00005	0.00019	0.00015	0.00004	0.00001	0.00000	0.00008	0.00008
Hipótesis Nula	ACEPT	ACEPT	ACEPT	ACEPT	ACEPT	ACEPT	ACEPT	ACEPT	ACEPT	ACEPT	ACEPT	ACEPT	ACEPT	ACEPT	ACEPT
Efecto NP	Negativo	Positivo	Negativo	Negativo	Positivo	Positivo	Positivo	Negativo	Negativo	Positivo	Negativo	Negativo	Negativo	Negativo	Positivo
Delta Prod (Nm ³ /m ³)	-0.0020	0.0005	0.0000	-0.0007	0.0001	0.0004	0.0001	-0.0002	-0.0002	0.0001	0.0000	0.0000	-0.0001	-0.0001	0.0000
Cambio Prod (%)	-27.07	21.66	-0.76	-100.00	14.97	125.16	139.12	-80.09	-46.17	97.55	-54.54	-67.77	-100.00	-39.60	27.07
Mejora Especifica (Nm ³ /gr _{NP})	-0.1220	0.0319	-0.0004	-0.0429	0.0064	0.0227	0.0033	-0.0130	-0.0099	0.0043	-0.0027	-0.0018	-0.0032	-0.0030	0.0010

Composición H ₂ S															
Día	1	2	3	4	7	8	9	10	11	14	15	16	17	18	21
Comp B (p.u.)	0.0009	0.0006	0.0004	0.0004	0.0006	0.0005	0.0002	0.0004	0.0008	0.0003	0.0005	0.0003	0.0002	0.0004	0.0003
Comp BN (p.u.)	0.0007	0.0008	0.0004	0.0003	0.0003	0.0009	0.0003	0.0003	0.0005	0.0002	0.0002	0.0001	0.0000	0.0003	0.0003
Hipótesis Nula	ACEPT	ACEPT	ACEPT	ACEPT	ACEPT	ACEPT	ACEPT	ACEPT	ACEPT	ACEPT	RECH	RECH	RECH	ACEPT	ACEPT
Efecto NP	Positivo	Negativo	Negativo	Positivo	Positivo	Negativo	Negativo	Positivo	Positivo	Positivo	Positivo	Positivo	Positivo	Positivo	Positivo
Delta Comp (p.u.)	-0.0003	0.0002	0.0000	-0.0001	-0.0004	0.0004	0.0001	-0.0001	-0.0003	-0.0001	-0.0003	-0.0003	-0.0002	-0.0001	-0.0001
Cambio Comp (%)	-26.93	33.99	4.23	-20.82	-56.15	78.92	41.21	-17.96	-34.68	-44.50	-64.06	-79.97	-100.00	-23.49	-19.50
Mejora Especifica (p.u./gr _{NP})	-0.0150	0.0120	0.0009	-0.0044	-0.0216	0.0226	0.0049	-0.0045	-0.0172	-0.0089	-0.0174	-0.0156	-0.0101	-0.0054	-0.0038

Como se puede apreciar en la Tabla 7, la hipótesis nula solo se puede rechazar (al igual que en la especie anterior) entre los días 15 y 17, en el análisis de la composición, ya que al producirse la interacción la poca producción en ambos grupos de ensayo no permite rechazar la igualdad de medias.

Sin embargo, al igual que en los análisis anteriores, se comprueba un efecto deseado en las nanopartículas, las cuales reducen la producción media a partir del día 10 llegando a presentar una reducción de hasta el 100% en la composición al no detectarse ácido sulhídrico en el día 17; como se ha mencionado antes, esto puede deberse no solo a la mejora de la composición, sino también a la relación escala-precisión del análisis. Asimismo, esta reducción se ve compensada por el incremento en composición y producción de algunos días en la primera semana del experimento

Pese a que en la composición se observan estos efectos positivos, es necesario señalar que en las botellas ensayadas estos efectos son reducidos en mejora específica, lo cual resulta en el retraso de la aparición de este efecto reductor hasta el día 15 de manera consistente, oscilando entre valores positivos y negativos en la producción de sulhídrico a partir del día 10. Por último, estos efectos se muestran al final de la sección en la Ilustración 11.

Análisis de la Producción Media Diaria de los Residuos de las Botellas

En este apartado se procederá del mismo modo que en el anterior, analizándose la composición de la especie estudiada, así como la interacción que presenta con la producción bruta de biogás del apartado 4.1. de este documento. En este caso, se estudia los efectos de las nanopartículas sobre la producción media de los residuos.

Tabla 8: Análisis estadístico de la media de RES

Producción RES															
Día	1	2	3	4	7	8	9	10	11	14	15	16	17	18	21
Prod B (Nm ³ /m ³)	0.76527	0.28211	0.16577	0.12214	0.09065	0.04935	0.02551	0.03206	0.02407	0.01804	0.01093	0.00660	0.00994	0.01148	0.01293
Prod BN (Nm ³ /m ³)	0.73384	0.26791	0.21538	0.00000	0.19845	0.12834	0.03980	0.03099	0.03091	0.04767	0.02304	0.01594	0.02258	0.01911	0.02839
Hipótesis Nula	ACEPT	ACEPT	ACEPT	ACEPT	ACEPT	ACEPT	ACEPT	ACEPT	ACEPT	ACEPT	ACEPT	ACEPT	ACEPT	ACEPT	ACEPT
Efecto NP	Positivo	Positivo	Negativo	Positivo	Negativo	Negativo	Negativo	Positivo	Negativo	Negativo	Negativo	Negativo	Negativo	Negativo	Negativo
Delta Prod (Nm ³ /m ³)	-0.0314	-0.0142	0.0496	-0.1221	0.1078	0.0790	0.0143	-0.0011	0.0068	0.0296	0.0121	0.0093	0.0126	0.0076	0.0155
Cambio Prod (%)	-4.11	-5.04	29.93	-100.00	118.93	160.06	56.00	-3.36	28.43	164.30	110.74	141.43	127.26	66.42	119.64
Mejora Específica (Nm ³ /gr _{NP})	-1.8724	-0.8461	2.9548	-7.2748	6.4208	4.7046	0.8509	-0.0642	0.4075	1.7651	0.7211	0.5563	0.7532	0.4542	0.9211

Composición RES															
Día	1	2	3	4	7	8	9	10	11	14	15	16	17	18	21
Comp B (p.u.)	0.0948	0.0783	0.0719	0.0720	0.0677	0.0713	0.0713	0.0701	0.0727	0.0688	0.0715	0.0697	0.0686	0.0642	0.0528
Comp BN (p.u.)	0.0910	0.0812	0.0816	0.0776	0.0776	0.1503	0.0748	0.0699	0.0761	0.0695	0.0705	0.0683	0.0677	0.0698	0.0662
Hipótesis Nula	ACEPT	ACEPT	ACEPT	ACEPT	ACEPT	ACEPT	ACEPT	ACEPT	ACEPT	ACEPT	ACEPT	ACEPT	ACEPT	ACEPT	ACEPT
Efecto NP	Positivo	Negativo	Negativo	Negativo	Negativo	Negativo	Negativo	Positivo	Negativo	Negativo	Positivo	Positivo	Positivo	Negativo	Negativo
Delta Comp (p.u.)	-0.0037	0.0028	0.0098	0.0056	0.0099	0.0790	0.0035	-0.0002	0.0034	0.0007	-0.0011	-0.0014	-0.0009	0.0056	0.0134
Cambio Comp (%)	-3.93	3.61	13.59	7.80	14.62	110.85	4.91	-0.29	4.71	1.00	-1.52	-2.00	-1.27	8.79	25.38
Mejora Específica (p.u./gr _{NP})	-0.2218	0.1685	0.5815	0.3347	0.5897	4.7069	0.2086	-0.0119	0.2041	0.0411	-0.0646	-0.0833	-0.0519	0.3361	0.7975

Al igual que en los apartados anteriores, la hipótesis nula no puede ser rechazada, por lo que no se puede asegurar que la composición o la producción media de residuos sean distintas entre las muestras. En lo que respecta a la composición, se puede observar que las nanopartículas presentan un ligero incremento en la composición del biogás al aumentar su peso en la composición de las muestras analizadas en la mayoría de los días ensayados salvo los días 1 y 10 y de los días 15 a 17, durante los cuales se registra una reducción máxima del 3,93% en el día 1 y un 2% durante el día 17. En cambio, el incremento producido en los días restantes tiene su pico en el día 8, cuando se produce un aumento del 110,85% al producirse más del doble en BN que en B. Sin embargo, este es un punto aislado, siendo el siguiente mayor pico el del día 7 (14,62%). Estos cambios pueden considerarse significativos en la composición ya que los residuos representan en torno al 7% de la composición.

En lo que respecta a la producción, el aumento de la producción de biogás bruto causa que el efecto de las nanopartículas sea mayor, presentando varios días en los que se supera el 100% de incremento y solo 3 días en los que se producen menos residuos. Lo cual se ve reflejado también en la mejora específica, siendo esta predominantemente negativa, pese a que el pico de efectividad no supera los 7,28 Nm³/gr_{NP}, lo cual contrasta con el pronunciado efecto que estas tienen en otras especies. Esto puede llegar a justificar su uso pese a empeorar la calidad del biogás. Para finalizar, estos efectos se muestran al final de la sección en la Ilustración 12.

Gráficas de los efectos de las Nanopartículas sobre la media

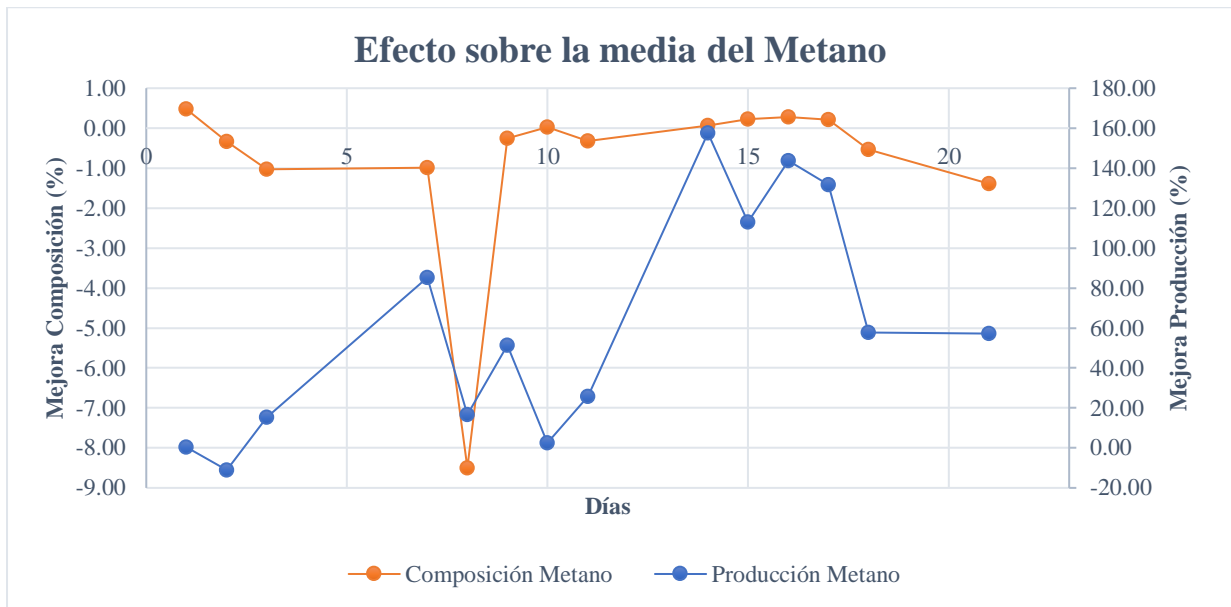


Ilustración 9: Efecto sobre sobre la media del Metano

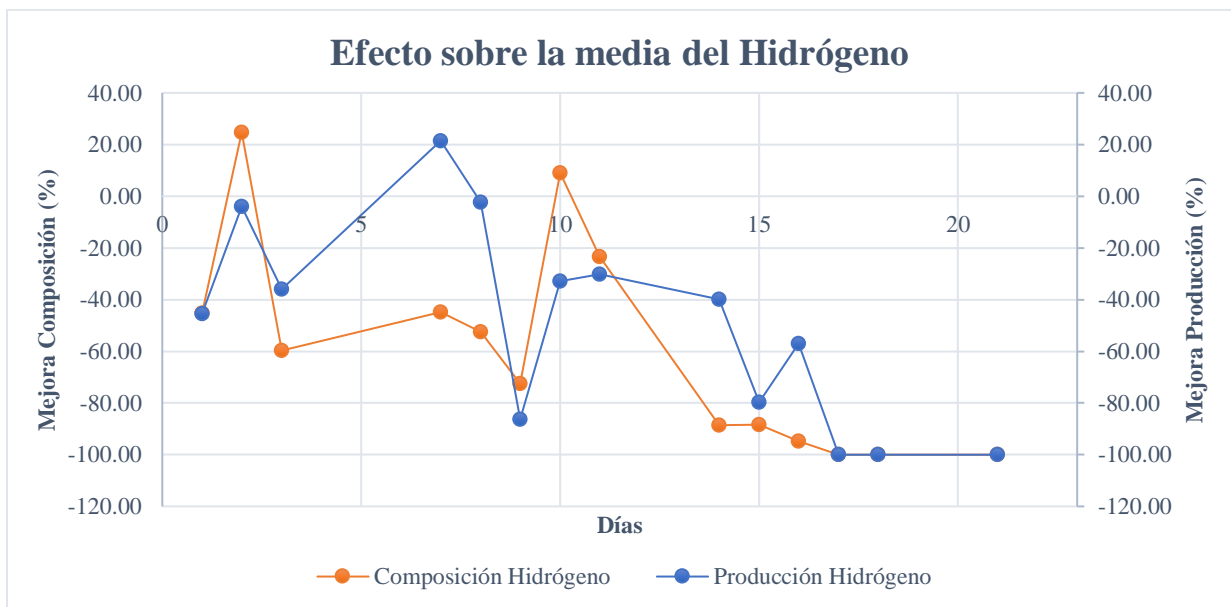


Ilustración 10: Efecto sobre la media del Hidrógeno

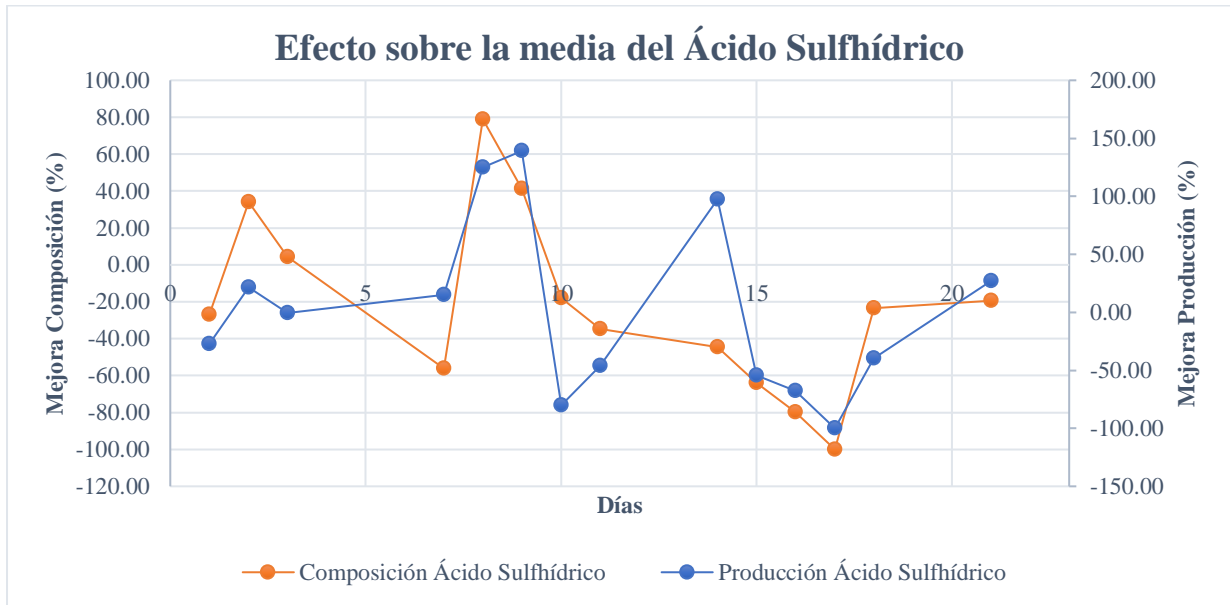


Ilustración 11: Efecto sobre sobre la media del Ácido Sulfhídrico

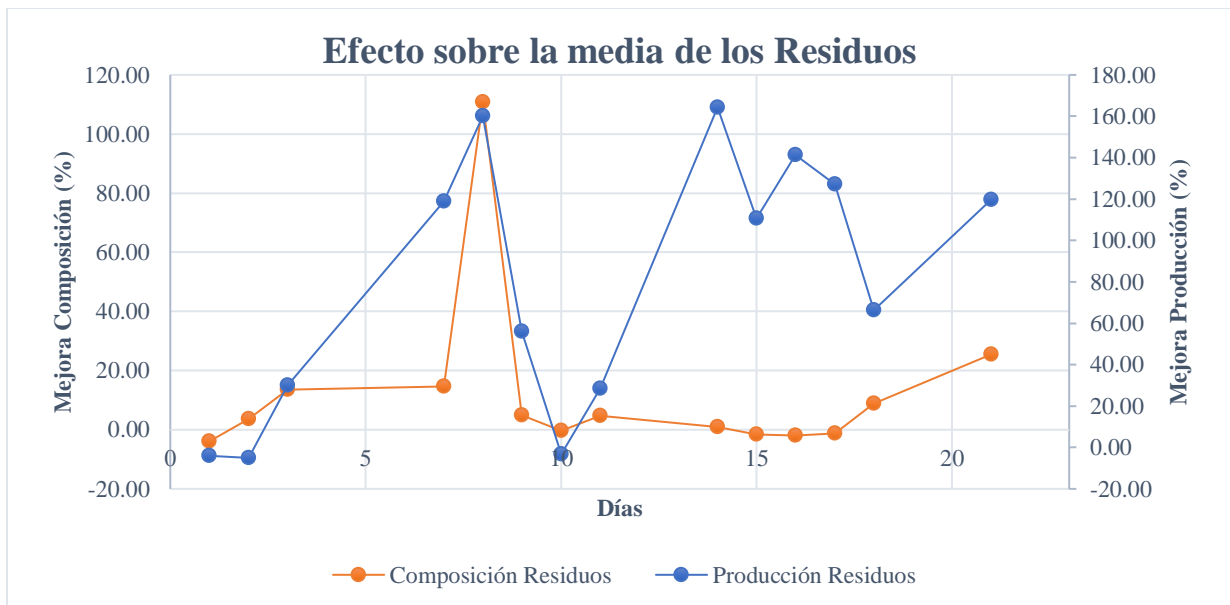


Ilustración 12: Efecto sobre la media de los Residuos

c. Análisis de la Varianza Diaria

La última prueba estadística realizada es la referente a la varianza de las poblaciones de cada grupo de muestras, como se ha mencionado antes. Siguiendo la estructura del apartado anterior, los resultados de cada compuesto se muestran a continuación de la Tabla 9 a la Tabla 12.

Análisis de la Varianza Diaria del Metano de las Botellas

Tabla 9: Análisis estadístico de la varianza de CH₄

Producción CH ₄															
Día	1	2	3	4	7	8	9	10	11	14	15	16	17	18	21
STD B (Nm ³ /m ³)	0.1314	1.8777	1.2789	1.0135	1.1705	0.5105	0.3073	0.3699	0.2307	0.3034	0.1471	0.1159	0.1303	0.1471	0.3160
STD BN (Nm ³ /m ³)	0.1476	1.2472	0.9139	0.0000	1.1881	0.2368	0.3335	0.2092	0.1357	0.4740	0.1286	0.0264	0.0461	0.0714	0.2077
Hipótesis Nula	ACCEPT	ACCEPT	ACCEPT	RECH	ACCEPT	ACCEPT	ACCEPT	ACCEPT	ACCEPT	ACCEPT	ACCEPT	RECH	ACCEPT	ACCEPT	ACCEPT
Efecto NP	Negativo	Positivo	Positivo	Positivo	Negativo	Positivo	Negativo	Positivo	Positivo	Negativo	Positivo	Positivo	Positivo	Positivo	Positivo
Delta Prod (Nm ³ /m ³)	0.0162	-0.6306	-0.3650	-1.0135	0.0175	-0.2738	0.0262	-0.1607	-0.0950	0.1706	-0.0185	-0.0895	-0.0842	-0.0757	-0.1082
Cambio Prod (%)	12.34	-33.58	-28.54	-100.00	1.50	-53.62	8.51	-43.43	-41.17	56.24	-12.59	-77.26	-64.63	-51.44	-34.25
Mejora Específica (Nm ³ /gr _{NP})	0.9656	-37.5557	-21.7380	-60.3606	1.0441	-16.3047	1.5575	-9.5691	-5.6580	10.1626	-1.1031	-5.3325	-5.0148	-4.5075	-6.4462

Composición CH ₄															
Día	1	2	3	4	7	8	9	10	11	14	15	16	17	18	21
STD B (p.u.)	0.0080	0.0080	0.0080	0.0052	0.0049	0.0073	0.0092	0.0078	0.0066	0.0078	0.0052	0.0038	0.0050	0.0080	0.0081
STD BN (p.u.)	0.0186	0.0130	0.0062	0.0034	0.0034	0.1769	0.0111	0.0109	0.0061	0.0037	0.0052	0.0026	0.0024	0.0030	0.0048
Hipótesis Nula	RECH	ACCEPT	ACCEPT	ACCEPT	ACCEPT	RECH	ACCEPT	ACCEPT	ACCEPT	ACCEPT	ACCEPT	ACCEPT	ACCEPT	ACCEPT	ACCEPT
Efecto NP	Negativo	Negativo	Positivo	Positivo	Positivo	Negativo	Negativo	Negativo	Positivo	Positivo	Negativo	Positivo	Positivo	Positivo	Positivo
Delta Comp (p.u.)	0.0106	0.0050	-0.0018	-0.0018	-0.0014	0.1696	0.0019	0.0031	-0.0005	-0.0041	0.0000	-0.0012	-0.0027	-0.0050	-0.0033
Cambio Comp (%)	132.54	62.58	-22.03	-34.20	-29.53	2,309.74	20.91	39.88	-6.99	-52.23	0.44	-32.16	-53.16	-61.94	-41.05
Mejora Específica (p.u./gr _{NP})	0.6327	0.2987	-0.1049	-0.1063	-0.0857	10.1005	0.1145	0.1845	-0.0274	-0.2431	0.0014	-0.0734	-0.1590	-0.2956	-0.1990

El análisis de la varianza del metano produce unos resultados de gran interés, ya que, pese a no rechazar la hipótesis nula y por tanto no poder asegurar que las varianzas poblacionales son distintas ni en composición ni en producción, salvo algunos días específicos, se ve una clara mejora en el proceso de digestión.

Comenzando por la composición, se observa que la desviación típica se reduce a partir del día 11, ya que en el día 8 apenas hay un empeoramiento del 2% y los días 9 y 10 aumenta la desviación. Esto sugiere que el efecto principal de las nanopartículas en la codigestión es la estabilización del proceso al reducir la variabilidad de esta especie. Para comprobar que estos no son resultados aislados, se deberán comprobar los efectos sobre el resto de los compuestos analizados en el cromatograma.

Continuando con la producción, en esta se observa un efecto similar, resultando en una interacción que es beneficiosa para el proceso ya que, al aumentar la producción bruta de biogás, junto con esta reducción de la desviación estándar se consigue un marcado efecto específico, desde el día 10 salvo el 14, consiguiéndose una mejora específica máxima de 9,57 Nm³/gr_{NP}. Estos efectos, al igual que en la sección anterior, se muestran al final de esta en la Ilustración 13.

Análisis de la Varianza Diaria del Hidrógeno de las Botellas

En este apartado se procederá del mismo modo que en el anterior, analizándose la composición de la especie estudiada, así como la interacción que presenta con la producción bruta de biogás del apartado 4.1. de este documento. En este caso, se estudia los efectos de las nanopartículas sobre la varianza del hidrógeno.

Tabla 10: Análisis estadístico de la varianza de H₂

Producción H ₂															
Día	1	2	3	4	7	8	9	10	11	14	15	16	17	18	21
STD B (Nm ³ /m ³ _f)	0.0067	0.0045	0.0016	0.0005	0.0006	0.0006	0.0005	0.0003	0.0007	0.0001	0.0001	0.0000	0.0001	0.0001	0.0000
STD BN (Nm ³ /m ³ _f)	0.0031	0.0035	0.0008	0.0000	0.0009	0.0003	0.0001	0.0001	0.0003	0.0001	0.0000	0.0000	0.0000	0.0000	0.0000
Hipótesis Nula	ACEPT	ACEPT	ACEPT	RECH	ACEPT	ACEPT	RECH	ACEPT	ACEPT	ACEPT	RECH	ACEPT	RECH	RECH	RECH
Efecto NP	Positivo	Positivo	Positivo	Positivo	Negativo	Positivo	Positivo	Positivo	Positivo	Positivo	Positivo	Positivo	Positivo	Positivo	Positivo
Delta Prod (Nm ³ /m ³ _f)	-0.0037	-0.0010	-0.0008	-0.0005	0.0003	-0.0003	-0.0004	-0.0002	-0.0005	0.0000	-0.0001	0.0000	-0.0001	-0.0001	0.0000
Cambio Prod (%)	-54.35	-22.44	-48.08	-100.00	42.96	-52.53	-81.34	-61.58	-62.84	-19.84	-76.73	-62.78	-100.00	-100.00	-100.00
Mejora Específica (Nm ³ /gr _{NP})	-0.2184	-0.0596	-0.0465	-0.0310	0.0158	-0.0187	-0.0226	-0.0103	-0.0269	-0.0014	-0.0046	-0.0018	-0.0065	-0.0074	-0.0010

Composición H ₂															
Día	1	2	3	4	7	8	9	10	11	14	15	16	17	18	21
STD B (p.u.)	0.0008	0.0009	0.0007	0.0009	0.0008	0.0008	0.0017	0.0006	0.0016	0.0019	0.0006	0.0007	0.0009	0.0006	0.0003
STD BN (p.u.)	0.0004	0.0010	0.0003	0.0008	0.0008	0.0002	0.0008	0.0006	0.0011	0.0003	0.0001	0.0001	0.0000	0.0000	0.0000
Hipótesis Nula	ACEPT	ACEPT	ACEPT	ACEPT	ACEPT	RECH	ACEPT	ACEPT	ACEPT	RECH	RECH	RECH	RECH	RECH	RECH
Efecto NP	Positivo	Negativo	Positivo	Positivo	Negativo	Positivo	Positivo	Negativo	Positivo	Positivo	Positivo	Positivo	Positivo	Positivo	Positivo
Delta Comp (p.u.)	-0.0004	0.0001	-0.0004	0.0000	0.0001	-0.0006	-0.0008	0.0000	-0.0005	-0.0017	-0.0005	-0.0006	-0.0009	-0.0006	-0.0003
Cambio Comp (%)	-54.06	13.55	-57.49	-5.50	6.38	-70.22	-50.91	6.12	-30.84	-86.64	-76.99	-89.83	-100.00	-100.00	-100.00
Mejora Específica (p.u./gr _{NP})	-0.0268	0.0071	-0.0254	-0.0029	0.0030	-0.0340	-0.0501	0.0021	-0.0297	-0.0985	-0.0292	-0.0384	-0.0509	-0.0330	-0.0188

Al contrario que en el metano, la varianza del hidrógeno si se ve muy afectada por la adición de nanopartículas, ya que se consigue rechazar la hipótesis nula durante la última semana del ensayo en lo que respecta la composición, ya que la desviación típica se reduce de una manera drástica en al menos 1 orden de magnitud frente a la codigestión sin estas. Lo que resulta en una mejora del 100% debido al redondeo por número de decimales. También hay que destacar que este proceso comienza en el día 8 con una reducción del 70,22%, salvo por el día 10, el cual rompe la racha de resultados negativos. Como último apunte, debido a la baja varianza del proceso, el efecto específico es reducido.

Sin embargo, la producción no muestra unos resultados tan marcados debido a la interacción, reduciendo el rechazo de la hipótesis nula al día 17, durante el periodo de metanogénesis. En cambio, las nanopartículas si consiguen reducir ligeramente la desviación típica a partir del día 8, con reducción siempre entre el 20 y el 80% (sin considerar los días finales cuando la muestra se está cerca de agotarse). Asimismo, estas mejoras, comparativamente menores, que en la composición presentan una menor especificidad de en torno a 1 orden de magnitud.

Asimismo, es de notar que este es el campo donde se han obtenido los mejores resultados en los ensayos. Finalmente, el cambio porcentual se ha incluido en la Ilustración 14 al final de esta sección.

Análisis de la Varianza Diaria del Ácido Sulfhídrico de las Botellas

En este apartado se procederá del mismo modo que en el anterior, analizándose la composición de la especie estudiada, así como la interacción que presenta con la producción bruta de biogás del apartado 4.1. de este documento. En este caso, se estudia los efectos de las nanopartículas sobre la varianza del ácido sulfhídrico.

Tabla 11: Análisis estadístico de la varianza de H₂S

Producción H ₂ S															
Día	1	2	3	4	7	8	9	10	11	14	15	16	17	18	21
STD B (Nm ³ /m ³ _f)	0.0080	0.0032	0.0013	0.0010	0.0009	0.0008	0.0001	0.0006	0.0004	0.0002	0.0001	0.0001	0.0002	0.0002	0.0001
STD BN (Nm ³ /m ³ _f)	0.0066	0.0030	0.0022	0.0000	0.0014	0.0015	0.0001	0.0001	0.0003	0.0003	0.0001	0.0000	0.0000	0.0001	0.0001
Hipótesis Nula	ACEPT	ACEPT	ACEPT	RECH	ACEPT	ACEPT	ACEPT	RECH	ACEPT	ACEPT	ACEPT	RECH	RECH	ACEPT	ACEPT
Efecto NP	Positivo	Positivo	Negativo	Positivo	Negativo	Negativo	Negativo	Positivo	Positivo	Negativo	Positivo	Positivo	Positivo	Positivo	Negativo
Delta Prod (Nm ³ /m ³ _f)	-0.0014	-0.0002	0.0009	-0.0010	0.0005	0.0008	0.0000	-0.0005	-0.0001	0.0002	-0.0001	-0.0001	-0.0002	-0.0001	0.0000
Cambio Prod (%)	-17.89	-6.93	72.81	-100.00	55.95	100.02	54.33	-86.53	-31.81	109.88	-41.09	-75.98	-100.00	-59.77	5.47
Mejora Específica (Nm ³ /gr _{NP})	-0.0850	-0.0133	0.0556	-0.0577	0.0301	0.0457	0.0025	-0.0297	-0.0074	0.0102	-0.0032	-0.0059	-0.0097	-0.0086	0.0004

Composición H ₂ S															
Día	1	2	3	4	7	8	9	10	11	14	15	16	17	18	21
STD B (p.u.)	0.0010	0.0007	0.0005	0.0003	0.0007	0.0009	0.0003	0.0008	0.0008	0.0004	0.0007	0.0006	0.0005	0.0007	0.0006
STD BN (p.u.)	0.0008	0.0008	0.0008	0.0005	0.0005	0.0019	0.0003	0.0006	0.0008	0.0003	0.0003	0.0001	0.0000	0.0003	0.0004
Hipótesis Nula	ACEPT	ACEPT	ACEPT	ACEPT	ACEPT	ACEPT	ACEPT	ACEPT	ACEPT	ACEPT	ACEPT	RECH	RECH	ACEPT	ACEPT
Efecto NP	Positivo	Negativo	Negativo	Negativo	Positivo	Negativo	Negativo	Positivo	Positivo	Positivo	Positivo	Positivo	Positivo	Positivo	Positivo
Delta Comp (p.u.)	-0.0002	0.0001	0.0003	0.0001	-0.0002	0.0011	0.0000	-0.0002	0.0000	-0.0002	-0.0003	-0.0005	-0.0005	-0.0003	-0.0002
Cambio Comp (%)	-17.99	17.98	55.54	37.69	-33.44	121.56	0.71	-20.92	-5.16	-37.72	-51.69	-75.93	-100.00	-48.98	-32.75
Mejora Específica (p.u./gr _{NP})	-0.0106	0.0072	0.0176	0.0075	-0.0138	0.0628	0.0001	-0.0095	-0.0026	-0.0098	-0.0205	-0.0276	-0.0303	-0.0192	-0.0109

Procediendo con el primero de los productos indeseados, el ácido sulfhídrico no rechaza la hipótesis nula salvo en los días 16 y 17 en la composición, también reflejado en la producción de esos días. Esto se debe a que el su bajo peso en la mezcla analizada resulte en una desviación típica mucho menor en esos días, en especial el día 17 cuando se reduce en al menos 1 orden de magnitud y por tanto se produce una mejora del 100% debido al redondeo.

Sin embargo, si se aprecia a partir del día 10 una mejora al reducirse su desviación en un 20%, siendo las subsecuentes mejoras porcentuales mayores salvo el día 11 durante el cual la mejora es solo del 5,16%. Al igual que en el resto de las especies analizadas en la desviación típica, el efecto específico es reducido.

Continuando con la producción, la interacción aumenta la dispersión de los datos durante los días iniciales, magnificando lo observado durante la primera mitad del ensayo, llegando a doblarse la desviación típica en el día 8. Pese a este aumento de la dispersión, el cual atenúa lo observado, sí que se aprecia el efecto reductor de las nanopartículas en la mejora específica. Por último, los cambios porcentuales de producción y composición se han incluido en la Ilustración 15 al final de esta sección

Análisis de la Varianza Diaria de los Residuos de las Botellas

En este apartado se procederá del mismo modo que en el anterior, analizándose la composición de la especie estudiada, así como la interacción que presenta con la producción bruta de biogás del apartado 4.1. de este documento. En este caso, se estudia los efectos de las nanopartículas sobre la varianza de los residuos.

Tabla 12: Análisis estadístico de la varianza de RES

Producción RES															
Día	1	2	3	4	7	8	9	10	11	14	15	16	17	18	21
STD B (Nm ³ /m ³ _f)	0.0569	0.1563	0.1013	0.0760	0.0792	0.0360	0.0207	0.0277	0.0182	0.0221	0.0108	0.0085	0.0096	0.0113	0.0153
STD BN (Nm ³ /m ³ _f)	0.1422	0.1199	0.0842	0.0000	0.0909	0.1357	0.0219	0.0144	0.0095	0.0362	0.0086	0.0014	0.0029	0.0047	0.0154
Hipótesis Nula	RECH	ACEPT	ACEPT	RECH	ACEPT	RECH	ACEPT	ACEPT	ACEPT	ACEPT	ACEPT	RECH	RECH	ACEPT	ACEPT
Efecto NP	Negativo	Positivo	Positivo	Positivo	Negativo	Negativo	Negativo	Positivo	Positivo	Negativo	Positivo	Positivo	Positivo	Positivo	Negativo
Delta Prod (Nm ³ /m ³ _f)	0.0853	-0.0364	-0.0171	-0.0760	0.0117	0.0997	0.0012	-0.0133	-0.0087	0.0141	-0.0022	-0.0071	-0.0067	-0.0066	0.0000
Cambio Prod (%)	149.96	-23.30	-16.86	-100.00	14.79	277.34	5.63	-47.94	-47.84	63.71	-20.10	-83.73	-69.46	-58.30	0.11
Mejora Específica (Nm ³ /gr _{NP})	5.0816	-2.1682	-1.0173	-4.5283	0.6975	5.9384	0.0694	-0.7899	-0.5175	0.8400	-0.1292	-0.4249	-0.3991	-0.3932	0.0010

Composición RES															
Día	1	2	3	4	7	8	9	10	11	14	15	16	17	18	21
STD B (p.u.)	0.0069	0.0073	0.0074	0.0049	0.0041	0.0062	0.0075	0.0067	0.0048	0.0068	0.0044	0.0031	0.0043	0.0079	0.0078
STD BN (p.u.)	0.0176	0.0120	0.0055	0.0030	0.0030	0.1749	0.0103	0.0101	0.0053	0.0033	0.0049	0.0026	0.0024	0.0028	0.0046
Hipótesis Nula	RECH	ACEPT	ACEPT	ACEPT	ACEPT	RECH	ACEPT	ACEPT	ACEPT	ACEPT	ACEPT	ACEPT	ACEPT	ACEPT	ACEPT
Efecto NP	Negativo	Negativo	Positivo	Positivo	Positivo	Negativo	Negativo	Negativo	Negativo	Positivo	Negativo	Positivo	Positivo	Positivo	Positivo
Delta Comp (p.u.)	0.0107	0.0047	-0.0019	-0.0019	-0.0011	0.1687	0.0027	0.0034	0.0004	-0.0035	0.0005	-0.0005	-0.0019	-0.0051	-0.0032
Cambio Comp (%)	154.06	63.97	-25.31	-38.37	-26.08	2,709.92	36.56	50.96	8.97	-51.06	11.35	-15.58	-45.19	-65.07	-40.49
Mejora Específica (p.u./gr _{NP})	0.6354	0.2791	-0.1118	-0.1123	-0.0637	10.0474	0.1637	0.2036	0.0257	-0.2059	0.0297	-0.0291	-0.1155	-0.3056	-0.1878

El último efecto por estudiar en los ensayos de botellas, al igual que en la anterior sección es el de los residuos, los cuales presentan un comportamiento contrario al resto de especies, ya que en este caso aparecen más rechazos de la hipótesis nula en la producción en lugar de en la composición, concretamente en los días 16 y 17, por lo que podemos asegurar que esta es la interacción con mayores efectos positivos.

Pese al efecto de la interacción, se puede observar cómo en este ensayo el uso de las nanopartículas aumenta considerablemente la desviación típica en las botellas, así como los efectos porcentuales y específicos de estas, llegando a un pico del 2700%, lo cual puede deberse a un error de escala en el procesado de los datos. Obviando ese dato singular, sí que se puede apreciar la mayor dispersión de las mejoras en ambas variables, ya que no entran en valores negativos de manera estable hasta los días 15 y 16, donde se produce una clara reducción de las desviaciones típicas.

Como apunte adicional, esta mayor dispersión en las medidas obtenidas causa una mayor especificidad en ambas variables, muy superior al resto de compuestos, por lo que se puede deducir que una menor especificidad es deseable para las varianzas del proceso. Para finalizar, los efectos se muestran en la Ilustración 16 al final de esta sección.

Gráficas de los efectos de las Nanopartículas sobre la desviación típica

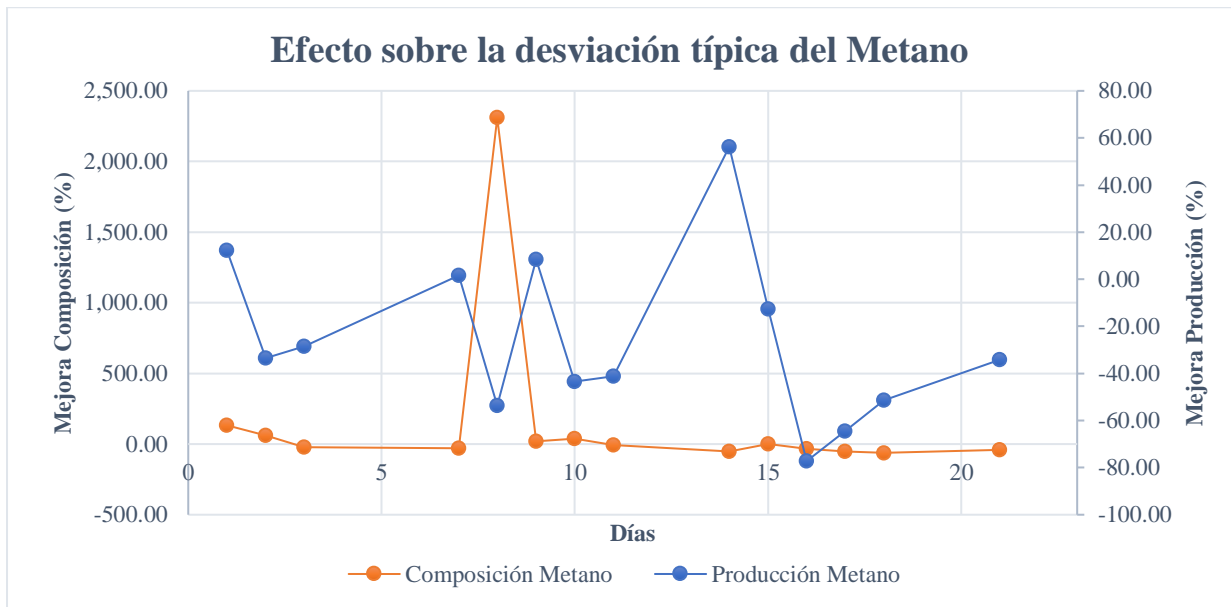


Ilustración 13: Efecto sobre la desviación estándar del Metano

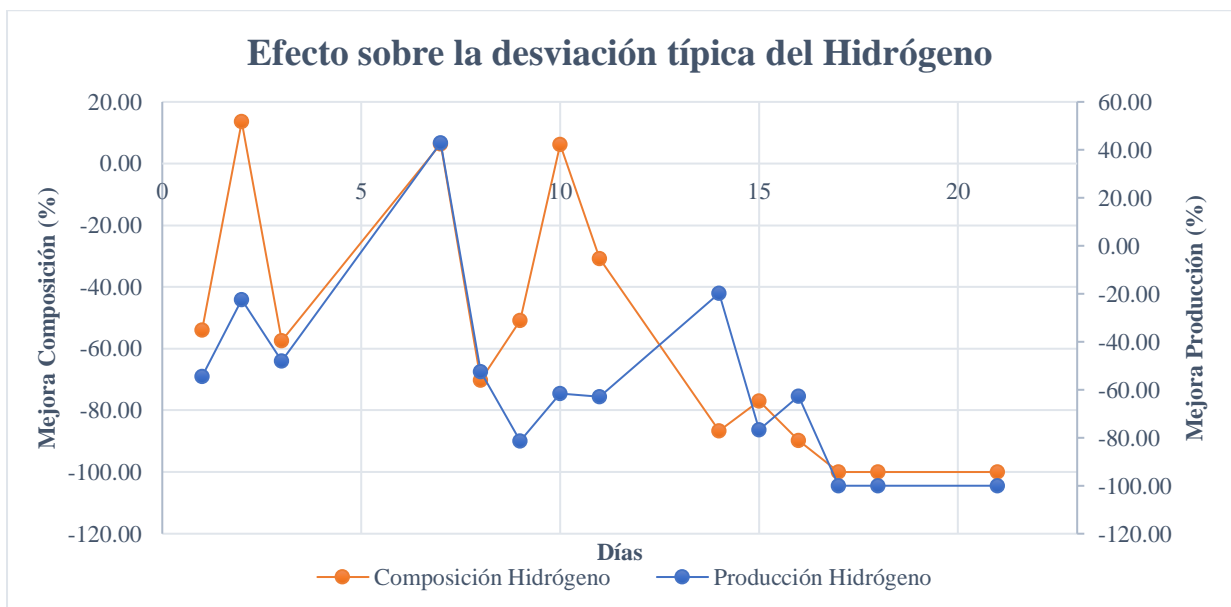


Ilustración 14: Efecto sobre la desviación estándar del Hidrógeno

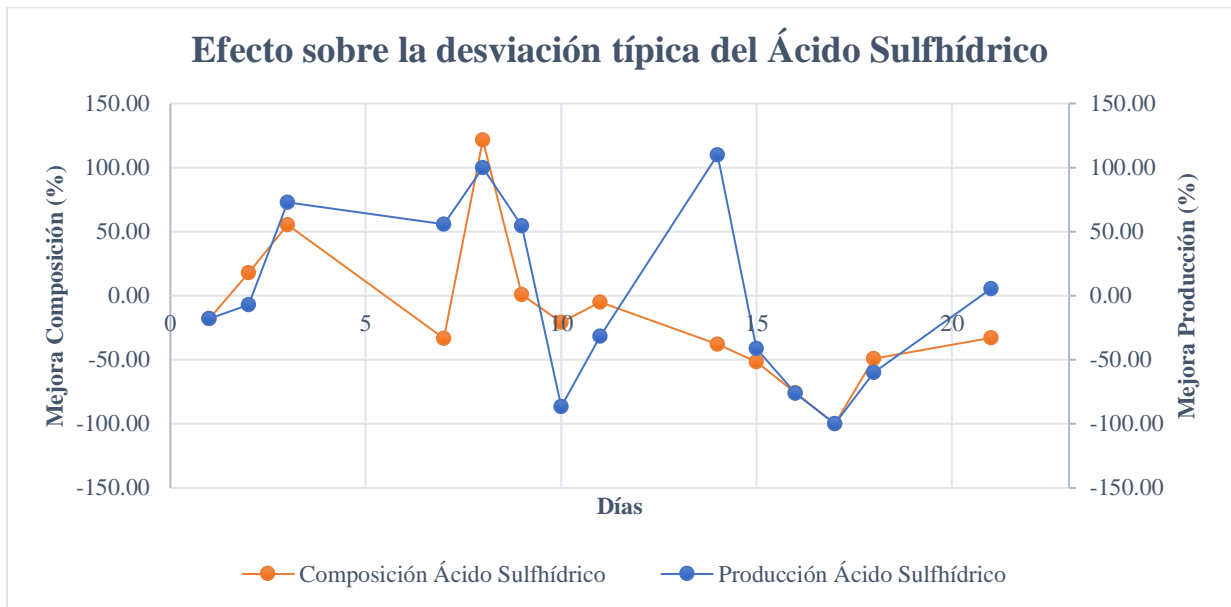


Ilustración 15: Efecto sobre la desviación estándar del Ácido Sulhídrico



Ilustración 16: Efecto sobre la desviación estándar de los Residuos

4. Análisis de los Resultados de los Reactores

Tras el análisis de los efectos de las nanopartículas en las botellas y comprobar los efectos prometedores de estas, se procedió con el análisis de las medidas reactores discontinuos de 2 litros empleados.

A priori, es de esperar que se obtengan resultados similares a los de las secciones anteriores al ser estos en esencia el mismo ensayo en un volumen mayor; lo cual podría mostrar tendencias previamente no observadas debido a la escala.

Por último, se ha de señalar que, debido a las restricciones temporales, solo se pudo ensayar 1 reactor en cada caso, por lo que se necesitará repetir este ensayo para obtener una muestra y realizar los mismos contrastes de hipótesis y comprobar si los reactores y botellas pertenecen a las mismas poblaciones. Además, debido a problemas con la pérdida de carga entre el gasómetro empleado para medir la producción y la salida del reactor, así como una fuga en la junta entre la varilla de agitación y su camisa (desvelada por la volatilización y acumulación de nanopartículas en este); no se registraron medidas de producción durante la mayoría de los días, por lo que no se analizaran.

Asimismo, este problema de volatilización de las nanopartículas implica que los ensayos se deben repetir ya que será de esperar que si se consigue un método de mezcla y disolución robusto (a realizar en futuras investigaciones) se amplificarán los efectos observados.

Finalmente, el análisis del efecto de las nanopartículas sobre la composición de los reactores se muestra a continuación de la Tabla 13 a la Tabla 16 para el metano, hidrógeno, ácido sulfhídrico y residuos respectivamente.

Análisis de la Composición del Metano de los Reactores

Tabla 13: Composición del Metano en los Reactores

Metano															
Día	1	2	3	4	7	8	9	10	11	14	15	16	17	18	21
Comp R (p.u.)	0.3794	0.8208	0.0439	0.6834	0.1738	0.7271	0.0994	0.1087	0.5711	0.3412	0.3971	0.4319	0.0531	0.3871	0.5082
Comp RN (p.u.)	0.8271	0.6811	0.7335	0.6420	0.6420	0.5159	0.6157	0.5863	0.3463	0.6197	0.0116	0.0000	0.0000	0.0000	0.0000
Efecto NP	Positivo	Negativo	Positivo	Negativo	Positivo	Negativo	Positivo	Positivo	Negativo	Positivo	Negativo	Negativo	Negativo	Negativo	Negativo
Delta Comp (p.u.)	0.4477	-0.1397	0.6896	-0.0414	0.4683	-0.2112	0.5163	0.4777	-0.2247	0.2785	-0.3855	-0.4319	-0.0531	-0.3871	-0.5082
Cambio Comp (%)	118.01	-17.02	1,571.07	-6.05	269.49	-29.05	519.42	439.60	-39.35	81.63	-97.08	-100.00	-100.00	-100.00	-100.00
Mejora Específica (p.u./gGNP)	3.9976	-1.2474	6.1568	-0.3694	4.1810	-1.8858	4.6098	4.2648	-2.0065	2.4867	-3.4419	-3.8563	-0.4740	-3.4559	-4.5372

Como se puede apreciar en la Tabla 13, las nanopartículas tuvieron un efecto positivo entre los días 9 y 14, con mejoras muy superiores a las observadas en las botellas, obteniéndose unos picos del 519 % y del 439%; lo cual sugiere que en volúmenes mayores el efecto acelerador de las nanopartículas es más pronunciado. Sin embargo, a partir del día 15 el peso del metano en la composición decae hasta 0, dando señales del agotamiento del reactor. En este caso, sería necesario realizar más ensayos en estos volúmenes para comprobar si este es un efecto real o este reactor se comportó de forma anómala. Por último, el efecto de las nanopartículas sobre la composición en metano se muestra junto con el efecto del hidrógeno en la Ilustración 17 al final de la sección.

Análisis de la Composición del Hidrógeno de los Reactores

Tabla 14: Composición del Hidrógeno en los Reactores

Hidrógeno															
Día	1	2	3	4	7	8	9	10	11	14	15	16	17	18	21
Comp R (p.u.)	0.2525	0.0420	0.4358	0.0926	0.2705	0.0646	0.2898	0.2617	0.1116	0.2485	0.1608	0.1705	0.2788	0.1671	0.1676
Comp RN (p.u.)	0.0502	0.1161	0.0739	0.1102	0.1102	0.1273	0.1002	0.1145	0.1692	0.0919	0.3683	0.2931	0.2802	0.2618	0.2269
Efecto NP	Negativo	Positivo	Negativo	Positivo	Negativo	Positivo	Negativo	Negativo	Positivo	Negativo	Positivo	Positivo	Positivo	Positivo	Positivo
Delta Comp (p.u.)	-0.2023	0.0741	-0.3619	0.0176	-0.1603	0.0627	-0.1896	-0.1472	0.0576	-0.1566	0.2074	0.1227	0.0014	0.0947	0.0593
Cambio Comp (%)	-80.11	176.65	-83.04	18.95	-59.27	97.07	-65.42	-56.23	51.58	-63.02	128.99	71.95	0.52	56.68	35.38
Mejora Específica (p.u./gr _{NP})	-1.8060	0.6618	-3.2314	0.1567	-1.4314	0.5599	-1.6929	-1.3140	0.5140	-1.3981	1.8522	1.0951	0.0128	0.8456	0.5294

En lo que respecta a la composición del hidrógeno, se observa un efecto contrario al que ocurre en el metano, siendo estos opuestos en la mayoría de los días reforzando la teoría de que existe una relación inversa, formando un ciclo. Se necesitan más estudios para determinar la veracidad de esta hipótesis.

Asimismo, se comprueba que el hidrógeno se ve afectado positivamente por las nanopartículas, produciéndose grandes mejoras en periodos cortos, en especial a partir del día 15, cuando la mejora específica deja de alternar rachas de valores positivos y negativos y produce mejoras entre 0,5 p.u./gr_{NP} y 1,85 p.u./gr_{NP}, con su mejora porcentual asociada. Por último, estas mejoras porcentuales se han incluido en la Ilustración 17.

Análisis de la Composición del Ácido Sulphídrico

Tabla 15: Composición del Ácido Sulphídrico en los Reactores

Ácido Sulphídrico															
Día	1	2	3	4	7	8	9	10	11	14	15	16	17	18	21
Comp R (p.u.)	0.0000	0.0022	0.0014	0.0000	0.0000	0.0018	0.0034	0.0000	0.0041	0.0000	0.0048	0.0000	0.0026	0.0022	0.0044
Comp RN (p.u.)	0.0012	0.0000	0.0003	0.0000	0.0000	0.0034	0.0003	0.0005	0.0000	0.0019	0.0018	0.0033	0.0000	0.0018	0.0017
Efecto NP	Positivo	Negativo	Negativo	Negativo	Negativo	Positivo	Negativo	Positivo	Negativo	Positivo	Negativo	Positivo	Negativo	Negativo	Negativo
Delta Comp (p.u.)	0.0012	-0.0022	-0.0011	0.0000	0.0000	0.0016	-0.0030	0.0005	-0.0041	0.0019	-0.0029	0.0033	-0.0026	-0.0005	-0.0027
Cambio Comp (%)	NaN	-100.00	-79.07	NaN	NaN	87.42	-90.37	NaN	-100.00	NaN	-61.98	NaN	-100.00	-20.59	-61.96
Mejora Específica (p.u./gr _{NP})	0.0104	-0.0198	-0.0102	0.0000	0.0000	0.0142	-0.0272	0.0048	-0.0367	0.0168	-0.0263	0.0294	-0.0236	-0.0041	-0.0245

Continuando con los efectos sobre el ácido sulfhídrico, en el reactor se presentan mejoras aún mayores que las observadas en las botellas, ya que en este se ha conseguido que los primeros días (hasta el día 8) se redujese considerablemente su peso en la composición de los gases analizados. Además, en la mayoría de los días se consigue una reducción en la composición, sin llegar a las mejoras mencionadas previamente; aunque siguen siendo proporcionalmente mayores a las mostradas en las botellas. Finalmente, los efectos se muestran en la Ilustración 18.

Análisis de la Composición de los Residuos de los Reactores

Tabla 16: Composición de los Residuos en los Reactores

Residuos															
Día	1	2	3	4	7	8	9	10	11	14	15	16	17	18	21
Comp R (p.u.)	0.3681	0.1350	0.5188	0.2240	0.5558	0.2064	0.6074	0.6296	0.3132	0.4104	0.4373	0.3976	0.6655	0.4436	0.3198
Comp RN (p.u.)	0.1215	0.2028	0.1923	0.2478	0.2478	0.3533	0.2838	0.2986	0.4845	0.2865	0.6183	0.7036	0.7198	0.7364	0.7714
Efecto NP	Negativo	Positivo	Negativo	Positivo	Negativo	Positivo	Negativo	Negativo	Positivo	Negativo	Positivo	Positivo	Positivo	Positivo	Positivo
Delta Comp (p.u.)	-0.2466	0.0678	-0.3265	0.0238	-0.3080	0.1469	-0.3236	-0.3310	0.1713	-0.1238	0.1810	0.3060	0.0543	0.2928	0.4516
Cambio Comp (%)	-67.00	50.21	-62.93	10.64	-55.41	71.16	-53.28	-52.57	54.69	-30.17	41.39	76.95	8.16	66.00	141.22
Mejora Especifica (p.u./gr _{NP})	-2.2020	0.6054	-2.9152	0.2127	-2.7496	1.3117	-2.8897	-2.9556	1.5293	-1.1054	1.6160	2.7319	0.4848	2.6143	4.0322

El último componente por analizar es el de residuos, los cuales muestran un comportamiento similar a los residuos en las botellas; ya que estos se reducen durante la mayoría del ensayo, concretamente a partir del día 7, pese a presentar un pequeño repunte en el día 11, aumentando se presencia en un 50%.

Asimismo, los días finales del ensayo su peso aumenta hasta alcanzar los 0,7714 p.u. debido al agotamiento del reactor, el cual se ha visto anteriormente en el análisis del metano. Este incremento es su peso unitario se corresponde con el observado en las botellas, pese a que en este volumen mayor se ve ligeramente magnificado. Por último, al igual que en los casos anteriores, el efecto porcentual se muestra en la Ilustración 18.

Gráficas de los efectos de las Nanopartículas sobre la composición de los Reactores

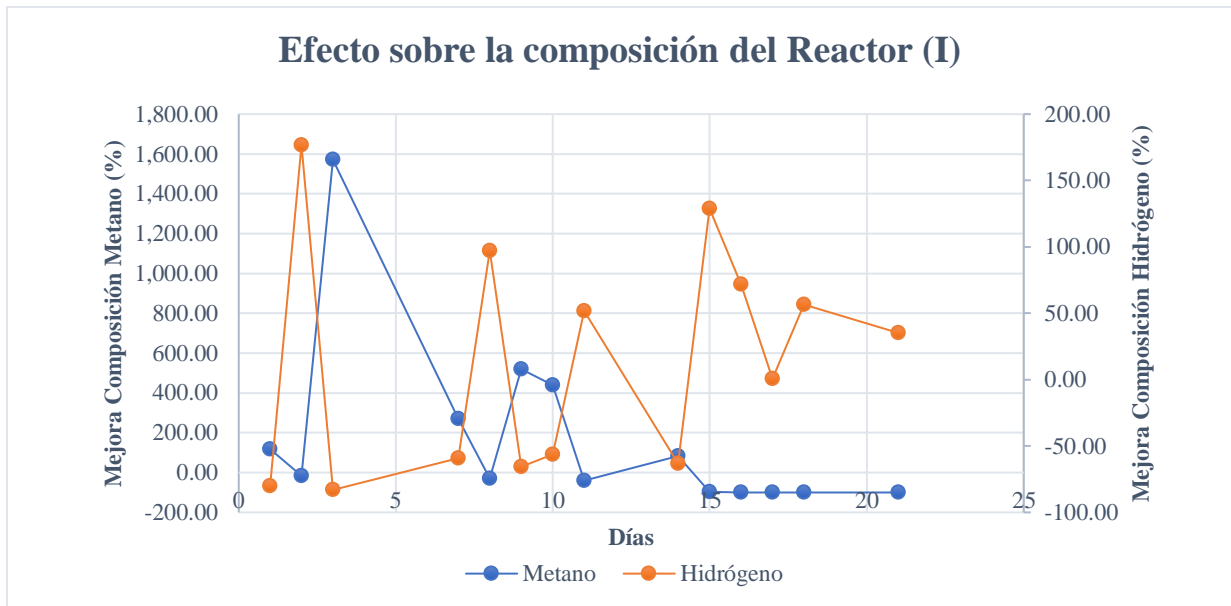


Ilustración 17: Efecto sobre la composición del Reactor (I)

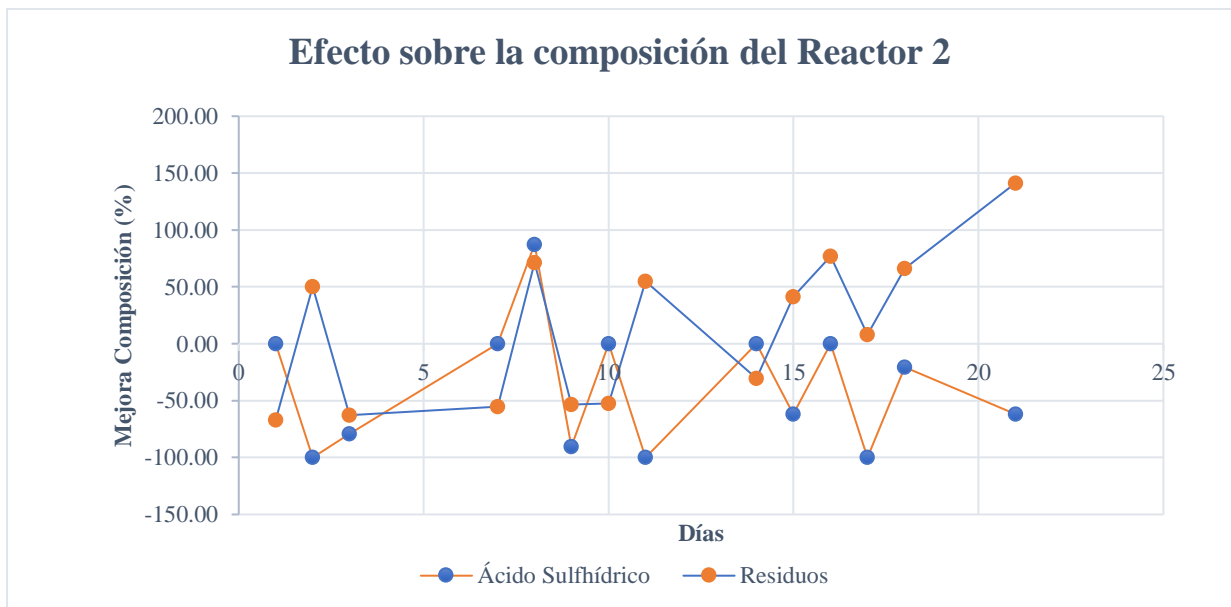


Ilustración 18: Efecto sobre la composición del Reactor (II)

5. Conclusiones

Tras el análisis de los resultados tanto de los ensayos normalizados en botellas, como de los ensayos realizados en reactores discontinuos, se han llegado a las siguientes conclusiones:

En primer lugar, pese a haber observado tendencias prometedoras en los dos tipos de ensayos realizados, no se ha dispuesto de suficientes muestras como para asegurar que las nanopartículas afectan a la producción media de biogás o a la variabilidad de este salvo en casos específicos como el de la desviación típica en la composición de las botellas, respecto del hidrógeno. Por tanto, se recomienda que en un futuro se realicen más tandas de ensayos normalizados para obtener muestras suficientes tal que se obtengan resultados estadísticos significativos.

Pese a esto, se han observado tendencias muy positivas en todas las muestras, con efectos específicos altos tanto en el metano como en la producción bruta de biogás, llegando a causar un aumento de $23,2928 \text{ Nm}^3/\text{gr}_{\text{NP}}$ y $25,0605 \text{ Nm}^3/\text{gr}_{\text{NP}}$ en el día 14, respectivamente.

Al mismo tiempo, se producía el efecto contrario en la composición del biogás, al reducir el peso unitario del metano en este en favor de los residuos y el ácido sulfhídrico, en especial en los días finales del ensayo, indicativo de que además de conseguir una mejora en la cantidad producida, las nanopartículas también aceleran el proceso y causan que se agote más rápido el reactor. Sin embargo, se requieren más ensayos para corroborar esto. Otro aspecto importante es la correlación inversa entre el hidrógeno y el metano, como se ha expuesto anteriormente en varias secciones.

Respecto del ácido sulfhídrico, las nanopartículas reducen tanto su producción como su peso en la composición de manera notable en la segunda mitad del ensayo, pese a tener el efecto contrario en los primeros 9 días. Sin embargo, a partir del pico del 78,92% del día 8, la composición desciende drásticamente hasta reducirse en al menos 3 órdenes de magnitud, tal que se puede considerar nulo a 4 cifras decimales. Como detalle adicional, esto también se ve reflejado en la varianza de este compuesto, consiguiendo que su desviación típica se reduzca a la mitad hacia los días finales del ensayo.

La última especie analizada fueron los residuos, siendo estos los compuestos no adsorbidos ni identificados en los cromatogramas. En estos, se producía una reducción tanto en producción como en composición en las muestras analizadas. Sin embargo, en los días finales se produjo un aumento de estos en la composición fruto de la reducción en la producción de metano y del resto de compuestos, lo que sugiere una aceleración del proceso de digestión, como se ha mencionado anteriormente. En cambio, su varianza sí que se redujo de manera significativa en la segunda mitad del ensayo, mostrando mejoras de hasta el 83,73% en el día 16 como máximo salto en una tendencia que se inició en el día 10.

Por último, los reactores discontinuos se comportaron de una manera similar a las botellas, como era de esperar dado que se realizó el mismo ensayo en distintos volúmenes. Esto permitió observar nuevas tendencias como la interacción del hidrógeno previamente mencionada; así como la volatilización de las nanopartículas, lo cual requiere de un cambio en el método para obtener una buena disolución y evitar su escape, lo que también se traducirá en unos resultados más marcados.

7.3. Anejo III: Hannah HI 902 Potentiometric Titrator Manual



MÁSTER UNIVERSITARIO EN INGENIERÍA INDUSTRIAL

MANUAL DE USO
HANNAH HI 902
Potentiometric Titrator

Madrid

Enero 2022

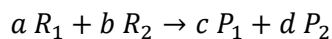
1. Introducción

Las valoraciones son una herramienta básica para la química analítica, ya que nos permiten determinar concentraciones de disoluciones, pH, y composiciones de estas según los reactivos que se empleen en ella, así como el método a seguir en estas.

Tanto es así que, a lo largo de la formación universitaria del alumno, se realizan desde primero de grado en la asignatura de Química. Estos primeros ensayos se realizan de manera manual empleando pipetas para medir de manera exacta la disolución, agitadores para conseguir mezclas homogéneas; indicadores para determinar el fin de la reacción y buretas para medir el volumen de reactivo empleado.

Sin embargo, pese a ser un método válido para prácticas didácticas, en los ensayos de investigación a veces es necesaria una precisión que no se puede conseguir con ensayos manuales, ya sea por la sensibilidad de la muestra (por ejemplo, el agua destilada) o por el nivel de la investigación (como el análisis de lixiviados en un doctorado) (Morales Polo, Co-Digestión anaerobia y pretratamiento de residuos agroalimentarios con fangos UASB de depuradora, 2019). Para estos casos, se emplean equipos como el Hanna HI 902 **Invalid source specified.**, cuyo funcionamiento se explica en esta guía.

Antes de proceder con el equipo, se considera de utilidad para el usuario tener las fórmulas empleadas en una valoración accesibles. Por ello, se incluyen a continuación para una reacción cualquiera a partir de una reacción general del tipo:



Esta reacción balanceada genérica ha de conocerse de antemano, así como el volumen de disolución a analizar y del reactivo (V_{R1} y V_{R2} , respectivamente) y la molaridad o normalidad del reactivo empleado (M_{R2} o N_{R2}). Se recuerda que para pasar de normalidad a molaridad se ha de emplear la siguiente ecuación, empleando la valencia de la reacción (V):

$$M \left[\frac{\text{mol}}{\text{l}} \right] = \frac{N \left[\frac{\text{mol}_{eq}}{\text{l}} \right]}{V}$$

Por tanto, la concentración desconocida en la muestra inicial R_1 será:

$$M_{R_1} \left[\frac{\text{mol}}{\text{l}} \right] = \frac{b * M_{R_2} * V_{R_2}}{a * V_{R_1}}$$

$$n_{R_1} = M_{R_1} * V_{R_1}$$

2. Componentes

Al tratarse de un equipo de valoración automático, este cuenta con varios componentes propios para este fin. A tal efecto, sus componentes son:

1. Equipo Central.
2. Motor.
3. Bureta de 25ml.
4. Botella de reactivo.
5. Pipeta.
6. Sonda de pH.
7. Agitador.
8. Termómetro.

Los componentes 1 a 5 se encuentran numerados en la Ilustración 19, mientras que los componentes 6 a 8 en el detalle de la Ilustración 20.

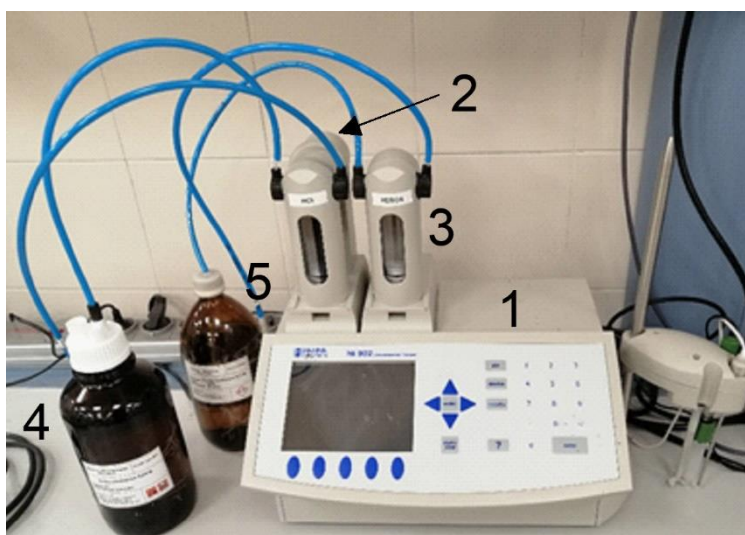


Ilustración 19: Componentes del equipo



Ilustración 20: Detalle Sondas

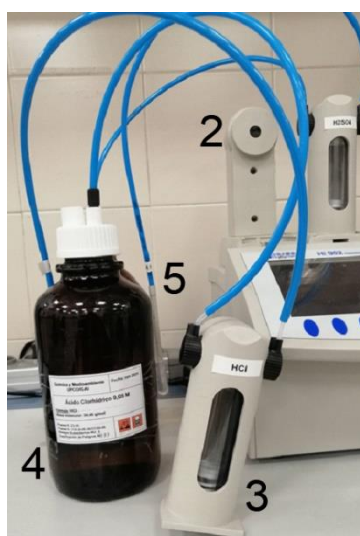


Ilustración 21: Detalle Conjunto Bureta

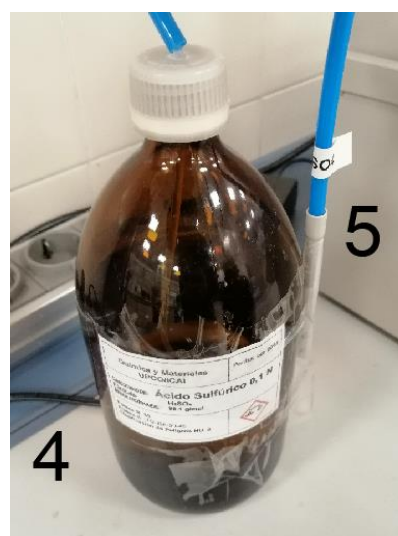


Ilustración 22: Detalle Botella y Pipeta

Como se puede observar en la Ilustración 19, se cuenta con 2 conjuntos de reactivo (botella, bureta y pipeta), sin embargo, el equipo cuenta con un único motor lineal para accionar estas. Por tanto, cuando

se requiera una valoración con paso intermedio, se ha de cambiar la bureta una vez esta se ha vuelto a llenar, lo cual ocurre de manera automática, que se explicará más adelante. Para extraer la bureta del motor, basta con tirar de esta horizontalmente y saldrá de su posición. Esta se puede cambiar por la segunda bureta, que se ha de insertar hasta que se oiga un “clic”, señal de que el motor ha enganchado con la bureta. Para facilitar estos cambios, ambas posiciones de buretas cuentan con railes. El montaje bureta se muestra en la Ilustración 21.

La pipeta se emplea para suministrar el reactivo durante la valoración. Esta se inserta en la sonda en los talaros disponibles a tal fin. En la Ilustración se muestra la pipeta junto con la botella. Para evitar que esta se dañe entre usos del equipo, se mantiene en la pipeta de plástico adherida a la botella de su reactivo correspondiente. Tras esta breve descripción de los componentes se procederá a explicar su uso.

3. Modo de Funcionamiento

Pantalla de Ensayo

En primer lugar, se ha de encender el equipo accionando el interruptor general que se encuentra en la parte trasera del equipo. Una vez se acciona, el dispositivo se enciende y comienza su propia secuencia de encendido. Durante este tiempo, se ha de evitar introducir comandos o pulsar botones en el equipo para evitar posibles fallos en el arranque. Cuando aparezca la pantalla de ensayo que se muestra en la Ilustración 23 este proceso de arranque ha finalizado y se puede proceder a su uso.



Ilustración 23: Pantalla de Ensayo

Como se puede observar, esta pantalla contiene los botones necesarios para operar el equipo, así como datos recogidos durante el ensayo. En el centro de esta se muestra la cantidad de reactivo dispensado durante el ensayo. Asimismo, encima de esta se muestra el método de ensayo seleccionado, el cual se explicará más adelante. Finalmente, en la parte inferior se muestran, de izquierda a derecha: Temperatura de la muestra, Condición de final del ensayo (configurable) y pH de la muestra. Los botones inferiores permiten modificar la configuración del equipo y del método a emplear. Estas se explicarán más adelante.

Panel de Control

El equipo cuenta con un panel de control para introducir comandos y valores al escribir los métodos. Para este fin, el panel de control cuenta con un teclado numérico, control del equipo, flechas de navegación y el botón “start/stop” el cual inicia y detiene ensayos.

Como apunte del teclado numérico, cuando se introduzcan datos en un método, así como para seleccionar los distintos campos a modificar, se ha de presionar la tecla “enter”. Asimismo, la tecla “stir” enciende el agitador de la sonda de manera independiente del ensayo. La tecla “results” accede a la memoria del equipo donde se muestran los resultados de los últimos 100 ensayos. Por último, la tecla “device” permite configurar el equipo para realizar varios ensayos de manera consecutiva. El panel de control se muestra en la Ilustración 24.

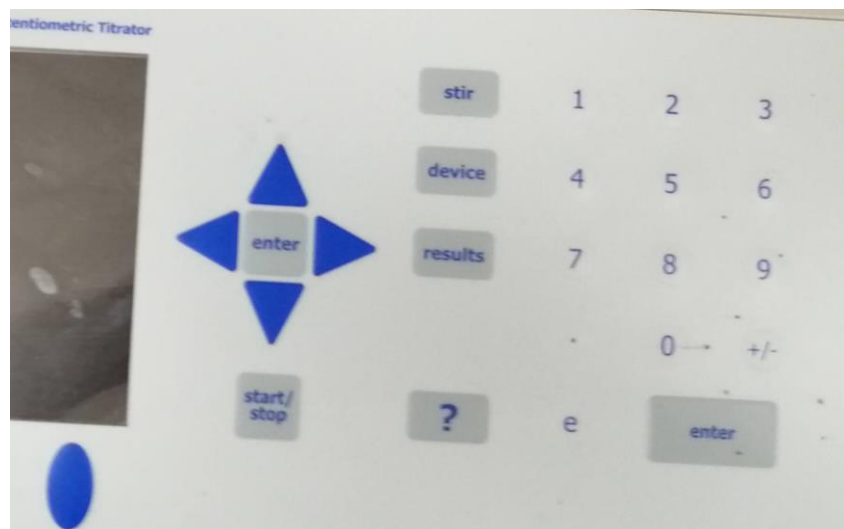


Ilustración 24: Panel de Control

Menú General

Este menú muestra la configuración del equipo. **Se recomienda no entrar en este menú** salvo que se vaya a conectar un equipo externo para guardar los datos de los ensayos, aunque de manera preestablecida permite guardar los resultados en un pendrive.

Las funcionalidades propias de este menú son el control de las bombas, seleccionando la bomba que operará (“Bomba Activada”), ya que el equipo admite 2 motores para la realización de valoraciones en 2 etapas. Sin embargo, se decidió no instalar la segunda bomba, por lo que solo aparece la Bomba 1. Este menú también permite cambiar las unidades de la temperatura, así como seleccionar la entrada de datos de esta, que por defecto es el termómetro integrado. Finalmente, permite ajustar la fecha, hora, idioma y otros parámetros del equipo. Este se muestra en la Ilustración 7.

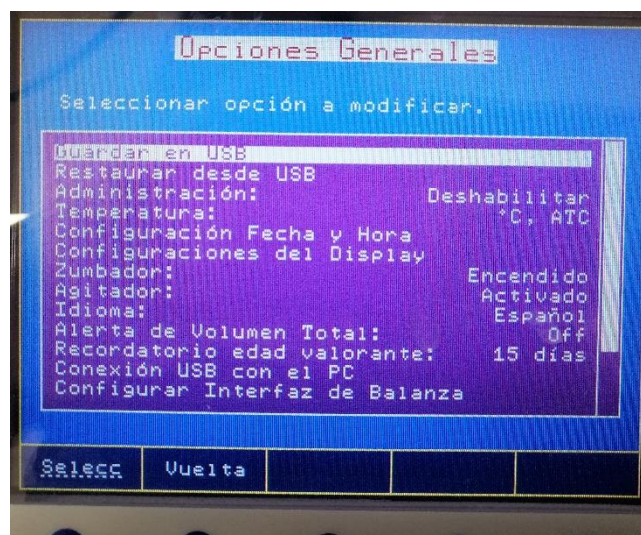


Ilustración 25: Menú General

Menú Selección Método

Una vez se ha iniciado el equipo, se ha de seleccionar el método de valoración a emplear según la muestra y los reactivos contenidos en las botellas. Para ello, pulsar el botón de “Selec. Método”, este abre el menú de selección de los métodos a emplear; estos se ordenan de manera descendiente desde el más antiguo al más reciente. El equipo cuenta con métodos preinstalados para realizar ensayos básicos y mediciones típicas como la concentración de cloro en el agua. También cuenta con 2 métodos para identificar errores en el equipo. Para seleccionar el método a emplear, utilizar las flechas o los botones “Página Anterior” y “Página Siguiente” para moverse por la lista y presionar “Selecc” para seleccionar el método y volver al menú general.

Con respecto al resto de las opciones, “Nuevo Método” crea una copia del método sobre el que se encuentre el cursor para modificarlo posteriormente. El proceso de crear y configurar un nuevo método se explicará en otra sección. De manera similar, el botón “Borrar” elimina el método seleccionado con el cursor tras una doble confirmación. Este menú se muestra en la Ilustración 26.

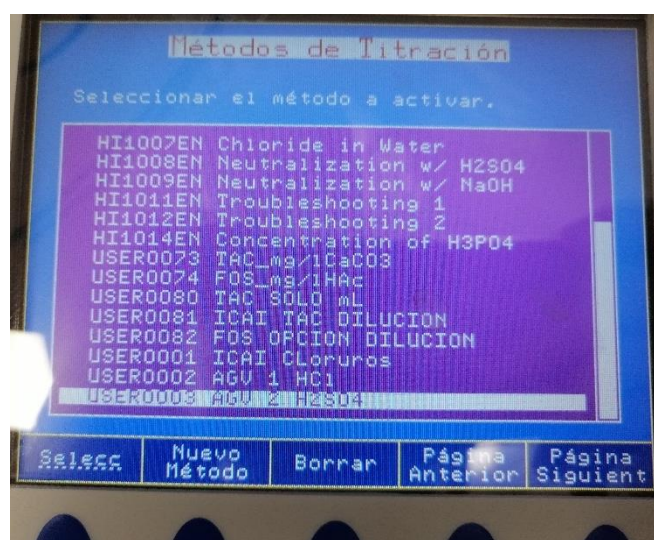


Ilustración 26: Menú Selección Método

Menú Bureta

Este menú permite el control de la bureta fuera sin la necesidad de que haya un método en proceso. Contiene 4 comandos posibles. El primer comando es “Cebiar Bureta”, el cual se emplea para lavar y llenar una bureta vacía, por lo que se recomienda usar después del comando “Purgar Bureta”. Adicionalmente, esta función requiere de un número de enjuagues (entre 1 y 5), cuando se haya repuesto la botella, se recomienda 1 enjuague y cuando se haya cambiado el reactivo, se recomiendan 3 enjuagues para asegurar que la bureta no tiene reactivo residual, según el manual del fabricante.

De manera análoga, la función “Purgar Bureta” lava esta 1 vez y la vacía, permitiendo cambiar el reactivo. Asimismo, se cuenta con la función “Lavar Punta”, la cual dispensa 2ml de reactivo para asegurarse de que no hay burbujas de aire en la punta. Se recomienda que esta función se use antes de iniciar una valoración y al finalizarla, antes de guardar la pipeta. Por último, se puede realizar un dosado manual de reactiva con “Dosificación Manual”. Esta función no se debe usar, ya que el dispositivo es automático para evitar esto. Si por cualquier motivo se necesitase, los límites de dosificación proporcionados por el fabricante se muestran en la Ilustración 27. El menú se muestra en la Ilustración 28.

0,001	a	4,500 ml	para una bureta de 5 ml
0,001	a	9,000 ml	para una bureta de 10 ml
0,005	a	22,500 ml	para una bureta de 25 ml
0,005	a	45,000 ml	para una bureta de 50 ml

Ilustración 27: Límites de dosado manual. Obtenido de (Laboquimica, 2022).

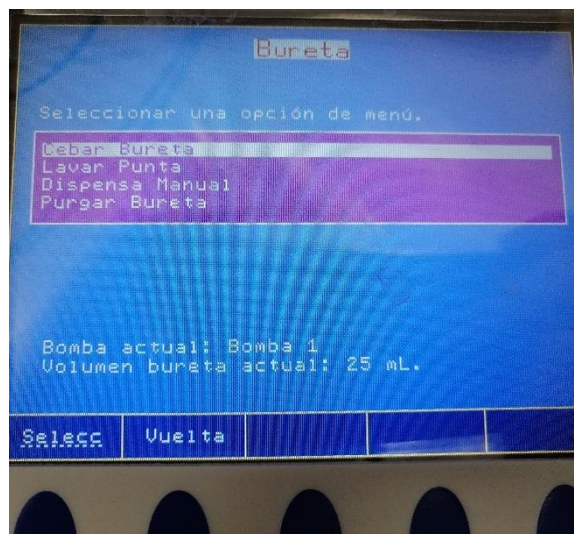


Ilustración 28: Menú Bureta

Menú Ver Método

El menú final permite ver y modificar el método seleccionado. Al ser el menú más extenso y complejo, se explicará en detalle a la par que la creación de un nuevo método en una sección posterior. A resaltar de esta pantalla es que indica el reactivo usado y los límites operativos en el caudal y volumen máximo de la valoración. Parte de este menú se muestra en la Ilustración 29.

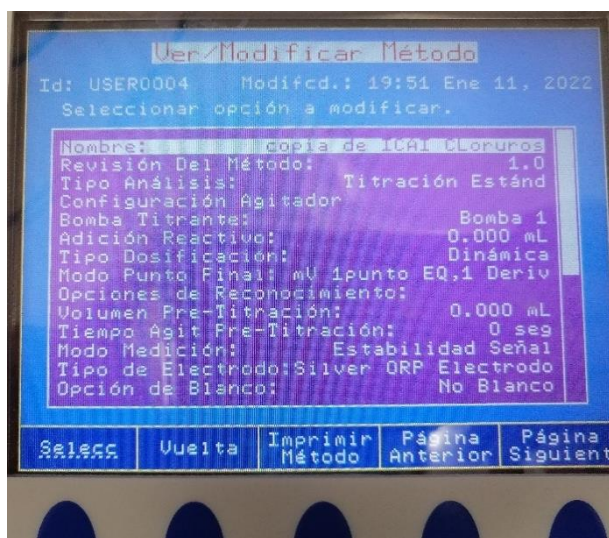


Ilustración 29: Menú Ver Método

4. Valoración indirecta de AGVs

El principal uso de este equipo es la determinación de Ácidos Grasos Volátiles (AGVs) mediante la adaptación del método indirecto propuesto en (Tran, 2017), el cual se basa en la alcalinidad total (AT), la alcalinidad parcial (AP) y la alcalinidad intermedia (AI), la cual se debe a los AGVs.

Para iniciar el ensayo, primero se ha de recoger una muestra del líquido a valorar de 25ml de lixiviados diluidos en 25ml de agua destilada en un cilindro graduado de 250ml.

En primer lugar, se han de limpiar las dos buretas con la función “Limpiar Bureta”, la cual dispensa 3ml de la solución. Al ser una operación estándar, no es necesario que se seleccione el método específico y basta con cambiar la bomba conectada al motor para lavar ambas. Se ha de recoger el líquido dispensado en un cilindro graduado auxiliar con agua destilada, la cual también se usará para lavar las buretas y las sondas después de realizar la valoración.

Para realizar la valoración primero se ha de colocar la bomba marcada como “HCl” en la posición del motor. A continuación, seleccionar el método “AGV 1 HCl”; el cual emplea HCl a 0,05M (igual a 0,05N) Antes de iniciar el ensayo, anotar los valores iniciales de temperatura (T_o); pH (pH_o); volumen de lixiviado (V_l); volumen de disolución (V_d) y volumen total (V).

$$V = V_m + V_d$$

Tras anotar los valores iniciales se puede iniciar el ensayo pulsando el botón “Start”. Este ensayo puede tardar hasta 10 minutos según la velocidad de dispensación y el comportamiento de la muestra. Una vez el ensayo haya finalizado, el equipo emitirá un pitido, tras el cual se han de anotar los valores mostrados en la pantalla de volumen dispensado (ml) y pH intermedio (-).

El segundo ensayo requiere cambiar la bomba acoplada al motor a la marcada como “H₂SO₄”. Si no se ha lavado la bureta antes del primer ensayo, se ha de hacer ahora, cambiando el cilindro graduado al auxiliar para no contaminar el ensayo. También se ha de seleccionar el método “AGV 2 H₂SO₄”; el cual emplea H₂SO₄ a 0,05M (igual a 0,1N). Tras realizar estos pasos, se puede iniciar la segunda valoración, la cual evoluciona dispensará H₂SO₄ hasta un valor de pH de 4,3. Este segundo ensayo es más rápido al usar un ácido más concentrado. Al igual que al finalizar el primer ensayo, se han de recoger los valores de volumen dispensado (ml) y pH final (-).

Con todos los datos obtenidos se puede proceder al cálculo de las alcalinidades intermedia (AI), parcial (AP) siguiendo las fórmulas obtenidas de (Tran, 2017).

$$AI \left(\frac{mg \text{ CaCO}_3}{L_{frac.solluble}} \right) = \frac{V_1 * N_1 * 5000}{V}$$

$$AP \left(\frac{mg \text{ CaCO}_3}{L_{frac.solluble}} \right) = \frac{V_2 * N_2 * 5000}{V}$$

Para calcular la alcalinidad total (AT), existen varios métodos, ya que se emplea el volumen total dispensado si solo se ha usado un reactivo ($V_3=V_1+V_2$), en este caso, al emplear dos ácidos distintos, se ha de usar la siguiente fórmula, la cual es igual a sumar las alcalinidades previas:

$$AT \left(\frac{mg \text{ CaCO}_3}{L_{frac.solluble}} \right) = \frac{(V_1 * N_1 + V_2 * N_2) * 5000}{V} = AI + AP$$

Si solo se ha empleado un único ácido, la fórmula es:

$$AT \left(\frac{mg \text{ CaCO}_3}{L_{frac.soluble}} \right) = \frac{V_3 * N_3 * 5000}{V}$$

Al acabar todas las valoraciones se han de lavar las sondas con el cilindro graduado auxiliar y desechar tanto la muestra como el agua de lavado en el contenedor de ácidos del laboratorio. Los datos que se han de recoger se muestran a continuación en Tabla 17.

Tabla 17: Variables a recoger en el ensayo de AGVs

Variable	Unidad	Símbolo
Volumen Lixiviados	ml	V _l
Volumen Dilución	ml	V _d
Volumen Inicial	ml	V
Temperatura Inicial	°C	T _o
pH Inicial	-	pH _o
Volumen HCL Dispensado	ml	V ₁
pH Intermedio	-	pH ₁
Normalidad HCl	Mol-eq/l	N ₁
Volumen H ₂ SO ₄ Dispensado	ml	V ₂
pH Final	-	pH _f
Normalidad H ₂ SO ₄	Mol-eq/l	N ₂
Alcalinidad Intermedia	mg CaCO ₃ /L _{frac.soluble}	AI
Alcalinidad Parcial	mg CaCO ₃ /L _{frac.soluble}	AP
Alcalinidad Total	mg CaCO ₃ /L _{frac.soluble}	AT

5. Realizar Valoración

En esta sección se explicará brevemente como realizar una valoración de 1 etapa con este equipo. Para realizar una valoración en 2 etapas se ha de cambiar el método y la bureta conectada a la Bomba 1 antes de continuar la valoración. Se recomienda que en caso de necesitar realizar una valoración de 2 etapas se numeren los métodos y se etiqueten las buretas y pipetas.

Para emplear este equipo se recomienda usar vasos graduados de 250ml. Previo a la valoración, se ha de quitar el cilindro protector de la sonda de pH e insertar la pipeta en uno de los taladros realizados en las sondas y ajustar la altura de estas para que quepa el vaso graduado y el agitador, sonda de pH y termómetro están bien posicionados en dentro de la solución a analizar. Para colocarlo basta con levantar las sondas manualmente y recolocarlas una vez se ha puesto la muestra, asegurándose de que la espiga de la abrazadera se inserta y bloquea las sondas en su posición correcta como se muestra en la Ilustración 12.

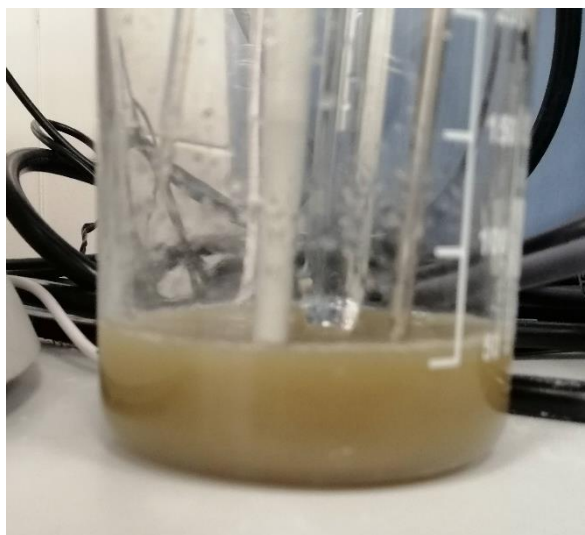


Ilustración 30: Posición de las sondas en la muestra

Una vez se ha preparado el equipo, se recomienda emplear un vaso graduado con agua destilada para lavar la pipeta y la sonda. Para ello, colocar las sondas dentro y activar el agitador. Tras unos segundos, lavar la pipeta desde el menú bureta. Para el lavado posterior a la valoración se puede reutilizar este vaso.

A continuación, se puede proceder a la valoración; para ello, comprobar el método seleccionado y presionar el botón “start/stop”. La valoración se realizará de manera automática y avisará cuando haya acabado con un pitido. El volumen empleado, así como el pH final se mostrarán en la pantalla del equipo. Finalmente, se han de lavar las sondas antes de la siguiente valoración, así como lavar la pipeta y guardarla si no se van a realizar más ensayos.

En caso de no realizarse más ensayos, también se ha de colocar el cilindro protector en la sonda de pH, asegurándose de que hay suficiente solución de mantenimiento en este.

Nota: Si se excede el límite de volumen titrante, la pantalla se volverá roja informando del error con varios pitidos. Si no se ha completado el ensayo se puede volver a iniciar pulsando “start/stop” y anotando el volumen usado.

6. Mantenimiento

Bureta

El mantenimiento de la bureta es relativamente simple, ya que el propio equipo es capaz de avisar cuando se necesita realizarlo. Para realizar tareas de mantenimiento como el lavado o vaciado de la bureta, se ha de emplear la función “Purgar Bureta”, como se ha mencionado anteriormente. Del mismo modo, se recomienda que se lave la bureta siempre que se haya cambiado la botella de reactivo. Este proceso se explica a continuación.

Cambio de botella

Si se requiere un cambio de botella o reponer el titrante usado, ya sea porque se ha agotado y hay aire en la bureta, o por que el equipo haya avisado de un nivel bajo de depósito (se puede configurar esto en el menú general), el procedimiento a seguir ha de ser el siguiente.

En primer lugar, quitar el tapón de la botella y extraer el tubo de aspiración de esta, colocándolo en un lugar donde se evite ensuciar. A continuación, se ha de purgar la bureta. Esto asegura que en el circuito de la bureta no hay grandes cantidades del antiguo reactivo que pudiesen reaccionar con el nuevo compuesto a usar, lo cual puede ser peligroso (mezclando un ácido con una base en la bureta o su circuito de aspiración).

Antes de colocar la nueva botella, se ha de lavar con agua destilada o desionizada el tubo de aspiración para evitar contaminar el nuevo reactivo. Tras esto, se puede insertar el tubo en la nueva botella y colocar el tapón. Finalmente, cebar la bureta, recogiendo el exceso en un recipiente a parte para evitar mezclar los compuestos.

Métodos

El primer método de mantenimiento “Troubleshooting 1” comprueba el funcionamiento de la dosificación lineal a 20ml, empleando agua destilada para ensayar la Bomba 1. En cambio, el método “Troubleshooting 2” realiza una dosificación lineal de 0,5ml, permitiendo evaluar el funcionamiento en regiones críticas. También emplea agua destilada para la valoración.

Desmontar motor

En primer lugar, siempre se ha de realizar esta operación con las buretas extraídas de la máquina y esta apagada. La bomba se encuentra sujeta a la carcasa del equipo con un tornillo en su parte trasera. Para quitar la bomba basta con desatornillarla y sacar el componente. Es importante no tirar con fuerza ni retirar la bomba sin antes desconectar el bus que la conecta con un puerto en el interior del equipo.

Vaciar Memoria de Resultados

El equipo cuenta con una memoria interna en la cual se almacenan los resultados de ensayos previos, hasta 50. Por tanto, cada cierto tiempo, según el uso del equipo, se ha de vaciar, apareciendo un mensaje en la pantalla. Este mensaje no permite realizar más test hasta vaciar la memoria. Para ello, basta con pulsar la tecla “Results”, accediendo a la memoria, y pulsar el botón “Eliminar” que aparecerá, eliminando las pruebas almacenadas uno a uno.

7. Crear Método Propio

En esta sección se procederá a explicar los distintos campos del menú Ver Método, ya que estos se pueden modificar para crear un nuevo método.

En primer lugar, como se ha mencionado anteriormente, se ha de crear una copia de un método existente desde el menú Selección Método. Se recomienda que se seleccione un método similar para facilitar el proceso. Una vez se ha copiado el método, el equipo vuelve a la pantalla de ensayo. Para acceder a los detalles del método usar el menú Ver Método.

Al ser este un menú muy extenso, se muestra en la Ilustración 31 y la Ilustración 32 a continuación. Para modificar cualquier campo se ha de pulsar el botón “Selecc” cuando el cursor esté sobre este. Siempre que se realice una modificación, el equipo pide doble confirmación.



Ilustración 31: Menú Ver Método, Detalle 1

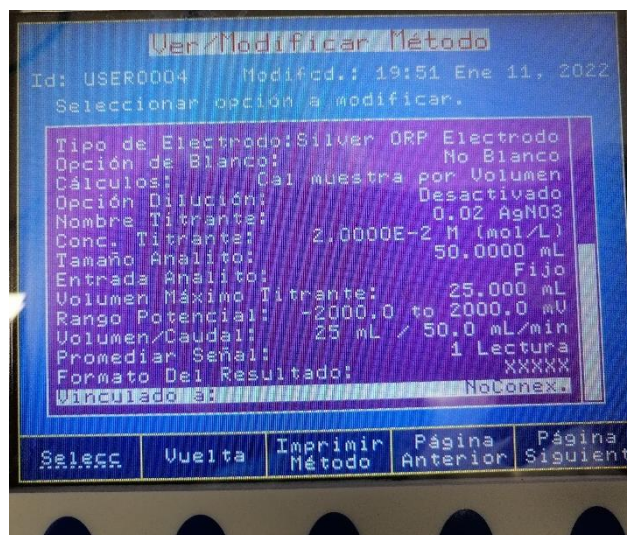


Ilustración 32: Menú Ver Método, Detalle 2

Los primeros campos que se pueden ver son “Nombre” y “Revisión del Método”, estos campos son meramente informativos, se pueden modificar libremente. Al seleccionarlos, aparece un teclado QWERTY en la pantalla por el que se puede navegar con las flechas y la tecla de “enter”. Una vez se ha cambiado el nombre y versión del método, se pueden cambiar los parámetros del método.

Tipo de Titración

El equipo permite realizar una titración estándar, la cual se realiza hasta un punto final establecido (la que se realiza siempre en esta máquina al no contar con 2 bombas independientes).

Sin embargo, si en algún momento se decidiera instalar una segunda bomba, se podría realizar una Retro-titración, la cual emplea 2 bombas de manera secuencial, empleando el titrante 1 hasta un punto dado y el segundo titrante cuando se ha completado la primera fase. Si se selecciona este método, se han de configurar ambas bombas. También se puede asignar una pausa en el cambio de titrante para realizar tareas intermedias.

El equipo cuenta con la tercera opción de lectura directa, la cual crea un ensayo simple sin las opciones de cálculo incluidas en los otros métodos y sin la posibilidad de automatizar el método. Para ensayos que requieran precisión se ha de evitar este tipo de titraciones. Las opciones se muestran en la Ilustración 33.

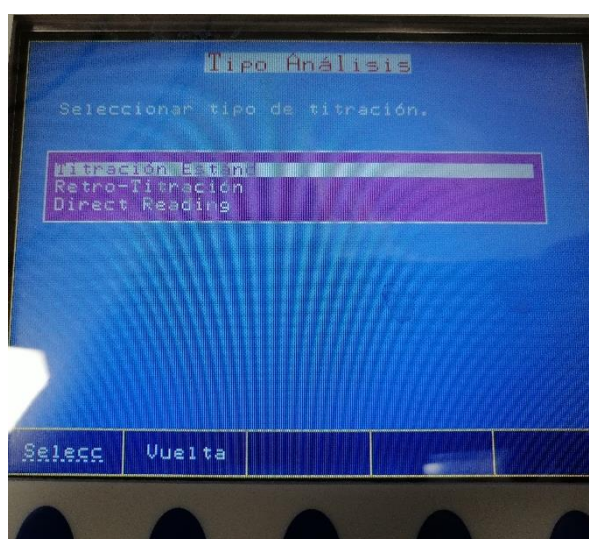


Ilustración 33: Tipo de Análisis.

Configuración Agitador

Permite ajustar la velocidad del agitador, la cual usa siempre que el método seleccionado sea este. Se mantiene constante durante el ensayo, pero puede aumentarse o reducirse con las flechas.

Bomba Titrante

En este caso, como solo se cuenta con una bomba, solo aparece como opción Bomba 1.

Adición Reactivo

En este menú se permite añadir manualmente el volumen de adición a añadir, se emplea para los cálculos internos si estos se configuran y no afectan al desarrollo del método.

Tipo Dosificación

El equipo permite seleccionar dos modos de dosificación de dosis: Lineal y Dinámica. La Dosificación Lineal emplea una tabla interna de intervalos de dosado fijo. Este tipo de valoraciones son más lentas y pueden causar problemas en la región crítica, sin embargo, se puede introducir la dosis óptima si esta se conoce y así eliminar el problema de la precisión.

En cambio, la Dosificación Dinámica analiza el cambio del potencial en la muestra para calcular la siguiente dosis a administrar al comparar con una tabla interna. Al emplear el cambio de potencial en lugar del volumen administrado como indicador de la reacción, permite añadir dosis más grandes cuando se está lejos del punto crítico (y por tanto hay menores cambio de potencial), mientras que se administran dosados menores cerca del punto crítico. Esto causa que el proceso sea por lo general más rápido, así como más exacto si no se conoce la dosis óptima. Se recomienda siempre usar una dosificación dinámica. El menú de dosificación se muestra a continuación en la Ilustración 34.

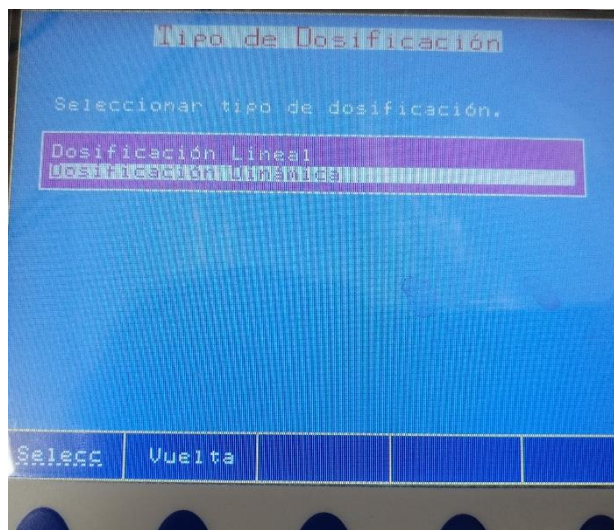


Ilustración 34: Menú Tipo Dosificación

Modo Punto Final

En este apartado se introducen las condiciones de finalización de la valoración; pudiendo introducirse en pH o en mV. Se recomienda siempre introducirlo en pH ya que los mV medidos dependen de la calibración de la sonda, pudiendo sufrir pequeñas variaciones.

Además, se distinguen dos puntos finales, el primero es “Punto Final Fijo”, en este, se introduce el valor objetivo. La valoración finalizará cuando este se alcance. Este tipo de ensayos tiene un rango entre -2 y 20 de pH, equivalente a -2000 y +2000mV.

El segundo tipo de punto final es “Punto Final Equivalente”, el cual requiere conocer previamente la ecuación química de la ecuación balanceada, así como los moles disueltos en la muestra a analizar. Este método añade titrante hasta llegar al volumen que se le ha indicado hasta llegar al punto estequiométrico. Como apunte final, permite realizar hasta 5 ensayos dentro de un mismo método.

Este método determina el punto estequiométrico se determina mediante el análisis de la primera o segunda derivada de la curva del ensayo. Se ha de escoger el cual se desea utilizar para este método. Si se escoge la primera derivada, el algoritmo detendrá el ensayo cuando encuentre un máximo en la pendiente. Si se escoge la segunda derivada, el algoritmo finalizará cuando se detecte el punto de inflexión en la segunda derivada.

Por último, se ha de añadir que la valoración, por necesidades del algoritmo, realiza 3 adiciones más allá del punto final seleccionado, lo cual ha de ser tenido en cuenta para posibles errores de cálculo. En la pantalla al finalizar el ensayo se muestra el punto final determinado, no el último valor leído. La pantalla de selección de punto final se muestra a continuación en Ilustración 35.

Se recomienda emplear la valoración de Punto Fijo (pH), ya que es la más usada, aunque algunos ensayos complejos pueden requerir el uso del Punto Final Equivalente.

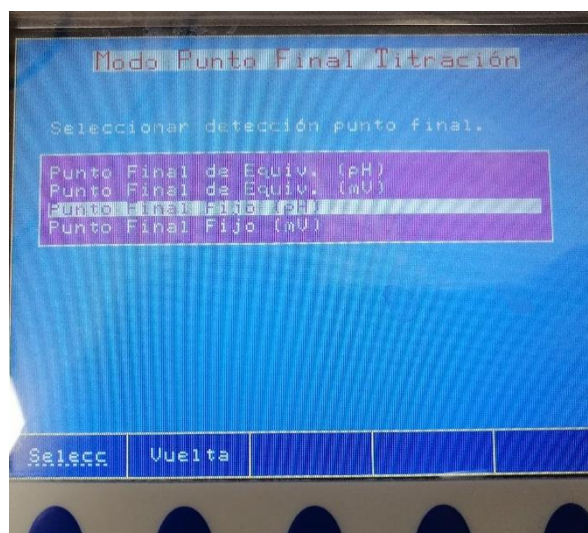


Ilustración 35: Menú Punto Final

Volumen Pre-Titración

En esta opción se puede fijar un volumen a añadir antes de iniciar el ensayo. Esto permite ahorrar tiempo si se conoce de antemano el punto final y el volumen necesario para alcanzarlo, por lo que no se realizan mediciones cuando se añade este volumen y se reduce el tiempo de ensayo.

Tiempo Agit. Pre-Titración

Permite activar el agitador durante un tiempo preestablecido antes de iniciar el ensayo, de 0 a 180, se recomiendan 10 segundos para asegurar una mezcla homogénea, lo cual estabilizará el pH.

Modo Medición

Este campo permite controlar el proceso de adición de titulante, pudiendo realizarse a intervalos regulares o cuando se ha alcanzado el equilibrio de la anterior adición.

El modo de “Incremento Temporizado” solo requiere como entrada el tiempo entre dosados, limitado entre 2 y 180 segundos, sin analizar la estabilidad de la señal.

El modo “Estabilidad de la Señal” añade más solución cuando se detecta que la reacción ha finalizado. Para ello, este requiere que se introduzcan un incremento mínimo de tensión (ΔE entre 0,1 y 99,9 mV) y un periodo mínimo de tiempo (Δt entre 0,5 y 10 segundos), dentro de los cuales se determina el equilibrio. También se pueden configurar tiempos de espera mínimo y máximo entre dosados, estando el intervalo siempre entre 2 y 180 segundos.

Para obtener valoraciones precisas, se recomienda usar el modo “Estabilidad de la señal” con ΔE de 1mV y Δt de 2 segundos.

El menú de Modo Medición se muestra en la Ilustración 36 y los parámetros de estabilidad en la Ilustración 37.

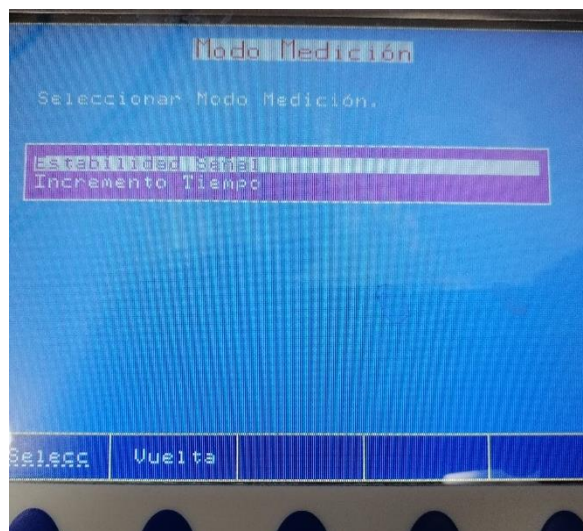


Ilustración 36: Menú Modo Medición

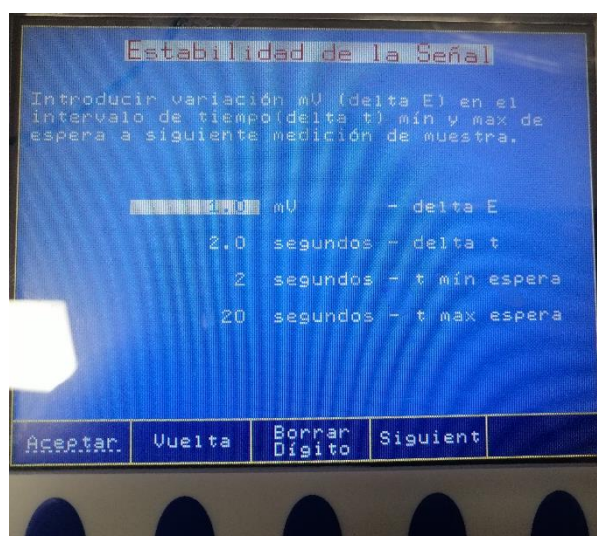


Ilustración 37: Menú Estabilidad de la Señal

Tipo Electrodo

Esta opción permite añadir una descripción del electrodo empleado, similar a los campos de nombre y versión, no modifica el ensayo.

Opción de Blanco

Esta opción configura los cálculos que realiza el equipo, si se configuran, permite realizar los cálculos entre el volumen de titrante usado (V) y el titrante consumido por un volumen objetivo (Blanco), el cual se ha de especificar. El cálculo se puede calcular en ambos sentidos. Para no realizarlos, seleccionar "No Blanco". Este menú se muestra en la Ilustración 38.

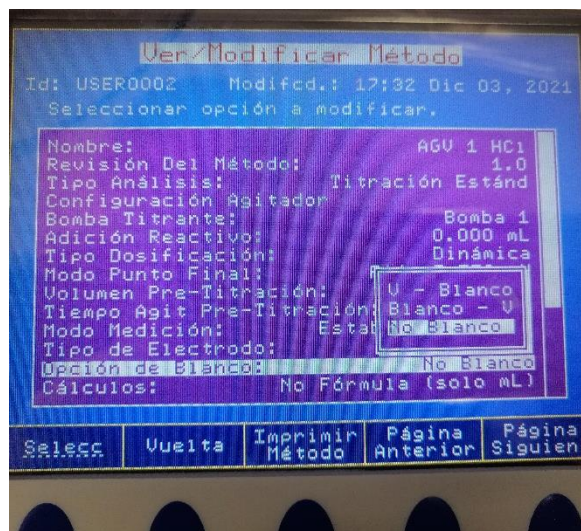


Ilustración 38: Opción de Blanco

Cálculos

Si se desea, se pueden configurar el equipo para que realice cálculos a partir del volumen de titrante usado, su concentración y otras variables que se introducen en el método. Estos cálculos se pueden realizar en volumen o masa, empleando fórmulas precargadas en el equipo o escribiendo una operación personalizada. Los detalles de este proceso se encuentran en el manual del fabricante (Laboquímica, 2022). Se recomienda no usar si no es estrictamente necesario. Las opciones de cálculo se muestran en la Ilustración 39.

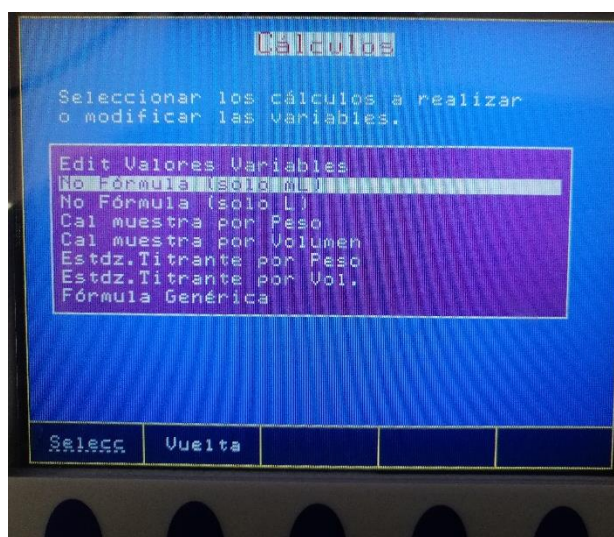


Ilustración 39: Menú de Cálculos

Opción Dilución

En este campo se puede introducir el volumen usado para diluir la muestra inicial (si se ha necesitado), permitiendo el cálculo en masa.

Nombre Titrante

Este es un campo descriptivo en el cual se puede introducir el nombre y la concentración del titrante para informar al usuario, no afecta al método.

Conc. Titrante

Relacionada con los cálculos, permite introducir la concentración del titrante para realizar los cálculos, solo se puede emplear si se realizan los cálculos en sentido directo, ya que en el sentido inverso se determina la concentración del titrante a usar. Como toda la sección de cálculos, evitar su uso a menos que sea imprescindible y crítico.

Tamaño Analito

Para los cálculos internos, aquí se introduce el volumen inicial de muestra que se ha ensayado empleando el teclado numérico.

Entrada Analito

Para los cálculos internos; permite indicar si la variable de entrada del analito será fija (constante en todos los ensayos), o manual (debiendo introducirse siempre antes de realizar el cálculo)

Volumen Máximo Titrante

Configuración necesaria para determinar el fallo del análisis, configura el volumen máximo de titrante a emplear hasta 100ml. Como se ha explicado, si se produce el fallo se puede reiniciar el ensayo desde cero.

Rango Potencial

Permite al usuario establecer los límites del potencial. Si se superan alguno de estos durante el ensayo la titración se detiene de manera automática y la clasifica como reacción anómala. Se muestra en la Ilustración 40.

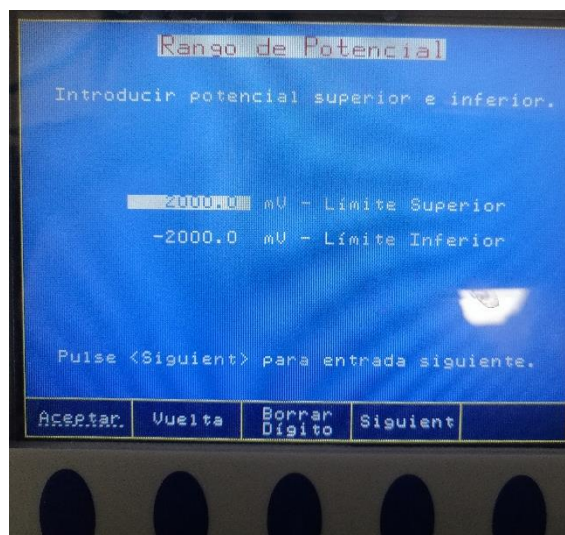


Ilustración 40: Menú de Rango de Potencial

Volumen/Caudal

Permite fijar el caudal máximo en la valoración en l/min. Su máximo es el doble del volumen de la burate (en una bureta de 25ml, el caudal máximo es 50ml/min).

Promediar Señal

En este campo se fija el número de lecturas a promediar para realizar cálculos, pudiendo usarse para eliminar ruido de la señal. Se puede fijar en 1, 2, 3 o 4 medidas.

7.4. Anejo IV: Chromatogram Manual



MÁSTER UNIVERSITARIO EN INGENIERÍA INDUSTRIAL

MANUAL DE USO
Aglient GC 7820A
Gas Chromatographer

Madrid

Junio 2022

1. Introducción

A la hora de analizar muestras gaseosas, se requieren técnicas específicas no basadas en análisis visuales o en densidades, ya que las mezclas acostumbran a ser transparentes. En consecuencia, las técnicas se han de basar en las propiedades físicas y químicas de estos compuestos.

A raíz de esto han surgido varias técnicas analíticas basadas en las distintas especies (tanto elementales como isotópicas), destacando entre ellas la espectrometría de masas (Broad Institute, 2022) y la cromatografía (Technology Networks, 2022). Este manual se centra en el uso y operación del equipo disponible en el laboratorio de Química, el cromatógrafo de gases Agilent GC7820A (Agilent Technologies, Inc., 2011), fabricado por Agilent (Agilent Technologies. Inc., 2022).

Este se basa en la cromatografía gas-sólido (Hage, 1991). Este tipo de análisis emplea el fenómeno de la adsorción en las columnas internas para retener la muestra gaseosa insertada. Una vez se inicia el ensayo, las válvulas se cierran, atrapando la muestra, y se procede a ejecutar un método específico el cual separa los distintos compuestos de la muestra en base a su tiempo de retención, el cual es

La cromatografía es una técnica de análisis de gases capaz de separar varios compuestos mediante su tiempo de retención (Sociedad Española de Cromatografía y Técnicas Afines, 2014); siendo este el tiempo que un compuesto queda retenido dentro de la columna, lo cual permitirá separarlo de otro compuesto distinto.

De manera teórica, el proceso puede asemejarse a una columna de destilación de platos, pudiendo obtenerse el número de platos de acuerdo con la siguiente fórmula (Bushra, 2018) para equipos de captación electrónica a partir del tiempo de retención (t_R) y la anchura del pico a mitad de la altura de este ($W_{h/2}$), datos que pueden obtenerse de manera teórica o empírica.

$$N = 5,54 * \left(\frac{t_R}{W_{h/2}} \right)^2$$

Por último, se ha de mencionar que este equipo se basa en el uso de gas nitrógeno (N_2) como gas portador, siendo de uso menos común que el hidrógeno (H_2), el cual tiene un mayor uso en la industria debido a su mayor calidad en las medidas del equipo y por tanto mejor resolución en el cromatograma; fruto de su menor masa molecular.

La elección de gas portador es de suma importancia ya que ha de ser indetectable por el sensor. En consecuencia, se optó por nitrógeno portador para poder analizar los picos de hidrógeno en el cromatograma, lo cual servirá para determinar en qué etapa del proceso se encuentra la muestra analizada. Por último, en la Ilustración 1 se muestra el cromatógrafo con su ordenador y balas de nitrógeno asociadas.



Ilustración 41: Cromatógrafo, balas de nitrógeno y ordenador

2. Componentes

Al ser un equipo complejo, este consta de varias partes para su correcto funcionamiento, y por tanto es necesario conocerlos y saber su función. A tal efecto, sus componentes son:

1. Equipo central.
2. Ordenador de control.
3. Bala de nitrógeno.
4. Bala de gas de calibración.
5. Jeringa de Muestreo de gases.

Los componentes 1 a 4 se muestran en la Ilustración 2, mientras que los componentes 5 y 6 se muestran en las Ilustraciones 3 y 4, respectivamente. En la Ilustración 5 se muestra un detalle de las llaves de control de caudal de las balas, estando la válvula de paso en la botella.



Ilustración 42: Componentes Principales del Equipo



Ilustración 43: Detalle de Inyección de Muestras



Ilustración 44: Detalle Balas de Nitrógeno



Ilustración 45: Detalle Manómetros de las Balas

Como se puede observar en la Ilustración 2, se cuenta con un único cromatógrafo, el cual se ha de conectar al ordenador de control mediante su software propio para realizar el análisis de la muestra gaseosa. Se ha de señalar que el equipo es capaz de analizar muestras sin estar conectado, pero los resultados no se guardarán. Asimismo, en la imagen se observan tanto las balas de nitrógeno, siendo este el gas portador, como la bala que contiene el gas de calibración, cuya composición es conocida.

Para inyectar la muestra en el equipo, se ha de usar la jeringa mostrada en la Ilustración 3, si se trata de una muestra de ensayo, o conectando la bala antes mencionada mediante un adaptador propio.

3. Modo de Funcionamiento

Cromatograma Aglient 7820A

Como se ha explicado previamente, el equipo hace uso de la adsorción en distintas columnas entre las cuales alterna para separar la muestra gaseosa insertada en sus distintos componentes. Estas columnas se encuentran dentro del horno del equipo, el cual está controlado por temperatura y junto con el flujo de gas portador determinan el método de ensayo y por tanto la separación de muestras. En la Ilustración 46: Interior del Horno se muestra tanto el horno como las columnas equipadas en el equipo.

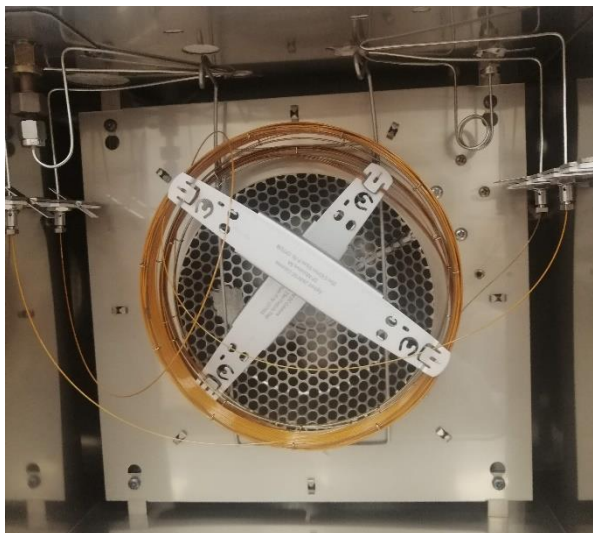


Ilustración 46: Interior del Horno

En el caso de este equipo, al emplearse para analizar muestras de biogás, se encuentra equipado con una columna de adsorción CP-Molsieve 5Å de 25m (Aglient Technologies, Inc., 2022). Asimismo, el equipo también cuenta con una columna capilar PoraPLOT Q de 12.5m (Aglient Technologies, Inc., 2022) y un sensor térmico TCD (Aglient Technologies, Inc., 2022) para la identificación de los picos de tensión causados por las distintas especies en la muestra a analizar (Morales Polo, Co-Digestión Anaerobia y Pretratamientos de Residuos Agroalimentarios con Fangos UASB de Depuradora, 2019).

Otro aspecto importante que señalar es la necesidad de emplear una muestra de composición conocida para poder determinar que pico del cromatograma corresponde a cada especie. En el caso de este equipo, se emplea una bala de composición conocida. La composición de la bala empleada se muestra a continuación en la Tabla 18.

Tabla 18: Composición de la Bala de Calibración

Especie	Peso (%)
CO ₂	35.00%
H ₂	2.00%
H ₂ S	3.00%
CH ₄	60.00%

Por último, en la Ilustración 47 se muestra un cromatograma de la muestra de esta bala con sus picos marcados por especie, así como los compuestos no separados.

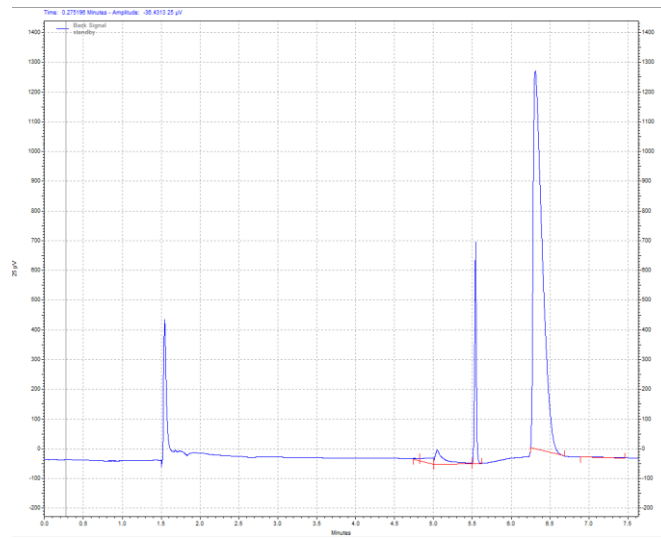


Ilustración 47: Cromatograma de Bala de Calibración

Programas de Control

Al tratarse de un equipo externo, este requiere de programas de control específicos para poder ser utilizado. En este caso, se cuenta con varios de estos programas, ya sean para la configuración del equipo, realizar ensayos o acceder a su propio panel de control. Estos programas se muestran a continuación en la Ilustración 6.

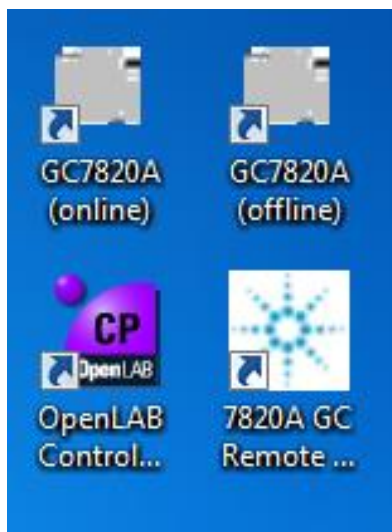


Ilustración 48: Programas de control del Cromatógrafo

En esta Ilustración se aprecian los siguientes programas, junto con sus funciones asociadas. Se listan de izquierda a derecha y de arriba abajo, en ese orden:

- GC7820A (online): Realización de ensayos y análisis simple de los resultados con conexión continua al equipo.
- GC7820A (offline): Realización de ensayos y análisis simple de los resultados sin conexión continua al equipo.
- OpenLAB Control Panel: Gestión y configuración del equipo.
- 7820A GC Remote Control Panel: Panel de control digital del equipo.

Barra de Pestañas

Pestaña File

Al igual que la mayoría de los programas, desde esta pestaña se pueden guardar los distintos archivos de este, así crear nuevos o abrir existentes. En este programa es de mencionar la posibilidad de tratar con informes, métodos y sets de resultados, que son los tipos de archivos que genera este programa. Los campos de la pestaña se muestran a continuación en la Ilustración 50

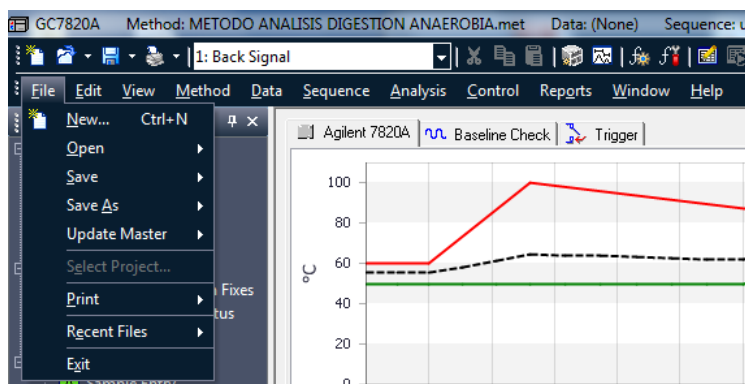


Ilustración 50: Pestaña File

Pestaña Edit

Pestaña de carácter genérico en la que se encuentran las herramientas de Cortar, Copiar y Pegar. Su uso en el programa está limitado a Informes o datos que puedan introducirse en cuadros de texto. La lista de opciones se incluye en la Ilustración 51

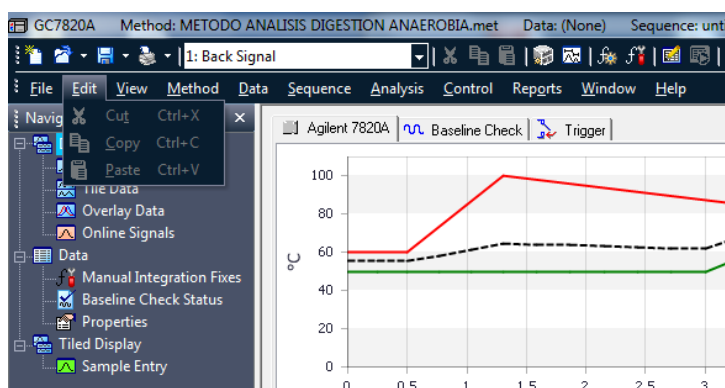


Ilustración 51: Pestaña Edit

Pestaña View

Esta pestaña permite mostrar distintos resultados y análisis que realiza el programa, principalmente los cromatogramas con las líneas base; así como datos del análisis de picos/grupos. Las opciones de esta pestaña se muestran en la Ilustración 52.

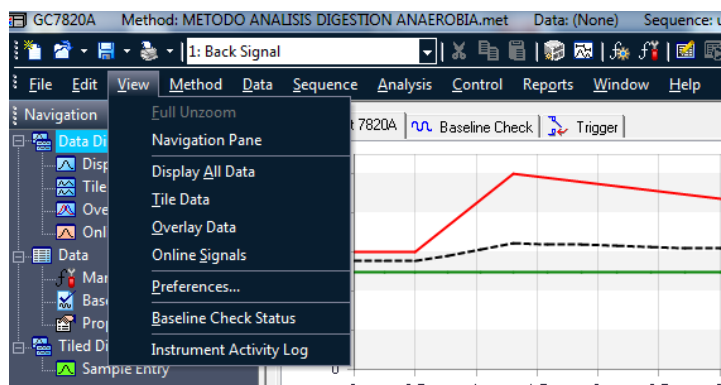


Ilustración 52: Pestaña View

Pestaña Method

A través de esta pestaña se puede acceder a la herramienta de creación y modificación del Método activo. Para ello se ha de emplear la entrada de “*Instrument Setup*”. Del mismo modo, esta permite importar un Método desde el equipo que se encuentre conectado a través de “*Import Instrument Setup*”.

Por último, las funciones restantes están relacionadas con procesos de automatización de análisis cuando se construye el cromatograma. Estos procesos ocurren durante la “*Post-Run Sequence*” del equipo. Asimismo, estas herramientas se explican en detalle en la sección de Barra de Iconos. La pestaña se muestra a continuación en la Ilustración 53

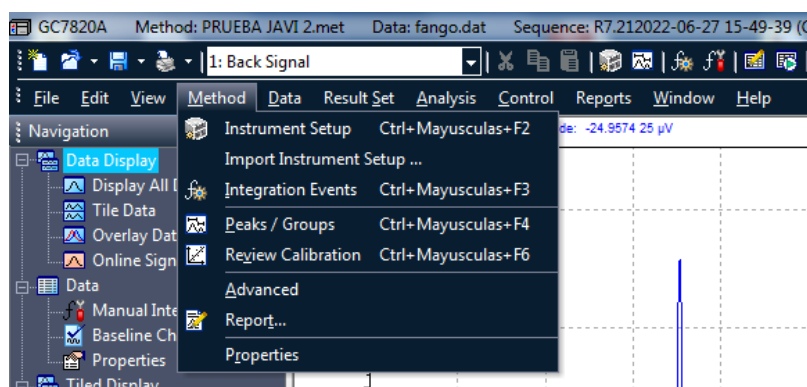


Ilustración 53: Pestaña Method

Pestaña Data

De manera similar a la pestaña anterior, a través de esta se puede realizar un análisis del set de resultados actualmente abierto. Para ello se cuenta con la herramienta de integración manual “*Manual Integration Fixes*”, la cual se explica en la sección de Barra de Iconos.

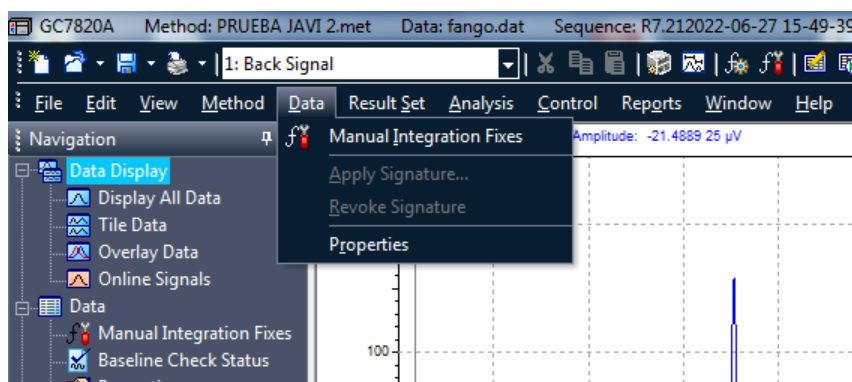


Ilustración 54: Pestaña Data

Pestaña Result Set

En esta pestaña se incluyen las herramientas necesarias para configurar el proceso de muestreo, permitiendo editar secuencias de análisis, si el equipo contase con la torreta “*Autosampler*” necesaria para ello.

Además, la entrada de “*Process*” permite abrir la herramienta de “*Run Queue*”, la cual se ha explicado en la siguiente sección. La pestaña se muestra en la Ilustración 55.

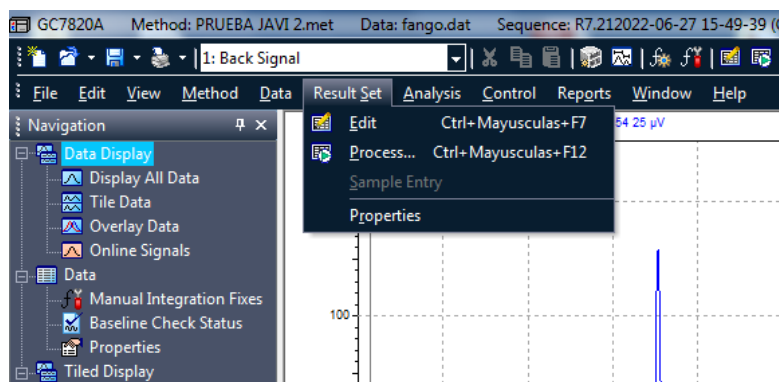


Ilustración 55: Pestaña Result Set

Pestaña Analysis

A través de esta sección en el programa se pueden iniciar las herramientas de análisis y calibración. Estas se abren en la misma ventana, como se explica en la sección de iconos. Estas herramientas permiten el análisis de especies separadas en el proceso, así como su capilarización en las columnas del equipo. Esta es de especial utilidad en las secuencias de muestreo, ya que puede mostrar todos los resultados de una especie y determinar una línea de tendencia. La pestaña se muestra en la Ilustración 56.

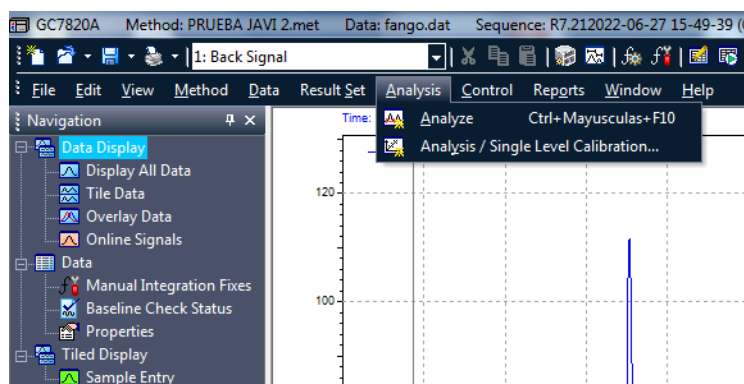


Ilustración 56: Pestaña Analysis

Pestaña Control

La siguiente pestaña contiene las herramientas necesarias para controlar el equipo y los ensayos que en este se realizan. En consecuencia, contiene la mayor cantidad de herramientas. Entre estas la más importante es la de “Single Run”, la cual se explica en la siguiente sección. Esta herramienta permite configurar el equipo para realizar un ensayo y almacenar los resultados. También permite entrar a la secuencia de muestreo y unificar ensayos con resultados, ya que estos se pueden almacenar en archivos separados.

Otra funcionalidad importante que este contiene es la de “Monitor GC7820A”, la cual es la que permite determinar cuándo el equipo se encuentra listo para ser usado o este presenta un problema. **Es la herramienta que diferencia la versión Online de la Offline**, por lo que siempre estará activa y siempre estará bloqueada.

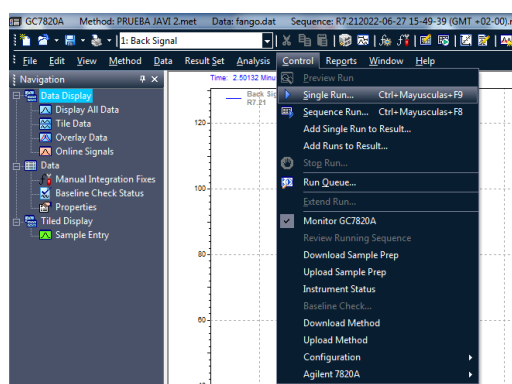


Ilustración 57: Pestaña Control

Pestaña Reports

A través de esta pestaña se puede acceder al editor de informes, los cuales se pueden producir de manera genérica a partir de las plantillas existentes, ya sean propias del equipo o creadas por su usuario; o a través de informes avanzados que permiten incluir varios datos específicos que se pueden seleccionar para producir un documento ad-hoc. Al no poder guardarse estos informes más que en formato.pdf, su utilidad principal es la comunicación externa de resultados. Las opciones disponibles en esta ventana se muestran en la Ilustración 58.

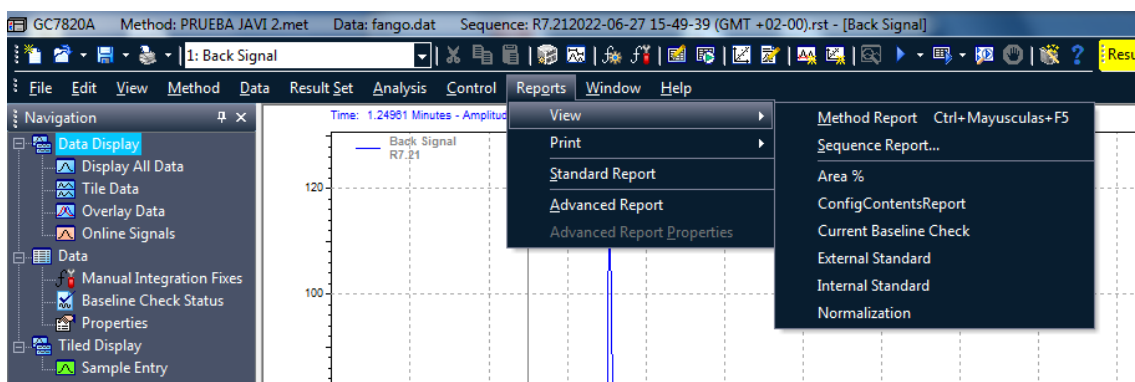


Ilustración 58: Pestaña Reports

Pestaña Window

Al igual que varias pestañas anteriores, esta contiene funciones genéricas. En este caso opciones de gestión de las múltiples ventanas internas del programa.

Pestaña Help

En esta última pestaña se encuentra el menú de ayuda. Al ser un equipo tan complejo, el menú de ayuda abre una nueva ventana en la cual se puede realizar una búsqueda por términos de aquello que se desee. La pestaña de búsqueda se muestra a continuación en Ilustración 59.

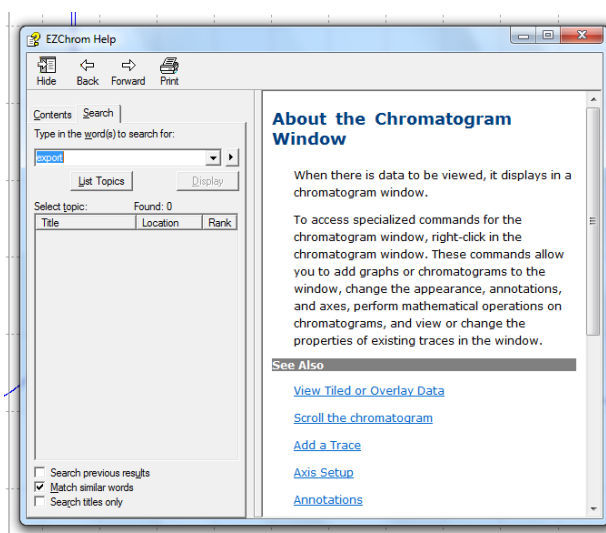


Ilustración 59: Ventana Instrument Wizard

Barra de Iconos

Encima a de las pestañas del equipo, también se cuenta con una barra de iconos, los cuales son atajos dentro del programa para acceder a herramientas específicas. Los 4 primeros iconos, comenzando por la izquierda, son de carácter genérico: Nuevo Método, Abrir, Guardar e Imprimir. De estos, el icono Abrir permite abrir no solo un método, sino también un informe o los resultados de un ensayo anterior. También se ha de señalar el selector del cromatograma, el cual deberá estar siempre en “1: Back Signal”, ya que es el puerto asignado al sensor TCD antes descrito.

Icono Instrument Set Up

Al ser este el primer icono de acceso rápido contiene información más general del equipo, mientras que los restantes contienen datos y herramientas específicos para cubrir las varias funciones del cromatógrafo. En esta herramienta, la cual se muestra en la Ilustración 60, se incluyen los datos genéricos como el método actualmente cargado en el equipo, además de la configuración de varios componentes de este.

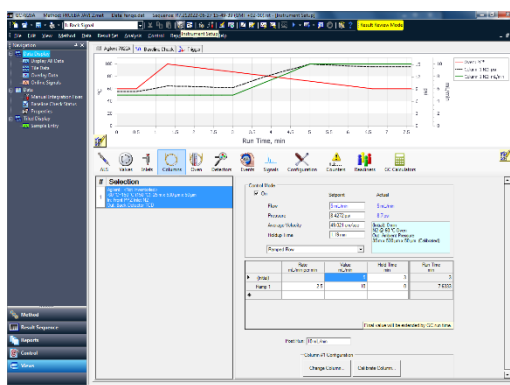


Ilustración 60: Icono Instrument Set Up

Icono Picos/Tablas de los picos

Este icono redirige a la sección de Grupos/Tablas, la cual contiene las definiciones de las especies que se desean analizar dentro de una muestra sometida a un Método (quedando esta tabla almacenada dentro de este). Es empleada internamente por el programa para determinar los campos a presentar y analizar cuando se genera un informe con resultados. Debido a su naturaleza, no deberá alterarse ni modificarse nunca salvo que se haya realizado una modificación sustancial del Método de ensayo empleado. La tabla producida se muestra en la Ilustración 60

JAVI 2.met Data: fango.dat Sequence: R7.212022-06-27 15-49-39 (GMT +02-00).rst - [Peak / Group Tables -- Back Signal]

Signal

Data Result Set Analysis Control Reports **Peak / Group Tables**

Named Peaks		Groups						
#		Name	ID	Ret. Time	Window	Ref. ID #	ISTD. ID #	Resolu
1	<input checked="" type="checkbox"/>	CO2	1	3.67	0.1835	0	0	
2	<input checked="" type="checkbox"/>	H2	3	5.68833	0.228442	0	0	
3	<input checked="" type="checkbox"/>	SH2	2	6.53083	0.326542	0	0	
4	<input checked="" type="checkbox"/>	CH4	4	7.18917	0.359458	0	0	
5	<input checked="" type="checkbox"/>							

Ilustración 61: Icono Peak/ Group Tables

Icono Eventos de Integración

A través de esta herramienta se puede automatizar un análisis del cromatograma empleando las secuencias de integración propias del programa, de las cuales se emplean comúnmente 3 que se explican en la siguiente subsección. Al ser una parte esencial del proceso “*Post-run*”, una modificación en esta tabla implica la necesidad de guardar el Método como un nuevo. La tabla de Integración del Método activo se muestra en la Ilustración 62

#	Event	Start Time	Stop Time	Value
1	Width	0.000	0.000	0.2
2	Threshold	0.000	0.000	15000
3	Integration Off	0.000	3.500	0
4	Width	5.200	5.688	0
5	Threshold	5.300	5.707	0
6	Integration Off	5.710	6.250	0
7	Width	6.294	6.996	0.701354
8	Threshold	6.323	7.071	1844.75
9	Integration Off	7.501	7.512	0
10				

Ilustración 62: Eventos de Integración

Herramientas de Integración

Para la realización de una integración de manera automática, esta se ha de programar en el método a emplear. Al ser un programa complejo, permite analizar tanto la primera como la segunda derivada del cromatograma, siendo más estable el análisis de la segunda derivada al suavizarse los picos y los escalones, pero perdiéndose detalles importantes como el comienzo de un pico si no hay un cambio de pendiente.

Para evitar estos problemas, el equipo realiza ambos análisis y los conjuga para determinar el comienzo del pico de tensión de una especie, así como su cola en el proceso de integración automática. Para ello se requiere del uso de 3 herramientas de integración: “*Width*”; “*Threshold*” e “*Integration Off*”, los cuales se explican a continuación:

- *Width*: Se emplea para marcar temporalmente la anchura máxima del pico de la especie a analizar. Se requiere establecer los límites de este para evitar el solape de estos.
- *Threshold*: Herramienta que determina el pico en μV de la especie. Esta herramienta necesita determinar el cambio de pendiente correspondiente a la cabeza y cola de la especie, por lo que necesita que su extensión temporal sea ligeramente mayor a “*Width*”, sin solaparse con ningún otro evento.
- *Integration Off*: Este evento desactiva la herramienta de integración entre los límites temporales que se definen. Se ha de usar siempre entre picos a analizar, así como en los tramos que no se quieran determinar, ya que, si no serán evaluados por la herramienta y asignados a una especie, alterando el resultado.

Icono Integración Manual

Del mismo modo que se puede programar un evento de integración en el propio Método, el programa permite realizar la integración manual de un cromatograma siguiendo los mismos pasos antes descritos. A valor informativo, la tabla de integración manual se muestra a continuación en la Ilustración 63.

#	Event	Start Time	Stop Time	Value
1	<input checked="" type="checkbox"/>			

Ilustración 63: Tabla de Integración Manual

Icono Selección de Secuencia

Como se ha mencionado anteriormente, el equipo permite la posibilidad de automatizar el proceso de análisis de muestras si el equipo cuenta con la torreta necesaria para ello, así como alguna modificación adicional. Para su proceso interno en el equipo, se ha de seleccionar el enrutamiento donde se almacenarán todos los resultados de la secuencia. Al no contarse con este equipo, y debido a la naturaleza de los ensayos, nunca se realizarán secuencias, por lo que la ventana mostrada en la Ilustración 64 es informativa. Se ha de señalar que el proceso para analizar una muestra se describe más abajo en el documento, en el apartado “Single Run”.

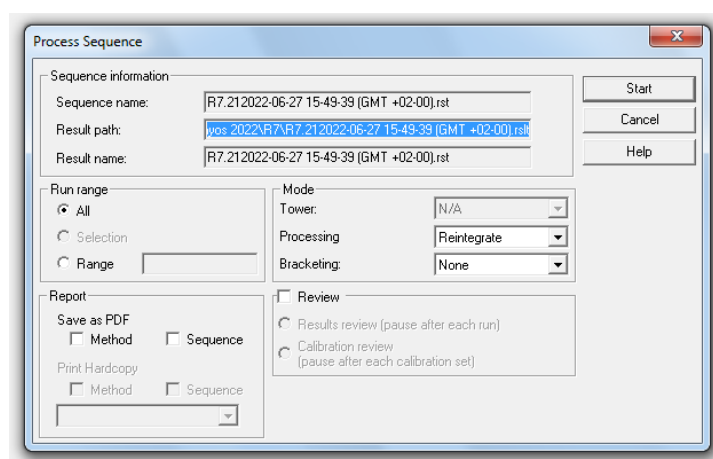


Ilustración 64: Ventana de Secuencia de Ensayos

Icono Editor de informes

Al tratarse de un programa de captura de datos, este cuenta con la posibilidad de realizar informes rudimentarios en su propia herramienta interna, los cuales se imprimen en formato pdf. Esta funcionalidad es útil cuando se ha preprogramado el formato del informe y se desea almacenar de manera independiente. Sin embargo, como se ha mencionado en otras secciones, el análisis de los datos se realiza mediante MATLAB a partir de las capturas de pantalla. En consecuencia, esta herramienta es de poca utilidad al solo poder proporcionar los datos brutos de la integración del cromatograma, la cual se ha explicado que no es fiable.

Icono Analyze

La herramienta de analyze permite el análisis por componentes los grupos anteriormente definidos en el método. Al ejecutarla, se abre una nueva ventana desde la cual se puede seleccionar la especie y se realiza el cálculo automático de esta.

Al abrirse en formato tabla, esta permite el seguimiento de varias muestras a la vez, mostrando la variación en cada una de ellas si se está analizando una secuencia de muestras. Además, en la parte inferior de la ventana se muestra una gráfica con la evolución de la presencia de la muestra en la especie, según lo estimado por la herramienta de integración. Esta se muestra en la Ilustración 65.

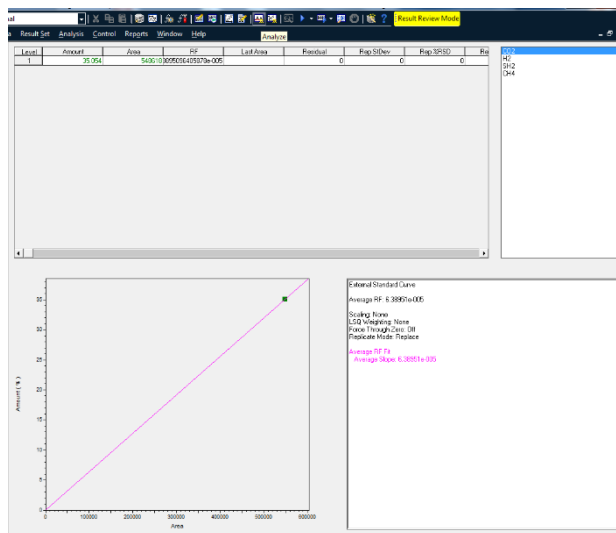


Ilustración 65: Ventana Analyze

Icono Analyze Single Run

Esta funcionalidad del programa abre una ventana a través de la cual se puede analizar resultados previos obtenidos en otro ensayo o con otro método, ya que aplica el proceso de integración automático explicado anteriormente. Esto permite la retrocompatibilidad de métodos y resultados si se modifica este primero. En la Ilustración 66 se muestra la ventana que este abre.

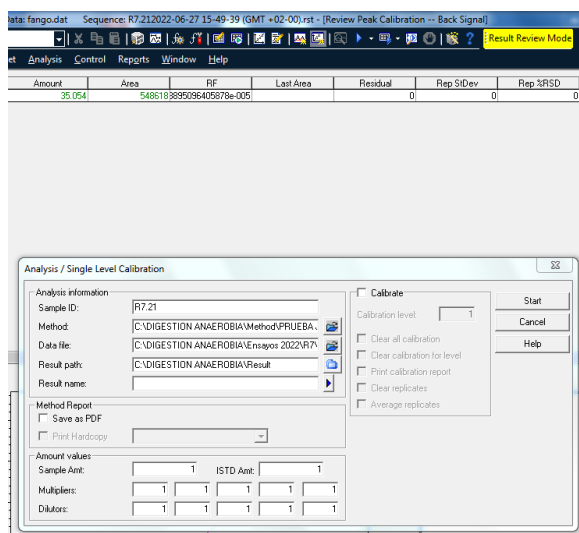


Ilustración 66: Ventana Analyze Single Run

Icono Single Run

Este es el icono incluye la función principal del equipo, el análisis de muestras. En este caso, se realiza únicamente el análisis de la muestra que se inserte cuando el equipo se encuentre listo y se presione el botón de “Start”, siguiendo el procedimiento descrito en otros apartados.

Debido a su importancia, se describe a continuación el proceso para la creación de un nuevo ensayo. En primer lugar, al presionarse el icono aparecerá en el centro de la pantalla la ventana mostrada en la Ilustración 67.

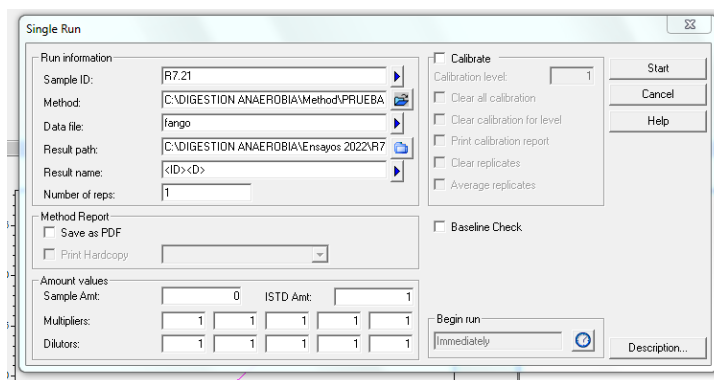


Ilustración 67: Ventana Single Run

Como se puede apreciar, en esta primero se ha de asignar el nombre de la muestra. Se recomienda que se siga un código que incluya el tipo de muestra (en este caso, F para fango, B para botella, R para reactor discontinuo y RC para reactor continuo), seguido del número de muestra y del día del ensayo.

Tras esto se ha de seleccionar el Método apropiado para el ensayo a realizar, así como el Data File, que es el nombre que tendrá el archivo con los resultados. Por último, se ha de seleccionar el “Results Path”. Al igual que en la asignación del nombre, se recomienda que se siga la misma estructura. El enrutamiento asociado a la muestra de la Ilustración 67 se muestra a continuación en la Ilustración 68.

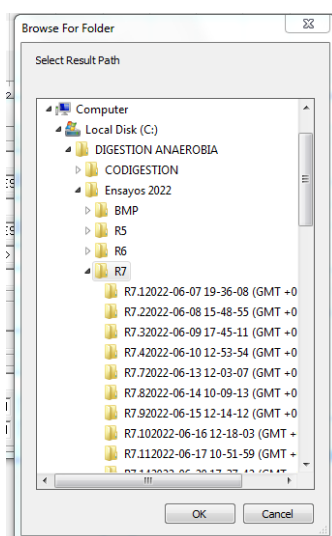


Ilustración 68: Ventana del Result Path de un ensayo Single Run

Icono Sequence Run

De una manera similar al icono anterior, en el cual se explica el proceso para crear una Single Run, el equipo puede, a través de una torre de auto muestreo ejecutar varios ensayos hasta agotar las muestras o realizar un número indicado de estas, lo cual se ajusta con “Run Usage”. Además, permite producir

un informe posterior. Sin embargo, no se cuenta con el equipo necesario para realizar este tipo de ensayos. La ventana se muestra en la Ilustración 69 a continuación.

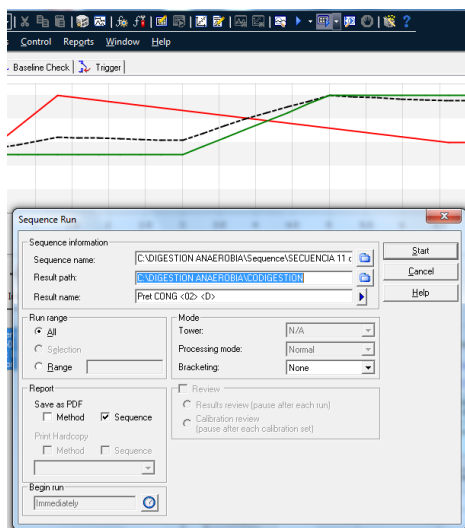


Ilustración 69: Ventana Sequence Run

Icono Run Queue

Al igual sé que se pueden realizar varios ensayos en una secuencia si se dispone del equipo necesario, el equipo también es capaz de programar varios ensayos, pudiendo incluirse en esta herramienta para mostrar la cola de espera de muestras a ensayar. Al no disponer del equipo necesario, no se pueden programar los ensayos a realizar, ya que también se necesitaría una manera de conectar de manera permanente el reactor a muestrear e incluir válvulas de control. La ventana de la herramienta se muestra en la Ilustración 70

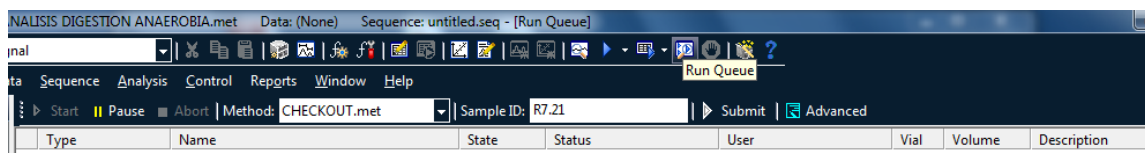


Ilustración 70: Ventana Run Queue

Icono Review Capillarization

Este icono abre la herramienta de analyze, mostrada en la Ilustración 65, en la cual se pueden observar los datos técnicos de la capilarización de la muestra a través de la columna en la esquina inferior derecha. Al tratarse de una herramienta de carácter muy específico, no tiene utilidad general en los ensayos realizados de manera común en este equipo.

Icono Wizard

Este icono abre el menú rápido del equipo, desde el que se facilitan los accesos a las principales funcionalidades y usos del equipo como la creación y modificación de métodos, secuencias y ensayos únicos. Estas opciones se muestran a continuación en la Ilustración 71.

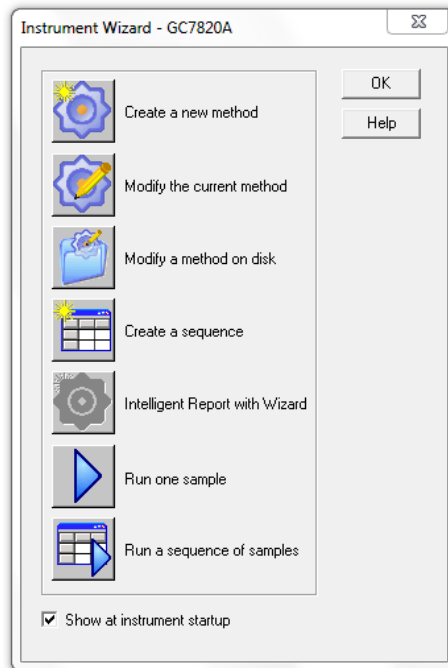


Ilustración 71: Ventana Instrument Wizard

Icono Help

Con este atajo se abre la herramienta de “*Help*” descrita anteriormente.

OpenLab Control Panel

Este programa del equipo, el cual no tiene uso de manera habitual, es empleado para la gestión de los dispositivos Agilent conectados al ordenador. Este se instala como parte del paquete de software OpenLAB CDS, incluido con todos los equipos de este fabricante.

Estas gestiones incluyen la posibilidad de gestionar varios proyectos de investigación de manera conjunta, así como la posibilidad de supervisar la actividad y estatus del equipo.

También permite la gestión de notificaciones y la configuración del equipo. Sin embargo, su función más importante es almacenar y controlar las licencias de los varios equipos que se conecten al equipo (Agilent Technologies, Inc., 2017). En consecuencia, este programa no deberá abrirse nunca salvo que se detecte un problema con la licencia del equipo.

La pantalla de inicio del programa se muestra a continuación en la Ilustración 72.

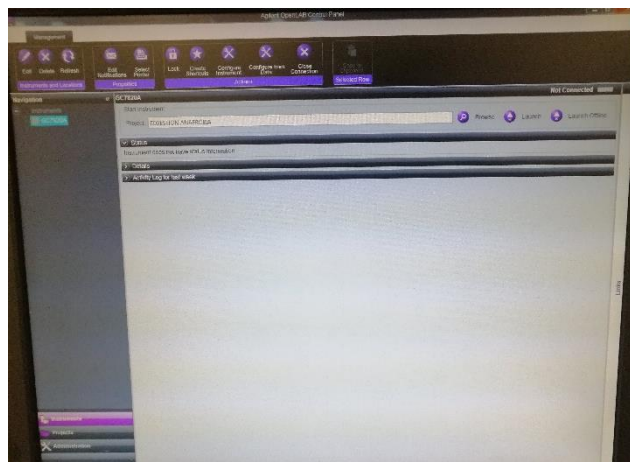


Ilustración 72: OpenLAB Control Panel

7820A Remote Control Panel

El equipo no cuenta con un teclado externo físico, por lo que para interactuar con el equipo se necesita de la conexión con el ordenador de control asociado, el cual se ha mostrado anteriormente.

En caso de necesitar emplear el teclado de control del equipo, por no poder controlarse desde sus programas específicos, se deberá usar el programa “7820A GC Remote Controller”. Al iniciar este programa, el equipo deberá conectar con el cromatógrafo, tras lo cual aparecerá la ventana con el teclado, la cual se muestra en la Ilustración 73.

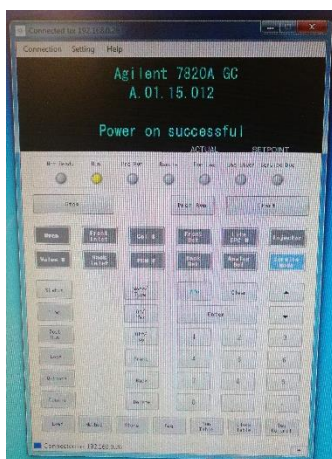


Ilustración 73: 7820A Remote Control Panel

Teclas de Ensayo

Este teclado permite controlar el equipo de manera independiente al ordenador. Para ello cuenta con varias funciones. La primera de ellas es la posibilidad de realizar los ensayos antes mencionados.

Para ello, se deberá presionar la tecla “*Prep Run*”, la cual inicia un nuevo ensayo, interrumpiendo el proceso actual, llevando el equipo al estado inicial. Asimismo, la tecla “*Start*” inicia el ensayo de manera manual, estando replicada físicamente en el equipo. La última tecla de ensayo que aparece en el teclado es la tecla de “*Stop*”, la cual detiene el ensayo actual.

Tecla de Mantenimiento

Esta es la tecla azul que se encuentra en la esquina inferior derecha de la sección con las teclas grises. Con ella se accede al menú de mantenimiento del equipo, pudiendo realizar diagnósticos y otras operaciones que se recogen en la guía avanzada de usuario (Agilent Technologies, Inc., 2016). Se recomienda no presionar nunca esta tecla, ya que es preferible llamar al servicio técnico si el equipo requiere mantenimiento.

Teclas de Componentes

Esta serie de teclas grises, debajo de las Teclas de Ensayo, permite consultar el estado de cada elemento representado en ellas, así como su modificación pulsando la tecla “*Enter*” en el teclado numérico debajo.

Sin embargo, se recomienda que, si solo se quieren comprobar los estados de cada componente como la temperatura del horno o el flujo de gas portador, se usen las teclas físicas del equipo, ya que evitan que se modifique uno de los valores por accidente.

Tecla Info

Esta tecla permite obtener información más detallada de los rangos de operación de cada componente del equipo; no se recomienda su uso a menos que se desee crear un método nuevo y se necesite emplear esos rangos.

Teclado numérico

Este conjunto de teclas permite modificar los valores de los distintos campos de funcionamiento del equipo, como se ha explicado antes. De esta sección merece la pena señalar las teclas “*Front*” y “*Back*” las cuales permiten seleccionar el puerto de entrada a controlar, ya que el equipo cuenta con 2 de estos. En el caso de este equipo, solo el puerto trasero se encuentra conectado a la bala de gas portador.

Teclas de Apoyo

Estas teclas secundarias permiten realizar funciones adicionales, tales como la programación del equipo al finalizar un ensayo o acceder a los resultados almacenados en el equipo. En caso de necesitar emplear estas teclas en lugar del software de control, consultar la guía de operación (Aglient, 2011). Asimismo, las teclas situadas debajo del teclado general permiten realizar controles de secuencia, método y automatización del equipo. Al no disponer actualmente de los componentes tales como la torre de muestreo, que permiten la automatización del proceso, no se incluyen en este manual.

4. Análisis de Gases de Digestión Anaerobia

El principal uso de este equipo es el análisis de muestras de biogás producido tanto en las botellas discontinuas de ensayo BMP (AENOR, 1999), como las obtenidas de los reactores tanto discontinuos como semicontinuos. Para ello, se deberá utilizar el método desarrollado en (Morales Polo, Co-Digestión Anaerobia y Pretratamientos de Residuos Agroalimentarios con Fangos UASB de Depuradora, 2019). Este método, mediante el uso de variaciones térmicas y el paso por las dos columnas del equipo, es capaz de separar en el tiempo 3 de las especies a analizar, siendo estas el metano (CH_4), hidrógeno (H_2) y el ácido sulfhídrico (H_2S), quedando el CO_2 restante en la bala de muestra retenido por las válvulas, por lo que se encontrará en los picos tras la apertura de estas, junto con otras especies no adsorbidas por las columnas. El método que emplear se muestra a continuación en la Ilustración 74.

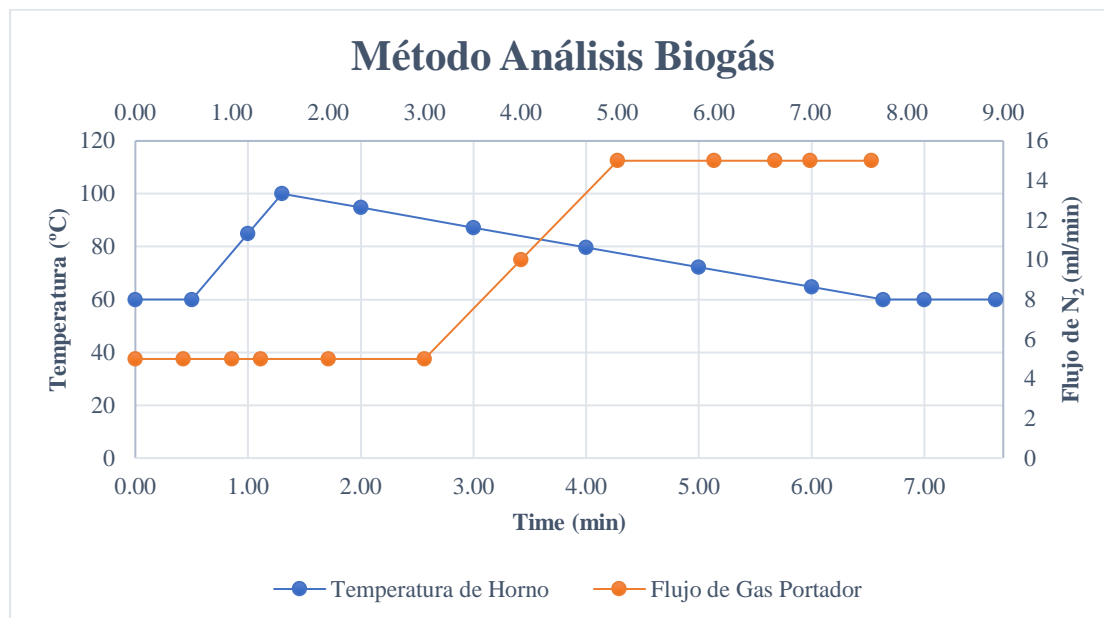


Ilustración 74: Gráfica del Método de Análisis de Muestras de Biogás

Como paso previo a la realización de un ensayo, se deberá encender el ordenador principal y emparejarlo con el equipo mediante el software de control. Una vez arrancado el programa, siguiendo las indicaciones de la sección previa se deberá preparar un nuevo ensayo, asegurándose de que el enrutamiento de los resultados, así como el método seleccionado son correctos. Se recuerda que para los ensayos del biogás se deberá utilizar el método “METODO ANALISIS DIGESTION ANAEROBIA”, el cual incluye integraciones automáticas del área del cromatograma. Sin embargo, se ha de señalar que el procesamiento de este se realizará con el código de Matlab “Lectura Imágenes GC”.

Asimismo, es necesario colocar un cilindro graduado con un volumen suficiente de agua desionizada como para que el final de la manguera de salida de muestras se encuentre sumergida y burbujee si se inyecta una muestra.

Una vez se ha programado el equipo correctamente, se deberá esperar a que la luz de “Run” pase de un amarillo intermitente a un verde sólido y en el programa se muestre el mensaje “Waiting for Trigger”. A partir de ese momento se puede insertar la aguja en el adaptador, asegurándose de que el sello es hermético. A continuación, se puede presionar el émbolo de la jeringa para insertar la muestra. Cuando se deje de presionar, se debe de observar el cilindro, el cual debería estar burbujeeando. Cuando la última burbuja haya salido de la manguera, se deberá presionar el botón de “Run” en el cromatógrafo para iniciar el ensayo. Se sabrá que este se ha iniciado correctamente cuando a los 5 segundos se escuche el sonido de la primera válvula. Para facilitar el proceso, se recomienda que se esté preparado con la mano izquierda sujetando la jeringa ya insertada y la mano derecha sobre el botón de “Run”, sin presionarlo.

Una vez iniciado el ensayo, el alumno no necesita realizar ninguna otra operación hasta su finalización al ser un proceso automático. Una vez este ha finalizado, si se desea se puede proceder con el análisis del cromatograma.

Para ello, primero se debe maximizar este en el programa e imprimir la imagen, guardándola en un lugar en el que sea fácil recuperar y/o transferir este para poder ser analizada en un equipo que tenga Matlab instalado.

Al no disponer aún del programa para el análisis del cromatograma, se procederá a realizar un tratamiento de la imagen como una matriz de bits tridimensional con valores (con los valores R, G y B en las capas 1, 2 y 3 del mapa de bits).

El código requiere que la imagen se guarde en la misma carpeta que el código y se guarde en este su nombre y extensión. Tras esto se puede ejecutar la primera sección del código, la cual recorta y extrae el cromatograma, abriendo este recorte como figura para poder anotar distintos píxeles significativos para permitir el cálculo gráfico.

En primer lugar, se debe establecer los píxeles de inicio y fin de la línea base. Estos serán aquellos entre el inicio del cromatograma y la apertura de la primera válvula (B_{start} y B_{end} , respectivamente). Una vez se han definido estos, la línea base se define como la moda de las coordenadas y de los puntos entre estos, ya que comúnmente estos puntos se concentran entre 2 píxeles de altura y se necesita un número natural para realizar el conteo, cuya fórmula se muestra a continuación.

$$BL = mode(B_{start}, B_{end})$$

Del mismo modo, en el programa se deberá indicar los píxeles de comienzo y fin de los gases residuales no adsorbidos, los cuales escapan tras la apertura de las válvulas, como se ha explicado anteriormente. Estos píxeles serán $Res1_{start}$; $Res2_{start}$ y $Res1_{end}$; $Res2_{end}$; respectivamente para el comienzo y final de cada tramo de integración.

Por último, se necesitan también los límites para la integración manual de los distintos compuestos, siendo en este caso el CH_4 (CH_{4start} y CH_{4end}); el H_2 (H_{2start} y H_{2end}) junto con el H_2S ($H_{2Sstart}$ y H_{2Send}). Con los límites ya registrados, el código procederá al cálculo de las áreas de la siguiente manera, representando la X la especie a analizar:

$$\begin{aligned} &for\ i = (X_{start}:X_{end}) \\ &X = X + Crom(i) - BL; \\ &end; \end{aligned}$$

Una vez recorrido todos los tramos especificados, se determina el peso unitario de cada especie en la muestra analizada.

$$X = \frac{X}{CH_4 + H_2 + H_2S + Res_1 + Res_2}$$

Con este análisis finaliza la ejecución del programa y se obtiene el resultado de la muestra analizada. A modo de resumen, todas las variables a recoger en el ensayo se incluyen en la Tabla 19.

Tabla 19: Variables a recoger en el ensayo de biogás

Variable	Unidad	Símbolo
Comienzo Línea Base	Píxel	B_{start}
Final Línea Base	Píxel	B_{end}
Comienzo Residuo 1	Píxel	Res_{1start}
Final Residuo 1	Píxel	Res_{1end}
Comienzo Residuo 2	Píxel	Res_{2start}
Final Residuo 2	Píxel	Res_{2end}
Comienzo Hidrógeno	Píxel	H_{2start}
Final Hidrógeno	Píxel	H_{2end}
Comienzo Metano	Píxel	CH_{4start}
Final Metano	Píxel	CH_{4end}
Comienzo Ácido Sulfhídrico	Píxel	H_2S_{start}
Final Ácido Sulfhídrico	Píxel	H_2S_{end}

5. Realizar Ensayo

En esta sección se explicará brevemente como realizar el ensayo de una muestra genérica en el equipo, sin el tratamiento de los cromatogramas, el cual se ha presentado en la sección anterior. Para ello, se deberá configurar el equipo con el método deseado, así como el enrutamiento de los resultados. En caso de realizar varios ensayos de distintas muestras, se recomienda seguir un método de numeración y almacenamiento de los cromatogramas para facilitar su posterior tratamiento. Además, el equipo debe estar en estado de espera del disparador, lo cual se indica en la pantalla del ordenador con el mensaje “*Waiting for Trigger*”, como se ha mencionado en otras ocasiones. También se ha de colocar la manguera de salida de muestra en un cilindro graduado con agua suficiente como para que su salida quede completamente sumergida.

Para realizar el ensayo se recomienda emplear muestras de 50ml recogidas con la jeringa propia del equipo, para asegurar que se dispone de muestra suficiente o la bala de muestras si se decide emplear esta. Es importante señalar que en caso de emplear una bala se ha de limitar la presión de salida a 1 bar como máximo para evitar la rotura de las columnas internas. Asimismo, se deberá instalar en el equipo el adaptador correspondiente, ya sea el adaptador de la jeringa o de la bala. En la Ilustración 75 a continuación se muestra un ejemplo de esto con la jeringa.

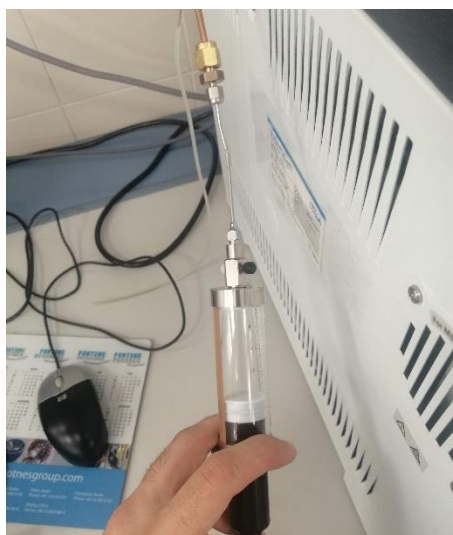


Ilustración 75: Inyección de muestra en el cromatógrafo desde jeringa

Una vez se ha insertado la jeringa y se ha preparado el equipo, se deberá presionar el émbolo de la jeringa lentamente, para evitar sobrepresiones internas, pero con la velocidad suficiente como para observar el escape de burbujas en el vaso de salida. Cuando se haya inyectado muestra suficiente, se deberá presionar el botón de “*Run*” en el instante en el cual sale la última burbuja de la manguera de salida. Se sabrá si el ensayo se ha iniciado correctamente si al cabo de unos pocos segundos de presionar el botón se escucha el cierre de una válvula en el cromatógrafo.

Cuando se realice este ensayo con jeringa, se recomienda emplear 10ml de la muestra, reservando el sobrante dentro de esta cerrando su válvula de paso para evitar escapes o contaminación de esta.

Una vez se ha iniciado el ensayo, no se podrá introducir otra muestra o iniciar otro ensayo hasta que haya finalizado la actual, ya que esto causaría un fallo en el análisis actual.

6. Mantenimiento

Al tratarse de un equipo muy sensible, se han de tener ciertas consideraciones a la hora de arrancarlo, usarlo y apagarlo. Esto se debe a la delicadeza de los aparatos de medida y de ciertos componentes como las columnas internas del equipo, las cuales son susceptibles de romperse. En consecuencia, esta sección está dividida en las distintas operaciones de mantenimiento del equipo.

Arranque de operación diaria

Debido a la naturaleza de las tandas de ensayos, el equipo se ha de usar a diario varias veces para analizar la composición de las muestras extraídas de reactores y botellas. En este caso, el equipo no deberá apagarse al acabar los ensayos diarios ni cerrar la llave de paso de la bala de nitrógeno portador, ya que interrumpir la alimentación de gas causará que la columna quede inundada de gas del ambiente y quede saturada, por lo que se requeriría regenerar la columna, lo cual requiere en torno a 1 hora.

Por ello, durante los ensayos, no se debe apagar el equipo, basta con cerrar el programa de control desde el ordenador y apagarlo. De esta manera, el cromatógrafo permanecerá en “*Standby*” con el método cargado, manteniendo un flujo suficiente.

Arranque tras apagado de larga duración

Cuando se enciende el equipo por primera vez en 14 o más días (Agilent Technologies, Inc., 2011), se necesita realizar una serie de tareas y permitir que se regeneren las columnas antes de poder utilizar el equipo. Para ello, se debe arrancar en primer lugar el ordenador de control y abrir las llaves de paso de la bala de nitrógeno conectada al equipo, iniciando el flujo de gas. Tras esto, se puede pulsar el botón de encendido del equipo.

Una vez encendido, el horno comenzará a calentarse a la par que se realizan las comprobaciones internas del equipo, siendo una de estas la conexión a equipo externo y la detección de flujo de gas. Asimismo, la luz “*Prep Run*” comenzará a parpadear, indicando que el equipo no puede usarse. Esta luz se apagará cuando el horno alcance la temperatura de consigna, basada en el método que se encuentre cargado (este debe ser el método “*Standby*”). Cuando se haya apagado la luz y el horno haya alcanzado la consigna, se deberá arrancar el programa de conexión y crear una nueva run, cargando el método que se vaya a emplear en la tanda de ensayos.

Finalmente, se ha de dejar que el equipo permanezca encendido con el flujo abierto para conseguir la desorción de las columnas, dependiendo del periodo de inactividad. Como referencia, en ocasiones anteriores como el arranque en septiembre tras el verano, así como el arranque en enero, ambos tras vacaciones, fue de 7 días.

Cambio de bala de nitrógeno

Si se requiere un cambio de bala, se recomienda que este se realice una vez se hayan completado todos los ensayos diarios. Además, de manera preventiva, se recomienda cambiar la bala cuando su presión ronda los 20psi; idealmente por una bala nueva con una presión en torno a los 220psi. Estas balas deberían durar en torno a 20 semanas, a razón de 20psi por semana (realizando en torno a 70-80 análisis por semana), una pérdida de presión más rápida es indicativa de una fuga en el circuito neumático, comúnmente en los racores metálicos de las balas.

Para realizar el cambio de bala, primero se ha de apagar el equipo y cerrar la válvula de la bala; esperando a que decaiga la presión.

Tras esto se puede desconectar la manguera de la bala y conectarla a la nueva. Una vez se ha conectado, se deberá abrir las válvulas para restaurar la presión y el flujo de nitrógeno. Posteriormente, volver a arrancar el cromatógrafo, permitiendo que este realice sus comprobaciones necesarias y se regenere la columna. Finalmente, notificar del cambio de bala para que esta pueda ser sustituida por otra nueva.

Apagado de corta duración

Este tipo de apagado se refiere a aquel que dure menos de 14 días, a partir del cual el manual del fabricante recomienda el apagado de larga duración (más de 7 días) (Aglient, 2011). Para realizar este apagado, se ha de apagar el cromatógrafo una vez se hayan finalizado los ensayos y cerrar las válvulas de las balas. Una vez hecho esto, apagar el ordenador de control.

Apagado de larga duración

Este proceso es similar al apagado de corta duración, pero se requiere cargar el método de “*Standby*” y permitir que el cromatógrafo se estabilice antes de proceder con el apagado y cierre de válvulas.

Limpieza de la jeringa

Debido a la utilización diaria de la jeringuilla, se recomienda la limpieza semanal de esta para evitar que la suciedad se acumule sobre ella debido a la grasa de vacío o vaselina que inevitablemente acaba sobre esta.

Al ser un equipo delicado, se recomienda que se limpie siempre con paño humedecido con etanol, el cual es menos efectivo que la acetona, pero no ataca el plástico. Se puede limpiar con sustancias más fuertes si se desmonta la jeringa y se realiza la operación con sumo cuidado.

También se ha de señalar la importancia de apretar la válvula de paso blanco-negro de la jeringa, ya que si no se rosca correctamente se pierde la estanqueidad de esta y por tanto se comprometen las muestras. Como último detalle, antes de reensamblar la jeringa, se recomienda comprobar que no hay gotas de agua en su interior, ya que estas persisten en el interior de la jeringa.

Limpieza general del equipo

Al tratarse de un equipo electrónico delicado, su limpieza exterior se debe limitar a retirar el polvo que se acumule sobre el equipo con un paño húmedo en los lugares donde se acumula, como las rejillas de ventilación del equipo o la tapa superior del equipo, la cual protege el sensor de medición y las entradas y salidas de gases.

Mover y recolocar el equipo

En ocasiones puede ser necesario desplazar el equipo, para ello, se ha de mover entre 2 o más personas, ya que el equipo es demasiado pesado y voluminoso para 1 persona. En estos casos, si se quiere recolocar el equipo en otra mesa o zona, consultar el manual sobre el desplazamiento del equipo.

Si solo se quiere mover sin necesidad de desconectar los tubos, hacerlo despacio y cuidadosamente para evitar dañar ningún componente. Además, se ha de comprobar tras que ninguno de los tubos y mangueras del equipo está doblados, ya que esto causará que en operación las aperturas de válvulas sacudan violentamente el equipo.

7.5. Anejo V: MATLAB Code

```

%Lectura de imagenes TFM
%%
%%Leer todos los archivos de las carpetas
%%Meter el numero de botellas, botellas continuas, recatores,
reactores continuos y fango a analizar
%%Meter el número de muestras de cada uno
n_s=3;
n_b=14;
n_b_np=5;
n_bc=2;
n_f=2;
n_f_np=1;
n_r=2;
n_r_np=1;
n_rc=1;

n_s_s=5;
n_s_b=15;
n_s_bc=15;
n_s_f=15;
n_s_r=15;
n_s_rc=30;

%Limites del cromatograma
x_i=121;
y_i=262;
x_f=902;
y_f=1224;

%Cálculos de cromatogramas
%Parámetros
b_start=10; %Desde donde se calcula la línea base
b_end=180; %Hasta donde se calcula la línea base
ch4_start=770;
ch4_end=930;
h2_start=725;
h2_end=760;
h2s_start=700;
h2s_end=720;
res_1_start=210;
res_1_end=280;
res_2_start=630;
res_2_end=690;

%Constatare gases ideales
R=8.314; %J/mol-K
V_botella=(20.5+900+150); %V botellas en m^3
Temp_b=(273.15+38);
Conv_p_v=10^5*V_botella/(R*Temp_b)*22.4/10^6;
V_fango_b=0.1125;
V_fango_bc=0.1125;
V_fango_f=0.15;

```

```

%Directorio Base
%Copiar la dirección donde estan las carpetas con las imagenes
dir='C:\Users\javie\OneDrive\Desktop\ICAI\6\TFM\MATLAB';
%%
%Cargar imagenes a tratar, guardadas en i_X
%Obtener cromatogramas a analizar, guardados en c_X

%Gas Muestra
if(n_s>0 && n_s_s>0)
    i_b=cell(n_s,n_s_s,1024,1380,3);
    c_b=cell(n_s,n_s_s);
    for i=1:n_s
        for j=1:n_s_s
            name=fullfile(dir,sprintf('S%d/S%d.%d.png',i,i,j));
            i_s{i,j}=imread(name);
            c_s{i,j}=i_s{i,j}(x_i:x_f,y_i:y_f,:);
        end
    end
end

%Botellas
if(n_b>0 && n_s_b>0)
    i_b=cell(n_b,n_s_b,1024,1380,3);
    c_b=cell(n_b,n_s_b);
    for i=1:n_b
        for j=1:n_s_b
            name=fullfile(dir,sprintf('B%d/B%d.%d.png',i,i,j));
            i_b{i,j}=imread(name);
            c_b{i,j}=i_b{i,j}(x_i:x_f,y_i:y_f,:);
        end
    end
end

%Botellas Continuas
if(n_bc>0&& n_s_bc>0)
    i_bc=cell(n_bc,n_s_bc);
    c_bc=cell(n_bc,n_s_bc);
    for i=1:n_bc
        for j=1:n_s_bc
            name=fullfile(dir,sprintf('BC%d/BC%d.%d.png',i,i,j));
            i_bc{i,j}=imread(name);
            c_bc{i,j}=i_bc{i,j}(x_i:x_f,y_i:y_f,:);
        end
    end
end

%Fango
if(n_f>0&& n_s_f>0)
    i_f=cell(n_f,n_s_f);
    c_f=cell(n_f,n_s_f);
    for i=1:n_f
        for j=1:n_s_f
            name=fullfile(dir,sprintf('F%d/F%d.%d.png',i,i,j));
            i_f{i,j}=imread(name);

```

```

        c_f{i,j}=i_f{i,j}(x_i:x_f,y_i:y_f,:);
    end
end
end

%Reactores Discontinuos
if(n_r>0 && n_s_r>0)
    i_r=cell(n_r,n_s_r);
    c_r=cell(n_r,n_s_r);
    for i=1:n_r
        for j=1:n_s_r

name=fullfile(dir,sprintf('R%d/R%d.%d.png',(i+4),(i+4),j));
            i_r{i,j}=imread(name);
            c_r{i,j}=i_r{i,j}(x_i:x_f,y_i:y_f,:);
        end
    end
end

%Reactores Continuos
if(n_rc>0 && n_s_rc>0)
    i_rc=cell(n_rc,n_s_rc);
    c_rc=cell(n_rc,n_s_rc);
    for i=1:n_rc
        for j=1:n_s_rc
            name=fullfile(dir,sprintf('RC%d/RC%d.%d.png',i,i,j));
            i_rc{i,j}=imread(name);
            c_rc{i,j}=i_rc{i,j}(x_i:x_f,y_i:y_f,:);
        end
    end
end

%Leer los datos producción y calcular la producción de biogás
T_b=readtable('Measurements.xlsx','Sheet','B','Range','A1:O17');
T_f=readtable('Measurements.xlsx','Sheet','B','Range','A19:C35');
T_bc=readtable('Measurements.xlsx','Sheet','B','Range','A37:U53');
T_r=readtable('Measurements.xlsx','Sheet','R','Range','A1:G17');
T_rc=readtable('Measurements.xlsx','Sheet','R','Range','A21:X52');
T_pH_cal=readtable('Measurements.xlsx','Sheet','Aux','Range','A1:C3');
T_N_DQO=readtable('Measurements.xlsx','Sheet','Aux','Range','A6:G14');
T_AGV=readtable('Measurements.xlsx','Sheet','Aux','Range','A17:N33');
;

%%
%Tratamiento del cromatograma
%Eliminar grises a blanco:[169 169 169] a [256 256 256]
%Eliminar vertical negra: [127 127 127] a [256 256 256]
%Eliminar base roja [255 0 0]
%Reinstaurar el azul [0 0 255]

%Muestras

```

```

if(n_s>0 && n_s_s>0)
    t_s=c_s;
    crom_s=zeros(1,1,1);
    for i=1:n_s
        for j=1:n_s_s
            [l_y,l_x,l_z]=size(t_s{i,j});
            for l=1:l_x
                blue_found=0;
                red_col=0;
                i_red=1;
                for m=1:l_y
                    %Encontrar linea vertical negra y ejes, a blanco
                    cond_1=t_s{i,j}(m,l,1)==169 &&
t_s{i,j}(m,l,2)==169 && t_s{i,j}(m,l,3)==169;
                    cond_2=t_s{i,j}(m,l,1)==127 &&
t_s{i,j}(m,l,2)==127 && t_s{i,j}(m,l,3)==127;
                    if(cond_2 && l>1 && m>1)
                        cond_2_1=t_s{i,j}(m,l+1,1)==0 &&
t_s{i,j}(m,l+1,2)==0 && t_s{i,j}(m,l+1,3)==255;
                    else
                        cond_2_1=0;
                    end
                    if(cond_1|| (cond_2 && ~cond_2_1))
                        t_s{i,j}(m,l,1)=255;
                        t_s{i,j}(m,l,2)=255;
                        t_s{i,j}(m,l,3)=255;
                    elseif(cond_2 && cond_2_1)
                        t_s{i,j}(m,l,1)=0;
                        t_s{i,j}(m,l,2)=0;
                        t_s{i,j}(m,l,3)=255;
                    end
                    cond_b=t_s{i,j}(m,l,1)==0 && t_s{i,j}(m,l,2)==0
&& t_s{i,j}(m,l,3)==255;
                    if(cond_b && blue_found==0)
                        crom_s(i,j,l)=(l_x-m);
                        blue_found=1;
                    end
                    cond_r=t_s{i,j}(m,l,1)==255 &&
t_s{i,j}(m,l,2)==0 && t_s{i,j}(m,l,3)==0;
                    if(cond_r)
                        red_col(i_red)=m;
                        i_red=i_red+1;
                    end
                end
            end
            if(blue_found==0)
                crom_s(i,j,l)=l_x-
red_col(round(length(red_col)/2));
            end
        end
    end
    save('crom_s.mat','crom_s');
end

%Botellas
if(n_b>0 && n_s_b>0)

```

```

t_b=c_b;
crom_b=zeros(1,1,1);
for i=1:n_b
    for j=1:n_s_b
        [l_y,l_x,l_z]=size(t_b{i,j});
        for l=1:l_x
            blue_found=0;
            red_col=0;
            i_red=1;
            for m=1:l_y
                %Encontrar linea vertical negra y ejes, a blanco
                cond_1=t_b{i,j}(m,l,1)==169 &&
t_b{i,j}(m,l,2)==169 && t_b{i,j}(m,l,3)==169;
                cond_2=t_b{i,j}(m,l,1)==127 &&
t_b{i,j}(m,l,2)==127 && t_b{i,j}(m,l,3)==127;
                if(cond_2 && l>1 && m>1)
                    cond_2_1=t_b{i,j}(m,l+1,1)==0 &&
t_b{i,j}(m,l+1,2)==0 && t_b{i,j}(m,l+1,3)==255;
                else
                    cond_2_1=0;
                end
                if(cond_1|| (cond_2 && ~cond_2_1))
                    t_b{i,j}(m,l,1)=255;
                    t_b{i,j}(m,l,2)=255;
                    t_b{i,j}(m,l,3)=255;
                elseif(cond_2 && cond_2_1)
                    t_b{i,j}(m,l,1)=0;
                    t_b{i,j}(m,l,2)=0;
                    t_b{i,j}(m,l,3)=255;
                end
                cond_b=t_b{i,j}(m,l,1)==0 && t_b{i,j}(m,l,2)==0
&& t_b{i,j}(m,l,3)==255;
                if(cond_b && blue_found==0)
                    crom_b(i,j,l)=(l_x-m);
                    blue_found=1;
                end
                cond_r=t_b{i,j}(m,l,1)==255 &&
t_b{i,j}(m,l,2)==0 && t_b{i,j}(m,l,3)==0;
                if(cond_r)
                    red_col(i_red)=m;
                    i_red=i_red+1;
                end
            end
            if(blue_found==0)
                crom_b(i,j,l)=l_x-
red_col(round(length(red_col)/2));
            end
        end
    end
end
end
save('crom_b.mat','crom_b');
end

%Botellas Continuas
if(n_bc>0 && n_s_bc>0)
    t_bc=c_bc;

```

```

crom_bc=zeros(1,1,1);
for i=1:n_bc
    for j=1:n_s_bc
        [l_y,l_x,l_z]=size(t_bc{i,j});
        for l=1:l_x
            blue_found=0;
            red_col=0;
            i_red=1;
            for m=1:l_y
                %Encontrar linea vertical negra y ejes, a blanco
                cond_1=t_bc{i,j}(m,l,1)==169 &&
t_bc{i,j}(m,l,2)==169 && t_bc{i,j}(m,l,3)==169;
                cond_2=t_bc{i,j}(m,l,1)==127 &&
t_bc{i,j}(m,l,2)==127 && t_bc{i,j}(m,l,3)==127;
                if(cond_2 && l>1 && m>1)
                    cond_2_1=t_bc{i,j}(m,l+1,1)==0 &&
t_bc{i,j}(m,l+1,2)==0 && t_bc{i,j}(m,l+1,3)==255;
                else
                    cond_2_1=0;
                end
                if(cond_1|| (cond_2 && ~cond_2_1))
                    t_bc{i,j}(m,l,1)=255;
                    t_bc{i,j}(m,l,2)=255;
                    t_bc{i,j}(m,l,3)=255;
                elseif(cond_2 && cond_2_1)
                    t_bc{i,j}(m,l,1)=0;
                    t_bc{i,j}(m,l,2)=0;
                    t_bc{i,j}(m,l,3)=255;
                end
                cond_b=t_bc{i,j}(m,l,1)==0 &&
t_bc{i,j}(m,l,2)==0 && t_bc{i,j}(m,l,3)==255;
                if(cond_b && blue_found==0)
                    crom_bc(i,j,l)=(l_x-m);
                    blue_found=1;
                end
                cond_r=t_bc{i,j}(m,l,1)==255 &&
t_bc{i,j}(m,l,2)==0 && t_bc{i,j}(m,l,3)==0;
                if(cond_r)
                    red_col(i_red)=m;
                    i_red=i_red+1;
                end
            end
            if(blue_found==0)
                crom_bc(i,j,l)=l_x-
red_col(round(length(red_col)/2));
            end
        end
    end
end
save('crom_bc.mat','crom_bc');
end

%Fango
if(n_f>0 && n_s_f>0)
    t_f=c_f;
    crom_f=zeros(1,1,1);

```

```

for i=1:n_f
    for j=1:n_s_f
        [l_y,l_x,l_z]=size(t_f{i,j});
        for l=1:l_x
            blue_found=0;
            red_col=0;
            i_red=1;
            for m=1:l_y
                %Encontrar linea vertical negra y ejes, a blanco
                cond_1=t_f{i,j}(m,l,1)==169 &&
t_f{i,j}(m,l,2)==169 && t_f{i,j}(m,l,3)==169;
                cond_2=t_f{i,j}(m,l,1)==127 &&
t_f{i,j}(m,l,2)==127 && t_f{i,j}(m,l,3)==127;
                if(cond_2 && l>1 && m>1)
                    cond_2_1=t_f{i,j}(m,l+1,1)==0 &&
t_f{i,j}(m,l+1,2)==0 && t_f{i,j}(m,l+1,3)==255;
                else
                    cond_2_1=0;
                end
                if(cond_1|| (cond_2 && ~cond_2_1))
                    t_f{i,j}(m,l,1)=255;
                    t_f{i,j}(m,l,2)=255;
                    t_f{i,j}(m,l,3)=255;
                elseif(cond_2 && cond_2_1)
                    t_f{i,j}(m,l,1)=0;
                    t_f{i,j}(m,l,2)=0;
                    t_f{i,j}(m,l,3)=255;
                end
                cond_b=t_f{i,j}(m,l,1)==0 && t_f{i,j}(m,l,2)==0
&& t_f{i,j}(m,l,3)==255;
                if(cond_b && blue_found==0)
                    crom_f(i,j,l)=(l_x-m);
                    blue_found=1;
                end
                cond_r=t_f{i,j}(m,l,1)==255 &&
t_f{i,j}(m,l,2)==0 && t_f{i,j}(m,l,3)==0;
                if(cond_r)
                    red_col(i_red)=m;
                    i_red=i_red+1;
                end
            end
            if(blue_found==0)
                crom_f(i,j,l)=l_x-
red_col(round(length(red_col)/2));
            end
        end
    end
end
save('crom_f.mat','crom_f');
end

%Reactor Continuo
if(n_rc>0 && n_s_rc>0)
    t_rc=c_rc;
    crom_rc=zeros(1,1,1);
    for i=1:n_rc

```

```

    for j=1:n_s_rc
        [l_y,l_x,l_z]=size(t_rc{i,j});
        for l=1:l_x
            blue_found=0;
            red_col=0;
            i_red=1;
            for m=1:l_y
                %Encontrar linea vertical negra y ejes, a blanco
                cond_1=t_rc{i,j}(m,l,1)==169 &&
t_rc{i,j}(m,l,2)==169 && t_rc{i,j}(m,l,3)==169;
                cond_2=t_rc{i,j}(m,l,1)==127 &&
t_rc{i,j}(m,l,2)==127 && t_rc{i,j}(m,l,3)==127;
                if(cond_2 && l>1 && m>1)
                    cond_2_1=t_rc{i,j}(m,l+1,1)==0 &&
t_rc{i,j}(m,l+1,2)==0 && t_rc{i,j}(m,l+1,3)==255;
                else
                    cond_2_1=0;
                end
                if(cond_1|| (cond_2 && ~cond_2_1))
                    t_rc{i,j}(m,l,1)=255;
                    t_rc{i,j}(m,l,2)=255;
                    t_rc{i,j}(m,l,3)=255;
                elseif(cond_2 && cond_2_1)
                    t_rc{i,j}(m,l,1)=0;
                    t_rc{i,j}(m,l,2)=0;
                    t_rc{i,j}(m,l,3)=255;
                end
                cond_b=t_rc{i,j}(m,l,1)==0 &&
t_rc{i,j}(m,l,2)==0 && t_rc{i,j}(m,l,3)==255;
                if(cond_b && blue_found==0)
                    crom_rc(i,j,l)=(l_x-m);
                    blue_found=1;
                end
                cond_r=t_rc{i,j}(m,l,1)==255 &&
t_rc{i,j}(m,l,2)==0 && t_rc{i,j}(m,l,3)==0;
                if(cond_r)
                    red_col(i_red)=m;
                    i_red=i_red+1;
                end
            end
            if(blue_found==0)
                crom_rc(i,j,l)=l_x-
red_col(round(length(red_col)/2));
            end
        end
    end
    end
    save('crom_rc.mat','crom_rc');
end

%Reactor
if(n_r>0 && n_s_r>0)
    t_r=c_r;
    crom_r=zeros(1,1,1);
    for i=1:n_r
        for j=1:n_s_r

```

```

        [l_y,l_x,l_z]=size(t_r{i,j});
        for l=1:l_x
            blue_found=0;
            red_col=0;
            i_red=1;
            for m=1:l_y
                %Encontrar linea vertical negra y ejes, a blanco
                cond_1=t_r{i,j}(m,l,1)==169 &&
t_r{i,j}(m,l,2)==169 && t_r{i,j}(m,l,3)==169;
                cond_2=t_r{i,j}(m,l,1)==127 &&
t_r{i,j}(m,l,2)==127 && t_r{i,j}(m,l,3)==127;
                if(cond_2 && l>1 && m>1)
                    cond_2_1=t_r{i,j}(m,l+1,1)==0 &&
t_r{i,j}(m,l+1,2)==0 && t_r{i,j}(m,l+1,3)==255;
                else
                    cond_2_1=0;
                end
                if(cond_1|| (cond_2 && ~cond_2_1))
                    t_r{i,j}(m,l,1)=255;
                    t_r{i,j}(m,l,2)=255;
                    t_r{i,j}(m,l,3)=255;
                elseif(cond_2 && cond_2_1)
                    t_r{i,j}(m,l,1)=0;
                    t_r{i,j}(m,l,2)=0;
                    t_r{i,j}(m,l,3)=255;
                end
                cond_b=t_r{i,j}(m,l,1)==0 && t_r{i,j}(m,l,2)==0
&& t_r{i,j}(m,l,3)==255;
                if(cond_b && blue_found==0)
                    crom_r(i,j,l)=(l_x-m);
                    blue_found=1;
                end
                cond_r=t_r{i,j}(m,l,1)==255 &&
t_r{i,j}(m,l,2)==0 && t_r{i,j}(m,l,3)==0;
                if(cond_r)
                    red_col(i_red)=m;
                    i_red=i_red+1;
                end
            end
            if(blue_found==0)
                crom_r(i,j,l)=l_x-
red_col(round(length(red_col)/2));
            end
        end
    end
end
save('crom_r.mat','crom_r');
end
%%
%Cálculo de linea base de integracion y agregados
if(n_s>0 && n_s_s>0)
    [l_1, l_2, l_3]=size(crom_s);
    for i=1:n_s
        for j=1:n_s_s
            base_s(i,j)=round(mode(crom_s(i,j,b_start:b_end)));
            for k=1:l_3

```

```

        area_s(i,j,k)=crom_s(i,j,k)-base_s(i,j);
    end
    ch4_s(i,j)=max(0,sum(area_s(i,j,ch4_start:ch4_end)));
    h2_s(i,j)=max(0,sum(area_s(i,j,h2_start:h2_end)));
    h2s_s(i,j)=max(0,sum(area_s(i,j,h2s_start:h2s_end)));

res_s(i,j)=max(0,sum(area_s(i,j,res_1_start:res_1_end))+sum(area_s(i
,j,res_2_start:res_2_end)));
    total_s(i,j)=ch4_s(i,j)+h2_s(i,j)+h2s_s(i,j)+res_s(i,j);
    results_s(i,j,1:4)=[ch4_s(i,j)/total_s(i,j)
h2_s(i,j)/total_s(i,j) h2s_s(i,j)/total_s(i,j)
res_s(i,j)/total_s(i,j)];
    end
end
save('comp_s.mat','results_s');
end

if(n_b>0 && n_s_b>0)
    [l_1, l_2, l_3]=size(crom_b);
    for i=1:n_b
        for j=1:n_s_b
            base_b(i,j)=round(mode(crom_b(i,j,b_start:b_end)));
            for k=1:l_3
                area_b(i,j,k)=crom_b(i,j,k)-base_b(i,j);
            end
            ch4_b(i,j)=max(0,sum(area_b(i,j,ch4_start:ch4_end)));
            h2_b(i,j)=max(0,sum(area_b(i,j,h2_start:h2_end)));
            h2s_b(i,j)=max(0,sum(area_b(i,j,h2s_start:h2s_end)));

res_b(i,j)=max(0,sum(area_b(i,j,res_1_start:res_1_end))+sum(area_b(i
,j,res_2_start:res_2_end)));
            total_b(i,j)=ch4_b(i,j)+h2_b(i,j)+h2s_b(i,j)+res_b(i,j);
            results_b(i,j,1:4)=[ch4_b(i,j)/total_b(i,j)
h2_b(i,j)/total_b(i,j) h2s_b(i,j)/total_b(i,j)
res_b(i,j)/total_b(i,j)];
        end
    end
end

if(n_bc>0 && n_s_bc>0)
    [l_1, l_2, l_3]=size(crom_bc);
    for i=1:n_bc
        for j=1:n_s_bc
            base_bc(i,j)=round(mode(crom_bc(i,j,b_start:b_end)));
            for k=1:l_3
                area_bc(i,j,k)=crom_bc(i,j,k)-base_bc(i,j);
            end
            ch4_bc(i,j)=max(0,sum(area_bc(i,j,ch4_start:ch4_end)));
            h2_bc(i,j)=max(0,sum(area_bc(i,j,h2_start:h2_end)));
            h2s_bc(i,j)=max(0,sum(area_bc(i,j,h2s_start:h2s_end)));

res_bc(i,j)=max(0,sum(area_bc(i,j,res_1_start:res_1_end))+sum(area_b
c(i,j,res_2_start:res_2_end)));

total_bc(i,j)=ch4_bc(i,j)+h2_bc(i,j)+h2s_bc(i,j)+res_bc(i,j);

```

```

                results_bc(i,j,1:4)=[ch4_bc(i,j)/total_bc(i,j)
h2_bc(i,j)/total_bc(i,j) h2s_bc(i,j)/total_bc(i,j)
res_bc(i,j)/total_bc(i,j)];
            end
        end
    end

    if(n_f>0 && n_s_f>0)
        [l_1, l_2, l_3]=size(crom_f);
        for i=1:n_f
            for j=1:n_s_f
                base_f(i,j)=round(mode(crom_f(i,j,b_start:b_end)));
                for k=1:l_3
                    area_f(i,j,k)=crom_f(i,j,k)-base_f(i,j);
                end
                ch4_f(i,j)=max(0,sum(area_f(i,j,ch4_start:ch4_end)));
                h2_f(i,j)=max(0,sum(area_f(i,j,h2_start:h2_end)));
                h2s_f(i,j)=max(0,sum(area_f(i,j,h2s_start:h2s_end)));

                res_f(i,j)=max(0,sum(area_f(i,j,res_1_start:res_1_end))+sum(area_f(i
,j,res_2_start:res_2_end)));
                total_f(i,j)=ch4_f(i,j)+h2_f(i,j)+h2s_f(i,j)+res_f(i,j);
                results_f(i,j,1:4)=[ch4_f(i,j)/total_f(i,j)
h2_f(i,j)/total_f(i,j) h2s_f(i,j)/total_f(i,j)
res_f(i,j)/total_f(i,j)];
            end
        end
    end

    if(n_r>0 && n_s_r>0)
        [l_1, l_2, l_3]=size(crom_r);
        for i=1:n_r
            for j=1:n_s_r
                base_r(i,j)=round(mode(crom_r(i,j,b_start:b_end)));
                for k=1:l_3
                    area_r(i,j,k)=crom_r(i,j,k)-base_r(i,j);
                end
                ch4_r(i,j)=max(0,sum(area_r(i,j,ch4_start:ch4_end)));
                h2_r(i,j)=max(0,sum(area_r(i,j,h2_start:h2_end)));
                h2s_r(i,j)=max(0,sum(area_r(i,j,h2s_start:h2s_end)));

                res_r(i,j)=max(0,sum(area_r(i,j,res_1_start:res_1_end))+sum(area_r(i
,j,res_2_start:res_2_end)));
                total_r(i,j)=ch4_r(i,j)+h2_r(i,j)+h2s_r(i,j)+res_r(i,j);
                results_r(i,j,1:4)=[ch4_r(i,j)/total_r(i,j)
h2_r(i,j)/total_r(i,j) h2s_r(i,j)/total_r(i,j)
res_r(i,j)/total_r(i,j)];
            end
        end
    end

    if(n_rc>0 && n_s_rc>0)
        [l_1, l_2, l_3]=size(crom_rc);
        for i=1:n_rc
            for j=1:n_s_rc
                base_rc(i,j)=round(mode(crom_rc(i,j,b_start:b_end)));

```

```

        for k=1:l_3
            area_rc(i,j,k)=crom_rc(i,j,k)-base_rc(i,j);
        end
        ch4_rc(i,j)=max(0,sum(area_rc(i,j,ch4_start:ch4_end)));
        h2_rc(i,j)=max(0,sum(area_rc(i,j,h2_start:h2_end)));
        h2s_rc(i,j)=max(0,sum(area_rc(i,j,h2s_start:h2s_end)));

res_rc(i,j)=max(0,sum(area_rc(i,j,res_1_start:res_1_end))+sum(area_r
c(i,j,res_2_start:res_2_end)));

total_rc(i,j)=ch4_rc(i,j)+h2_rc(i,j)+h2s_rc(i,j)+res_rc(i,j);
    results_rc(i,j,1:4)=[ch4_rc(i,j)/total_rc(i,j)
h2_rc(i,j)/total_rc(i,j) h2s_rc(i,j)/total_rc(i,j)
res_rc(i,j)/total_rc(i,j)];
    end
end
if(n_rc>0 && n_s_rc>0)
[l_1, l_2, l_3]=size(crom_rc);
for i=1:n_rc
    for j=1:n_s_rc
        base_rc(i,j)=round(mode(crom_rc(i,j,b_start:b_end)));
        for k=1:l_3
            area_rc(i,j,k)=crom_rc(i,j,k)-base_rc(i,j);
        end
        ch4_rc(i,j)=max(0,sum(area_rc(i,j,ch4_start:ch4_end)));
        h2_rc(i,j)=max(0,sum(area_rc(i,j,h2_start:h2_end)));
        h2s_rc(i,j)=max(0,sum(area_rc(i,j,h2s_start:h2s_end)));

res_rc(i,j)=max(0,sum(area_rc(i,j,res_1_start:res_1_end))+sum(area_r
c(i,j,res_2_start:res_2_end)));

total_rc(i,j)=ch4_rc(i,j)+h2_rc(i,j)+h2s_rc(i,j)+res_rc(i,j)
    results_rc(i,j,1:4)=[ch4_rc(i,j)/total_rc(i,j)
h2_rc(i,j)/total_rc(i,j) h2s_rc(i,j)/total_rc(i,j)
res_rc(i,j)/total_rc(i,j)];
    end
end
end
end

if(n_b>0 && n_s_b>0)
    for i=1:n_b
        for j=1:n_s_b
            biogas_b(i,j)=T_b{j+1,i+1}*Conv_p_v/V_fango_b;
            prod_b(i,j,1)=biogas_b(i,j)*results_b(i,j,1);
            prod_b(i,j,2)=biogas_b(i,j)*results_b(i,j,2);
            prod_b(i,j,3)=biogas_b(i,j)*results_b(i,j,3);
            prod_b(i,j,4)=biogas_b(i,j)*results_b(i,j,4);
        end
    end
    save('comp_b.mat','results_b','prod_b','biogas_b');
end

if(n_f>0 && n_s_f>0)
    for i=1:n_f
        for j=1:n_s_f

```

```

        biogas_f(i,j)=T_f{j+1,i+1}*Conv_p_v/V_fango_f;
        prod_f(i,j,1)=biogas_f(i,j)*results_f(i,j,1);
        prod_f(i,j,2)=biogas_f(i,j)*results_f(i,j,2);
        prod_f(i,j,3)=biogas_f(i,j)*results_f(i,j,3);
        prod_f(i,j,4)=biogas_f(i,j)*results_f(i,j,4);
    end
end
save('comp_f.mat','results_f','prod_f','biogas_f');
end

if(n_bc>0 && n_s_bc>0)
    for i=1:n_bc
        for j=1:n_s_bc
            biogas_bc(i,j)=T_bc{j+1,i+1}*Conv_p_v/V_fango_bc;
            prod_bc(i,j,1)=biogas_bc(i,j)*results_bc(i,j,1);
            prod_bc(i,j,2)=biogas_bc(i,j)*results_bc(i,j,2);
            prod_bc(i,j,3)=biogas_bc(i,j)*results_bc(i,j,3);
            prod_bc(i,j,4)=biogas_bc(i,j)*results_bc(i,j,4);
        end
    end
    save('comp_bc.mat','results_bc','prod_bc','biogas_bc');
end

if(n_r>0 && n_s_r>0)
    for i=1:n_r
        for j=1:n_s_r
            biogas_r(i,j)=T_r{j+1,i+1}/1000;
            prod_r(i,j,1)=biogas_r(i,j)*results_r(i,j,1);
            prod_r(i,j,2)=biogas_r(i,j)*results_r(i,j,2);
            prod_r(i,j,3)=biogas_r(i,j)*results_r(i,j,3);
            prod_r(i,j,4)=biogas_r(i,j)*results_r(i,j,4);
        end
    end
    save('comp_r.mat','results_r','prod_r','biogas_r');
end

if(n_rc>0 && n_s_rc>0)
    for i=1:n_rc
        for j=1:n_s_rc
            biogas_rc(i,j)=T_rc{j+1,i+1}/1000;
            prod_rc(i,j,1)=biogas_rc(i,j)*results_rc(i,j,1);
            prod_rc(i,j,2)=biogas_rc(i,j)*results_rc(i,j,2);
            prod_rc(i,j,3)=biogas_rc(i,j)*results_rc(i,j,3);
            prod_rc(i,j,4)=biogas_rc(i,j)*results_rc(i,j,4);
        end
    end
    save('comp_rc.mat','results_rc','prod_rc','biogas_rc');
end

end

%%
%Tests estadísticos
%T-test de las botellas día a día
%Biogas generado al día y anova
%ANOVA de todos los datos
%Construcción de los grupos para ANOVAs
for i=1:n_b

```

```

for j=1:n_s_b
    G_anova_d(i+(n_b*(j-1)),1)=j;
    if(i<=n_b_np)
        G_anova_b_np_d(i+(n_b_np*(j-1)),1)=j;
    end
    if (i<=(n_b-n_b_np))
        G_anova_g(i+(n_b*(j-1)),1)="B";
        G_anova_b_d(i+((n_b-n_b_np)*(j-1)),1)=j;
        G_anova_g_d(i+(n_b*(j-
1)),1)=join(["B",num2str((j))],"_");
        elseif (i<=n_b)
            G_anova_g(i+(n_b*(j-1)),1)="NP";
            G_anova_g_d(i+(n_b*(j-
1)),1)=join(["NP",num2str((j))],"_");
        end
    end
end
end
%%

%Test a hacer: Lillefors, t_Student y F_Snedecor. Se ha el de
Lillefors
% por que comprueba si la muestra proviene de una normal sin conocer
mu o
%sigma
%Para comprobar la normalidad tambien usamos Jarque-Bera y Anderson
Darling

%Biogas
Biogas_b=biogas_b(:);
B_b=biogas_b(1:(n_b-n_b_np),:);
B_b=B_b(:);
B_b_np=biogas_b((n_b-n_b_np+1):n_b,:);
B_b_np=B_b_np(:);
%ANOVA por nanoparticulas
[p,tbl,stats]=anoval(Biogas_b,G_anova_g,'varname',{'Grupo_B'});
p_B_g=p;
tbl_B_g=tbl;
stats_B_g=stats;
h_B_1=figure;
multcompare(stats_B_g);
%ANOVA por días
[p,tbl,stats]=anoval(Biogas_b,G_anova_d,'varname',{'Dia_B'});
p_B_d=p;
tbl_B_d=tbl;
stats_B_d=stats;
h_B_2=figure;
multcompare(stats_B_d);
%ANOVA1 por grupos y días
[p,tbl,stats]=anoval(Biogas_b,G_anova_g_d,'varname',{'GrupoyDia_B'})
;
p_B_gd=p;
tbl_B_gd=tbl;
stats_B_gd=stats;
h_B_3=figure;
multcompare(stats_B_gd);
%ANOVA n por grupos y días

```

```

[p,tbl,stats]=anovan(Biogas_b,{G_anova_g
G_anova_d},'model','interaction','varnames',{'Dia_B','Grupo_B'});
p_B_g_d=p;
tbl_B_g_d=tbl;
stats_B_g_d=stats;
h_B_4=figure;
multcompare(stats_B_d);
%ANOVA de B por día
[p,tbl,stats]=anoval(B_b,G_anova_b_d,'varname',{'Dia_B_b'});
p_B_b_d=p;
tbl_B_b_d=tbl;
stats_B_b_d=stats;
h_B_5=figure;
multcompare(stats_B_b_d);
%ANOVA de B_NP por día
[p,tbl,stats]=anoval(B_b_np,G_anova_b_np_d,'varname',{'Dia_B_b_np'})
;
p_B_b_np_d=p;
tbl_B_b_d=tbl;
stats_B_b_np_d=stats;
h_B_6=figure;
multcompare(stats_B_b_np_d);

%Test de Normalidad
for i=1:n_s_b
    b_norm=biogas_b(1:(n_b-n_b_np),i);
    b_np_norm=biogas_b((n_b-n_b_np+1):n_b,i);

    %JBtest
    [h,p,stats,ci]=jbtest(b_norm);
    h_jbtest_b(i)=h;
    p_jbtest_b(i)=p;
    stats_jbtest_b{i}=stats;
    ci_jbtest_b(i,:)=ci;

    [h,p,stats,ci]=jbtest(b_np_norm);
    h_jbtest_b_np(i)=h;
    p_jbtest_b_np(i)=p;
    stats_jbtest_b_np{i}=stats;
    ci_jbtest_b_np(i,:)=ci;

    %Anderson-Darling
    [h,p,stats,ci]=adtest(b_norm);
    h_adtest_b(i)=h;
    p_adtest_b(i)=p;
    stats_adtest_b{i}=stats;
    ci_adtest_b(i,:)=ci;

    [h,p,stats,ci]=adtest(b_np_norm);
    h_adtest_b_np(i)=h;
    p_adtest_b_np(i)=p;
    stats_adtest_b_np{i}=stats;
    ci_adtest_b_np(i,:)=ci;

    %Lillefors
    [h,p,stats,ci]=lillietest(b_norm);

```

```

h_lillietest_b(i)=h;
p_lillietest_b(i)=p;
stats_lillietest_b{i}=stats;
ci_lillietest_b(i,:)=ci;

[h,p,stats,ci]=lillietest(b_np_norm);
h_lillietest_b_np(i)=h;
p_lillietest_b_np(i)=p;
stats_lillietest_b_np{i}=stats;
ci_lillietest_b_np(i,:)=ci;

%Ttest
[h,p,ci,stats]=ttest2(b_norm,b_np_norm);
h_ttest_biogas(i)=h;
p_ttest_biogas(i)=p;
ci_ttest_biogas(i,:)=ci(:);
stats_ttest_biogas{i}=stats;
mean_biogas(i,1)=mean(b_norm(:));
mean_biogas(i,2)=mean(b_np_norm(:));

%Ftest
std_biogas(i,1)=sqrt(var(b_norm(:)));
std_biogas(i,2)=sqrt(var(b_np_norm(:)));
[h,p,ci,stats]=vartest2(b_norm,b_np_norm);
h_ftest_biogas(i)=h;
p_ftest_biogas(i)=p;
ci_ftest_biogas(i,:)=ci(:);
stats_ftest_biogas{i}=stats;
end

%Composicion CH4
Comp_ch4=results_b(:, :, 1);
Comp_ch4=Comp_ch4(:);
Comp_ch4_b=results_b(1:(n_b-n_b_np), :, 1);
Comp_ch4_b=Comp_ch4_b(:);
Comp_ch4_b_np=results_b((n_b-n_b_np+1):n_b, :, 1);
Comp_ch4_b_np=Comp_ch4_b_np(:);

%ANOVA por nanoparticulas
[p,tbl,stats]=anoval(Comp_ch4,G_anova_g,'varname',{'Grupo_C_ch4'});
p_Comp_ch4_g=p;
tbl_Comp_ch4_g=tbl;
stats_Comp_ch4_g=stats;
h_Comp_ch4_1=figure;
multcompare(stats_Comp_ch4_g);
%ANOVA por días
[p,tbl,stats]=anoval(Comp_ch4,G_anova_d,'varname',{'Dia_C_ch4'});
p_Comp_ch4_d=p;
tbl_Comp_ch4_d=tbl;
stats_Comp_ch4_d=stats;
h_Comp_ch4_2=figure;
multcompare(stats_Comp_ch4_d);
%ANOVA1 por grupos y días
[p,tbl,stats]=anoval(Comp_ch4,G_anova_g_d,'varname',{'GrupoyDia_C_ch4'});
p_Comp_ch4_gd=p;

```

```

tbl_Comp_ch4_gd=tbl;
stats_Comp_ch4_gd=stats;
h_Comp_ch4_3=figure;
multcompare(stats_Comp_ch4_gd);
%ANOVA por grupos y días
[p,tbl,stats]=anovan(Comp_ch4,{G_anova_g
G_anova_d},'model','interaction','varnames',{'Dia_C_ch4','Grupo_C_ch
4'});
p_Comp_ch4_g_d=p;
tbl_Comp_ch4_g_d=tbl;
stats_Comp_ch4_g_d=stats;
h_Comp_ch4_4=figure;
multcompare(stats_Comp_ch4_d);
%ANOVA de Comp_ch4 B por día
[p,tbl,stats]=anoval(Comp_ch4_b,G_anova_b_d,'varname',{'Dia_C_ch4_b'
});
p_Comp_ch4_b_d=p;
tbl_Comp_ch4_b_d=tbl;
stats_Comp_ch4_b_d=stats;
h_Comp_ch4_5=figure;
multcompare(stats_Comp_ch4_b_d);
%ANOVA de B_NP por día
[p,tbl,stats]=anoval(Comp_ch4_b_np,G_anova_b_np_d,'varname',{'Dia_C_
ch4_b_np'});
p_Comp_ch4_b_np_d=p;
tbl_Comp_ch4_b_d=tbl;
stats_Comp_ch4_b_np_d=stats;
h_Comp_ch4_6=figure;
multcompare(stats_Comp_ch4_b_np_d);

%Test de normalidad
for i=1:n_s_b
    comp_ch4_b=results_b(1:(n_b-n_b_np),i,1);
    comp_ch4_b_np=results_b((n_b-n_b_np+1):n_b,i,1);

    %JBtest
    [h,p,stats,ci]=jbstest(comp_ch4_b);
    h_jbstest_comp_b_ch4_b(i)=h;
    p_jbstest_comp_b_ch4_b(i)=p;
    stats_jbstest_comp_b_ch4_b{i}=stats;
    ci_jbstest_comp_b_ch4_b(i,:)=ci;

    [h,p,stats,ci]=jbstest(comp_ch4_b_np);
    h_jbstest_comp_b_ch4_b_np(i)=h;
    p_jbstest_comp_b_ch4_b_np(i)=p;
    stats_jbstest_comp_b_ch4_b_np{i}=stats;
    ci_jbstest_comp_b_ch4_b_np(i,:)=ci;

    %Anderson-Darling
    [h,p,stats,ci]=adtest(comp_ch4_b);
    h_adtest_comp_b_ch4_b(i)=h;
    p_adtest_comp_b_ch4_b(i)=p;
    stats_adtest_comp_b_ch4_b{i}=stats;
    ci_adtest_comp_b_ch4_b(i,:)=ci;

    [h,p,stats,ci]=adtest(comp_ch4_b_np);

```

```

h_adtest_comp_b_ch4_b_np(i)=h;
p_adtest_comp_b_ch4_b_np(i)=p;
stats_adtest_comp_b_ch4_b_np{i}=stats;
ci_adtest_comp_b_ch4_b_np(i,:)=ci;

%Lillefors
[h,p,stats,ci]=lillietest(comp_ch4_b);
h_lillietest_comp_b_ch4_b(i)=h;
p_lillietest_comp_b_ch4_b(i)=p;
stats_lillietest_comp_b_ch4_b{i}=stats;
ci_lillietest_comp_b_ch4_b(i,:)=ci;

[h,p,stats,ci]=lillietest(comp_ch4_b_np);
h_lillietest_comp_b_ch4_b_np(i)=h;
p_lillietest_comp_b_ch4_b_np(i)=p;
stats_lillietest_comp_b_ch4_b_np{i}=stats;
ci_lillietest_comp_b_ch4_b_np(i,:)=ci;

[h,p,ci,stats]=ttest2(comp_ch4_b,comp_ch4_b_np);
h_ttest_comp_b_ch4(i)=h;
p_ttest_comp_b_ch4(i)=p;
ci_ttest_comp_b_ch4(i,:)=ci(:);
stats_ttest_comp_b_ch4{i}=stats;
mean_comp_b_ch4(i,1)=mean(comp_ch4_b(:));
mean_comp_b_ch4(i,2)=mean(comp_ch4_b_np(:));

std_comp_b_ch4(i,1)=sqrt(var(comp_ch4_b(:)));
std_comp_b_ch4(i,2)=sqrt(var(comp_ch4_b_np(:)));
[h,p,ci,stats]=vartest2(comp_ch4_b,comp_ch4_b_np);
h_ftest_comp_b_ch4(i)=h;
p_ftest_comp_b_ch4(i)=p;
ci_ftest_comp_b_ch4(i,:)=ci(:);
stats_ftest_comp_b_ch4{i}=stats;
end

%Composición H2
Comp_h2=results_b(:, :, 2);
Comp_h2=Comp_h2(:);
Comp_h2_b=results_b(1:(n_b-n_b_np), :, 2);
Comp_h2_b=Comp_h2_b(:);
Comp_h2_b_np=results_b((n_b-n_b_np+1):n_b, :, 2);
Comp_h2_b_np=Comp_h2_b_np(:);

%ANOVA por nanoparticulas
[p,tbl,stats]=anoval(Comp_h2,G_anova_g,'varname',{'Grupo_C_h2'});
p_Comp_h2_g=p;
tbl_Comp_h2_g=tbl;
stats_Comp_h2_g=stats;
h_Comp_h2_1=figure;
multcompare(stats_Comp_h2_g);
%ANOVA por días
[p,tbl,stats]=anoval(Comp_h2,G_anova_d,'varname',{'Dia_C_h2'});
p_Comp_h2_d=p;
tbl_Comp_h2_d=tbl;
stats_Comp_h2_d=stats;

```

```

h_Comp_h2_2=figure;
multcompare(stats_Comp_h2_d);
%ANOVA1 por grupos y días
[p,tbl,stats]=anoval(Comp_h2,G_anova_g_d,'varname',{'GrupoyDia_C_h2'
});
p_Comp_h2_gd=p;
tbl_Comp_h2_gd=tbl;
stats_Comp_h2_gd=stats;
h_Comp_h2_3=figure;
multcompare(stats_Comp_h2_gd);
%ANOVA n por grupos y días
[p,tbl,stats]=anovan(Comp_h2,{G_anova_g
G_anova_d},'model','interaction','varnames',{'Dia_C_h2','Grupo_C_h2'
});
p_Comp_h2_g_d=p;
tbl_Comp_h2_g_d=tbl;
stats_Comp_h2_g_d=stats;
h_Comp_h2_4=figure;
multcompare(stats_Comp_h2_d);
%ANOVA de Comp_h2 B por día
[p,tbl,stats]=anoval(Comp_h2_b,G_anova_b_d,'varname',{'Dia_C_h2_b'})
;
p_Comp_h2_b_d=p;
tbl_Comp_h2_b_d=tbl;
stats_Comp_h2_b_d=stats;
h_Comp_h2_5=figure;
multcompare(stats_Comp_h2_b_d);
%ANOVA de B_NP por día
[p,tbl,stats]=anoval(Comp_h2_b_np,G_anova_b_np_d,'varname',{'Dia_C_h
2_b_np'});
p_Comp_h2_b_np_d=p;
tbl_Comp_h2_b_d=tbl;
stats_Comp_h2_b_np_d=stats;
h_Comp_h2_6=figure;
multcompare(stats_Comp_h2_b_np_d);

%Test de Normalidad
for i=1:n_s_b
    comp_h2_b=results_b(1:(n_b-n_b_np),i,2);
    comp_h2_b_np=results_b((n_b-n_b_np-1):n_b,i,2);

    %JBtest
    [h,p,stats,ci]=jbtest(comp_h2_b);
    h_jbtest_comp_b_h2_b(i)=h;
    p_jbtest_comp_b_h2_b(i)=p;
    stats_jbtest_comp_b_h2_b{i}=stats;
    ci_jbtest_comp_b_h2_b(i,:)=ci;

    [h,p,stats,ci]=jbtest(comp_h2_b_np);
    h_jbtest_comp_b_h2_b_np(i)=h;
    p_jbtest_comp_b_h2_b_np(i)=p;
    stats_jbtest_comp_b_h2_b_np{i}=stats;
    ci_jbtest_comp_b_h2__np(i,:)=ci;

    %Anderson-Darling
    [h,p,stats,ci]=adtest(comp_h2_b);

```

```

h_adtest_comp_b_h2_b(i)=h;
p_adtest_comp_b_h2_b(i)=p;
stats_adtest_comp_b_h2_b{i}=stats;
ci_adtest_comp_b_h2_b(i,:)=ci;

[h,p,stats,ci]=adtest(comp_h2_b_np);
h_adtest_comp_b_h2_b_np(i)=h;
p_adtest_comp_b_h2_b_np(i)=p;
stats_adtest_comp_b_h2_b_np{i}=stats;
ci_adtest_comp_b_h2_b_np(i,:)=ci;

%Lillefors
[h,p,stats,ci]=lillietest(comp_ch4_b);
h_lillietest_comp_b_h2_b(i)=h;
p_lillietest_comp_b_h2_b(i)=p;
stats_lillietest_comp_b_h2_b{i}=stats;
ci_lillietest_comp_b_h2_b(i,:)=ci;

[h,p,stats,ci]=lillietest(comp_h2_b_np);
h_lillietest_comp_b_h2_b_np(i)=h;
p_lillietest_comp_b_h2_b_np(i)=p;
stats_lillietest_comp_b_h2_b_np{i}=stats;
ci_lillietest_comp_b_h2_b_np(i,:)=ci;

[h,p,ci,stats]=ttest2(comp_h2_b,comp_h2_b_np);
h_ttest_comp_b_h2(i)=h;
p_ttest_comp_b_h2(i)=p;
ci_ttest_comp_b_h2(i,:)=ci(:);
stats_ttest_comp_b_h2{i}=stats;
mean_comp_b_h2(i,1)=mean(comp_h2_b(:));
mean_comp_b_h2(i,2)=mean(comp_h2_b_np(:));

std_comp_b_h2(i,1)=sqrt(var(comp_h2_b(:)));
std_comp_b_h2(i,2)=sqrt(var(comp_h2_b_np(:)));
[h,p,ci,stats]=vartest2(comp_h2_b,comp_h2_b_np);
h_ftest_comp_b_h2(i)=h;
p_ftest_comp_b_h2(i)=p;
ci_ftest_comp_b_h2(i,:)=ci(:);
stats_ftest_comp_b_h2{i}=stats;
end

%Composición H2S
Comp_h2s=results_b(:, :, 3);
Comp_h2s=Comp_h2s(:);
Comp_h2s_b=results_b(1:(n_b-n_b_np), :, 3);
Comp_h2s_b=Comp_h2s_b(:);
Comp_h2s_b_np=results_b((n_b-n_b_np+1):n_b, :, 3);
Comp_h2s_b_np=Comp_h2s_b_np(:);

%ANOVA por nanoparticulas
[p,tbl,stats]=anova1(Comp_h2s,G_anova_g,'varname',{'Grupo_C_h2s'});
p_Comp_h2s_g=p;
tbl_Comp_h2s_g=tbl;
stats_Comp_h2s_g=stats;
h_Comp_h2s_1=figure;

```

```

multcompare(stats_Comp_h2s_g);
%ANOVA por días
[p,tbl,stats]=anoval(Comp_h2s,G_anova_d,'varname',{'Dia_C_h2s'});
p_Comp_h2s_d=p;
tbl_Comp_h2s_d=tbl;
stats_Comp_h2s_d=stats;
h_Comp_h2s_2=figure;
multcompare(stats_Comp_h2s_d);
%ANOVA1 por grupos y días
[p,tbl,stats]=anoval(Comp_h2s,G_anova_g_d,'varname',{'GrupoyDia_C_h2s'});
p_Comp_h2s_gd=p;
tbl_Comp_h2s_gd=tbl;
stats_Comp_h2s_gd=stats;
h_Comp_h2s_3=figure;
multcompare(stats_Comp_h2s_gd);
%ANOVA n por grupos y días
[p,tbl,stats]=anovan(Comp_h2s,{G_anova_g
G_anova_d},'model','interaction','varnames',{'Dia_C_h2s','Grupo_C_h2s'});
p_Comp_h2s_g_d=p;
tbl_Comp_h2s_g_d=tbl;
stats_Comp_h2s_g_d=stats;
h_Comp_h2s_4=figure;
multcompare(stats_Comp_h2s_d);
%ANOVA de Comp_h2s B por día
[p,tbl,stats]=anoval(Comp_h2s_b,G_anova_b_d,'varname',{'Dia_C_h2s_b'});
p_Comp_h2s_b_d=p;
tbl_Comp_h2s_b_d=tbl;
stats_Comp_h2s_b_d=stats;
h_Comp_h2s_5=figure;
multcompare(stats_Comp_h2s_b_d);
%ANOVA de B_NP por día
[p,tbl,stats]=anoval(Comp_h2s_b_np,G_anova_b_np_d,'varname',{'Dia_C_h2s_b_np'});
p_Comp_h2s_b_np_d=p;
tbl_Comp_h2s_b_np_d=tbl;
stats_Comp_h2s_b_np_d=stats;
h_Comp_h2s_6=figure;
multcompare(stats_Comp_h2s_b_np_d);

%Test de Normalidad
for i=1:n_s_b
    comp_h2s_b=results_b(1:(n_b-n_b_np),i,3);
    comp_h2s_b_np=results_b((n_b-n_b_np+1):n_b,i,3);

    %JBtest
    [h,p,stats,ci]=jbtest(comp_h2s_b);
    h_jbtest_comp_b_h2s_b(i)=h;
    p_jbtest_comp_b_h2s_b(i)=p;
    stats_jbtest_comp_b_h2s_b{i}=stats;
    ci_jbtest_comp_b_h2s_b(i,:)=ci;

    [h,p,stats,ci]=jbtest(comp_h2s_b_np);
    h_jbtest_comp_b_h2s_b_np(i)=h;

```

```

p_jbtest_comp_b_h2s_b_np(i)=p;
stats_jbtest_comp_b_h2s_b_np{i}=stats;
ci_jbtest_comp_b_h2s_b_np(i,:)=ci;

%Anderson-Darling
[h,p,stats,ci]=adtest(comp_h2s_b);
h_adtest_comp_b_h2s_b(i)=h;
p_adtest_comp_b_h2s_b(i)=p;
stats_adtest_comp_b_h2s_b{i}=stats;
ci_adtest_comp_b_h2s_b(i,:)=ci;

[h,p,stats,ci]=adtest(comp_h2s_b_np);
h_adtest_comp_b_h2s_b_np(i)=h;
p_adtest_comp_b_h2s_b_np(i)=p;
stats_adtest_comp_b_h2s_b_np{i}=stats;
ci_adtest_comp_b_h2s_b_np(i,:)=ci;

%Lillefors
[h,p,stats,ci]=lillietest(comp_ch4_b);
h_lillietest_comp_b_h2s_b(i)=h;
p_lillietest_comp_b_h2s_b(i)=p;
stats_lillietest_comp_b_h2s_b{i}=stats;
ci_lillietest_comp_b_h2s_b(i,:)=ci;

[h,p,stats,ci]=lillietest(comp_h2s_b_np);
h_lillietest_comp_b_h2s_b_np(i)=h;
p_lillietest_comp_b_h2s_b_np(i)=p;
stats_lillietest_comp_b_h2s_b_np{i}=stats;
ci_lillietest_comp_b_h2s_b_np(i,:)=ci;

[h,p,ci,stats]=ttest2(comp_h2s_b,comp_h2s_b_np);
h_ttest_comp_b_h2s(i)=h;
p_ttest_comp_b_h2s(i)=p;
ci_ttest_comp_b_h2s(i,:)=ci(:);
stats_ttest_comp_b_h2s{i}=stats;
mean_comp_b_h2s(i,1)=mean(comp_h2s_b(:));
mean_comp_b_h2s(i,2)=mean(comp_h2s_b_np(:));

std_comp_b_h2s(i,1)=sqrt(var(comp_h2s_b(:)));
std_comp_b_h2s(i,2)=sqrt(var(comp_h2s_b_np(:)));
[h,p,ci,stats]=vartest2(comp_h2s_b,comp_h2s_b_np);
h_ftest_comp_b_h2s(i)=h;
p_ftest_comp_b_h2s(i)=p;
ci_ftest_comp_b_h2s(i,:)=ci(:);
stats_ftest_comp_b_h2s{i}=stats;
end

%Composición Residuos
Comp_res=results_b(:, :, 4);
Comp_res=Comp_res(:);
Comp_res_b=results_b(1:(n_b-n_b_np), :, 4);
Comp_res_b=Comp_res_b(:);
Comp_res_b_np=results_b((n_b-n_b_np+1):n_b, :, 4);
Comp_res_b_np=Comp_res_b_np(:);

%ANOVA por nanoparticulas

```

```

[p,tbl,stats]=anoval(Comp_res,G_anova_g,'varname',{'Grupo_C_res'});
p_Comp_res_g=p;
tbl_Comp_res_g=tbl;
stats_Comp_res_g=stats;
h_Comp_res_1=figure;
multcompare(stats_Comp_res_g);
%ANOVA por días
[p,tbl,stats]=anoval(Comp_res,G_anova_d,'varname',{'Dia_C_res'});
p_Comp_res_d=p;
tbl_Comp_res_d=tbl;
stats_Comp_res_d=stats;
h_Comp_res_2=figure;
multcompare(stats_Comp_res_d);
%ANOVA1 por grupos y días
[p,tbl,stats]=anoval(Comp_res,G_anova_g_d,'varname',{'GrupoyDia_C_re
s'});
p_Comp_res_gd=p;
tbl_Comp_res_gd=tbl;
stats_Comp_res_gd=stats;
h_Comp_res_3=figure;
multcompare(stats_Comp_res_gd);
%ANOVA n por grupos y días
[p,tbl,stats]=anovan(Comp_res,{G_anova_g
G_anova_d},'model','interaction','varnames',{'Dia_C_ch4','Grupo_C_re
s'});
p_Comp_res_g_d=p;
tbl_Comp_res_g_d=tbl;
stats_Comp_res_g_d=stats;
h_Comp_res_4=figure;
multcompare(stats_Comp_res_d);
%ANOVA de Comp_res B por día
[p,tbl,stats]=anoval(Comp_res_b,G_anova_b_d,'varname',{'Dia_C_res_b'
});
p_Comp_res_b_d=p;
tbl_Comp_res_b_d=tbl;
stats_Comp_res_b_d=stats;
h_Comp_res_5=figure;
multcompare(stats_Comp_res_b_d);
%ANOVA de B_NP por día
[p,tbl,stats]=anoval(Comp_res_b_np,G_anova_b_np_d,'varname',{'Dia_C_
res_b_np'});
p_Comp_res_b_np_d=p;
tbl_Comp_res_b_d=tbl;
stats_Comp_res_b_np_d=stats;
h_Comp_res_6=figure;
multcompare(stats_Comp_res_b_np_d);

%Test de Normalidad
for i=1:n_s_b
    comp_res_b=results_b(1:(n_b-n_b_np),i,4);
    comp_res_b_np=results_b((n_b-n_b_np+1):n_b,i,4);

    %JBtest
    [h,p,stats,ci]=jbtest(comp_res_b);
    h_jbtest_comp_b_res_b(i)=h;
    p_jbtest_comp_b_res_b(i)=p;

```

```

stats_jbtest_comp_b_res_b{i}=stats;
ci_jbtest_comp_b_res_b(i,:)=ci;

[h,p,stats,ci]=jbtest(comp_res_b_np);
h_jbtest_comp_b_res_b_np(i)=h;
p_jbtest_comp_b_res_b_np(i)=p;
stats_jbtest_comp_b_res_b_np{i}=stats;
ci_jbtest_comp_b_res__np(i,:)=ci;

%Anderson-Darling
[h,p,stats,ci]=adtest(comp_res_b);
h_adtest_comp_b_res_b(i)=h;
p_adtest_comp_b_res_b(i)=p;
stats_adtest_comp_b_res_b{i}=stats;
ci_adtest_comp_b_res_b(i,:)=ci;

[h,p,stats,ci]=adtest(comp_res_b_np);
h_adtest_comp_b_res_b_np(i)=h;
p_adtest_comp_b_res_b_np(i)=p;
stats_adtest_comp_b_res_b_np{i}=stats;
ci_adtest_comp_b_res_b_np(i,:)=ci;

%Lillefors
[h,p,stats,ci]=lillietest(comp_ch4_b);
h_lillietest_comp_b_res_b(i)=h;
p_lillietest_comp_b_res_b(i)=p;
stats_lillietest_comp_b_res_b{i}=stats;
ci_lillietest_comp_b_res_b(i,:)=ci;

[h,p,stats,ci]=lillietest(comp_res_b_np);
h_lillietest_comp_b_res_b_np(i)=h;
p_lillietest_comp_b_res_b_np(i)=p;
stats_lillietest_comp_b_res_b_np{i}=stats;
ci_lillietest_comp_b_res_b_np(i,:)=ci;

[h,p,ci,stats]=ttest2(comp_res_b,comp_res_b_np);
h_ttest_comp_b_res(i)=h;
p_ttest_comp_b_res(i)=p;
ci_ttest_comp_b_res(i,:)=ci(:);
stats_ttest_comp_b_res{i}=stats;
mean_comp_b_res(i,1)=mean(comp_res_b(:));
mean_comp_b_res(i,2)=mean(comp_res_b_np(:));

std_comp_b_res(i,1)=sqrt(var(comp_res_b(:)));
std_comp_b_res(i,2)=sqrt(var(comp_res_b_np(:)));
[h,p,ci,stats]=vartest2(comp_res_b,comp_res_b_np);
h_ftest_comp_b_res(i)=h;
p_ftest_comp_b_res(i)=p;
ci_ftest_comp_b_res(i,:)=ci(:);
stats_ftest_comp_b_res{i}=stats;
end

%Producción de CH4 en Nm3
Prod_ch4=prod_b(:, :, 1);
Prod_ch4=Prod_ch4(:);

```

```

Prod_ch4_b=prod_b(1:(n_b-n_b_np),:,1);
Prod_ch4_b=Prod_ch4_b(:);
Prod_ch4_b_np=prod_b((n_b-n_b_np+1):n_b, :,1);
Prod_ch4_b_np=Prod_ch4_b_np(:);

%ANOVA por nanoparticulas
[p,tbl,stats]=anoval(Prod_ch4,G_anova_g,'varname',{'Grupo_P_ch4'});
p_Prod_ch4_g=p;
tbl_Prod_ch4_g=tbl;
stats_Prod_ch4_g=stats;
h_Prod_ch4_1=figure;
multcompare(stats_Prod_ch4_g);
%ANOVA por días
[p,tbl,stats]=anoval(Prod_ch4,G_anova_d,'varname',{'Dia_P_ch4'});
p_Prod_ch4_d=p;
tbl_Prod_ch4_d=tbl;
stats_Prod_ch4_d=stats;
h_Prod_ch4_2=figure;
multcompare(stats_Prod_ch4_d);
%ANOVA1 por grupos y días
[p,tbl,stats]=anoval(Prod_ch4,G_anova_g_d,'varname',{'GrupoyDia_P_ch
4'});
p_Prod_ch4_gd=p;
tbl_Prod_ch4_gd=tbl;
stats_Prod_ch4_gd=stats;
h_Prod_ch4_3=figure;
multcompare(stats_Prod_ch4_gd);
%ANOVA n por grupos y días
[p,tbl,stats]=anovan(Prod_ch4,{G_anova_g
G_anova_d},'model','interaction','varnames',{'Dia_P_ch4','Grupo_P_ch
4'});
p_Prod_ch4_g_d=p;
tbl_Prod_ch4_g_d=tbl;
stats_Prod_ch4_g_d=stats;
h_Prod_ch4_4=figure;
multcompare(stats_Prod_ch4_d);
%ANOVA de Prod_ch4 B por día
[p,tbl,stats]=anoval(Prod_ch4_b,G_anova_b_d,'varname',{'Dia_P_ch4_b'
});
p_Prod_ch4_b_d=p;
tbl_Prod_ch4_b_d=tbl;
stats_Prod_ch4_b_d=stats;
h_Prod_ch4_5=figure;
multcompare(stats_Prod_ch4_b_d);
%ANOVA de B_NP por día
[p,tbl,stats]=anoval(Prod_ch4_b_np,G_anova_b_np_d,'varname',{'Dia_P_
ch4_b_np'});
p_Prod_ch4_b_np_d=p;
tbl_Prod_ch4_b_d=tbl;
stats_Prod_ch4_b_np_d=stats;
h_Prod_ch4_6=figure;
multcompare(stats_Prod_ch4_b_np_d);

%Test de Normalidad
for i=1:n_s_b
    prod_ch4_b=prod_b(1:(n_b-n_b_np),i,1);

```

```

prod_ch4_b_np=prod_b((n_b-n_b_np+1):n_b,i,1);

%JBtest
[h,p,stats,ci]=jbttest(prod_ch4_b);
h_jbttest_prod_b_ch4_b(i)=h;
p_jbttest_prod_b_ch4_b(i)=p;
stats_jbttest_prod_b_ch4_b{i}=stats;
ci_jbttest_prod_b_ch4_b(i,:)=ci;

[h,p,stats,ci]=jbttest(prod_ch4_b_np);
h_jbttest_prod_b_ch4_b_np(i)=h;
p_jbttest_prod_b_ch4_b_np(i)=p;
stats_jbttest_prod_b_ch4_b_np{i}=stats;
ci_jbttest_prod_b_ch4__np(i,:)=ci;

%Anderson-Darling
[h,p,stats,ci]=adtest(prod_ch4_b);
h_adtest_prod_b_ch4_b(i)=h;
p_adtest_prod_b_ch4_b(i)=p;
stats_adtest_prod_b_ch4_b{i}=stats;
ci_adtest_prod_b_ch4_b(i,:)=ci;

[h,p,stats,ci]=adtest(prod_ch4_b_np);
h_adtest_prod_b_ch4_b_np(i)=h;
p_adtest_prod_b_ch4_b_np(i)=p;
stats_adtest_prod_b_ch4_b_np{i}=stats;
ci_adtest_prod_b_ch4_b_np(i,:)=ci;

%Lillefors
[h,p,stats,ci]=lillietest(comp_ch4_b);
h_lillietest_prod_b_ch4_b(i)=h;
p_lillietest_prod_b_ch4_b(i)=p;
stats_lillietest_prod_b_ch4_b{i}=stats;
ci_lillietest_prod_b_ch4_b(i,:)=ci;

[h,p,stats,ci]=lillietest(prod_ch4_b_np);
h_lillietest_prod_b_ch4_b_np(i)=h;
p_lillietest_prod_b_ch4_b_np(i)=p;
stats_lillietest_prod_b_ch4_b_np{i}=stats;
ci_lillietest_prod_b_ch4_b_np(i,:)=ci;

[h,p,ci,stats]=ttest2(prod_ch4_b,prod_ch4_b_np);
h_ttest_prod_b_ch4(i)=h;
p_ttest_prod_b_ch4(i)=p;
ci_ttest_prod_b_ch4(i,:)=ci(:);
stats_ttest_prod_b_ch4{i}=stats;
mean_prod_b_ch4(i,1)=mean(prod_ch4_b(:));
mean_prod_b_ch4(i,2)=mean(prod_ch4_b_np(:));

std_prod_b_ch4(i,1)=sqrt(var(prod_ch4_b(:)));
std_prod_b_ch4(i,2)=sqrt(var(prod_ch4_b_np(:)));
[h,p,ci,stats]=vartest2(prod_ch4_b,prod_ch4_b_np);
h_ftest_prod_b_ch4(i)=h;
p_ftest_prod_b_ch4(i)=p;
ci_ftest_prod_b_ch4(i,:)=ci(:);

```

```

    stats_ftest_prod_b_ch4{i}=stats;
end

%Producción de H2 en Nm3
Prod_h2=prod_b(:, :, 2);
Prod_h2=Prod_h2(:);
Prod_h2_b=prod_b(1:(n_b-n_b_np), :, 2);
Prod_h2_b=Prod_h2_b(:);
Prod_h2_b_np=prod_b((n_b-n_b_np+1):n_b, :, 2);
Prod_h2_b_np=Prod_h2_b_np(:);

%ANOVA por nanoparticulas
[p,tbl,stats]=anoval(Prod_h2,G_anova_g,'varname',{'Grupo_P_h2'});
p_Prod_h2_g=p;
tbl_Prod_h2_g=tbl;
stats_Prod_h2_g=stats;
h_Prod_h2_1=figure;
multcompare(stats_Prod_h2_g);
%ANOVA por días
[p,tbl,stats]=anoval(Prod_h2,G_anova_d,'varname',{'Dia_P_h2'});
p_Prod_h2_d=p;
tbl_Prod_h2_d=tbl;
stats_Prod_h2_d=stats;
h_Prod_h2_2=figure;
multcompare(stats_Prod_h2_d);
%ANOVA1 por grupos y días
[p,tbl,stats]=anoval(Prod_h2,G_anova_g_d,'varname',{'GrupoyDia_P_h2'});
p_Prod_h2_gd=p;
tbl_Prod_h2_gd=tbl;
stats_Prod_h2_gd=stats;
h_Prod_h2_3=figure;
multcompare(stats_Prod_h2_gd);
%ANOVA n por grupos y días
[p,tbl,stats]=anovan(Prod_h2,{G_anova_g
G_anova_d},'model','interaction','varnames',{'Dia_P_h2','Grupo_P_h2'});
p_Prod_h2_g_d=p;
tbl_Prod_h2_g_d=tbl;
stats_Prod_h2_g_d=stats;
h_Prod_h2_4=figure;
multcompare(stats_Prod_h2_d);
%ANOVA de Prod_h2 B por día
[p,tbl,stats]=anoval(Prod_h2_b,G_anova_b_d,'varname',{'Dia_P_h2_b'});
;
p_Prod_h2_b_d=p;
tbl_Prod_h2_b_d=tbl;
stats_Prod_h2_b_d=stats;
h_Prod_h2_5=figure;
multcompare(stats_Prod_h2_b_d);
%ANOVA de B_NP por día
[p,tbl,stats]=anoval(Prod_h2_b_np,G_anova_b_np_d,'varname',{'Dia_P_h2_b_np'});
p_Prod_h2_b_np_d=p;
tbl_Prod_h2_b_np_d=tbl;
stats_Prod_h2_b_np_d=stats;

```

```

h_Prod_h2_6=figure;
multcompare(stats_Prod_h2_b_np_d);

for i=1:n_s_b
    prod_h2_b=prod_b(1:(n_b-n_b_np),i,2);
    prod_h2_b_np=prod_b((n_b-n_b_np+1):n_b,i,2);

    %JBtest
    [h,p,stats,ci]=jbttest(prod_h2_b);
    h_jbttest_prod_b_h2_b(i)=h;
    p_jbttest_prod_b_h2_b(i)=p;
    stats_jbttest_prod_b_h2_b{i}=stats;
    ci_jbttest_prod_b_h2_b(i,:)=ci;

    [h,p,stats,ci]=jbttest(prod_ch4_b_np);
    h_jbttest_prod_b_h2_b_np(i)=h;
    p_jbttest_prod_b_h2_b_np(i)=p;
    stats_jbttest_prod_b_h2_b_np{i}=stats;
    ci_jbttest_prod_b_h2__np(i,:)=ci;

    %Anderson-Darling
    [h,p,stats,ci]=adtest(prod_h2_b);
    h_adtest_prod_b_h2_b(i)=h;
    p_adtest_prod_b_h2_b(i)=p;
    stats_adtest_prod_b_h2_b{i}=stats;
    ci_adtest_prod_b_h2_b(i,:)=ci;

    [h,p,stats,ci]=adtest(prod_h2_b_np);
    h_adtest_prod_b_h2_b_np(i)=h;
    p_adtest_prod_b_h2_b_np(i)=p;
    stats_adtest_prod_b_h2_b_np{i}=stats;
    ci_adtest_prod_b_h2_b_np(i,:)=ci;

    %Lilliefors
    [h,p,stats,ci]=lillietest(comp_h2_b);
    h_lillietest_prod_b_h2_b(i)=h;
    p_lillietest_prod_b_h2_b(i)=p;
    stats_lillietest_prod_b_h2_b{i}=stats;
    ci_lillietest_prod_b_h2_b(i,:)=ci;

    [h,p,stats,ci]=lillietest(prod_h2_b_np);
    h_lillietest_prod_b_h2_b_np(i)=h;
    p_lillietest_prod_b_h2_b_np(i)=p;
    stats_lillietest_prod_b_h2_b_np{i}=stats;
    ci_lillietest_prod_b_h2_b_np(i,:)=ci;

    [h,p,ci,stats]=ttest2(prod_h2_b,prod_h2_b_np);
    h_ttest_prod_b_h2(i)=h;
    p_ttest_prod_b_h2(i)=p;
    ci_ttest_prod_b_h2(i,:)=ci(:);
    stats_ttest_prod_b_h2{i}=stats;
    mean_prod_b_h2(i,1)=mean(prod_h2_b(:));
    mean_prod_b_h2(i,2)=mean(prod_h2_b_np(:));

    std_prod_b_h2(i,1)=sqrt(var(prod_h2_b(:)));

```

```

std_prod_b_h2(i,2)=sqrt(var(prod_h2_b_np(:)));
[h,p,ci,stats]=vartest2(prod_h2_b,prod_h2_b_np);
h_ftest_prod_b_h2(i)=h;
p_ftest_prod_b_h2(i)=p;
ci_ftest_prod_b_h2(i,:)=ci(:);
stats_ftest_prod_b_h2{i}=stats;
end

%Producción de H2S en Nm3
Prod_h2s=prod_b(:, :, 3);
Prod_h2s=Prod_h2s(:);
Prod_h2s_b=prod_b(1:(n_b-n_b_np), :, 3);
Prod_h2s_b=Prod_h2s_b(:);
Prod_h2s_b_np=prod_b((n_b-n_b_np+1):n_b, :, 3);
Prod_h2s_b_np=Prod_h2s_b_np(:);

%ANOVA por nanoparticulas
[p,tbl,stats]=anoval(Prod_h2s,G_anova_g,'varname',{'Grupo_P_h2s'});
p_Prod_h2s_g=p;
tbl_Prod_h2s_g=tbl;
stats_Prod_h2s_g=stats;
h_Prod_h2s_1=figure;
multcompare(stats_Prod_h2s_g);
%ANOVA por días
[p,tbl,stats]=anoval(Prod_h2s,G_anova_d,'varname',{'Dia_P_h2s'});
p_Prod_h2s_d=p;
tbl_Prod_h2s_d=tbl;
stats_Prod_h2s_d=stats;
h_Prod_h2s_2=figure;
multcompare(stats_Prod_h2s_d);
%ANOVA1 por grupos y días
[p,tbl,stats]=anoval(Prod_h2s,G_anova_g_d,'varname',{'GrupoyDia_P_h2s'});
p_Prod_h2s_gd=p;
tbl_Prod_h2s_gd=tbl;
stats_Prod_h2s_gd=stats;
h_Prod_h2s_3=figure;
multcompare(stats_Prod_h2s_gd);
%ANOVA n por grupos y días
[p,tbl,stats]=anovan(Prod_h2s,{G_anova_g
G_anova_d},'model','interaction','varnames',{'Dia_P_h2s','Grupo_P_h2s'});
p_Prod_h2s_g_d=p;
tbl_Prod_h2s_g_d=tbl;
stats_Prod_h2s_g_d=stats;
h_Prod_h2s_4=figure;
multcompare(stats_Prod_h2s_d);
%ANOVA de Prod_h2s B por día
[p,tbl,stats]=anoval(Prod_h2s_b,G_anova_b_d,'varname',{'Dia_P_h2s_b'});
p_Prod_h2s_b_d=p;
tbl_Prod_h2s_b_d=tbl;
stats_Prod_h2s_b_d=stats;
h_Prod_h2s_5=figure;
multcompare(stats_Prod_h2s_b_d);
%ANOVA de B_NP por día

```

```

[p,tbl,stats]=anova1(Prod_h2s_b_np,G_anova_b_np_d,'varname',{'Dia_P_
h2s_b_np'});
p_Prod_h2s_b_np_d=p;
tbl_Prod_h2s_b_d=tbl;
stats_Prod_h2s_b_np_d=stats;
h_Prod_h2s_6=figure;
multcompare(stats_Prod_h2s_b_np_d);

%Test de Normalidad
for i=1:n_s_b
    prod_h2s_b=prod_b(1:(n_b-n_b_np),i,3);
    prod_h2s_b_np=prod_b((n_b-n_b_np+1):n_b,i,3);

    %JBtest
    [h,p,stats,ci]=jbtest(prod_h2s_b);
    h_jbtest_prod_b_h2s_b(i)=h;
    p_jbtest_prod_b_h2s_b(i)=p;
    stats_jbtest_prod_b_h2s_b{i}=stats;
    ci_jbtest_prod_b_h2s_b(i,:)=ci;

    [h,p,stats,ci]=jbtest(prod_h2s_b_np);
    h_jbtest_prod_b_h2s_b_np(i)=h;
    p_jbtest_prod_b_h2s_b_np(i)=p;
    stats_jbtest_prod_b_h2s_b_np{i}=stats;
    ci_jbtest_prod_b_h2s__np(i,:)=ci;

    %Anderson-Darling
    [h,p,stats,ci]=adtest(prod_h2s_b);
    h_adtest_prod_b_h2s_b(i)=h;
    p_adtest_prod_b_h2s_b(i)=p;
    stats_adtest_prod_b_h2s_b{i}=stats;
    ci_adtest_prod_b_h2s_b(i,:)=ci;

    [h,p,stats,ci]=adtest(prod_h2s_b_np);
    h_adtest_prod_b_h2s_b_np(i)=h;
    p_adtest_prod_b_h2s_b_np(i)=p;
    stats_adtest_prod_b_h2s_b_np{i}=stats;
    ci_adtest_prod_b_h2s_b_np(i,:)=ci;

    %Lillefors
    [h,p,stats,ci]=lillietest(comp_h2s_b);
    h_lillietest_prod_b_h2s_b(i)=h;
    p_lillietest_prod_b_h2s_b(i)=p;
    stats_lillietest_prod_b_h2s_b{i}=stats;
    ci_lillietest_prod_b_h2s_b(i,:)=ci;

    [h,p,stats,ci]=lillietest(prod_h2s_b_np);
    h_lillietest_prod_b_h2s_b_np(i)=h;
    p_lillietest_prod_b_h2s_b_np(i)=p;
    stats_lillietest_prod_b_h2s_b_np{i}=stats;
    ci_lillietest_prod_b_h2s_b_np(i,:)=ci;

    [h,p,ci,stats]=ttest2(prod_h2s_b,prod_h2s_b_np);
    h_ttest_prod_b_h2s(i)=h;
    p_ttest_prod_b_h2s(i)=p;

```

```

ci_ttest_prod_b_h2s(i,:)=ci(:);
stats_ttest_prod_b_h2s{i}=stats;
mean_prod_b_h2s(i,1)=mean(prod_h2s_b(:));
mean_prod_b_h2s(i,2)=mean(prod_h2s_b_np(:));

std_prod_b_h2s(i,1)=sqrt(var(prod_h2s_b(:)));
std_prod_b_h2s(i,2)=sqrt(var(prod_h2s_b_np(:)));
[h,p,ci,stats]=vartest2(prod_h2s_b,prod_h2s_b_np);
h_ftest_prod_b_h2s(i)=h;
p_ftest_prod_b_h2s(i)=p;
ci_ftest_prod_b_h2s(i,:)=ci(:);
stats_ftest_prod_b_h2s{i}=stats;
end

%Producción de Residuos en Nm3
Prod_res=prod_b(:, :, 4);
Prod_res=Prod_res(:);
Prod_res_b=prod_b(1:(n_b-n_b_np), :, 4);
Prod_res_b=Prod_res_b(:);
Prod_res_b_np=prod_b((n_b-n_b_np+1):n_b, :, 4);
Prod_res_b_np=Prod_res_b_np(:);

%ANOVA por nanoparticulas
[p,tbl,stats]=anoval(Prod_res,G_anova_g,'varname',{'Grupo_P_res'});
p_Prod_res_g=p;
tbl_Prod_res_g=tbl;
stats_Prod_res_g=stats;
h_Prod_res_1=figure;
multcompare(stats_Prod_res_g);
%ANOVA por días
[p,tbl,stats]=anoval(Prod_res,G_anova_d,'varname',{'Dia_P_res'});
p_Prod_res_d=p;
tbl_Prod_res_d=tbl;
stats_Prod_res_d=stats;
h_Prod_res_2=figure;
multcompare(stats_Prod_res_d);
%ANOVA1 por grupos y días
[p,tbl,stats]=anoval(Prod_res,G_anova_g_d,'varname',{'GrupoyDia_P_re
s'});
p_Prod_res_gd=p;
tbl_Prod_res_gd=tbl;
stats_Prod_res_gd=stats;
h_Prod_res_3=figure;
multcompare(stats_Prod_res_gd);
%ANOVA n por grupos y días
[p,tbl,stats]=anovan(Prod_res,{G_anova_g
G_anova_d},'model','interaction','varnames',{'Dia_P_res','Grupo_P_re
s'});
p_Prod_res_g_d=p;
tbl_Prod_res_g_d=tbl;
stats_Prod_res_g_d=stats;
h_Prod_res_4=figure;
multcompare(stats_Prod_res_d);
%ANOVA de Prod_res B por día
[p,tbl,stats]=anoval(Prod_res_b,G_anova_b_d,'varname',{'Dia_P_res_b'
});

```

```

p_Prod_res_b_d=p;
tbl_Prod_res_b_d=tbl;
stats_Prod_res_b_d=stats;
h_Prod_res_5=figure;
multcompare(stats_Prod_res_b_d);
%ANOVA de B_NP por día
[p,tbl,stats]=anova1(Prod_res_b_np,G_anova_b_np_d,'varname',{'Dia_P_
res_b_np'});
p_Prod_res_b_np_d=p;
tbl_Prod_res_b_d=tbl;
stats_Prod_res_b_np_d=stats;
h_Prod_res_6=figure;
multcompare(stats_Prod_res_b_np_d);

%Test de Normalidad
for i=1:n_s_b
    prod_res_b=prod_b(1:(n_b-n_b_np),i,4);
    prod_res_b_np=prod_b((n_b-n_b_np+1):n_b,i,4);

    %JBtest
    [h,p,stats,ci]=jbtest(prod_res_b);
    h_jbtest_prod_b_res_b(i)=h;
    p_jbtest_prod_b_res_b(i)=p;
    stats_jbtest_prod_b_res_b{i}=stats;
    ci_jbtest_prod_b_res_b(i,:)=ci;

    [h,p,stats,ci]=jbtest(prod_ch4_b_np);
    h_jbtest_prod_b_res_b_np(i)=h;
    p_jbtest_prod_b_res_b_np(i)=p;
    stats_jbtest_prod_b_res_b_np{i}=stats;
    ci_jbtest_prod_b_res__np(i,:)=ci;

    %Anderson-Darling
    [h,p,stats,ci]=adtest(prod_res_b);
    h_adtest_prod_b_res_b(i)=h;
    p_adtest_prod_b_res_b(i)=p;
    stats_adtest_prod_b_res_b{i}=stats;
    ci_adtest_prod_b_res_b(i,:)=ci;

    [h,p,stats,ci]=adtest(prod_res_b_np);
    h_adtest_prod_b_res_b_np(i)=h;
    p_adtest_prod_b_res_b_np(i)=p;
    stats_adtest_prod_b_res_b_np{i}=stats;
    ci_adtest_prod_b_res_b_np(i,:)=ci;

    %Lilliefors
    [h,p,stats,ci]=lillietest(comp_res_b);
    h_lillietest_prod_b_res_b(i)=h;
    p_lillietest_prod_b_res_b(i)=p;
    stats_lillietest_prod_b_res_b{i}=stats;
    ci_lillietest_prod_b_res_b(i,:)=ci;

    [h,p,stats,ci]=lillietest(prod_res_b_np);
    h_lillietest_prod_b_res_b_np(i)=h;
    p_lillietest_prod_b_res_b_np(i)=p;
    stats_lillietest_prod_b_res_b_np{i}=stats;

```

```

ci_lillietest_prod_b_res_b_np(i,:)=ci;

[h,p,ci,stats]=ttest2(prod_res_b,prod_res_b_np);
h_ttest_prod_b_res(i)=h;
p_ttest_prod_b_res(i)=p;
ci_ttest_prod_b_res(i,:)=ci(:);
stats_ttest_prod_b_res{i}=stats;
mean_prod_b_res(i,1)=mean(prod_res_b(:));
mean_prod_b_res(i,2)=mean(prod_res_b_np(:));

std_prod_b_res(i,1)=sqrt(var(prod_res_b(:)));
std_prod_b_res(i,2)=sqrt(var(prod_res_b_np(:)));
[h,p,ci,stats]=vartest2(prod_res_b,prod_res_b_np);
h_ftest_prod_b_res(i)=h;
p_ftest_prod_b_res(i)=p;
ci_ftest_prod_b_res(i,:)=ci(:);
stats_ftest_prod_b_res{i}=stats;
end
%Extraer datos
norm_b=[h_jbtest_b;h_jbtest_b_np;h_adtest_b;h_adtest_b_np;h_lillietest_b;h_lillietest_b_np];

norm_1=[h_jbtest_comp_b_ch4_b;h_jbtest_comp_b_ch4_b_np;h_adtest_comp_b_ch4_b;h_adtest_comp_b_ch4_b_np;h_lillietest_comp_b_ch4_b;h_lillietest_comp_b_ch4_b_np];
norm_2=[h_jbtest_comp_b_h2_b;h_jbtest_comp_b_h2_b_np;h_adtest_comp_b_h2_b;h_adtest_comp_b_h2_b_np;h_lillietest_comp_b_h2_b;h_lillietest_comp_b_h2_b_np];
norm_3=[h_jbtest_comp_b_h2s_b;h_jbtest_comp_b_h2s_b_np;h_adtest_comp_b_h2s_b;h_adtest_comp_b_h2s_b_np;h_lillietest_comp_b_h2s_b;h_lillietest_comp_b_h2s_b_np];
norm_4=[h_jbtest_comp_b_res_b;h_jbtest_comp_b_res_b_np;h_adtest_comp_b_res_b;h_adtest_comp_b_res_b_np;h_lillietest_comp_b_res_b;h_lillietest_comp_b_res_b_np];

norm_5=[h_jbtest_prod_b_ch4_b;h_jbtest_prod_b_ch4_b_np;h_adtest_prod_b_ch4_b;h_adtest_prod_b_ch4_b_np;h_lillietest_prod_b_ch4_b;h_lillietest_prod_b_ch4_b_np];
norm_6=[h_jbtest_prod_b_h2_b;h_jbtest_prod_b_h2_b_np;h_adtest_prod_b_h2_b;h_adtest_prod_b_h2_b_np;h_lillietest_prod_b_h2_b;h_lillietest_prod_b_h2_b_np];
norm_7=[h_jbtest_prod_b_h2s_b;h_jbtest_prod_b_h2s_b_np;h_adtest_prod_b_h2s_b;h_adtest_prod_b_h2s_b_np;h_lillietest_prod_b_h2s_b;h_lillietest_prod_b_h2s_b_np];
norm_8=[h_jbtest_prod_b_res_b;h_jbtest_prod_b_res_b_np;h_adtest_prod_b_res_b;h_adtest_prod_b_res_b_np;h_lillietest_prod_b_res_b;h_lillietest_prod_b_res_b_np];

%%
%Regresión de los resultados
%Construcción de la tabla

%Medias
DAY=transpose([1,2,3,4,7,8,9,10,11,14,15,16,17,18,21]);
MEAN_BIOGAS_B=mean_biogas(:,1);

```

```

MEAN_BIOGAS_NP=mean_biogas(:,2);
MEAN_C_CH4_B=mean_comp_b_ch4(:,1);
MEAN_C_CH4_NP=mean_comp_b_ch4(:,2);
MEAN_C_H2_B=mean_comp_b_h2(:,1);
MEAN_C_H2_NP=mean_comp_b_h2(:,2);
MEAN_C_H2S_B=mean_comp_b_h2s(:,1);
MEAN_C_H2S_NP=mean_comp_b_h2s(:,2);
MEAN_C_RES_B=mean_comp_b_res(:,1);
MEAN_C_RES_NP=mean_comp_b_res(:,2);
MEAN_P_CH4_B=mean_prod_b_ch4(:,1);
MEAN_P_CH4_NP=mean_prod_b_ch4(:,2);
MEAN_P_H2_B=mean_prod_b_h2(:,1);
MEAN_P_H2_NP=mean_prod_b_h2(:,2);
MEAN_P_H2S_B=mean_prod_b_h2s(:,1);
MEAN_P_H2S_NP=mean_prod_b_h2s(:,2);
MEAN_P_RES_B=mean_prod_b_res(:,1);
MEAN_P_RES_NP=mean_prod_b_res(:,2);

%Tablas de medias
T_medias_B=table(DAY,MEAN_BIOGAS_B,MEAN_C_CH4_B,MEAN_C_H2_B,MEAN_C_H
2S_B,MEAN_C_RES_B,MEAN_P_CH4_B,MEAN_P_H2_B,MEAN_P_H2S_B,MEAN_P_RES_B
);
T_medias_NP=table(DAY,MEAN_BIOGAS_NP,MEAN_C_CH4_NP,MEAN_C_H2_NP,MEAN
_C_H2S_NP,MEAN_C_RES_NP,MEAN_P_CH4_NP,MEAN_P_H2_NP,MEAN_P_H2S_NP,MEA
N_P_RES_NP);

T_medias_B(4,:)=[];
T_medias_NP(4,:)=[];

%Desviacion estandar
STD_BIOGAS_B=std_biogas(:,1);
STD_BIOGAS_NP=std_biogas(:,2);
STD_C_CH4_B=std_comp_b_ch4(:,1);
STD_C_CH4_NP=std_comp_b_ch4(:,2);
STD_C_H2_B=std_comp_b_h2(:,1);
STD_C_H2_NP=std_comp_b_h2(:,2);
STD_C_H2S_B=std_comp_b_h2s(:,1);
STD_C_H2S_NP=std_comp_b_h2s(:,2);
STD_C_RES_B=std_comp_b_res(:,1);
STD_C_RES_NP=std_comp_b_res(:,2);
STD_P_CH4_B=std_prod_b_ch4(:,1);
STD_P_CH4_NP=std_prod_b_ch4(:,2);
STD_P_H2_B=std_prod_b_h2(:,1);
STD_P_H2_NP=std_prod_b_h2(:,2);
STD_P_H2S_B=std_prod_b_h2s(:,1);
STD_P_H2S_NP=std_prod_b_h2s(:,2);
STD_P_RES_B=std_prod_b_res(:,1);
STD_P_RES_NP=std_prod_b_res(:,2);

%Tablas de desviaciones típicas
T_std_B=table(DAY,STD_BIOGAS_B,STD_C_CH4_B,STD_C_H2_B,STD_C_H2S_B,ST
D_C_RES_B,STD_P_CH4_B,STD_P_H2_B,STD_P_H2S_B,STD_P_RES_B);
T_std_NP=table(DAY,STD_BIOGAS_NP,STD_C_CH4_NP,STD_C_H2_NP,STD_C_H2S_
NP,STD_C_RES_NP,STD_P_CH4_NP,STD_P_H2_NP,STD_P_H2S_NP,STD_P_RES_NP);

T_std_B(4,:)=[];

```

```

T_std_NP(4,:)=[];

%%
%%Regresion de los resultados
x=T_std_B.DAY;
prod=[0:0.1:8.5];
comp=[0:0.01:1];

%Biogas Production B
y=(log(T_medias_B.MEAN_BIOGAS_B));
tbl=table(x,y);
mdl_mean_biogas_b=fitlm(tbl,'y~1+x')
p01ResidualAnalysis(mdl_mean_biogas_b);

y=T_std_B.STD_BIOGAS_B;
tbl=table(x,y);
mdl_std_biogas_b=fitlm(tbl,'y~1-x+x^2+x^3')
p01ResidualAnalysis(mdl_std_biogas_b);

norm_b=[];
for i=1:length(x)
    mu_b(i)=exp(1.4252-0.19205*x(i));
    std_b(i)=1.2177-0.011971*x(i)^2+0.00047875*x(i)^3;
    for j=1:length(prod)
        norm_b(j,i)=normpdf(prod(j),mu_b(i),std_b(i));
    end
end

y=(log(T_medias_NP.MEAN_BIOGAS_NP));
tbl=table(x,y);
mdl_mean_biogas_np=fitlm(tbl,'y~1+x')
p01ResidualAnalysis(mdl_mean_biogas_np);

y=T_std_NP.STD_BIOGAS_NP;
tbl=table(x,y);
mdl_std_biogas_np=fitlm(tbl,'y~1-x+x^2+x^3')
p01ResidualAnalysis(mdl_std_biogas_np);

norm_np=[];
for i=1:length(x)
    mu_np(i)=exp(1.4256-0.1531*x(i));
    std_np(i)=0.84945-0.0074038*x(i)^2+0.00028246*x(i)^3;
    for j=1:length(prod)
        norm_np(j,i)=normpdf(prod(j),mu_np(i),std_np(i));
    end
end

%
figure;
surf(x, prod, norm_b);
hold on;
title('B Binormal Distribution ');
xlabel('Day');
ylabel('Production (Nm^3 / m3_s)');
zlabel('Probability');

```

```
%  
figure;  
surf(x, prod, norm_np);  
hold on;  
title('B NP Binormal Distribution ');  
xlabel('Day');  
ylabel('Production (Nm^3 / m3_s)');  
zlabel('Probability');  
  
%%  
%%Salidas de los datos  
%plot(squeeze(crom_r(1,13,:)))  
%imshow(t_r{1,1})
```

Chapter 8: References

- AENOR. June UNE-EN ISO 11734:1999 Calidad del agua. Evaluación de la biodegradabilidad anaerobia "final" de los compuestos orgánicos con lodos en digestión. Método por medida de la producción de biogás. doi:EN ISO 11734:1998
- Agilent. (2011). *Agilent 7820A Gas Chromatography Operating Guide*. Shanghai: Agilent Technologies, Inc. <https://www.agilent.com/cs/library/usermanuals/public/g4350-90012.pdf>
- Agilent Technologies. (2011). *Agilent 7820A Cromatógrafo de gases*. Santa Clara.
- Agilent Technologies, Inc. (2011). *Agilent 7820A Cromatógrafo de gases*. Santa Clara.
- Agilent Technologies, Inc. (2016). *Agilent 7820A Gas Chromatography Advanced User Guide*. Shanghai: Agilent Technologies, Inc. <https://www.agilent.com/cs/library/usermanuals/public/G4350-90020.pdf>
- Agilent Technologies, Inc. (2017). *Agilent OpenLAB CDS*. Shanghai. <https://www.agilent.com/cs/library/usermanuals/public/WorkstationGuide.pdf>
- Agilent Technologies, Inc. CP-Molsieve 5A Columns: <https://www.agilent.com/en/product/gc-columns/plot-gc-columns/cp-molsieve-5a-columns#productdetails>
- Agilent Technologies, Inc. June *Agilent*. PoraPLOT Q Columns: <https://www.agilent.com/en/product/gc-columns/plot-gc-columns/poraplot-q-columns>
- Agilent Technologies, Inc. https://www.agilent.com/?gclid=Cj0KCQjwkruVBhCHARIsACViiOx0Iq0Giuu7UBxSwAPUr7O8OuvkVZ_6M8Dt5nWH_BM7Ycdh1j8X_w8aAoPTEALw_wcB&gclsrc=aw.ds
- June *Agilent*. 6890-Thermal Conductivity Detector (TCD): <https://www.agilent.com/en/support/gas-chromatography/a03127>
- Akratos, C. S., Tekerlekopoulou, A. G., Vasiliadou, I. A., & Vayenas, D. V. (2017). Chapter 8 - Cocomposting of olive mill waste for the production of soil amendments. *Olive Mill Waste* (161-182). Chania: Elsevier. doi:<https://doi.org/10.1016/B978-0-12-805314-0.00008-X>
- Al Seadi, T., Ruiz, D., Prassl, H., Kottner, M., Finsterwaldes, T., Volke, S., & Janssens, R. (2008). *Handbook of Biogas*. Esbjerg: University of Southern Denmark. doi:978-87-992962-0-0.
- Angelidaki, I., Xie, L., Luo, G., Zhang, Y., Oechsner, H., Lemmer, A., . . . Kougias, P. G. (2019). Chapter 33 - Biogas Upgrading: Current and Emerging Technologies. In I. Angelidaki, L. Xie, G. Luo, Y. Zhang, H. Oechsner, A. Lemmer, . . . P. G. Kougias, *Biofuels: Alternative Feedstocks and Conversion Processes for the Production of Liquid and Gaseous Biofuels (Second Edition)* (second ed., pp. 817-843). Academic Press. doi:<https://doi.org/10.1016/B978-0-12-816856-1.00033-6>
- Antonini, C., Treyer, K., Streb, A., Spek, M. v., Bauer, C., & Mazzotti, M. (2020, March 11). Hydrogen production from natural gas and biomethane with carbon capture and storage- A techno-environmental analysis. *Sustainable Energy Fuels*, 2967-2986. doi:10.1039/D0SE00222D
- Anukam, A., Mohammadi, A., Muhammad, N., & Granström, K. May A Review of the Chemistry of Anaerobic Digestion: Methods of Accelerating and Optimizing Process Efficiency. *MDPI*, 504-523. doi:10.3390/pr7080504

- APHA, AWWA, WEF. (2012). *Standard method for the examination of water and wastewater* (Vol. 23). doi:9780875532875
- B10NUMB3R5. Solubility of carbon dioxide in water at 25°C and 1 atm partial pressure: <https://bionumbers.hms.harvard.edu/bionumber.aspx?s=n&v=4&id=106207#:~:text=0.1449%20grams%20CO2%20per%20100%20ml%20H2O%20at%2025%C2%B0C>.
- november COP26: US and EU announce pledge to slash methane. London, Greater London, United Kingdom. <https://www.bbc.com/news/world-59137828>
- Benitez, J. (2009). *Principles and modern applications of mass transfer operations*. Hoboken: John Wiley and Sons. <https://www.wiley.com/en- ie/Principles+and+Modern+Applications+of+Mass+Transfer+Operations%2C+3rd+Edition- p-9781119276944>
- Benitez, J. (2016). *Principles and Modern Applications of Mass Transfer Operations* (3rd ed.). Wiley. <https://www.wiley.com/en- ie/Principles+and+Modern+Applications+of+Mass+Transfer+Operations%2C+3rd+Edition- p-9781119276944>
- Billet, R. (1989). *Packed column analysis and design*. Ruhr: Ruhr-University Bochum. <https://www.worldcat.org/title/packed-column-analysis-and-design/oclc/758858472>
- junio *Broad Institute*. What is mass spectrometry: <https://www.broadinstitute.org/technology- areas/what-mass- spectrometry#:~:text=Mass%20spectrometry%20is%20an%20analytical,the%20sample%20c omponents%20as%20well>.
- Bushra, R. (2018). Chapter 15: Functionalized Nanomaterials for Chromatography. C. M. Hussain, *Nanomaterials in Chromatography* (403-414). Elsevier. doi:<https://doi.org/10.1016/B978-0-12-812792-6.00015-7>
- Caicedo, L. M., Wang, H., Lu, W., De Clercq, D., Liu, Y., Xu, S., & Ni, Z. (2017, june). Effect of initial bulk density on high-solids anaerobic digestion of MSW: General mechanism. *Bioresource Technology*, 233, 332-341. doi:<https://doi.org/10.1016/j.biortech.2017.02.107>
- Chemistry LibreTexts. Lennard-Jones Potential: [https://chem.libretexts.org/Bookshelves/Physical_and_Theoretical_Chemistry_Textbook_Maps/Supplemental_Modules_\(Physical_and_Theoretical_Chemistry\)/Physical_Properties_of_Matter/Atomic_and_Molecular_Properties/Intermolecular_Forces/Specific_Interactions/Le](https://chem.libretexts.org/Bookshelves/Physical_and_Theoretical_Chemistry_Textbook_Maps/Supplemental_Modules_(Physical_and_Theoretical_Chemistry)/Physical_Properties_of_Matter/Atomic_and_Molecular_Properties/Intermolecular_Forces/Specific_Interactions/Le)
- septembre *Chesmitry LibreTexts*. 6.7: The Ideal Gas Law: [https://chem.libretexts.org/Courses/Sacramento_City_College/SCC%3A_CHEM_330_-_Adventures_in_Chemistry_\(Alviar- Agnew\)/06%3A_Gases_Liquids_Solids_..._and_Intermolecular_Forces/6.07%3A_The_Ideal_Gas_Law#:~:text=The%20ideal%20gas%20constant%20is,moles%20of%20](https://chem.libretexts.org/Courses/Sacramento_City_College/SCC%3A_CHEM_330_-_Adventures_in_Chemistry_(Alviar- Agnew)/06%3A_Gases_Liquids_Solids_..._and_Intermolecular_Forces/6.07%3A_The_Ideal_Gas_Law#:~:text=The%20ideal%20gas%20constant%20is,moles%20of%20)
- Cledera Castro, M. (2022). Contaminants. Introduction. *Water Pollutiong and Liquid Effluent Treatment* (2.1.1-2.1.64). Madrid: Universidad Pontificia Comillas.
- Comecta. (2022, august 1). *Comecta*. Retrieved from Ivymen Orbital Shaker Incubator: <https://www.comecta.es/model/33>
- CPI Inflation Calculator. Value of €100 from 2018 to 2022: <https://www.in2013dollars.com/europe/inflation/2018?amount=100>

- july *CPI Inflation Calculator*. Value of €100 from 2005 to 2022:
<https://www.in2013dollars.com/europe/inflation/2005?amount=100>
- Crynes, B. L., Albright, L. F., & Tan, L.-F. (2003). Thermal Cracking. R. A. Meyers, *Encyclopedia of Physical Science and Technology (Third Edition)* (613-626). West Lafayette, Indiana, United States of America: Academic Press.
 doi:<https://www.sciencedirect.com/science/article/pii/B0122274105001538>
- Doan Pham Minh, T. J.-V. (2018). Chapter 4 - Hydrogen Production From Biogas Reforming: An Overview of Steam Reforming, Dry Reforming, Dual Reforming, and Tri-Reforming of Methane. T. J.-V. Doan Pham Minh, *Hydrogen Supply Chains: Design, Deployment and Operation* (111-166). Academic Press.
- Dong, N., Bu, F., Zhou, Q., Khanal, S. K., & Xie, L. (2018). Performance and microbial community of hydrogenotrophic methanogenesis under thermophilic and extreme-thermophilic conditions. *Bioresource Technology*, 266, 454-462.
 doi:<https://doi.org/10.1016/j.biortech.2018.05.105>
- eckson Kamusoko, R. M. (2022). Chapter 25 - Biogas: microbiological research to enhance efficiency and regulation. 485-497). Academic Press. doi:<https://doi.org/10.1016/B978-0-12-822810-4.00025-7>
- november *ecoinvent*. <https://ecoinvent.org/>
- El Ibrahimy, M., Khay, I., El Maakoul, A., Moussa, M. O., Barkaoui, A., & Bakhouya, M. Anaerobic co-digestion in a liquid recirculation pilot-scale reactor: Thermal and hydraulic analysis. *Elsevier*, 496-502. doi:10.1016/j.egy.2019.09.01
http://www.enerblu-cogeneration.com/uploads/file/28/1028/CATALOGO_PRODOTTI_GB_05.2019.pdf
- Energy Information Agency. (2021, may 26). *Natural gas explained*. Retrieved from Energy Information Agency: <https://www.eia.gov/energyexplained/natural-gas/use-of-natural-gas.php#:~:text=Most%20U.S.%20natural%20gas%20use,other%20uses%20for%20natural%20gas.&text=The%20electric%20power%20sector%20uses,and%20produce%20useful%20thermal%20output>.
- European Biogas Association. (2020). *BioLNG in Transport: Making Climate Neutrality a Reality*. Belgium: European Biogas Association. https://www.europeanbiogas.eu/wp-content/uploads/2020/11/BioLNG-in-Transport_Making-Climate-Neutrality-a-Reality.pdf
- january Commision Work Programme 2020. *The Official Journal of the European Union*, 1-11. doi:COM*2020(37 final
- European Comission. (2020). *Implementing the SET Plan 2020 Report*. Brussels: Joint Research Centre. doi:JRC122587
- European Comission. European Green Deal: https://ec.europa.eu/info/strategy/priorities-2019-2024/european-green-deal_es
- november *F-Chart Software*. Engineering Equation Solver:
<https://fchartsoftware.com/ees/index.php/>
- Food and Agriculture Organization. (2002). The role of agriculture in the development of the least-developed countries and their integration into the world economy. *Commodities and Trade Division*, 3-6. <https://www.fao.org/3/y3997e/y3997e.pdf>

- Fraunhofer ISE. (2018). *Levelized Cost of Electricity Renewable Energy Technologies*. Fraunhofer ISE, Karlsruhe.
https://www.ise.fraunhofer.de/content/dam/ise/en/documents/publications/studies/EN2018_Fraunhofer-ISE_LCOE_Renewable_Energy_Technologies.pdf
- Fumey, J.-P. (2021, september 14). *startup.info*. Retrieved from <https://startup.info/es/el-biogas-es-una-alternativa-al-gas-natural-pero-es-una-fuente-de-energia-verde/>
- García Mingo, L. (2021). Depuración de Aguas Residuales. *Water Pollution & Liquid Effluent Treatment*. Madrid.
- Ghaly, A. E. december Effect of reseeded and ph control on the performance of a two-stage mesophilic anaerobic digester operating on acid cheese whey. *Canadian Agricultural Engineering*, 42(4), 173-183.
<http://citeseerx.ist.psu.edu/viewdoc/download?doi=10.1.1.1070.9493&rep=rep1&type=pdf>
- Gómez Camacho, C. E., Ruggeri, B., Mangialardi, L., Persico, M., & Luongo Malavé, A. C. (2019). Continuous two-step anaerobic digestion (TSAD) of organic market waste: rationalising process parameters. *International Journal of Energy and Environmental Engineering*, 413-427. doi:10.1007/s40095-019-0312-1
- Hage, D. S. (1991). Chapter 10: Gas Chromatography. 223-462). Elsevier.
doi:[https://doi.org/10.1016/S0166-526X\(05\)80100-X](https://doi.org/10.1016/S0166-526X(05)80100-X)
- june Baños con equipo termostático “Digiterm-TFT-200-20”. (J.P. Selecta) july 2022,
<https://grupo-selecta.com/productos/bano-con-equipo-termost-digiterm-tft-200--20-3000550>
- Kayode Coker, A. (2010). *Ludwig's Applied Process Design for Chemical and Petrochemical Plants* (Vols. 2: Distillation, packed towers, petroleum fractionation, gas processing and dehydration). Jubal, Saudi Arabia: Elsevier. doi:<https://doi.org/10.1016/C2009-0-27075-9>
- Kim, D.-H., & Oh, S.-E. (2011). Continuous high-solids anaerobic co-digestion of organic solid wastes under mesophilic conditions. *Wast Management*, 31(9-10), 1943-1948.
doi:10.1016/j.wasman.2011.05.007
- Kress, P., Hans-Joachim, N., Oechsner, H., & S., R. (2018). Effect of agitation time on nutrient distribution in full scale CSTR biogas digesters. *Elsevier*, 1-6.
- Laboquímica. (2022). *Valorador automático HI 901 y HI 902, HANNA®*.
http://www.laboquimia.es/catalogo/producto.php?codigo=2109HI902&sub_amarillo=yes
- Lampaya Nasarre, J. (2022). Waste to Energy Power Plants: Rejects and Optimization. *Solid Waste Management and Valorization* (1-147). Madrid: Universidad Pontificia Comillas.
- Lefers, M. <https://groups.molbiosci.northwestern.edu/holmgren/Glossary/Definitions/Def-H/hydrolysis.html>
- september Vapor-liquid equilibrium properties for confined binary mixtures involving CO₂, CH₄, and N₂ from Gibbs ensemble Monte Carlo simulations. *Science China-Chemistry*, 55(9), 1825-1833. doi:10.1007/s11426-012-4724-5
- Linares Hurtado, J. (2021). Tema 9.- Hidrógeno y Pilas de Combustible. 9.1-9.23). Madrid: Universidad Pontificia Comillas.
- J. I. Linares Hurtado, *Ingeniería Energética- Apuntes de Clase* (1.1-1.34). Madrid: Universidad Pontificia Comillas-ICAI.

- Linares Hurtado, J. I. (2020). Tema 5.- Cogeneración, renovables y Ciclos de potencia avanzados. 5.1-5.67). Madrid: Universidad Pontificia Comillas.
- J. I. Linares Hurtado, *Ingeniería Energética* (1.1.1-1.1.34). Madrid: Unversidad Pontificia Comillas.
- Linares Hurtado, J. I. (2021). Tema 5: Cogeneración, renovables y ciclos de potencia avanzados. Ejercicios de clase. 5.2.14). Madrid: Universidad Pontificia Comillas-ICAI.
- J. I. Linares Hurtado, *Ingeniería Energética* (5.1.1-5.1.35). Madrid: Universidad Pontificia Comillas.
- Liu, S., Cao, L., Xu, F., Yang, L., Li, Y., & Inalegwu, O. S. (2021). Chapter Five - Integration of algae cultivation to anaerobic digestion for biofuel and bioenergy production. 199-300). Elsevier. doi:<https://doi.org/10.1016/bs.aibe.2021.06.002>.
- Lorenzo Acosta, Y., & Obaya Abreu, M. C. (2005). La Disgestión Anaerobia. Aspectos Teóricos. Parte I. *Sobre los Derivados de la Caña de Azúcar*, XXXIX(1), 35-48. <https://www.redalyc.org/pdf/2231/223120659006.pdf>
- Marin Galvín, R. https://www.researchgate.net/publication/330359842_Sobre_la_sustitucion_de_la_DQO_por_el_COT_para_medidas_de_la_materiaorganica_en_aguas_residuales_ventajas_e_inconvenientes
- november *MathWorks*. MATLAB: <https://es.mathworks.com/products/matlab.html>
- MatWorks. (2022). *atlab & Simulink*. <https://es.mathworks.com/products/matlab.html>
- Meegoda, J. L. (2018). A Review of the Processes, Parameters, and Optimization of Anaerobic Digestion. *International Journal of Environmental Research and Public Health*, 16.
- Megegoda, J. L., Li, B., & Wang, L. B. october A Review of the Processes, Parameters, and Optimization of anaerobic Digestion. *International Journal of Environmental Research and Public Health*. doi:10.3390/ijerph15102224
- Memon, A., Li, A., Wencheng, H., & Tian, W. (2019). Effect of gas adsorption-induced pore radius and effective stress on shale gas permeability in slip flow: New Insights. *Open Geosciences*, 948-960. doi:10.1515/geo-2019-0073
- Menzel, T. N. (2020). Role of Microbial Hydrolysis in Anaerobic Digestion. *MDPI*, 29.
- Merck. COD Cell Test: <https://www.sigmaaldrich.com/ES/es/product/mm/114541>
- Merck. august *Merck*. Nitrogen (total) Cell Test: <https://www.sigmaaldrich.com/ES/es/product/mm/114537>
- Merck. (2022). *Prove 100*. <https://www.sigmaaldrich.com/ES/es/product/mm/173016>
- Ministerio de Industria, Energía y Turismo. junio Real Decreto 413/2014, de 6 de junio, por el que se regula la actividad de producción de energía eléctrica a partir de fuentes de energía renovables, cogeneración y residuos. *Boletín Oficial del Estado*, 43876-43978. doi:BOE-A-2014-6123
- Ministerio de Industria, Turismo y Comercio. july Real Decreto 661/2007, de 25 de mayo, por el que se regula la actividad de producción de energía eléctrica en régimen especial. *Boletín Oficial del Estado*, 1-66. doi:BOE-A-2007-10556

- Ministerio para la Transición Ecológica y el Reto Demográfico. (2020). *Plan Nacional Integrado de Energía y Clima*. Madrid: Ministerio para la Transición Ecológica y el Reto Demográfico. https://www.miteco.gob.es/images/es/pniecCompleto_tcm30-508410.pdf
- Ministerio para la Transición Ecológica y el Reto Demográfico. (2021). *El MITECO saca a información pública la propuesta de Hoja de Ruta del Biogás*. Madrid: Borrador Trámite de Audiencia.
- Ministerio para la Transición Ecológica y el Reto Demográfico. (2022). *Hoja de Ruta del Biogás*. Madrid: Ministerio para la Transición Ecológica y el Reto Demográfico. <https://drive.google.com/file/d/1Uw7iaML1Evh0e0nI91ZvNFWDCcwjprlN/view>
- Morales Polo, C. (2019). *Co-Digestión anaerobia y pretratamiento de residuos agroalimentarios con fangos UASB de depuradora*. Madrid: Universidad Pontificia Comillas-ICAI.
- Morales Polo, C. (2019). *Co-Digestión Anaerobia y Pretratamientos de Residuos Agroalimentarios con Fangos UASB de Depuradora*. Madrid, Madrid, Spain: Universidad Pontificia Comillas-ICAI.
- Morales Polo, C. (2022). Digestión Anaerobia. 4.2.1-4.2.19). Madrid: Universidad Pontificia Comillas-ICAI.
- Solid Waste Management and Valorizations* (4.1.1-4.4.33). Madrid: Universidad Pontificia Comillas.
- Morales Polo, C. (2022). Residuos Sólidos Urbanos. *Solid Waste Mangement and Valorization* (2.1.1-2.1.31). Madrid: Universidad Pontificia Comillas.
- Morozova, I., Nikulina, N., Oechsner, H., Krümpel, J., & Lemmer, A. Effects of Increasing Nitrogen Content on Process Stability and Reactor Performance in Anaerobic Digestions. *Energies*, 1139-1157. doi:<https://doi.org/10.3390/en13051139>
- august *Thermopedia*. Diffusion Coefficient: <https://www.thermopedia.com/content/696/>
- Nguyen, H., Morrison, A. L., & Nelson, P. F. (2005). *Analysis of Pollution Control Costs in Coal Based Electricity Generation. Technology Assessment Report 68*. Pullenvale: QCAT Technology Transfer Center. https://www.researchgate.net/publication/237460048_ANALYSIS_OF_POLLUTION_CONTROL_COSTS_IN_COAL_BASED_ELECTRICITY_GENERATION_TECHNOLOGY_ASSESSMENT_REPORT_68
- july *OMIP*. OMIP: <https://www.omip.pt/es>
- Owen, W. F., Stuckey, D. C., jr, J. H., Young, L., & MCarty, P. Bioassay for monitoring biochemical methane potential and anaerobic toxicity. *Water Research*, 485-492. doi:0043-1354 79 0601-0485802.00 0
- august Stabilization Wedges: Solving the Climate Problem for the Next 50 Years with Current Technologies. *Science*, 968-972. doi:10.1126/science.1100103
- Palomar, P. (2020). Contaminación agrícola y ganadera. Palomar, *Soil Pollution & Depletion- Apuntes de Clase* (2.2.1-2.2.44). Madrid: Universidad Pontificia Comillas-ICAI.
- Pavlov, K. F. (1981). *Problemas y ejemplos para el curso de operaciones básicas y aparatos en tecnología química*. Moscow: Mir. https://primo.utb.edu.co/discovery/fulldisplay?docid=alma990000024680205731&context=L&vid=57UTB_INST:57UTB_INST&lang=es&adaptor=Local%20Search%20Engine&tab=Everything&query=sub,exact,VIDRIO&offset=0

- septiembre Design of a packed-bed absorption column considering four packing types and applying Matlab. *Nexo Revista Científica*, 29(2), 83-.
doi:<https://www.camjol.info/index.php/NEXO/article/view/4577>
- Petchsri, P., Towprayoon, S., Chaiprasert, P., & Nopharatana, A. (2004). Biogas production from simulated landfill bioreactor with leachate recirculation under various waste densities. *Sustainable energy and Environment (SEE)*, 390-395.
- PRé. november *SimaPro*. <https://simapro.com/>
- Rabii, A., Aldin, S., Dahman, Y., & Elbeshbishy, E. march A Review on Anaerobic Co-Digestion with a Focus on the Microbial Populations and the Effect of Multi-Stage Configuration. *Energies*, 12(6), 1106-1130. doi:10.3390/en12061106
- Rakmak, N., & Wiyaratn, W. (2010). Effect of Operating Parameters on Double Packed Columns using Iron (Fe 3+) Doped MgO Catalyst for Removal of H₂S from Biogas. *The Eighth PSU Engineering Conference* (
https://www.researchgate.net/publication/267389413_Effect_of_Operating_Parameters_on_Double_Packed_Columns_using_Iron_Fe_3_Doped_MgO_Catalyst_for_Removal_of_H_2_S_from_Biogas
- november COP 26: Coal compromise as leaders near climate deal. London, Greater London, United Kingdom. <https://www.bbc.com/news/science-environment-59221790>
- Rathnasiri, P. G. (2016). Dynamic modelling and simulation of pilot scale anaerobic digestion plant treating source separated food waste and effect of recycling sludge. *Procedia*, 740-748.
- Ritter. (2022). *MilliGascounter*. july 2022, <https://www.ritter.de/es/productos/milligascounter/>
- Romero Mora, J. C., & Tatay Nieto, J. (2020). What is the circular economy. J. C. Romero Mora, & J. Tatay Nieto, *Sustainable Development Agenda- Apuntes de Clase* (5.1-5.53). Madrid: Universidad Pontificia Comillas-ICAI.
- Sander, R. (2015). Compilation of Henry's law constants (version 4.0) for water as solvent. *Atmospheric Chemistry and Physics*, 4399-4981. doi:10.5194/acp-15-4399-2015
- Scharlab. (2021). *Minireactor with mechanical stirring of 2000 ml*. july 2022, <https://www.scharlab.com/productos-producto-catalogo-productos-detalle-referencia.php?c=13&sc=55&p=9196&r=MR-00%2F2000>
- Scharlab. (2022). *Portable pH meter XS pH 70, complete with case, low cost pH electrode, CAT and buffers.Labprocess*. <https://www.scharlab.com/productos-producto-catalogo-productos-detalle-referencia.php?r=00G-PH70-3>
- Hydrothermal carbonization of biomass as a route for the sequestration of CO₂: Chemical and structural properties of the carbonized products*. Oviedo: Instituto Nacional del Carbón (CSIC).
- Siciliano, A., Limonti, C., Curcio, G. M., & Calabrò, V. (2019). Biogas Generation through Anaerobic Digestion of Compost Leachate in Semi-Continuous Completely Stirred Tank Reactors. *MDPI*.
- Smallops. november *Smallops*. <https://smallops.eu/>
- Sociedad Española de Cromatografía y Técnicas Afines. Parámetros, retención en cromatografía en columna: <https://www.secyta.es/es/node/29>

- april Effect of Spatial Differences in Microbial Activity, pH, and Substrate Levels on Methanogenesis Initiation in Refuse. *Appl Environ Microbiol*, 2381-2391. doi:10.1128/AEM.02349-10
- Statistics How To. (2022). *T Test (Student's T-Test): Definition and Examples*. <https://www.statisticshowto.com/probability-and-statistics/t-test/>
- august *The Engineering ToolBox*. Gases-Dynamic Viscosities: https://www.engineeringtoolbox.com/gases-absolute-dynamic-viscosity-d_1888.html
- Tran, T. (2017). *Standard Methods for the Examination of Water and Wastewater, 23rd edition*. Washington, DC.: American Public Health Association.
- United Nations. (2015, september 25). *Sustainable Development Goals*. Retrieved november 19, 2021, from United Nations: <https://www.un.org/sustainabledevelopment/climate-change/>
- United Nations. (2015, september 25). *Sustainable Development Goals*. Retrieved from United Nations: <https://www.un.org/sustainabledevelopment/infrastructure-industrialization/>
- United Nations. United Nations: <https://sdgs.un.org/goals/goal11>
- United Nations. november *UN Climate Change Conference UK 2021*. COP26: <https://ukcop26.org/>
- Universidad Pontificia Comillas. <https://www.comillas.edu/investigacion/grupos/contaminantes-emergentes-y-valorizacion-de-residuos>
- november *Universidad Pontificia Comillas*. Cátedra Rafael Maiño de Nuevas Tecnologías Energéticas: <https://www.comillas.edu/catedra-rafael-marino>
- Usack, J. G., & Angenent, L. (2012). Continuously-stirred Anaerobic Digester to Convert Organic Wastes into Biogas: System Setup and Basic Operation. *Journal of Visualized Experiments*. doi:10.379/3978
- van Lier, J. B., Mahmoud, N., & Zeeman, G. (2020). 16. Anaerobic Wastewater Treatment. *Biological Wastewater Treatment* (401-442). IWA Publishing. doi:<https://doi.org/10.2166/9781789060362>
- Verlag des Vereins Deutscher Ingenieure. (2006). *VDI-4630 (2006) Fermentation of Organic Materials: Characterisation of the Substrate, Sampling, Collection of Material Data, Fermentation Tests*. Düsseldorf: VDI. <https://www.vdi.de/richtlinien/details/vdi-4630-fermentation-of-organic-materials-characterization-of-the-substrate-sampling-collection-of-material-data-fermentation-tests>
- Vijayalakshmi Arelli, S. J. (2022). 16 - Solid state anaerobic digestion of organic waste for the generation of biogas and bio manure. *Advanced Organic Waste Management* (247-277). Hyderabad: Elsevier. doi:<https://doi.org/10.1016/B978-0-323-85792-5.00023-X>
- Walcoom Corporation. (2022). *Random Packing*. Hengshui, Hebei, People's Republic of China: Walcoom Corporation. <https://www.walcoom.com/pdf/random-packing-catalog.pdf>
- Whitehead, P. april *Elga*. (Veolia) july 2022, [https://www.elgalabwater.com/blog/total-organic-carbon-toc#:~:text=Total%20Organic%20Carbon%20\(TOC\)%20is,solution%20is%20for%20their%20processes.](https://www.elgalabwater.com/blog/total-organic-carbon-toc#:~:text=Total%20Organic%20Carbon%20(TOC)%20is,solution%20is%20for%20their%20processes.)
- Yang, Z., Wang, W., He, Y., Zhang, R., & Liu, G. september Effect of ammonia on methane production, methanogenesis pathway, microbial community and reactor performance under

- mesophilic and thermophilic conditions. *Renewable Energy*, 125, 915-925.
doi:<https://doi.org/10.1016/j.renene.2018.03.032>
- Zhang, B., Zhang, L. L., Zhang, S. C., Shi, H. Z., & Cai, W. M. (2005). The Influence of pH on Hydrolysis and Acidogenesis of Kitchen Wastes in Two-phase Anaerobic Digestion. *Environmental Technology*, 26(3), 329-339. doi:10.1080/09593332608618563
- Zhang, C., Su, H., Baeyens, J., & Tan, T. Reviewing the anaerobic digestion of food waste for biogas production. *Elsevier*, 383-392. doi:10.1016/j.rser.2014.05.038
- october Reviewing the anaerobic digestion of food waste for biogas production. *Renewable and Sustainable Energy Reviews*, 38, 383-392. doi:10.1016/j.rser.2014.05.038
- Zhao, Q., Gyebi Arhin, S., Yang, Z., Liu, H., Li, Z., Anwar, N., . . . Wang, W. pH regulation of the first phase could enhance the energy recovery from two-phase anaerobic digestion of food waste. *Water Environment Research*, 1370*-1380. doi:<https://doi.org/10.1002/wer.1527>